

University of Nebraska - Lincoln

DigitalCommons@University of Nebraska - Lincoln

Dissertations & Theses: Construction
Engineering and Management

Durham School of Architectural Engineering
and Construction

Spring 5-2022

Repair and Strengthening of Concrete Bridges Using Ultra-High-Performance Concrete (UHPC)

Antony Kodsy

University of Nebraska-Lincoln

Follow this and additional works at: <https://digitalcommons.unl.edu/constructiondiss>



Part of the [Construction Engineering and Management Commons](#)

Kodsy, Antony, "Repair and Strengthening of Concrete Bridges Using Ultra-High-Performance Concrete (UHPC)" (2022). *Dissertations & Theses: Construction Engineering and Management*. 29.
<https://digitalcommons.unl.edu/constructiondiss/29>

This Article is brought to you for free and open access by the Durham School of Architectural Engineering and Construction at DigitalCommons@University of Nebraska - Lincoln. It has been accepted for inclusion in Dissertations & Theses: Construction Engineering and Management by an authorized administrator of DigitalCommons@University of Nebraska - Lincoln.

REPAIR AND STRENGTHENING OF CONCRETE BRIDGES USING
ULTRA-HIGH-PERFORMANCE CONCRETE (UHPC)

by

Antony M. Kodsy

A DISSERTATION

Presented to the Faculty of

The Graduate College at the University of Nebraska

In Partial Fulfillment of Requirements

For the Degree of Doctor of Philosophy

Major: Engineering

(Construction Engineering and Management)

Under the Supervision of Professor George Morcous

Lincoln, Nebraska

May, 2022

REPAIR AND STRENGTHENING OF CONCRETE BRIDGES USING ULTRA-HIGH-PERFORMANCE CONCRETE (UHPC)

Antony Kodsy, Ph.D.

University of Nebraska, 2022

Advisor: George Morcous

Reinforced/Prestressed concrete bridges are subjected to environmental effects that cause premature deterioration and require structural repair and strengthening during their service life. Currently 42% of bridges in the United States are at least 50 years old, and 7.5% of them are structurally deficient and need to be repaired/strengthened. Recently, new repair and strengthening techniques using Ultra-High-Performance concrete (UHPC) have shown a great potential with respect to performance, economy, and speed. UHPC is a new class of concrete that has mechanical and durability properties that are far superior to those of conventional concrete (CC). In addition, UHPC offers several advantages compared to the current repair and strengthening techniques such as: ease of construction, ductility, and reduced material quantity. Limited cases of strengthening concrete bridge elements using UHPC are available in the literature. Also, predicting the behavior of composite CC-UHPC sections in flexure and shear is challenging due to the significant differences in the performance of both materials in tension and compression. The objective of this research is to develop flexure and shear prediction models of strengthened composite CC-UHPC beams. The flexure prediction model is based on strain compatibility, while shear prediction model is based on effective strain. The interface shear resistance between the two materials is also predicted to design the shear connectors between the CC beam and UHPC encasement. A non-proprietary UHPC mix is used, and its mechanical properties are evaluated. Three non-prestressed concrete beams were tested in flexure: one CC reference beam, and two beams strengthened in flexure using UHPC and different reinforcement ratios. Another three non-prestressed concrete beams were tested in shear: one CC reference beam, and two beams strengthened in shear using UHPC with different thickness. Test results were used to validate the prediction models and showed that the strengthened beams achieved their predicted strength.

DEDICATION

To my parents who made everything possible for me,
My Sister, and her lovely family (Marco, Marly, and Julia)

ACKNOWLEDGMENTS

First, I would like to express my gratitude to my advisor Dr. George Morcoux for his support, insights, and encouragement during my doctoral study. I consider myself to be very lucky to have him as my mentor during this journey. I cannot thank him enough for all what he did for me starting from giving me the opportunity to continue my doctoral research, and throughout all the journey until this dissertation was made possible.

I would also like to express my great appreciation to my advisory committee: Dr. Ece Erdogmus, Dr. Philip Barutha, and Dr. Richard Wood for serving in my committee and for their invaluable guidance and input on this research.

I would like to thank Dr. Mourad M. Bakhoun for encouraging me to continue my doctoral studies in the United States. I would not have taken the step to work on my doctoral studies in the University of Nebraska without his encouragement.

I wish to thank my fellow graduate student Soumitra Das for his help during the experimental testing and the production of UHPC. I also want to thank my friends in Omaha, Nebraska who made my life significantly easier and bearable: Micheal Asaad, Ramez Mina, and Mostafa Abo El-Khier. Also, I want to thank the lab manager Peter Hilsabeck, and lab technicians: Jose Lopez and Carlos Francis for their help during the experimental work.

This journey would not have been possible without the support of my parents for me to continue my research journey abroad. Their endless love and encouragement helped me overcome all negative feeling of loneliness and homesickness. I do not think I would have accomplished anything in my life without their support and prayers.

Table of Contents

List of Figures.....	v
List of Tables	xiii
Chapter 1 - Introduction	1
1.1 Background.....	1
1.2 Problem Statement.....	4
1.3 Objective and Scope	6
1.4 Dissertation Organization	6
Chapter 2 – Literature Review	8
2.1 Current Practices of Repair and Strengthening of CC Beams	8
2.1.1 Reinforced Concrete Encasement	8
2.1.2 FRP Wrapping	9
2.1.3 External Post-Tensioning.....	11
2.1.4 Steel Encasement	12
2.2 Current Practices of using UHPC in Repair and Strengthening.....	13
2.2.1 Encasement of Steel Bridge Girder Ends.....	13
2.2.2 Encasement of Columns	15
2.2.3 Deck Slab Overlays.....	19
2.2.4 UHPC Shotcrete.....	21
2.3 Flexural Strength of UHPC.....	21
2.3.1 Flexural Strength Prediction Models of UHPC Beams	21
2.3.2 Test Data of UHPC Beams in Flexure	24
2.3.3 Test Data of CC-UHPC Beams in Flexure	30
2.4 Shear Strength of UHPC	37
2.4.1 Shear Strength Prediction Models of UHPC Beams	37

2.4.2	Test Data of UHPC Beams in Shear	45
2.4.3	Test Data of CC-UHPC Beams in Shear	61
Chapter 3 – UHPC Material Characterization		70
3.1	Mix Design	70
3.2	Compressive Properties	72
3.2.1	Idealized Material Models	72
3.2.2	Compressive Strength Testing	75
3.2.3	Modulus of Elasticity Testing	78
3.3	Tensile Properties.....	79
3.3.1	Idealized Material Models	79
3.3.2	Direct Tension Testing.....	82
3.3.3	Indirect Tension Testing	84
3.3.4	Inverse Analysis.....	87
Chapter 4 – Flexural and Shear Strength of UHPC Beams.....		94
4.1	Flexural Strength of UHPC Beams.....	94
4.1.1	Analysis of UHPC Beams Flexure Test Data	94
4.1.2	Parameters Affecting Flexural Strength Prediction	100
4.1.3	Flexural Testing of a Ribbed UHPC Slab.....	102
4.2	Shear Strength of UHPC Beams.....	104
4.2.1	Analysis of UHPC Beams Shear Test Data	105
4.2.2	Parameters Affecting Shear Strength Prediction	112
Chapter 5 – Flexural Strengthening using UHPC		119
5.1	Construction Procedure and Design.....	119
5.1.1	Flexural Strengthening Procedure using UHPC	119
5.1.2	Development of Prediction Model of CC-UHPC Beams in Flexure	122

5.1.3	Interface Design for Flexural Strengthening.....	127
5.2	Flexural Testing of CC-UHPC Beams.....	129
5.2.1	Specimen Design	129
5.2.2	Fabrication	133
5.2.3	Strengthening Procedure.....	135
5.2.4	Test Results.....	139
5.2.5	Validation of The Prediction Model	148
Chapter 6	– Shear Strengthening using UHPC.....	151
6.1	Construction Procedure and Design.....	151
6.1.1	Shear Strengthening Procedure using UHPC	151
6.1.2	Development of Prediction Model of CC-UHPC Beams in Flexure	153
6.1.3	Interface Design for Shear Strengthening.....	159
6.2	Shear Testing of CC-UHPC Beams	159
6.2.1	Specimen Design	160
6.2.2	Fabrication	162
6.2.3	Strengthening Procedure.....	163
6.2.4	Test Results.....	169
6.2.5	Validation of The Prediction Model of CC-UHPC Beams in Shear	181
Chapter 7	– Design Examples	185
7.1	Flexure Design Example of a CC-UHPC Beam.....	185
7.2	Shear Design Example of a CC-UHPC Beam.....	187
Chapter 8	– Summary, Conclusions, and Recommendations.....	196
8.1	Summary	196
8.1.1	Flexure Strengthening of Conventional Concrete Beams.....	196
8.1.2	Shear Strengthening of Conventional Concrete Beams.....	197

8.1.3 Design Examples	197
8.2 Conclusions	198
8.3 Recommendations	200
References	201
Appendix	210

List of Figures

Figure 1: Deteriorated bridge girder end, Platte River South Bridge, courtesy of Nebraska Department of Transportation, Kodsy et al., 2020.....	1
Figure 2: Stress-strain behavior of CC and UHPC in compression, courtesy of El-Helou et al., 2019.....	5
Figure 3: Stress-strain behavior of CC and UHPC in tension, courtesy of El-Helou et al., 2019.....	5
Figure 4: Reinforced concrete encasement of a deteriorated bridge girder end, courtesy of MN/RC 2018-07 Report	9
Figure 5: FRP Wrapped Repair, courtesy of Iowa Dot, 2014.....	11
Figure 6: External post-tensioning end block, courtesy of Alberta Infrastructure and.....	12
Figure 7: Grouted steel encasement of a bridge girder, courtesy of Iowa Dot, 2014	13
Figure 8: Shear studs and additional reinforcement at the UHPC encasement, courtesy of Fan, 2020.....	14
Figure 9: Pouring UHPC from the top of a concrete bridge deck using pipes for strengthening a steel bridge girder, courtesy of Fan, 2020	15
Figure 10: Strengthened girder end after stripping the forms, courtesy of Fan, 2020.....	15
Figure 11: Casting UHPC using a chute for a thin jacket for a bridge pier from the top of formwork, courtesy from Ductal website and Doiron, 2017	16
Figure 12: UHPC jacket over the bridge pier, courtesy of Doiron, 2017	17
Figure 13: Casting a 9-inch thick UHPC jacket around a bridge pier using a hopper, courtesy of Doiron, 2017	18
Figure 14: Seismic strengthening with UHPC jackets around bridge piers, courtesy of Doiron, 2017	18
Figure 15: Precast UHPC column encasement, courtesy of Ductal website	19
Figure 16: Placing UHPC deck overlay, Mud Creek Bridge, Iowa, Wibowo et al., 2018	20
Figure 17: Pumping UHPC to repair the Caderousse Dam slab, courtesy of Guingot et al., 2013.....	20
Figure 18: UHPC shotcrete to strengthen and renovate a deteriorated metal culvert, courtesy of Ductal website.....	21

Figure 19: Strain and stress distribution in a UHPC beam cross section, courtesy of Bae et al., 2016.....	22
Figure 20: Material models combinations and stress blocks used for flexural strength prediction, courtesy of Bae et al., 2016	23
Figure 21: Schematic of the moment-curvature of non-prestressed UHPC components .	24
Figure 22: Beam cross-section parameters and test setup	25
Figure 23: Cross-sections of the beams used in the 12 experimental programs (dimensions in inches).....	25
Figure 24: Frequency distribution of the number of the tension reinforcement ratio in the test data	29
Figure 25: Measured flexural resistance factor versus tension reinforcement ratio of each experimental program in the test data.....	29
Figure 26: Tested specimens, courtesy of Safdar et al., 2016.....	30
Figure 27: Cantilever test setup specimens, courtesy of Noshiravani, and Bruhwiler, 2013	31
Figure 28: Four-point bending test setup and control beam cross-section, courtesy of Prem et al., 2016.....	33
Figure 29: Four-point bending test setup, courtesy of Yin et al., 2017	34
Figure 30: Four mechanisms of vertical shear transfer in concrete beams, courtesy of Abad et al., 2019.....	37
Figure 31: Tensile stresses carried by steel fibers in a general beam section according to the Modified Compression Field Theory, Crane, 2010	42
Figure 32: Girder cross-sections of the considered sixteen experimental programs, dimensions in inches	48
Figure 33: Shear failure mode, courtesy of Hegger et al., 2004	48
Figure 34: Girder cross-section (left), shear failure mode (right), courtesy of Voo et al., 2006.....	49
Figure 35: Girder cross-section (left), shear failure mode (right), courtesy of Graybeal, 2006.....	50
Figure 36: Girder cross-section, courtesy of Hegger and Bertram, 2008	51
Figure 37: Shear failure mode, courtesy of Graybeal, 2009	52

Figure 38: Girder cross-section (left), shear failure mode (right), courtesy of Wipf et al., 2009.....	53
Figure 39: Non-prestressed girder cross-section (left), prestressed girder cross-section (right), courtesy of Baby, et al., 2010	54
Figure 40: Girder cross-section (left), shear failure mode (right), courtesy of Crane, 2010	55
Figure 41: Shear test setup (left), beam cross-sections (right), courtesy of Fehling et al., 2012.....	55
Figure 42: Shear failure mode, courtesy of Fehling et al., 2012.....	56
Figure 43: Shear test setup (left), beam cross-section (right), courtesy of Ridha, et al., 2018	57
Figure 44: Three-point bending test of a strengthened beam, courtesy of Aghani et al., 2016	61
Figure 45: Tested specimens, (a) Control Beam, (b) BOT SJ, (c) 2 SJ, (d) 3SJ, courtesy of Al-Osta et al., 2016	63
Figure 46: Four-point bending test setup, courtesy of Bahraq et al., 2019.....	64
Figure 47: Four-point bending test setup, courtesy of Sakr et al., 2019.....	66
Figure 48: Beam strengthening schemes, courtesy of Sakr et al., 2019	66
Figure 49: Particle Size Gradations of Powders	71
Figure 50: Particle Size Gradation of Sand.....	71
Figure 51: UHPC compression model according to El-Helou et al., 2019 and AFGC, 2013	73
Figure 52: UHPC compression model according to Haber et al., 2018.....	74
Figure 53: Accelerated curing procedure and equipment	75
Figure 54: End grinding of UHPC cylinders (left), failed cylinder after compressive strength testing (right).....	76
Figure 55: Resulting spread of 8-inches	76
Figure 56: Average compressive strength of moist-cured UHPC cylinders at different ages	77
Figure 57: Average 4-day compressive strength of UHPC cylinders and cubes using different curing methods	78

Figure 58: Extensometer cage installed on a UHPC cylinder for the modulus of elasticity testing.....	79
Figure 59: UHPC simplified tension model according to AFGC, 2013 and El-Helou et al., 2019.....	80
Figure 60: UHPC strain-hardening tension model according to of AFGC, 2013 and Yoo et al., 2016.....	81
Figure 61: UHPC strain-softening tension model according to Qi et al., 2018 and Bae et al., 2016.....	82
Figure 62: Stress-strain behavior of UHPC in tension, courtesy of Graybeal et al., 2013	84
Figure 63: Flexural testing of UHPC prism.....	85
Figure 64: Stress-deflection plot of the UHPC prisms tested at 4 days of age.....	85
Figure 65: Stress-deflection plot of the UHPC prisms tested at 14 days of age.....	86
Figure 66: Stress-deflection plot of the UHPC prisms tested at 28 days of age.....	86
Figure 67: Tested prisms after failure at 4 days (top left), 14 days (top right), and 28 days (bottom).....	87
Figure 68: Assumed stress and strain profiles at the measured peak flexural stress, SIA 2052, 2016 (not to scale).....	88
Figure 69: Stress and strain profiles at the measured peak flexural stress, method 2 of inverse analysis.....	90
Figure 70: Stress and strain profiles at the measured peak flexural stress, method 3 of inverse analysis.....	91
Figure 71: Stress and strain profiles at the measured peak flexural stress, method 4 of inverse analysis.....	93
Figure 72: Moment-curvature plot of flexure test results of two specimens and the prediction provided by different inverse analysis methods.....	93
Figure 73: Strain and stress profiles of the prediction models at curvatures Φ_p and Φ_u : a) CC Model; b) Model A2 at curvature Φ_p ; c) Model A2 at curvature Φ_u ; d) Model B2 at curvature Φ_p ; e) Model B2 at curvature Φ_u ; f) Model C1 at curvature Φ_p ; g) Model C1 at curvature Φ_u (not to scale).....	96
Figure 74: Measured versus predicted flexural resistance using CC and A1 models at curvature Φ_p	97

Figure 75: Measured versus predicted flexural resistance using Model A1 at curvatures Φ_p and Φ_u	97
Figure 76: Measured versus predicted flexural resistance using Models A1 and A2 at curvature Φ_p	98
Figure 77: Measured versus predicted flexural resistance using Models A1, B1, and C1 at curvature Φ_p	99
Figure 78: Measured versus predicted flexural resistance using Models A1 and A1M at curvature Φ_p	99
Figure 79: Measured-to-predicted flexural resistance factors versus design parameters: . a) ρ ; b) ft ; c) $f'c$; and d) Vf	101
Figure 80: Ribbed slab dimensions and reinforcement	102
Figure 81: Test setup of the ribbed slab	103
Figure 82: Moment-deflection plot of the flexure test of the ribbed slab	104
Figure 83: Flexure failure mode in the ribbed slab	104
Figure 84: Measured versus predicted shear strength according to RILEM TC 162-TDF, 2003	107
Figure 85: Measured versus predicted shear strength according to the <i>fib</i> Model Code, 2010	108
Figure 86: Measured versus predicted shear strength according to French Standard NF P 18-710, 2016	109
Figure 87: Measured versus predicted shear strength according to PCI-UHPC Structures Design Guide, 2021	110
Figure 88: Measured versus predicted shear strength according to Draft of AASHTO Guide Specification for Structural Design with UHPC, 2021	111
Figure 89: Effect of key parameters on shear strength of prestressed UHPC beams	114
Figure 90: Effect of the level of prestressing ($6cp$) on the shear strength for prestressed beam with $Vf \geq 2.0\%$	115
Figure 91: Effect of key parameters on shear strength of non-prestressed UHPC beams	117
Figure 92: Effect of the longitudinal reinforcement ratio (Al/bwd) on the shear strength of non-prestressed UHPC beams with $Vf \geq 2.0\%$	118

Figure 93: General technique of using UHPC encasement for flexural strengthening of an existing CC beam.....	120
Figure 94: Schematic of possible failure modes in a CC beam strengthened with UHPC	123
Figure 95: Bases of analysis of the proposed CC-UHPC flexure strength prediction model	125
Figure 96: Cross-sections of the strengthened beams in flexure, reference beam (left), strengthened beam #1 (middle), and strengthened beam #2 (right).....	130
Figure 97: Schematic of the flexural test setup of a CC-UHPC beam.....	130
Figure 98: Predicted moment-curvature relationship of the reference and flexural strengthened beams	131
Figure 99: Double shear test setup of headed stud anchors in UHPC (left), anchor dimensions (right), courtesy of Cao et al., 2017	132
Figure 100: Formwork and reinforcement of one of the CC beams	134
Figure 101: Stripping formwork of two CC beams	134
Figure 102: Flexural strengthening procedure, step 1: roughening of the interface	135
Figure 103: Flexural strengthening procedure, step 2: installing anchors	136
Figure 104: Flexural strengthening procedure, step 3: installing additional reinforcement	136
Figure 105: Flexural strengthening procedure, step 4: assembling formwork	137
Figure 106: Flexural strengthening procedure, step 5: installing formwork	138
Figure 107: Flexural strengthening procedure, step 6: pouring UHPC	139
Figure 108: Reference beam test setup and instrumentation	140
Figure 109: Reference beam moment-deflection plot	140
Figure 110: Reference beam failure mode.....	141
Figure 111: Strengthened beam #1 test setup and instrumentation	142
Figure 112: measuring relative displacement between CC and UHPC in strengthened beam #1.....	142
Figure 113: Strengthened beam #1 moment-deflection plot.....	143
Figure 114: Strengthened beam #1 failure mode.....	144

Figure 115: Strengthened beam #1 failure mode, slippage of CC tension reinforcement	144
Figure 116: Strengthened beam #1 relative end displacements between CC and UHPC	145
Figure 117: Strengthened beam #2 failure mode	146
Figure 118: Strengthened beam #2 failure mode, CC tension reinforcement slippage ..	146
Figure 119: Strengthened beam #2 moment-deflection plot.....	147
Figure 120: Strengthened beam #2 relative end displacement between CC and UHPC	147
Figure 121: Moment versus measured extreme compressive strain	148
Figure 122: Moment-deflection results of the reference and two strengthened beams ..	149
Figure 123: Measured versus predicted moment-curvature relationship of the three tested beams in flexure	150
Figure 124: General technique of using 2 UHPC side layers at the web area for shear strengthening of an existing CC bridge girder	152
Figure 125: Principal strains at the diagonal tension cracking used to develop the MCFT for CC, courtesy of Bentz et al., 2006.....	157
Figure 126: Typical slip fields depending on critical shear crack, courtesy of Lu et al., 2009	157
Figure 127: Schematic of different crack angles at the existing girder and UHPC	158
Figure 128: Cross-sections of the strengthened beams in shear, reference beam (left), strengthened beam #1 (middle), and strengthened beam #2 (right).....	160
Figure 129: Schematic of two shear tests setup of a CC-UHPC beam, test #1 (top), and test #2 (bottom).....	161
Figure 130: Formwork and reinforcement of two CC beams	163
Figure 131: Stripping formwork of two CC beams	163
Figure 132: Shear strengthening procedure, steps 1 and 2: roughening of the interface and installing anchors	164
Figure 133: Shear strengthening procedure, step 3: drilling top flange openings	165
Figure 134: Shear strengthening procedure, step 4: installing formwork.....	166
Figure 135: Shear strengthening procedure, step 5 (left): fixing formwork, step 6 (right): pouring UHPC	167
Figure 136: Poor consolidation in strengthened beam #1	168

Figure 137: Poor consolidation in strengthened beam #2.....	168
Figure 138: Casting UHPC at the poorly consolidated locations in strengthened beam #2	168
Figure 139: Reference beam test setup and instrumentation	169
Figure 140: Reference beam load-deflection plot.....	170
Figure 141: Reference beam failure mode.....	170
Figure 142: Strengthened beam #1 – test #1, test setup and instrumentation.....	171
Figure 143: Measuring relative displacement between CC and UHPC in strengthened beam #1 – test #1	172
Figure 144: Strengthened beam #1 load-deflection plot for tests #1 and #2	173
Figure 145: Strengthened beam #1 – test #1 failure mode	173
Figure 146: Strengthened beam #1 – test #1 bar slippage in the CC beam	174
Figure 147: Strengthened beam #1 – test #2 failure mode and bar slippage in the CC beam	174
Figure 148: Strengthened beam #1 relative end displacements for tests #1 and #2	175
Figure 149: Strengthened beam #2 – test #1, test setup and failure mode.....	176
Figure 150: Strengthened beam #2 – test #2, test setup and failure mode.....	176
Figure 151: Strengthened beam #2 load-deflection plot for tests #1 and #2	177
Figure 152: Strengthened beam #2 relative end displacements for tests #1 and #2	177
Figure 153: Measured compressive strains.....	178
Figure 154: Measured tensile strains	179
Figure 155: Measured horizontal strains.....	180
Figure 156: Measured vertical strains.....	181
Figure 157: Load-deflection results of the shear testing done on the reference and two strengthened beams.....	182
Figure 158: UHPC contribution to the measured shear strength	184
Figure 159: Cross-section of the original (left) and strengthened (right) girders	185
Figure 160: Un-factored flexural strength of the original and strengthened girders	186
Figure 161: Factored flexural strength of the original and strengthened girders.....	186
Figure 162: Shear strengthening of the reference girder (left), CFRP strengthened girder (middle), and UHPC strengthened girder (right)	187

List of Tables

Table 1: Cases of using UHPC as a strengthening/repair material	3
Table 2: Summary of test data	27
Table 3: Summary of tested specimens and failure modes, Safdar et al., 2016.....	31
Table 4: Summary of tested specimens and failure load, Noshiravani, and Bruhwiler, 2013	32
Table 5: Summary of tested specimens and failure load, Prem et al., 2016	33
Table 6: Summary of tested specimens and failure load, Yin et al., 2017.....	35
Table 7: Summary of previous testing done on strengthened beams in flexure using UHPC	36
Table 8: Shear experiments review on prestressed UHPC beams	58
Table 9: Shear experiments review on non-prestressed UHPC beams.....	60
Table 10: Summary of tested specimens and failure modes, Aghani et al., 2016	62
Table 11: Summary of tested specimens and failure modes, Al-Osta et al., 2016	63
Table 12: Summary of tested specimens and failure load, Bahraq et al., 2019	65
Table 13: Summary of tested specimens and failure load, Sakr et al., 2019	66
Table 14: Summary of previous testing done on strengthening conventional concrete beams using UHPC jackets in shear.....	68
Table 15: Calculating UHPC contribution to the shear strength	69
Table 16: UHPC mix design constituents.....	70
Table 17: Compressive strength UNL UHPC 1900 cylinders and cubes at different age and curing conditions.....	77
Table 18: Modulus of elasticity test results (ksi) of three UHPC cylinders	79
Table 19: Prediction model combinations	95
Table 20: Summary of the evaluation of the prediction models.....	100
Table 21: Three-point bending tests on notched prisms to evaluate residual tensile strength	106
Table 22: Summary of evaluation of prediction models.....	112
Table 23: Cohesion and friction factors recommended for different CC surface conditions	128

Table 24: Summary of test specimens and predicted capacity	131
Table 25: CC mix design constituents	133
Table 26: Measured versus predicted flexural strength of the tested beams in flexure ..	150
Table 27: Summary of test specimens and predicted capacity	161
Table 28: Measured versus predicted load capacities of the tested beams in shear	183

Chapter 1 - Introduction

1.1 Background

Structural engineers are often faced with the challenge of required repair and strengthening projects for the ever-deteriorating concrete members in buildings and bridges. Strengthening projects are typically required when the structure use is modified, requiring certain elements to have higher load-carrying capacity. While, repair projects are typically required at the incidents of deterioration, or incidental damage (i.e., impact damage) causing section loss in concrete or reinforcement. Currently 42% of bridges in the United States bridges are at least 50 years old, and 46,154 of the nation's bridges are considered structurally deficient and require repair and strengthening, Infrastructure Report Card, 2021. Figure 1 shows an example of a deteriorated concrete bridge girder end. The deterioration was accelerated due to leaking joints on the concrete deck which led to the corrosion of prestressing strands and bearing assemblies and the bridge required immediate repairs.



Figure 1: Deteriorated bridge girder end, Platte River South Bridge, courtesy of Nebraska Department of Transportation, Kodsy et al., 2020

Recently, there are several repair and strengthening techniques using Ultra-High-Performance Concrete (UHPC) that have been documented by several agencies in the United States and other countries. The Federal Highway Administration (FHWA) has been leading efforts in the past two years to encourage the use of UHPC in bridge preservation, FHWA-HRT-21-002, 2021. An interactive map has been created and frequently updated by FHWA to show the cases of using UHPC in bridge preservation in the United States.

UHPC is a relatively newly developed material and its use in the reinforced concrete construction industry has been growing rapidly in the past two decades, which entitled it to be titled as a “Game Changer”, Binard, 2017. FHWA defines UHPC as: “A cementitious composite material composed of an optimized gradation of granular constituents, a water-to-cementitious materials ratio less than 0.25, and a high percentage of discontinuous internal fiber reinforcement. The mechanical properties include compressive strength greater than 21.7 ksi and sustained post-cracking tensile strength greater than 0.72 ksi”, Haber et al., 2018. The presence of fibers in UHPC enhances all tension-driven failure modes, especially shear strength which helps eliminate transverse reinforcement in beams and bridge girders.

One of the major challenges facing the growth of using UHPC is that it is a relatively new developed material compared to other cementitious materials. Limited cases of using UHPC in the repair and strengthening of conventional concrete elements have been reported. No cases of strengthening concrete beams have been reported to date. Table 1 shows some of the reported cases with the requirement for repair or strengthening and the advantages offered by UHPC compared to other options.

Table 1: Cases of using UHPC as a strengthening/repair material

Case	Requirement for Repair or Strengthening	Advantages offered by UHPC	Reference
Caderousse Dam's slab, 2010	Impact damage from heavy rocks	High impact and abrasion resistance. And high early-age compressive strength	Guingot et al., 2013
Rail Bridge Pier Jacketing, Montreal, 2013	Spalling and deterioration	Jacket thickness was minimized compared to other options, maintaining adequate road clearances	Doiron, 2017
Mission Bridge Piers Seismic Retrofit, 2014	Foundations in a high seismic zone and highly liquefiable soil	UHPC ductility would allow for high deformation capacity	Doiron, 2017
Encasement of Bent Legs, 2015	Local corrosion at steel bent legs. Increase load capacity	Better mechanical properties than other options minimizing the required encasement area	Doiron, 2017
Steel Bridge Girder, Zemtra, 2015	Corrosion damage	UHPC end-block increased shear and bearing resistance	Zemtra, 2015
Mud Creek Bridge Deck Overlay, Iowa, 2016	Cracking and spalling	High resistance to cracking and spalling, decrease water penetration, increasing deck rigidity, and girder flexural strength	Wibowo et al., 2018
Concrete bridge girder, 2016	Poorly consolidated closure pour	High bond strength with steel reinforcement and existing concrete. Highly flowable and self-consolidating for the congested area.	Haber et al., 2019
Ductal Shotcrete for Renovating a Metal Culvert	Deterioration	Minimizing jacket thickness (1.2 in.) and the reduction of the culvert cross-section	Ductal Website, 2020
Precast Column Jacket	Additional load from 2 extra stories	Minimizing jacket thickness	Ductal Website, 2021
Steel Bridge End Repair	Corrosion Damage	Provide 15-20 Years Additional Service Life	Fan, 2020

Using UHPC as a repair and strengthening material can offer several benefits than the other techniques such as:

1. Very low permeability, which increases durability and service life of the repaired/strengthened section, and will have higher resistance to further damage/vandalism of the element
2. Less sensitive to base concrete surface preparation than FRP wrapping
3. Can replace patching materials in restoring the loss in a concrete section (patching is required to be done prior to FRP wrapping)
4. High tension and shear resistance that can eliminate the need for additional transverse reinforcement
5. Increased bond strength to base concrete and reinforcement
6. Highly flowable and self-consolidating for congested areas
7. Smaller increase in section dimensions compared to CC jacketing

1.2 Problem Statement

The significant difference in mechanical properties between UHPC and CC causes the prediction of behavior of a composite CC-UHPC element to be complicated. Figure 2 shows an example of the compressive stress-strain behavior of CC (having compressive strength of 5 ksi) and UHPC (having compressive strength of 21.7 ksi). It can be noticed that the elastic modulus of UHPC is significantly higher than CC, causing it to attract more stresses than CC at any given strain. Figure 3 shows an example of the tensile stress-strain behavior, where the sustained post-cracking tensile strength of UHPC continues to a strain value of 0.01 and even larger. Under tensile stresses, CC will always crack earlier than UHPC and lose all tensile stress carrying capacity.

There are currently no prediction models describing the behavior or design of a composite section of CC beams or bridge girders repaired or strengthened using UHPC.

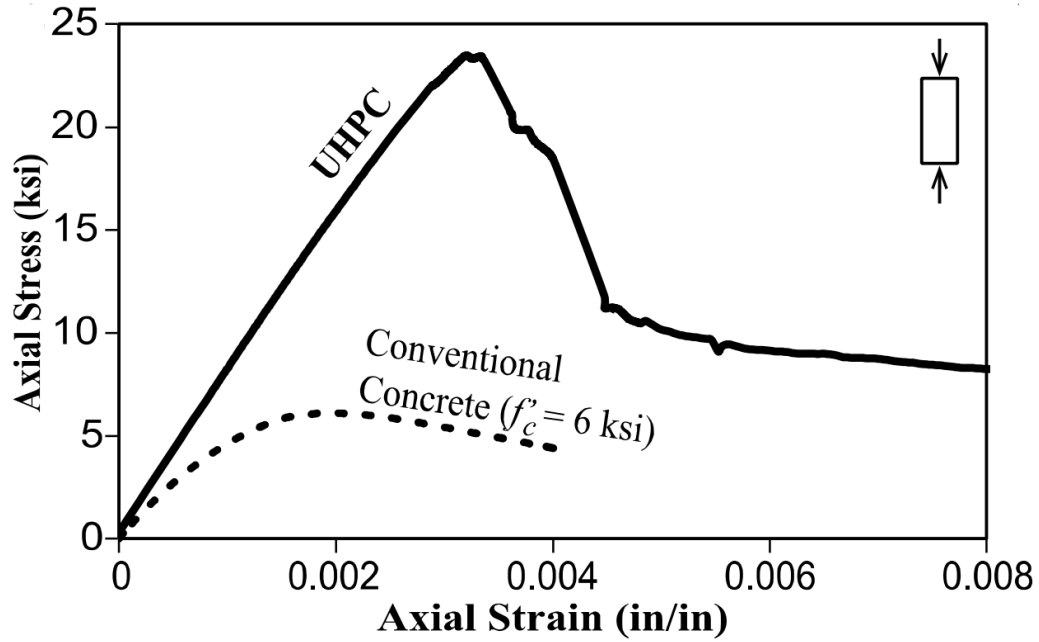


Figure 2: Stress-strain behavior of CC and UHPC in compression, courtesy of El-Helou et al., 2019

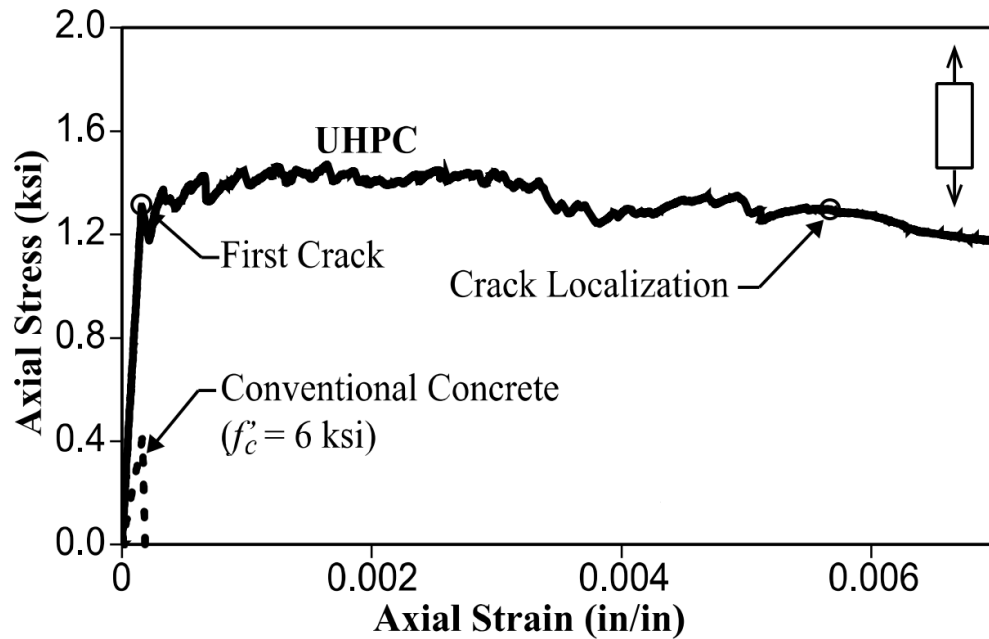


Figure 3: Stress-strain behavior of CC and UHPC in tension, courtesy of El-Helou et al., 2019

1.3 Objective and Scope

The main objective of this research is to develop prediction models for the shear and flexural strength of conventional concrete bridge components repaired or strengthened using UHPC. To achieve these objectives the following tasks needed to be performed:

1. Literature review of UHPC prediction models in flexure and shear.
2. Literature review of CC-UHPC test data in flexure and shear.
3. Evaluation of the existing prediction models of UHPC in flexure and shear using test data.
4. Develop prediction models of CC-UHPC composite sections in flexure and shear.
5. Validate the developed prediction models via experimental investigation.

The developed prediction models can be used for prestressed and non-prestressed concrete bridge components. However, the experimental investigation is limited to non-prestressed concrete components.

1.4 Dissertation Organization

The dissertation is organized into six chapters as follows:

Chapter 1: Background information, problem statement, objective, and organization of the dissertation.

Chapter 2: Literature review on the flexural and shear strength of UHPC, and CC-UHPC beams. Prediction models of UHPC beams are reviewed, then the test data of UHPC, and CC-UHPC beams are presented.

Chapter 3: UHPC Material Characterization. This chapter discusses the mix design and mechanical properties of UHPC in tension and compression which are used in the prediction models of UHPC and CC-UHPC components in flexure and shear.

Chapter 4: Flexural and Shear Strength of UHPC Beams. The chapter presents the work done on analyzing flexural and shear test data of UHPC beams collected from the literature. The parameters affecting flexural and shear strength of UHPC beams are also analyzed. Flexure testing of a ribbed UHPC slab is also presented to validate the analysis of flexural strength prediction models of UHPC beams.

Chapter 5: Flexural strengthening using UHPC. This chapter presents the proposed concept of using UHPC in flexural strengthening techniques and utilizing its advantages. The implementation of flexural strengthening techniques in actual projects is presented in the form of construction procedures for a beam example. Then, the design process of a composite (strengthened) CC-UHPC is presented in the form of developing the flexural strength prediction model. Flexure testing of CC-UHPC beams is also presented to validate the prediction of the developed model.

Chapter 6: Shear strengthening using UHPC. This chapter presents the proposed concept of using UHPC in shear strengthening techniques and utilizing its advantages. The implementation of shear strengthening techniques in actual projects is presented in the form of construction procedures for a beam example. Then, the design process of a composite (strengthened) CC-UHPC is presented in the form of developing the shear strength prediction model. Shear testing of CC-UHPC beams is also presented to validate the prediction of the developed model.

Chapter 7: Design examples on flexural and shear strengthening of conventional concrete members using UHPC. The design examples aim to show the calculation procedure of the developed prediction models of CC-UHPC members, and to show the capabilities of UHPC in these strengthening applications.

Chapter 8: Summary, conclusions, and Recommendations: the summary and benefits obtained from this research are presented, as well as recommendations for strengthening procedures and future research work are given.

Chapter 2 – Literature Review

This chapter presents a review of the current practices used in the repair and strengthening of conventional concrete beams, and the practices of using UHPC in repair and strengthening in general. Flexural and shear strength of UHPC beams are also reviewed with respect to the prediction models and test data of UHPC and composite CC-UHPC beams. The work presented in this chapter has been used as the reference to the proposed the prediction models of composite CC-UHPC beams.

2.1 Current Practices of Repair and Strengthening of CC Beams

This section provides an overview of the current repair practices and the advantages and disadvantages and what UHPC can offer as an alternative technique when used.

2.1.1 Reinforced Concrete Encasement

One of the commonly used techniques is to encase the element that requires strengthening in reinforced concrete. The encasement can be done from one side, two sides, U-wrap, full-wrap around the sides of the element. Casting a concrete end-block encasement is a common technique used in the repair and strengthening of deteriorated bridge girders, especially in Nebraska, Kody et al., 2020. The challenges that can be often accompanied with this technique is the significant increase in dimensions and weight of the member. In addition, there are several cases indicating that if the existing element is suffering from environmental deterioration, then the service life of the repair will be significantly shortened. Two cases of bridge girders suffered from extensive spalls in the concrete encasement in less than five years. The first case is documented in MN/RC 2018-07 Report, where the bridge girder was suffering from leaking expansion joints and the original cause of deterioration was not addressed before the concrete encasement was performed by shotcrete as shown in Figure 4. The encasement suffered major spalling in less than five years and the entire bridge had to be replaced. The second case occurred in Kearney South Platte River Bridge, Nebraska discussed in section 1.1 and Figure 1.

According to Tabatabai et al., 2004, reinforced concrete encasement do not typically retard chloride-induced corrosion in severe environments. This technique type of repair and

strengthening will typically fail prematurely if no measures are taken to mitigate the primary source of deterioration. In addition, since the newly placed concrete consists of minimal to no concentration of chlorides, a reverse chloride gradient is created between the patch repair and the existing concrete.



Figure 4: Reinforced concrete encasement of a deteriorated bridge girder end, courtesy of MN/RC 2018-07 Report

The major advantage that can be offered by UHPC compared to this technique is that UHPC porosity is much smaller than CC causing it to be practically impervious compared to CC. UHPC shall act as a moisture barrier against environmental attack which will increase the service life of the encasement significantly. UHPC also can reduce the dimensions of the encasement significantly, as well as eliminate the need for additional reinforcement in shear. The enhanced ductility of UHPC can also be a major advantage in axially loaded elements in seismic zones.

2.1.2 FRP Wrapping

Another commonly effective strengthening technique is wrapping the element with FRP sheets or laminates. This method is effective structurally in flexure and shear and can also protect against future corrosion damage by acting as a water barrier. Figure 5 shows an

example of an FRP U-shaped wrap repair and strengthening for a prestressed concrete girder in flexure. The ACI 440.2R-17 provides structural calculations for externally bonded FRP systems for the strengthening of concrete structures. When the FRP wrap is required to increase flexural resistance only of a section, FRP plies can be glued to the soffit of the girder. Strain in FRP reinforcement will be limited to the de-bonding limit, which can reduce the utilization of the FRP material. Different anchorage systems are provided in the ACI 440.2R-17. Anchoring the FRP layers can increase the effective strain up to its tensile rupture, which can significantly increase the strengthening effect of the FRP system. The FRP wraps can also be prestressed to optimize the use of both the existing element capacity and FRP materials.

The major disadvantage that can be accompanied by this technique is the possibility for debonding from the existing element when subjected to environmental attack or vandalism. Another major disadvantage is the high sensitivity to the existing surface preparation and that it requires skillful labor for its application.

UHPC can offer several advantages when compared to that technique such as significantly increased ductility and that it is less sensitive to existing surface preparation. The increased toughness of the material makes it also less sensitive to environmental attack and vandalism. The bonding properties of UHPC to CC are also superior than most of the other repair and strengthening materials which reduces the possibility of debonding. In addition, since UHPC is a cementitious material, it is more compatible to be used with CC in terms of coefficient of thermal expansion.



Figure 5: FRP Wrapped Repair, courtesy of Iowa Dot, 2014

2.1.3 External Post-Tensioning

This technique is considered to be most efficient when it comes to utilizing the existing and strengthening materials. However, the applicability of this technique is limited by the residual capacity of the un-strengthened beam which must safely resist any expected nominal load. According to Iowa DOT., 2014 the addition of external post-tensioning should be considered a temporary repair or strengthening even if the element removal is required. Another major disadvantage is that the strengthening materials requires environmental protection against external attacks and vandalism. Figure 6 shows an example of that technique, where an end block is casted and anchored to the existing beam, then the external post-tensioning steel is tensioned to apply an external compression force on the existing element.

The main advantage offered by UHPC as an alternative strengthening material/technique is that it does not depend on the un-strengthened element capacity in the case of environmental attack or vandalism. The strengthened UHPC element does not require special considerations for its protection due to the increased toughness and ductility of the material. Additionally, the strengthened UHPC element can also be externally post-tensioned to optimize the use of UHPC and the existing element.



Figure 6: External post-tensioning end block, courtesy of Alberta Infrastructure and Transportation, 2005

2.1.4 Steel Encasement

This technique is the least common method to strengthen a bridge girder because of the increased material cost and weight, in addition to the special considerations that must be considered to connect both the existing element material and the additional steel plates. The steel encasement is typically anchored with concrete anchors into the existing element, and then the space between concrete and the inside of the steel encasement would be injected with epoxy to bond the two elements together. Figure 7 shows an example of steel encasement to an exterior bridge girder to serve as an armor to the bottom of the girder against repeated vehicular collision impacts.

The main advantage offered by UHPC as an alternative strengthening material/technique is that it is less sensitive to surface preparation and construction procedure. Additionally it is much less likely that the UHPC strengthening element detach from the existing beam than the steel sleeves.



Figure 7: Grouted steel encasement of a bridge girder, courtesy of Iowa Dot, 2014

2.2 Current Practices of using UHPC in Repair and Strengthening

This section presents a review of the reported practices of UHPC production and construction procedure used in repair and strengthening of structures. Several cases of using UHPC in structural repair and strengthening have been reported with different construction procedures. A repair or strengthening case is presented for each construction practice discussed in this section.

2.2.1 Encasement of Steel Bridge Girder Ends

Two cases have been reported of using UHPC as an end block encasement at deteriorated steel bridge girder ends by Fan, 2020 and Hain et al., 2021 in the states of Texas and Connecticut. Another case of using the same approach was tested by Zemtra, 2015, where the UHPC end block encasement showed promising results and provided an alternate load path at the bearing area rather than the deteriorated web.

The main objective of the project reported by Fan, 2020 was to provide additional service life of 15 to 20 years to the entire bridge. Bearing assemblies were repaired and a UHPC encasement was added at the deteriorated girder ends. The strengthening procedure on-site

started by sandblasting to remove unsound surfaces, paint, and rusted steel. The shear studs were welded on the interface area and additional reinforcement for the UHPC encasement was tied to it as shown in Figure 8. The next step was to install the formwork for the required strengthening area as shown in Figure 9 on the left. Then deck openings and plastic pipes were used to cast UHPC from the top of the concrete deck as shown in Figure 9 on the right. The production of UHPC on-site was done by having two mixers and the mixing process was done entirely on-site. The poured UHPC showed no consolidation issues as shown in Figure 10 and UHPC provided an alternate solid load path at the deteriorated girder end.

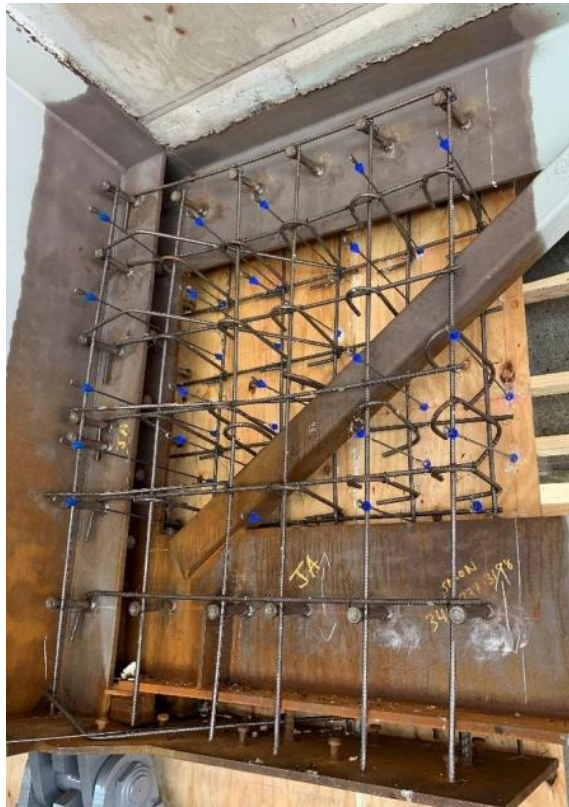


Figure 8: Shear studs and additional reinforcement at the UHPC encasement, courtesy of Fan, 2020



Figure 9: Pouring UHPC from the top of a concrete bridge deck using pipes for strengthening a steel bridge girder, courtesy of Fan, 2020



Figure 10: Strengthened girder end after stripping the forms, courtesy of Fan, 2020

2.2.2 Encasement of Columns

UHPC has been reported in several strengthening projects because of its superior mechanical properties, durability, and ductility compared to conventional encasement

materials. These superior properties enable the encasement dimensions to be minimized which can offer several advantages in tight areas. One case of adding a thin UHPC jacket over an impact damaged bridge pier is reported by Ductal website and Doiron, 2017 where UHPC was casted using a chute. The pier supported a railway bridge crossing over a 2-lane ramp and the lanes were narrow. The existing bridge pier showed some spalling and deterioration, and the selected strengthening method was adding a concrete jacket to protect against chloride ingress and freeze/thaw. The jacket thickness had to be optimized as possible in order to maintain adequate clearances, which lead to the choice of using UHPC. The deteriorated layer was removed, and a galvanized rebar cage was added. Afterwards, forms were installed to allow for a 4-inch-thick concrete jacket of UHPC. Top openings were made in the forms around the pier and UHPC was casted from the top of the bridge deck as shown in Figure 11. Figure 12 shows the final UHPC jacket over the damaged bridge pier. In addition to the top openings in the forms, intermediate openings were done to allow for mid-height UHPC pouring and better consolidation. This technique requires access from below the bridge and access to the top of the forms which might be challenging in some projects. However, the advantage offered by this technique is that no opening are needed to be drilled in the deck slab as in the previous technique of steel bridge girder ends.



Figure 11: Casting UHPC using a chute for a thin jacket for a bridge pier from the top of formwork, courtesy from Ductal website and Doiron, 2017



Figure 12: UHPC jacket over the bridge pier, courtesy of Doiron, 2017

Another case of column encasement was reported by Doiron, 2017 to cast a strengthening jacket for bridge columns subjected to significant seismic actions and the possibility of soil liquefaction. Two tapered, rectangular jackets with height of approximately 10.5 feet from the base were cast around the V-shaped concrete piers. Compared to other strengthening methods using traditional piles, a UHPC jacket provided significant cost savings, and allowed for a high seismic deformation capacity with a thin jacket. UHPC was placed using a conical shaped hopper to allow UHPC to be poured into tight places and small forms as shown in Figure 13. The main challenge facing this technique is the requirement for a clear access from the top of the forms, as well as crane access to the casting location. The main advantage offered by this technique is the minimized pouring time and required labor during casting.



Figure 13: Casting a 9-inch thick UHPC jacket around a bridge pier using a hopper, courtesy of Doiron, 2017



Figure 14: Seismic strengthening with UHPC jackets around bridge piers, courtesy of Doiron, 2017

Another case of using precast UHPC jacket components to strengthen concrete columns in a shopping center in the United Kingdom was reported by Ductal website. The building required redevelopment to add two more stories to its existing structure which required the columns on the ground floor to be strengthened. Two components of the jacket were installed against each other and were linked to the existing element by anchors along the height of the element as shown in Figure 15. The use of thin UHPC jackets resulted in minimized added dimensions for the existing columns, as well as significantly reduced installation time.



Figure 15: Precast UHPC column encasement, courtesy of Ductal website

2.2.3 Deck Slab Overlays

UHPC has been reported to be used as a structural overlay system for bridge decks to increase the resistance to cracking and spalling, decrease water penetration which significantly increases durability, in addition to the structural benefit of increasing the deck rigidity. A 1.5-inch thick UHPC bridge deck overlay was successfully constructed and tested in Mud Creek Bridge in Iowa, Wibowo et al., 2018 as shown in Figure 16. Three concrete deck panels with and without a UHPC overlay were tested in flexure in addition to the field implementation. It was found that adding the UHPC overlay increased the flexural strength by 18% in the positive moment region. While the increase in strength in the negative moment region was not significant because of the small reinforcement area used in the overlay. Another case was reported by Ductal website in Commodore Barry Bridge in New Jersey, where UHPC was selected as the overlay material to increase the service life of the roadway in general.



Figure 16: Placing UHPC deck overlay, Mud Creek Bridge, Iowa, Wibowo et al., 2018

Another case was reported by Guingot et al., 2013 where UHPC was used to strengthen the Caderousse Dam's slab in France in 2010. The dam slabs were subjected to damage by impact of rocks during floods. One of the slabs was repaired in 2008 but did not perform well and several holes in the repaired area were observed. In 2010, the slab was repaired again using UHPC to cast an overlay on top of the slab. UHPC was used for its high early age compressive strength which enabled the dam gate bay to be opened 20 days after casting. UHPC was also used because of its high abrasion and impact resistance. 14 cubic yards of UHPC were mixed in a local batching plant and transported by ready-mix trucks, then were pumped as shown in Figure 17. This main challenge using such technique is that it requires special equipment, very flowable UHPC mix, and experienced labor.



Figure 17: Pumping UHPC to repair the Caderousse Dam slab, courtesy of Guingot et al., 2013

2.2.4 UHPC Shotcrete

Two cases of using UHPC shotcrete were reported by Ductal website, where there are proprietary products for sprayable UHPC with the same properties of conventional UHPC. The main use for such products is for thin elements and architectural facades. In these cases, UHPC shotcrete was used to renovate deteriorated metal culverts with a 3-inch-thick layer of UHPC to provide structural strengthening and protect against future deterioration as shown in Figure 18.



Figure 18: UHPC shotcrete to strengthen and renovate a deteriorated metal culvert, courtesy of Ductal website

2.3 Flexural Strength of UHPC

This section presents a review on the current flexural strength prediction of UHPC, and CC-UHPC beams. Test data are also collected and analyzed to be used later for the evaluation of these models' accuracy.

2.3.1 Flexural Strength Prediction Models of UHPC Beams

Similar to conventional concrete beams, the basic principles of strain compatibility (plane sections remain plane after bending) and internal force equilibrium are valid in the prediction of the flexural strength of UHPC beams. Existing prediction models are all based on these two principles with the main difference in the representation of UHPC mechanical

properties, especially the tensile stresses. Figure 19 shows an example of the approach of setting the compressive strain to the maximum usable value (ϵ_{cu}) and a strain profile based on the neutral axis depth (c) is assumed. After assuming (c) and the strain profile, the material stress-strain models are used to obtain the stress profile, then the internal forces in UHPC and reinforcement are calculated based on their areas. The value of (c) is obtained by iteration so that the internal forces in the section are in equilibrium. Then the moment capacity of the section is calculated by taking the moment of all internal forces at the centroid (or any other point for pure flexure) of the section.

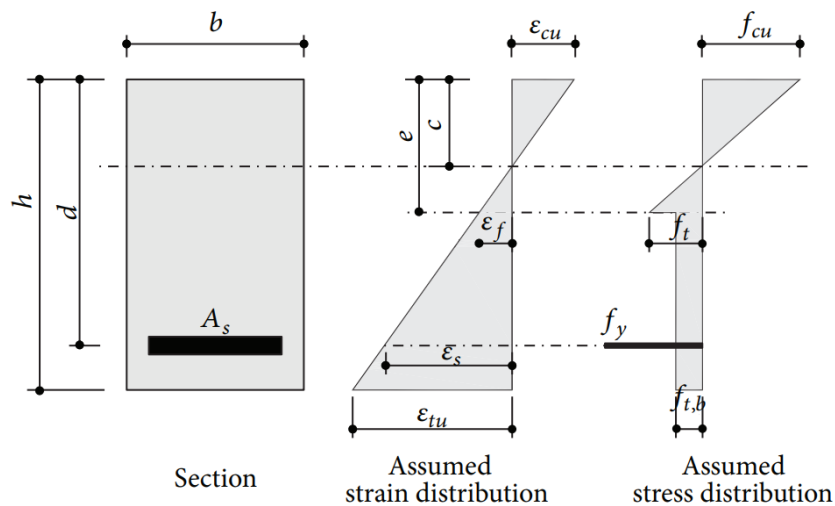


Figure 19: Strain and stress distribution in a UHPC beam cross section, courtesy of Bae et al., 2016

The stress-strain models of UHPC have a significant part on the flexural strength prediction. Chapter 3 presents a review of the commonly used models of UHPC in compression and tension. Figure 20 shows several combinations of idealizations and stress blocks that could be used to predict the flexural strength of a UHPC section. Bae et al., 2016 compared nine types of different material model combinations and compared their prediction against his own experimental test results. All the literature in that area of developing flexural strength prediction models of UHPC components followed the same approach with a variety of material model combinations. The next section presents a collection of the test data of non-prestressed UHPC beams, and a similar study was made using all test data to evaluate the prediction of different material model combinations.

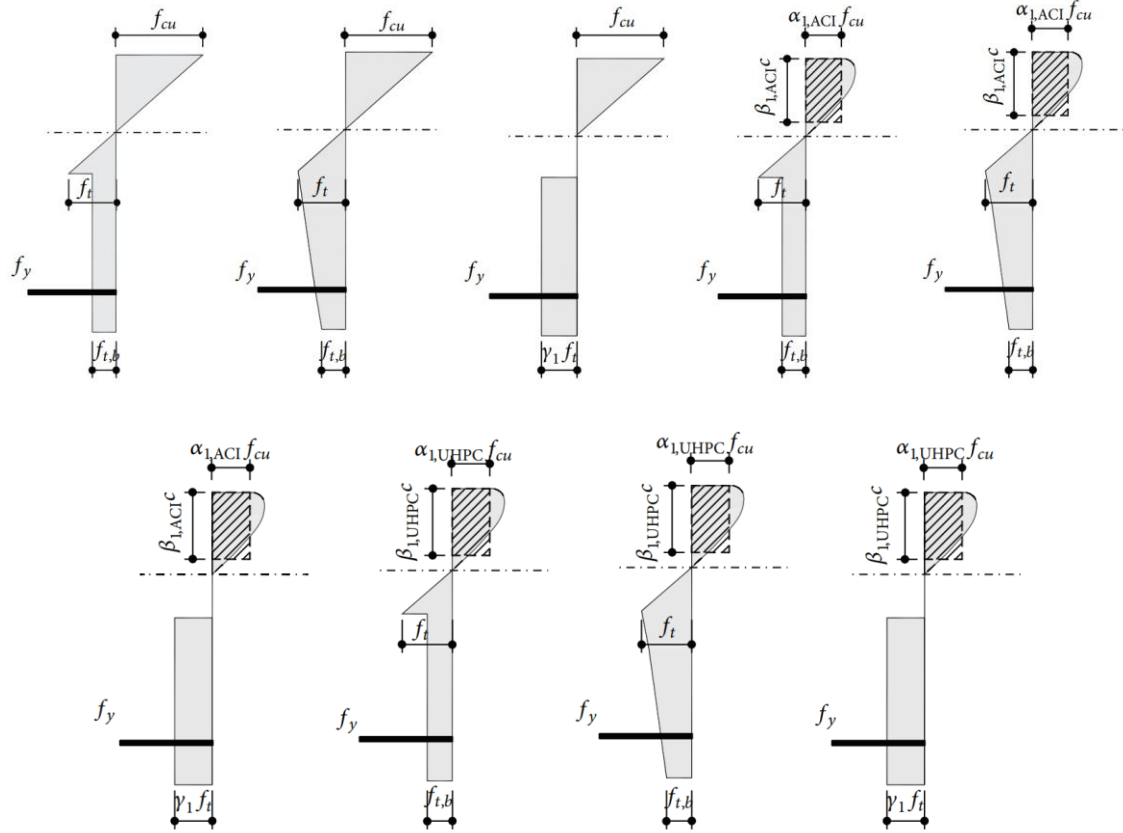


Figure 20: Material models combinations and stress blocks used for flexural strength prediction, courtesy of Bae et al., 2016

The moment-curvature behavior of UHPC components in flexure is significantly different from that of CC components due to the fiber contribution in tension. Figure 21 shows a schematic of the moment-curvature relationship of a non-prestressed UHPC section using El-Helou et al., 2019 material models in compression and tension. The moment increases linearly with curvature until the cracking moment (M_{cr}) is reached. After cracking, the moment continues to increase with curvature at a lower rate until the yield moment (M_y) is reached when the tension reinforcement starts yielding. Then, the moment continues to increase with curvature at a lower rate until the peak moment (M_p) is reached. The curvature at peak moment (Φ_p) typically occurs when the strain of the extreme tension fibers equals to the ultimate tensile strain of UHPC (\mathcal{E}_{tu}), which ranges between 0.004 and 0.01, according to El-Helou et al., 2019, Kodsý and Morcous, 2021, and Graybeal, 2008. After reaching the peak moment, the moment decreases with increased curvature until the ultimate moment (M_u) is reached. The curvature at ultimate moment (Φ_u) typically occurs

when the strain of the extreme compression fibers equals to the ultimate compressive strain of UHPC (ϵ_{cu}), which ranges between 0.0035 and 0.0047 El-Helou et al., 2019 and Haber et al., 2018.

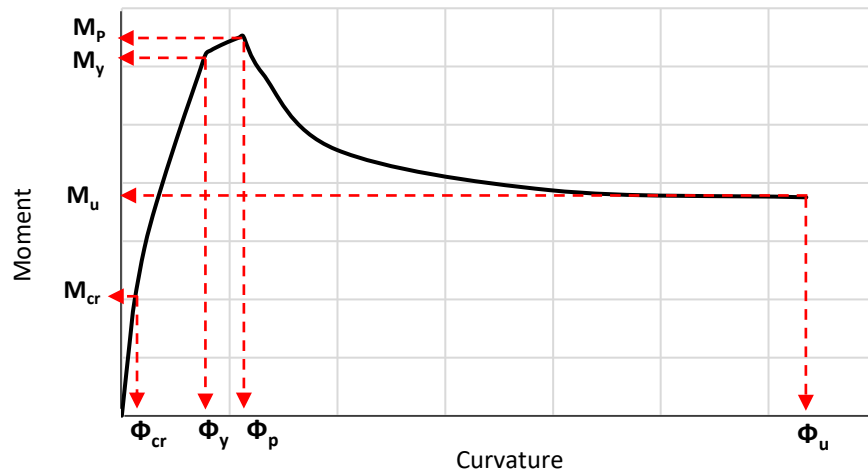


Figure 21: Schematic of the moment-curvature of non-prestressed UHPC components

For non-prestressed UHPC sections, the value of M_p is usually higher than M_u because as the curvature increases, the tensile stresses carried by UHPC occur at a smaller portion of the section resulting in a reduced moment capacity. The contribution of the tensile reinforcing steel is the same in both M_p and M_u as the lower bound of ϵ_{tu} is suggested as 0.004, which means tensile reinforcement steel is already yielding in both M_p and M_u .

2.3.2 Test Data of UHPC Beams in Flexure

Test data from 12 experimental programs conducted using four-point bending of UHPC non-prestressed beams were collected from the literature. Tested beams failed in either tension-controlled flexure (yielding of reinforcement) or compression-controlled flexure (crushing in UHPC). All beams had rectangular sections except those reported by Qiu et al., 2020, had flanged sections. Figure 22 shows a schematic of the test setup, while Figure 23 shows cross-sections of the tested beams.

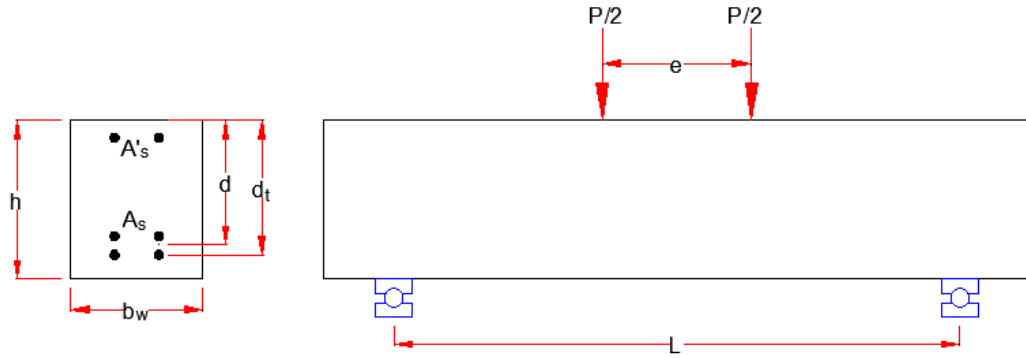


Figure 22: Beam cross-section parameters and test setup

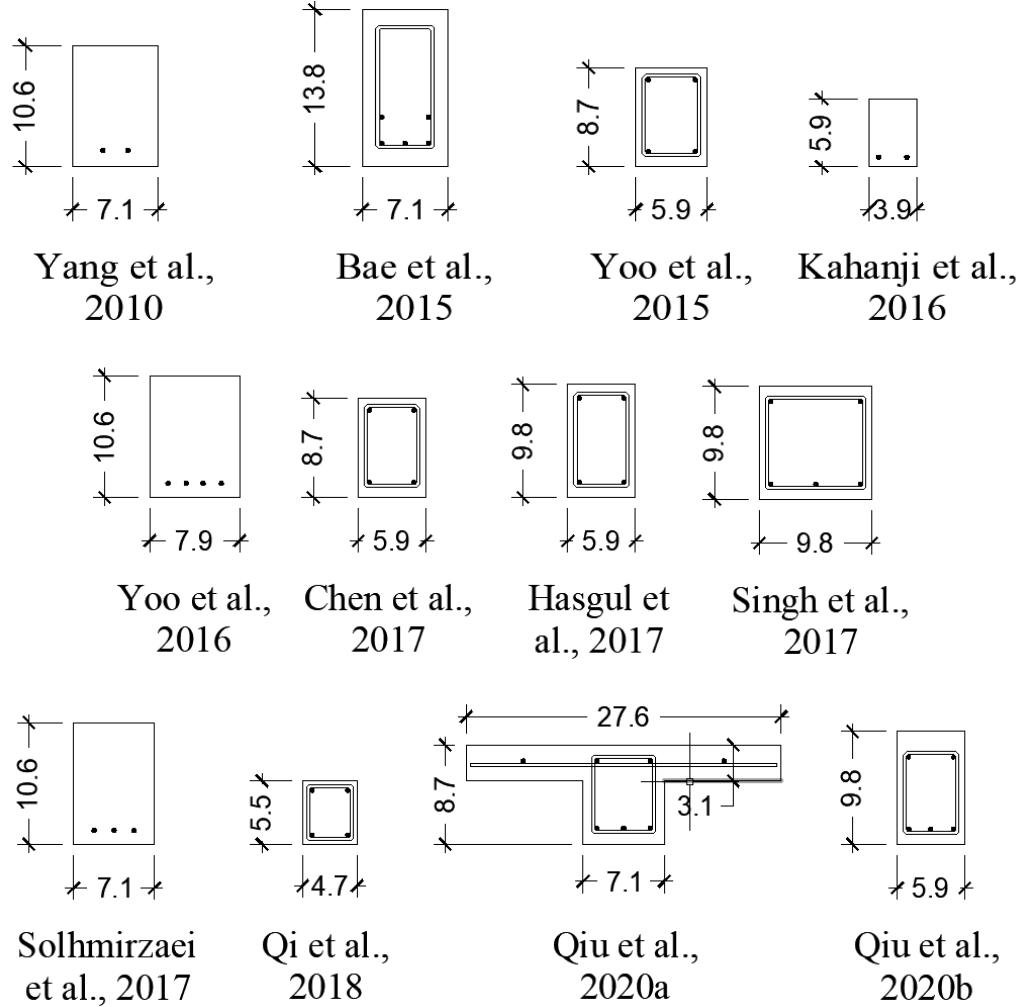


Figure 23: Cross-sections of the beams used in the 12 experimental programs (dimensions in inches)

Table 2 summarizes the test data and results, where b_w is the width of the beam at the web area, h is the height of the beam, d is the depth of the centroid of the reinforcement, d_t is the depth of the outermost layer of reinforcement, A_s is the reinforcement area in tension, ρ is the tension reinforcement ratio ($\frac{A_s}{b_w d}$), L is the span length of the beam, e is the distance between the concentrated loads acting on the beam, f'_c is the UHPC compressive strength, f_t is the UHPC tensile strength, f_y is the yield strength of the reinforcement, V_f is the steel fiber volume fraction.

Tensile strength of UHPC can be obtained by conducting a direct tensile test, splitting tensile test, or flexural test. For direct tensile test and splitting tensile test, the tensile strength is reported as shown in Table 2, while for flexural test, the modulus of rupture was multiplied by a factor of 0.377 to obtain the tensile strength. This factor is the average of the values recommended by SIA 2052, 2016 and DAfStb-Guideline, 2017.

Table 2: Summary of test data

Reference	Specimen ID	b_w (in.)	h (in.)	d (in.)	d_t (in.)	A_s (in ²)	ρ (%)	L (ft)	e (ft)	f'_c (ksi)	f_t (ksi)	f_y (ksi)	V_f (%)	Measured Resistance (kip.ft)
Yang et al., 2010	R12-1	7.1	10.6	9.3	9.3	0.39	0.59	8.9	1.4	27.8	1.6	60	2	64.2
	R12-2	7.1	10.6	9.3	9.3	0.39	0.59	8.9	1.4	27.8	1.6	60	2	61.5
	R13-1	7.1	10.6	9.3	9.3	0.59	0.89	8.9	1.4	27.8	1.6	60	2	72.0
	R13-2	7.1	10.6	9.3	9.3	0.59	0.89	8.9	1.4	27.8	1.6	60	2	78.6
	R13C-1	7.1	10.6	9.3	9.3	0.59	0.89	8.9	1.4	27.8	1.6	60	2	68.0
	R14-1	7.1	10.6	9.3	9.3	0.79	1.20	8.9	1.4	27.8	1.6	60	2	86.0
	R14-2	7.1	10.6	9.3	9.3	0.79	1.20	8.9	1.4	27.8	1.6	60	2	86.2
	R22-1	7.1	10.6	8.5	9.3	0.79	1.31	8.9	1.4	27.8	1.6	60	2	79.0
	R22-2	7.1	10.6	8.5	9.3	0.79	1.31	8.9	1.4	27.8	1.6	60	2	78.0
R23-2	7.1	10.6	8.5	9.3	1.18	1.96	8.9	1.4	27.8	1.6	60	2	97.2	
Bae et al., 2015	B1	7.9	13.8	10.9	11.8	3.8	4.44	14.1	1.6	31.3	1.4	61.2	2	237.5
Yoo et al., 2015	S13 - 0.94%	5.9	8.7	7.1	7.1	0.39	0.93	7.2	1.3	30.7	1.0	71.8	2	28.9
	S13 - 1.50%	5.9	8.7	7.1	7.1	0.62	1.48	7.2	1.3	30.7	1.0	74.0	2	41.1
Kahanji et al., 2016	RSC-1	3.9	5.9	4.9	4.9	0.35	1.83	3.9	1.3	18.9	0.5	60	1	13.1
	RSC-2	3.9	5.9	4.9	4.9	0.35	1.83	3.9	1.3	24.7	1.0	60	2	12.7
	RSH-1	3.9	5.9	4.9	4.9	0.35	1.83	3.9	1.3	21.4	0.5	60	1	11.7
	RSH-2	3.9	5.9	4.9	4.9	0.35	1.83	3.9	1.3	21.6	1.0	60	2	11.5
Yoo et al., 2016	UH-0.53%	7.9	10.6	9.5	9.5	0.39	0.52	8.2	1.3	28.5	1.6	75.8	2	72.3
	UH-1.06%	7.9	10.6	9.5	9.5	0.78	1.04	8.2	1.3	28.5	1.6	75.8	2	87.7
	UH-1.71%	7.9	10.6	8.8	9.5	1.18	1.70	8.2	1.3	28.5	1.6	75.8	2	96.8
Chen et al., 2017	B1	5.9	8.7	7.4	7.4	0.48	1.10	5.9	2.0	20.5	1.6	67	2	31.8
	B2	5.9	8.7	7.2	7.2	1.18	2.78	5.9	2.0	20.5	1.6	60	2	52.6
	B3	5.9	8.7	7.2	7.2	1.52	3.58	5.9	2.0	20.5	1.6	66	2	66.5
	B4	5.9	8.7	6.9	7.2	2.11	5.18	5.9	2.0	20.5	1.6	60	2	78.0
Hasgul et al., 2017	B1-F	5.9	9.8	8.8	8.8	0.48	0.92	6.9	2.3	22.8	0.8	65.7	1.5	38.8
	B2-F	5.9	9.8	8.7	8.7	0.98	1.91	6.9	2.3	24.2	0.8	67.1	1.5	66.3
	B3-F	5.9	9.8	8.6	8.6	1.4	2.76	6.9	2.3	22.8	0.8	66.1	1.5	82.7
	B4-F	5.9	9.8	7.1	8.7	1.96	4.68	6.9	2.3	24.1	0.8	67.4	1.5	99.2
Singh et al., 2017	B25-1	9.8	9.8	8.7	8.7	1.46	1.72	10.7	1.6	20.7	0.9	76.1	2.3	87.2
	B25-2	9.8	9.8	8.7	8.7	1.46	1.72	10.7	1.6	20.7	0.9	76.1	2.3	84.7
	B15-2	5.9	5.9	4.8	4.8	0.93	3.28	8.9	1.0	20.7	0.9	75.4	2.3	24.4
Solhmirzaei et al., 2017	B3	7.1	10.6	9.3	9.3	0.6	0.91	12.0	2.8	28.0	0.8	63	1.5	50.2
	B5	7.1	10.6	9.3	9.3	0.8	1.21	12.0	2.8	28.0	0.8	63	1.5	65.5
Qi et al., 2018	F-9	4.7	5.5	4.7	4.7	0.16	0.70	3.7	1.3	19.66	0.9	129	2	10.4
Qiu et al., 2020a	B-S65-16	7.1	8.7	7.3	7.3	0.93	1.79	11.5	4.6	19.1	1.4	60	2	48.4
	B-S65-20	7.1	8.7	7.3	7.3	1.46	2.81	11.5	4.6	19.1	1.4	66.7	2	75.2
	B-S81-20	7.1	8.7	7.3	7.3	1.46	2.81	11.5	4.6	18.3	1.4	66.7	2	78.1
	B-S83-20	7.1	8.7	7.3	7.3	1.46	2.81	11.5	4.6	18.8	1.4	66.7	2	75.3

Table 2: continued

Reference	Specimen ID	b_w (in.)	h (in.)	d (in.)	d_t (in.)	A_s (in ²)	ρ (%)	L (ft)	e (ft)	f'_c (ksi)	f_t (ksi)	f_y (ksi)	V_f (%)	Measured Resistance (kip.ft)
Qiu et al., 2020b	B-2S12-20	5.9	9.8	8.8	8.8	0.35	0.67	9.8	2.6	24.6	1.2	64.1	2	25.2
	B-2S16-20	5.9	9.8	8.7	8.7	0.62	1.20	9.8	2.6	24.6	1.2	65.6	2	41.9
	B-3S16-20	5.9	9.8	8.7	8.7	0.62	1.20	9.8	2.6	24.6	1.2	65.6	2	44.2
	B-3S20-20	5.9	9.8	8.7	8.7	0.97	1.90	9.8	2.6	24.6	1.2	68.2	2	83.3
	B-2S20-20	5.9	9.8	8.7	8.7	0.97	1.90	9.8	2.6	24.6	1.2	68.2	2	49.5
	B-2S25-20	5.9	9.8	8.6	8.6	1.52	3.00	9.8	2.6	24.6	1.2	70.5	2	92.3
	B-3S16-30	5.9	9.8	8.4	8.4	0.93	1.89	9.8	2.6	24.6	1.2	65.6	2	53.4
	B-3S16-40	5.9	9.8	8.0	8.0	0.93	1.98	9.8	2.6	24.6	1.2	65.6	2	56.8
Maximum	9.8	13.8	10.9	11.8	3.8	5.18	11.5	4.6	30.7	1.6	129	2.3	237.5	
Minimum	3.9	5.9	4.7	4.7	0.35	0.46	3.7	1.0	18.9	0.5	60	1	10.4	
Average	8.2	9.4	8.0	8.1	0.94	1.84	8.5	2.1	24.5	1.2	69	1.9	64	
Standard Deviation	6	2	2	2	0.63	1.09	2.4	1.0	3.7	0.3	12	0.3	36.8	

*Value not reported by the original research work and was reasonably assumed.

Figure 24 shows the frequency distribution of tensile reinforcement ratio (ρ) of the tested beams. The figure indicates that most tested beams had reinforcement ratios less than 2%, while few beams had reinforcement ratios between 2 to 5%, which is considerably higher than the typically used in flexural components. Figure 25 plots the measured flexural resistance factor (R) versus ρ for each point in the test data. The flexural resistance factor represents the normalized flexural resistance of a component that has width (b_w), and depth (d); and is calculated for conventional concrete (CC) beams as follows Wight, 2016:

$$R = \frac{M_u}{b_w d^2} = \omega f'_c (1 - 0.59 \omega) \quad [MPa] \quad (1)$$

$$\omega = \rho \frac{f_y}{f'_c} \quad (2)$$

Where, ω is the reinforcement index, f_y is the reinforcement yield strength, f'_c is the compressive strength, and M_u is the ultimate moment of resistance. For specific f'_c and f_y , the relationship between R and ρ becomes a straight line. Considering the average f'_c of the UHPC test data (24.5 ksi), and the commonly used f_y (60 ksi), the CC beams straight

line shown in Figure 25 was developed. The flexural resistance factors of all UHPC test beams exceeded that straight line regardless of the reinforcement ratio. This indicates the tensile strength of UHPC contributes significantly to the flexural strength of non-prestressed UHPC beams. This contribution is higher in beams with low reinforcement ratios than those with high reinforcement ratios.

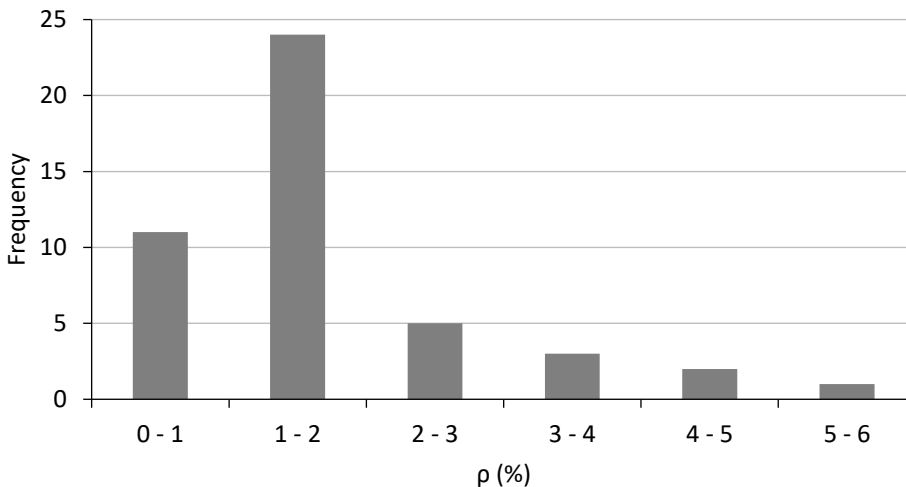


Figure 24: Frequency distribution of the number of the tension reinforcement ratio in the test data

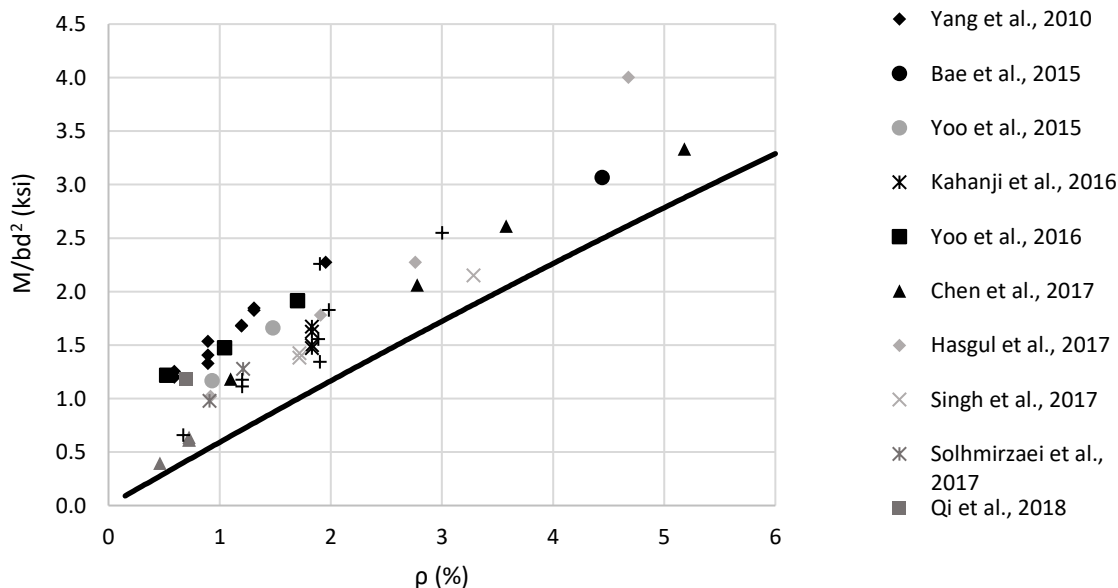


Figure 25: Measured flexural resistance factor versus tension reinforcement ratio of each experimental program in the test data

2.3.3 Test Data of CC-UHPC Beams in Flexure

This section will present a review on previous testing done on strengthening rectangular non-prestressed beams using UHPC. No testing has been published to date on the repair or strengthening of I-shaped or prestressed beams. In each testing program, a summary of the test setup, parameters, failure load, and failure mode will be presented. At the end of this section, a summary of all testing done is presented in a tabulated format.

2.3.3.1 Safdar et al., 2016

Seven rectangular beams (10 x 15.7 in.) shown in Figure 26 were tested in a four-point bending test as summarized in Table 3. One beam was considered as the control beam without having any UHPC, three beams were repaired in the compression zone (top layer) with 0.8, 1.6, and 2.4 in. UHPC thickness, and three beams were repaired in the tension zone (bottom layer) with 0.8, 1.6, and 2.4 in. UHPC thickness. UHPC was bonded to the conventional concrete by roughening the interface using water jetting. The conventional concrete had a compressive strength of 4.3 ksi. While, the used UHPC had a compressive strength of 22.7 ksi, and an average tensile strength of 1.4 ksi, reinforced with 0.5 in. long fibers having a diameter of 0.006 in. Longitudinal reinforcement (A_l) was 0.62 in.², and shear reinforcement (A_v) was 0.167 in.²/ft. Beam BU-60 was terminated before reaching the failure load, so the failure mode was not reported, and the failure load was below predictions. Using UHPC as a repair material was successful in increasing the flexural resistance of the beams with the increase of UHPC thickness.

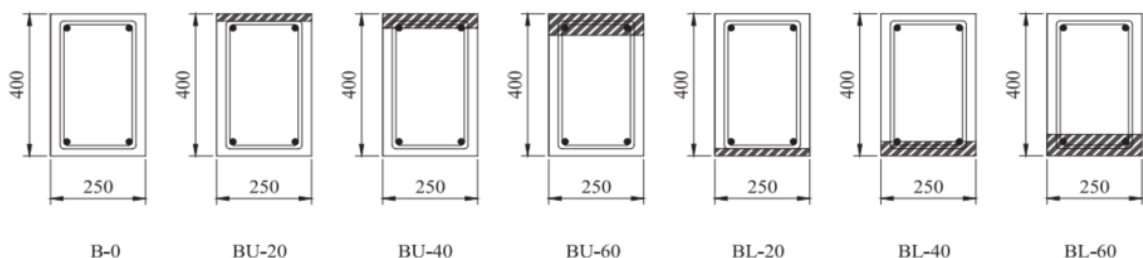


Figure 26: Tested specimens, courtesy of Safdar et al., 2016

Table 3: Summary of tested specimens and failure modes, Safdar et al., 2016

Specimen ID	Specimen Type	UHPC Thickness (in.)	Application of UHPC	Failure Load	Failure Mode
B-0	Control Beam	0	N/A	26.7	Concrete Crushing
BU-20	Upper Layer Repair	0.8	Protection	32.0	UHPC Crushing
BU-40		1.6		31.8	Rebar Fracture
BU-60		2.4	Protection and Strengthening	30.8	N/A
BL-20	Lower Layer Repair	0.8	Protection	26.7	Concrete Crushing
BL-40		1.6		32.7	Rebar Fracture
BL-60		2.4	Protection and Strengthening	35.1	Rebar Fracture

2.3.3.2 Noshiravani, and Bruhwiler, 2013

A series of beams were tested in a cantilever beam setup as shown in Figure 27 and summarized in Table 4. The test parameters were the shear span, shear reinforcement, longitudinal reinforcement in the UHPC or Conventional Concrete (CC). The conventional concrete beam dimensions were (5.9 x 9.8 in.). The beams were strengthened by a 2-inch UHPC top layer containing longitudinal reinforcement. The conventional concrete had a compressive strength of 6.0 ksi. While, the UHPC had a compressive strength of 23.2 ksi, and tensile strength of 1.7 ksi (from direct tension test on dog bone specimens). Steel fibers used had a volume fraction of 3%, length of 0.5 in., and diameter of 0.006 in. All the beams failed in a flexure, or a flexure-shear mode. Adding the 2-inch UHPC top layer increased the flexural strength significantly (from two to three times compared to control beams).

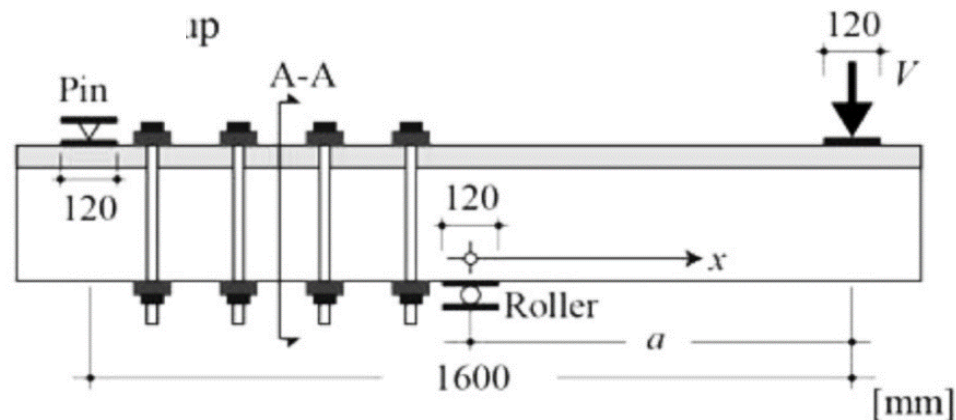


Figure 27: Cantilever test setup specimens, courtesy of Noshiravani, and Bruhwiler, 2013

Table 4: Summary of tested specimens and failure load, Noshiravani, and Bruhwiler, 2013

Specimen ID	Specimen Type	a (in.)	S (in.)	A_v (in. ² /ft)	A_l (UHPC) (in. ²)	A_l (CC) (in. ²)	Failure Load (kip)		
L0	Control	39.4	7.9	0.24	0	0.37	7.7		
L1	Long Span		15.7	0.12	0.31		9.8		
L2							21.7		
L3							7.9	0.24	0.31
MN0	Control	31.5	7.9	0.24	0	0.72	10.0		
MN1	Medium Span				9.8		0.11	0.31	21.8
MN2								0.31	20.8
MN3			0.31	30.3					
MW0	Control		15.7	0.12	0	0.37	9.7		
MW1	Medium Span				15.7		0.12	0.31	13.2
MW2								0.31	23.5
MW3		0.31						20.6	
MW4		0.31						20.4	
MW5		0.31						22.4	
MW6	0.31	0.72	20.4						
SN1	Short	23.6	7.9	0.24	0.31	0.37	25.9		
SW1	Span		15.7	0.1	0.31		28.0		

2.3.3.3 Prem et al., 2016

A series of rectangular beams were tested in a four-point bending setup as shown in Figure 28 and summarized in Table 5. The beams were divided into three main groups with variable longitudinal reinforcement (A through C). In each group the control beam was tested until failure. To simulate the damage occurring in the rest of the beams, they were loaded in flexure until reaching 90% of the failure load of the control beam. Then a UHPC

layer was bonded by any epoxy adhesive to the soffit of the beam. The conventional concrete in this study had a compressive strength of 5.0 ksi. The UHPC in this study had a compressive strength of 24.6 ksi, split tensile strength of 3.3 ksi. Fibers used had a length of 0.5 in. and diameter of 0.006 in. It was found that only an 0.4-inch thick UHPC layer was able to restore the flexural strength of the damaged beams to the control beams. Using a UHPC thickness of 0.6, and 0.8 inch increased the flexural strength to exceed the control beams.

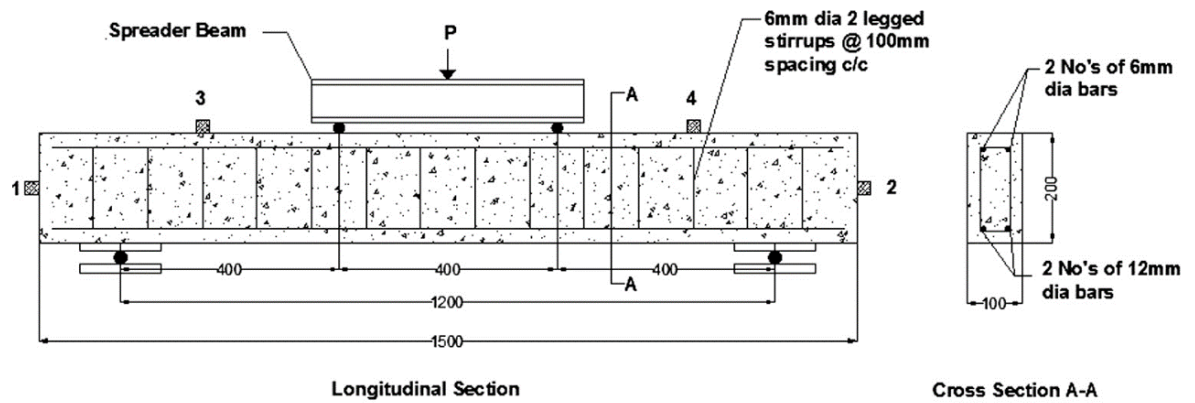


Figure 28: Four-point bending test setup and control beam cross-section, courtesy of Prem et al., 2016

Table 5: Summary of tested specimens and failure load, Prem et al., 2016

Specimen	Specimen Type	A_f (in. ²)	A_v (in. ² /ft)	Failure Load	Failure
A	Control	0.16	0.27	12.7	Flexure
A1	0.4			12.4	
A2	0.6			15.7	
A3	0.8			17.2	
B	Control	0.24		18.1	
B1	0.4			17.9	
B2	0.6			20.5	
B3	0.8			21.5	
C	Control	0.35		23.9	
C1	0.4			23.8	
C2	0.6			26.5	
C3	0.8			27.5	

2.3.3.4 Yin et al., 2017

Nine slab specimens were tested in a four-point bending configuration as shown in Figure 29 and summarized in Table 6. The slabs were strengthened in flexure by casting a UHPC layer on the bottom surface of the slab. Specimens labeled (RE) had the same depth before and after strengthening, which indicates a repair application. While, specimens labeled (OV) had the same conventional concrete section as the control specimen and the UHPC layer adds to the overall depth of the section indicating a strengthening application. The used UHPC in this study had an average compressive strength of 24.4 ksi and flexural strength of 4.0 ksi. The slabs did not contain any transverse reinforcement. Bonding between conventional concrete and UHPC was achieved by roughening the conventional concrete surface using a chisel and hammer randomly. Interface failure was evident in specimen (RE-20). For the (OV) specimens, diagonal shear cracks occurred initially followed by interface failure. Adding the UHPC layer significantly affected the failure load and behavior of all repaired or strengthened specimens. With the increase of UHPC thickness, the failure mode changed from brittle shear failure to ductile flexural failure. However, the failure load was not increased by the addition of the UHPC layer in the case of (RE) series specimens.

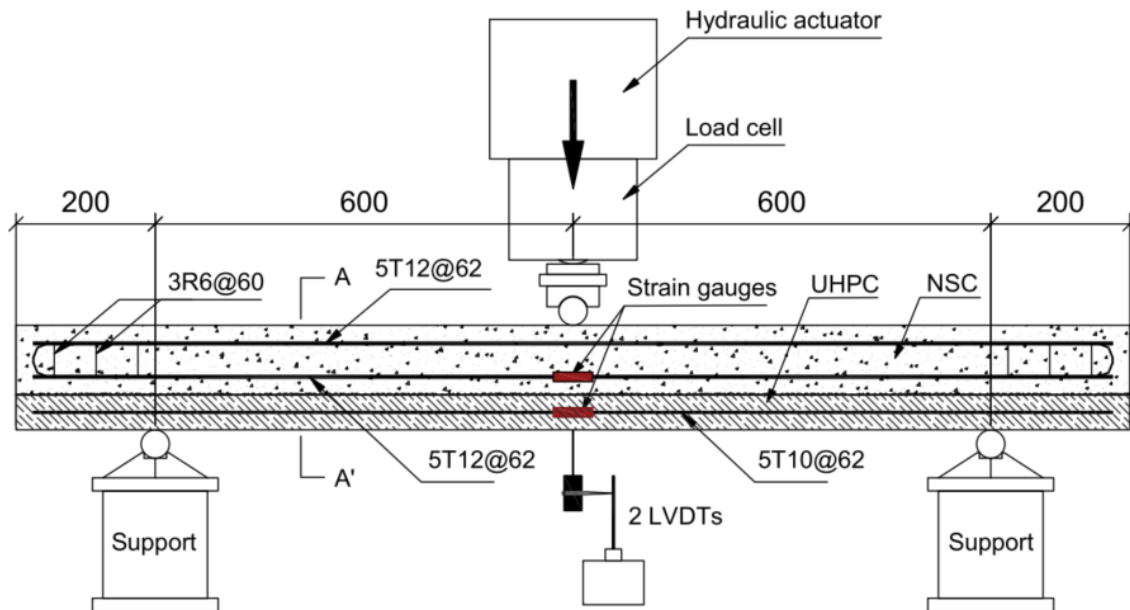


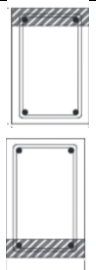
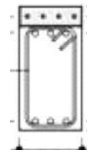
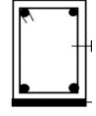
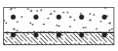
Figure 29: Four-point bending test setup, courtesy of Yin et al., 2017

Table 6: Summary of tested specimens and failure load, Yin et al., 2017

Specimen	Specimen Type/UHPC Bottom Layer	Overall Dimensions (in. x in.)	Longitudinal		Failure Load (kip)	Failure Mode
			Bottom	Top		
RE-0	Control	11.8 x 3.9	0.88	0.88	13.7	Shear
RE-20	1.0				12.8	Interface
RE-32	1.3				9.8	Flexure
RE-50	2.0				12.5	Flexure
RE-100	UHPC only				25.4	Flexure
OV-25	1.0	11.8 x 4.9	0.88	0.88	16.5	Shear
OV-25a	1.0 (with		0.88 + 0.61	0.88	17.5	Shear
OV-50	2.0	11.8 x 5.9	0.88	0.88	17.5	Shear
OV-50a	2.0 (with		0.88 + 0.61	0.88	21.4	Shear

Table 7 shows a summary review on the four testing programs where UHPC was used to strengthen non-prestressed rectangular concrete beams in flexure. Application of the material varied between casting on roughened surfaces (using sandblasting or water jetting) and using prefabricated sheets bonded to the existing concrete surface using epoxy.

Table 7: Summary of previous testing done on strengthened beams in flexure using UHPC

Reference	Conventional Concrete Section	Conventional Concrete Compressive Strength (ksi)	UHPC repair or strengthening scheme	UHPC Compressive Strength (ksi)	UHPC location	Bonding Mechanism	Test Type	Failure Mode	Main Findings	Descriptive Photo
Safdar et al., 2016	Rectangular 10 x 15.7 in ²	4.3	Thicknesses of 0.8, 1.6, and 2.4 in. (0.8 and 1.6 in. thicknesses are intended for protection only)	22.7	Top or bottom layers	Water jetting of the conventional concrete surface	4-point bending	Flexure (rebar fracture)	Smallest thickness of UHPC at the Top (0.8 inch) increased flexural resistance	
Noshiravani, and Bruhwiler, 2013	Rectangular 5.9 x 9.8 in ²	6.0	Thickness of 2 in.	23.2	Top Layer with and without RFT	Roughened Interface	Cantilever beam	Flexure	Adding a reinforced layer of UHPC in tension increased flexural resistance significantly	
Prem et al., 2016	Rectangular 3.9 x 7.9 in ²	5.0	Pre-fabricated UHPC with 0.4, 0.6, and 0.8 thick	24.6	Bottom layer	Epoxy adhesive	4-point bending	Flexure	UHPC thickness of 0.6 and 0.8 inch increased flexural resistance	
Yin et al., 2017	Rectangular 11.8 x 3.9 in ²	4.8	Thicknesses of 0.8, 1.6, and 2.0 in. for repair 1.0 and 2.0 for strengthening	24.4	Bottom layer	Roughening CC surface using a chisel and hammer randomly	4-point bending	Shear in un-strengthened beams tuned into flexure after strengthening	No significant increase in failure load in repaired series	

2.4 Shear Strength of UHPC

This section presents a review on the shear strength prediction models of UHPC beams, and previous literature of shear testing. A summary of the testing done on UHPC beams is presented in the end of the section in a tabulated form.

Vertical shear resistance in concrete beams is activated by four mechanisms after cracking: the action of the concrete in the compression zone, aggregate interlock, dowel action, and residual tension across the crack, Abad et al., 2019. Figure 30 shows a schematic of these mechanisms. In SFRC beams, the steel fibers provide additional tensile capacity across the crack. In the compression zone of the cross-section, the uncracked concrete provides shear resistance. Aggregate interlock results from the contact forces between the aggregates bridging the crack. Dowel action is the resistance of the flexural steel to shearing forces. In UHPC, the presence of steel fibers enhances all tension-driven failure modes especially vertical shear. The significant increase in shear resistance of UHPC beams enables the elimination of transverse reinforcement, which in turn reduces production and labor cost significantly.

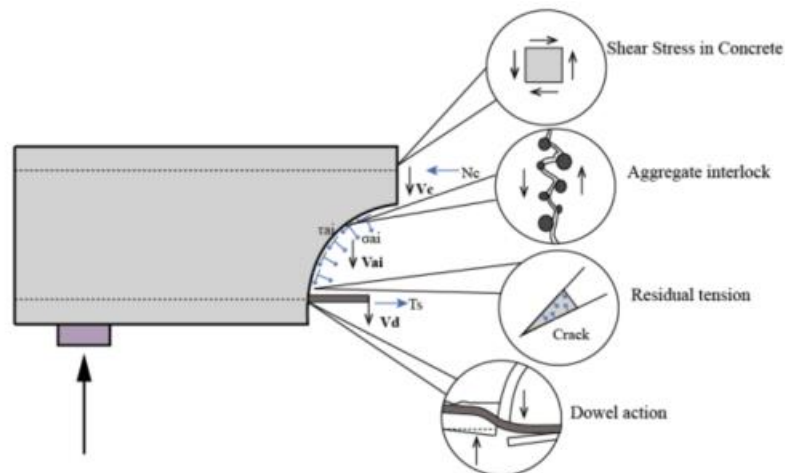


Figure 30: Four mechanisms of vertical shear transfer in concrete beams, courtesy of Abad et al., 2019

2.4.1 Shear Strength Prediction Models of UHPC Beams

This section presents a review of the current prediction models evaluating the shear strength of UHPC beams. Five prediction models from international codes/standards are

presented: RILEM TC 162-TDF, 2003, *fib* Model Code, 2010, French standard, NF P 18-710, 2016, PCI-UHPC Structures Design Guide, 2021, and Draft of AASHTO Guide Specification for Structural Design with UHPC, 2021. The first three models represent the historical evolution of shear strength prediction approaches from conventional concrete to fiber-reinforced concrete to UHPC internationally. While the last two models are recently published in the United States to promote the implementation of UHPC in structural applications. The main differences among these models are the terms that account for the post-cracking tensile strength of UHPC and safety factors.

2.4.1.1 RILEM TC 162-TDF, 2003

The Eurocode 2 part 1, 1991 shear strength prediction model of conventional concrete was used as the general framework to develop this prediction model Vandewalle, 2000. However, Eurocode 2 considers only the pre-peak behavior of concrete in tension, while this model considers the effect of steel fibers on the post-peak behavior of fiber-reinforced concrete. Therefore, the tensile stress-strain relationship of fiber-reinforced concrete is needed for this model. The ultimate shear load carrying capacity is taken as the sum of the contributions of concrete (V_{cd}), stirrups and/or inclined bars, and steel fibers (V_{fd}). Steel fibers contribution is calculated according to the following equation:

$$V_{fd} = 3.11k_f k b_w d \mathcal{T}_{fd} \quad [lbf] \quad (3)$$

Where (k_f) is a factor to account for the contribution of flanges in T-shaped sections (taken as 1.0 for other shapes) calculated as follows:

$$k_f = 1 + n \left(\frac{h_f}{b_w} \right) \left(\frac{h_f}{d} \right) \quad (4)$$

$$n = \frac{b_f - b_w}{h_f} \leq 3; \quad \text{and } n \leq \frac{3b_w}{h_f} \quad (5)$$

Where (b_f) is the width of flanges [in.]; (b_w) is the beam minimum web width [in.] over (d) [in.]; (d) is the effective depth [in.]; (h_f) is the height of flanges [in.]. And, (k) is the size effect factor taken as $1 + \sqrt{\frac{200}{d}} \leq 2$; (\mathcal{T}_{fd}) is the design value of the increase in shear strength due to steel fibers taken as $(0.12 f_{R,4})$ [psi]; ($f_{R,4}$) is the residual flexural tensile

strength corresponding to crack mouth opening displacement (CMOD) of 0.14 in. [psi]. Residual flexural tensile strengths ($f_{R,i}$) are determined experimentally by a three-point bending test on a 5.9 x 5.9 x 21.6 in. notched prism. The stress-strain relation is obtained from the load-deflection or load-CMOD of the notched prism. The load-CMOD curve is defined by four points ($i = 1$ through 4) corresponding to CMOD of 0.02, 0.06, 0.10, and 0.14 in., respectively. ($f_{R,i}$) is calculated as follows:

$$f_{R,i} = \frac{3 F_{R,i} x L}{2b x h_{sp}^2} \quad [psi] \quad (6)$$

Where ($F_{R,i}$) is the load recorded at crack mouth opening displacement (CMOD_{*i*}) [lbf]; (L) is the span of the prism [in.]; (b) is the width of the prism cross-section [in.]; (h_{sp}) is the distance between the tip of the notch to the top of the prism cross-section [in.]. Concrete contribution is calculated as follows:

$$V_{cd} = \left[0.53 k (0.69 \rho_1 f_{ck})^{\frac{1}{3}} + 0.67 \mathfrak{G}_{cp} \right] b_w d \quad [lbf] \quad (7)$$

$$\rho_1 = \frac{A_l}{b_w d} \quad (8)$$

$$\mathfrak{G}_{cp} = \frac{N_{sd}}{A_c} \quad [psi] \quad (9)$$

Where (ρ_1) is the longitudinal reinforcement ratio (recommended not to exceed 2%); (A_l) is the area of tension reinforcement extending not less than ($d +$ anchorage length) beyond the section considered [in.²]; (f_{ck}) is the characteristic cylinder compressive strength [psi]; (\mathfrak{G}_{cp}) is the level of axial loading or prestressing in the section [psi]; (N_{sd}) is the longitudinal force in the section due to loading or prestressing (compression: positive) [lbf]; (A_c) is the cross-sectional area of the beam [in.²].

2.4.1.2 *fib* Model Code, 2010

The prediction model is developed for steel fiber reinforced concrete with conventional strength and is not validated yet for UHPC. The approach used has a close resemblance to RILEM TC 162-TDF, 2003 prediction model except that the steel fibers contribution to the

resistance is coupled with the concrete contribution in one term. After cracking, the concrete contribution is weakly coupled with the transverse reinforcement contribution and is strongly coupled with the steel fibers contribution to the shear resistance.

The coupled contributions of concrete and fibers to the shear resistance of fiber reinforced concrete elements without transverse reinforcement is given by:

$$V_{Rd,F} = \left\{ \frac{0.8}{\gamma_c} \cdot k \cdot \left[0.69 \cdot \rho_1 \left(1 + 7.5 \frac{f_{Ftuk}}{f_{ctk}} \right) \cdot f_{ck} \right]^{1/3} + 0.67 \cdot \mathcal{G}_{cp} \right\} \cdot b_w \cdot d \quad [lbf] \quad (10)$$

Where terms like (k) , (ρ_1) , (\mathcal{G}_{cp}) , (b_w) , and (d) are defined similarly to RILEM TC 162-TDF, 2003. (γ_c) is the partial safety factor for concrete without fibers typically taken as 1.5. However, (γ_c) was not considered when calculating the ultimate shear resistance of UHPC beams in the evaluation of the prediction model in this paper. (f_{Ftuk}) is the characteristic value of the ultimate residual tensile strength determined as follows:

$$f_{Ftuk} = \frac{f_{R,3}}{3} \quad [psi] \quad (11)$$

$$f_{Ftuk} = f_{Fts} - \frac{w_u}{CMOD_3} (f_{Fts} - 0.5 f_{R,3} + 0.2 f_{R,1}) \geq 0 \quad [psi] \quad (12)$$

$$f_{Fts} = 0.45 f_{R,1} \quad [psi] \quad (13)$$

Similar to RILEM TC 162-TDF, 2003, $(f_{R,1})$ and $(f_{R,3})$ are the residual flexural tensile strengths corresponding to CMOD of 0.02 in. and 0.14 in. respectively [psi]; (f_{Fts}) is the characteristic service residual tensile strength (post-cracking strength at serviceability crack opening) [psi]; (w_u) is the maximum crack opening accepted in structural design (typically taken as 0.06 in.). The residual flexural tensile strengths are determined experimentally according to EN 14651 by a three-point bending test on a 5.9 x 5.9 x 21.6 in. notched prism. (f_{Ftuk}) can be determined based on the rigid-plastic model equation (9), or the linear model based on equations (10) and (11). (f_{ctk}) is the characteristic value of the tensile strength for the concrete without fibers [psi] determined as follows:

$$f_{ctk} = 2.12 \ln(1 + 0.1(f_{ck} + 1160 \text{ psi})) \quad [psi] \quad (\text{for } f_{ck} > 7250 \text{ psi}) \quad (14)$$

Where (f_{ck}) is the characteristic value of cylinder compressive strength [psi].

2.4.1.3 French standard, NF P 18-710, 2016

Similar shear prediction model to the AFGC, 2013, the shear resistance is equal to the smaller of the resistance of concrete compressive struts ($V_{Rd,max}$) and the tensile resistance of the ties (V_{Rd}). The general philosophy is similar to the AASHTO LRFD, 2017 simplified version of the Modified Compression Field Theory procedure dividing (V_{Rd}) into concrete contribution term ($V_{Rd,c}$) and shear reinforcement contribution term ($V_{Rd,s}$), with the addition of fibers contribution term ($V_{Rd,f}$), Crane, 2010. The concrete contribution term for prestressed beam sections is calculated as follows:

$$V_{Rd,c} = \frac{1.07}{\gamma_{cf}\gamma_E} k f_{ck}^{1/2} b_w z [lbf] \quad (15)$$

$$k = 1 + \frac{3 \mathfrak{G}_{cp}}{f_{ck}}, \text{ for } \mathfrak{G}_{cp} \geq 0 \quad (16)$$

The terms (k), (f_{ck}), (b_w), and (\mathfrak{G}_{cp}) are similar to what was described in the previous models. The terms (γ_{cf}) and (γ_E) are partial safety factors (typically taken as 1.5 after being multiplied). (γ_{cf}) is a partial factor for UHPC under tension typically taken as 1.3, while (γ_E) is a partial factor accounting for the uncertainty about extrapolating the model developed for high performance concrete with ($f_{ck} \leq 13.1$ ksi) to UHPC, (z) is the internal moment lever arm (typically taken as 90% of the section depth). A larger number of experimental results is required to lower the level of reduction in the estimation of concrete contribution. Safety factors were not considered when calculating the ultimate shear strength of UHPC beams in the evaluation of the prediction model in this paper. For non-prestressed sections, the only two differences in ($V_{Rd,c}$) are that the value (1.07) is replaced by (0.80), and section height (h) is used instead of (z). Fibers contribution term is determined by quantifying the post-crack residual tensile strength resisting the main crack across the angle (θ) over (z) as shown in Figure 31, Degen, 2006 and Crane, 2010. Fibers contribution term is calculated as follows:

$$V_{Rd,f} = \frac{A_{fv} \mathfrak{G}_{Rd,f}}{\tan(\theta)} [lbf] \quad (17)$$

$$\mathfrak{G}_{Rd,f} = \frac{1}{K \gamma_{cf}} \frac{1}{w_{lim}} \int_0^{w_{lim}} \mathfrak{G}_f(w). dw [psi] \quad (18)$$

Where, (A_{fv}) is the area of fiber effect ($A_{fv} = b_w z$) [in.²]; $(\sigma_{Rd,f})$ is the residual tensile strength of the fiber-reinforced cross-section [psi]; (θ) is the angle between the principal compression stress and the beam axis in degrees, a minimum value of 30 degrees is recommended. $(\sigma_{Rd,f})$ is estimated by the summation of the area under the stress-crack width curve of a three-point bending curve as shown in equation (14). (K) is a reduction factor used to consider the difference between fibers orientation of the prism and the actual orientation of the fibers in the future structure; the (K) factor typically ranges between 1.0 to 1.4. (w_{lim}) is the maximum of the ultimate crack width reached at the ultimate limit state bending moment of the section at the outer tension fiber, or the admissible crack width (recommended as 0.01 in.). Stress versus crack width ($\sigma_f(w)$) relation is determined by a bending test on UHPC prisms (six prisms are required). Three-point bending tests are performed on notched specimens, while four-point tests are used for un-notched specimens. The dimensions of the test prisms depend on the length of fibers (l_f). For ($l_f \leq 0.6$ inch), 2.8 x 2.8 x 11 in. prisms are recommended, and for ($0.6 \text{ in.} < l_f \leq 0.8 \text{ in.}$), 4.0 x 4.0 x 15.6 in. prisms shall be used. The depth of the notch is equal to 10% of the prism height to enable an efficient localization of the crack while minimizing the risk of cracking outside the notch location. The distance between bearing points must be three times the depth of the prism. The residual tensile strength can be also estimated by means of direct tension tests on un-notched prisms.

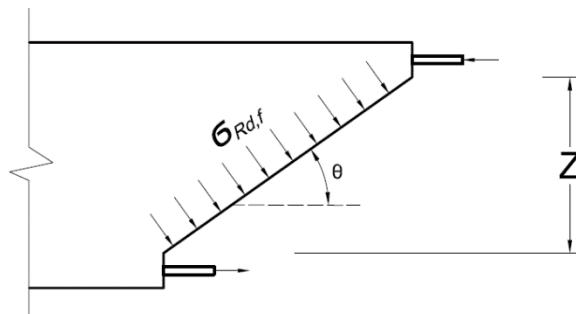


Figure 31: Tensile stresses carried by steel fibers in a general beam section according to the Modified Compression Field Theory, Crane, 2010

2.4.1.4 PCI-UHPC Structures Design Guide, 2021

The Precast/Prestressed Concrete Institute (PCI) recently published Phase II report for the implementation of using UHPC in precast bridges and buildings. The report provides guidelines for the design of UHPC members, as well as acceptance criteria for PCI-UHPC material mechanical properties and production. The model presented in the report is based on the MCFT and AASHTO LRFD, 2017. The ultimate shear load carrying capacity (V_n) is taken as the sum of the contributions of UHPC tensile strength (V_{cf}), shear reinforcement (V_s), and component of prestressing force resisting vertical shear (V_p). V_{cf} is calculated according to the following equation:

$$V_{cf} = 1.33 f_{rr} b_w d \cot(\theta) \quad (19)$$

Where f_{rr} is the residual tensile strength of UHPC and recommended to be taken as 0.75 ksi for UHPC meeting minimum PCI-UHPC tensile properties requirements; this value was calculated based on the minimum required peak flexural strength according to ASTM C1609, 2019 of 2.0 ksi multiplied by a 0.375 conversion factor according to DAfStb, 2017 and SIA 2052, 2016. Other parameters are similar to what was described in the previous models. The crack angle is estimated according to the following equations:

$$\theta = 29 + 3500 \mathcal{E}_s \quad (20)$$

Where \mathcal{E}_s is the strain at the level of tension reinforcement and calculated as follows for positive values of \mathcal{E}_s :

$$\mathcal{E}_s = \frac{\left(\frac{M_u}{d}\right) + (V_u - V_p) - P_e}{(E_s A_s + E_p A_{ps})} \leq 0.006 \quad (21)$$

Where M_u and V_u are the applied factored moment and vertical shear at the critical section under consideration; P_e is the effective axial prestressing force acting on the section; E_s and E_p are the moduli of elasticity of reinforcing and prestressing steel, respectively; A_s and A_{ps} are the area of reinforcing and prestressing steel, respectively. For negative values of \mathcal{E}_s the equation becomes as follows:

$$\mathcal{E}_s = \frac{\left(\frac{M_u}{d}\right) + (V_u - V_p) - P_e}{(E_s A_s + E_p A_{ps} + E_c A_{ct})} \geq -0.0004 \quad (22)$$

Where E_c is the UHPC modulus of elasticity, and A_{ct} is the area of UHPC on the flexural tension side of the member measured from the mid-height of the section. The upper and lower bounds of \mathcal{E}_s are selected to provide an angle between 27.6 and 50.0 degrees. It should be noted that this model is based on the load and resistance factor design which utilizes a strength reduction factor and a load magnification factor. Strength reduction factors were not considered when the shear strength was predicted using that model in that paper. Also, the model assumes proper reinforcement is provided and developed in the flexural tension side of the critical section to achieve the full diagonal tension strength.

2.4.1.5 Draft of AASHTO Guide Specification for Structural Design with UHPC, 2021

A draft guide specification for the design of concrete elements fabricated with UHPC is currently being considered by the AASHTO CBS T-10 committee to be included in the next revision of the AASHTO LRFD, 2017. The document was developed by the Federal Highway Administration (FHWA) Turner-Fairbank Highway Research Center. Similar to the French standard AFGC, 2013 and AASHTO LRFD, 2017, the model is based on the MCFT with the analysis of the principal strains at critical sections. The nominal shear resistance of a member (V_n) is taken as the sum of the contributions of UHPC tensile strength (V_{UHPC}), shear reinforcement (V_s), and component of prestressing force resisting vertical shear (V_p). V_{UHPC} is calculated according to the following equation:

$$V_{UHPC} = \gamma f_{t,loc} b_w d \cot(\theta) \quad (23)$$

Where γ is a reduction factor to account for the variability of tensile stresses carried by UHPC (recommended not to exceed 0.85), $f_{t,loc}$ is the localization tensile strength of UHPC estimated by means of direct tension testing on (2 x 2 in²) prisms, other parameters are similar to what was described before. The crack angle (θ) in this model is limited to range from 25 to 45 degrees, and is estimated according to the following equations:

$$\begin{aligned} \mathcal{E}_{t,loc} = & \frac{\mathcal{E}_s}{2} (1 + \cot^2 \theta) + \frac{2f_{t,loc}}{E_c} \cot^4 \theta \\ & + \frac{2\rho_v f_v}{E_c} \sin \alpha \cot^2 \theta [1 + \cot^2 \theta + \cot \alpha (\tan \theta + \cot \theta)] \end{aligned} \quad (24)$$

$$\mathcal{E}_2 = -\frac{2f_{t,loc}}{E_c} \cot^2 \theta - \frac{2\rho_v f_v}{E_c} \sin \alpha [1 + \cot^2 \theta + \cot \alpha (\tan \theta + \cot \theta)] \quad (25)$$

$$\mathcal{E}_v = \mathcal{E}_{t,loc} - 0.5 \mathcal{E}_s + \mathcal{E}_2 \quad (26)$$

$$f_v = E_s \mathcal{E}_v \leq f_y \quad (27)$$

Where, $\mathcal{E}_{t,loc}$ is the localization strain obtained by the direct tension testing when the tensile stresses carried by the UHPC prism starts to decrease consistently, and recommended to be taken between 0.004 to 0.010 as discussed in section 2.3.1; \mathcal{E}_s is longitudinal strain at the level of reinforcement calculated as follows:

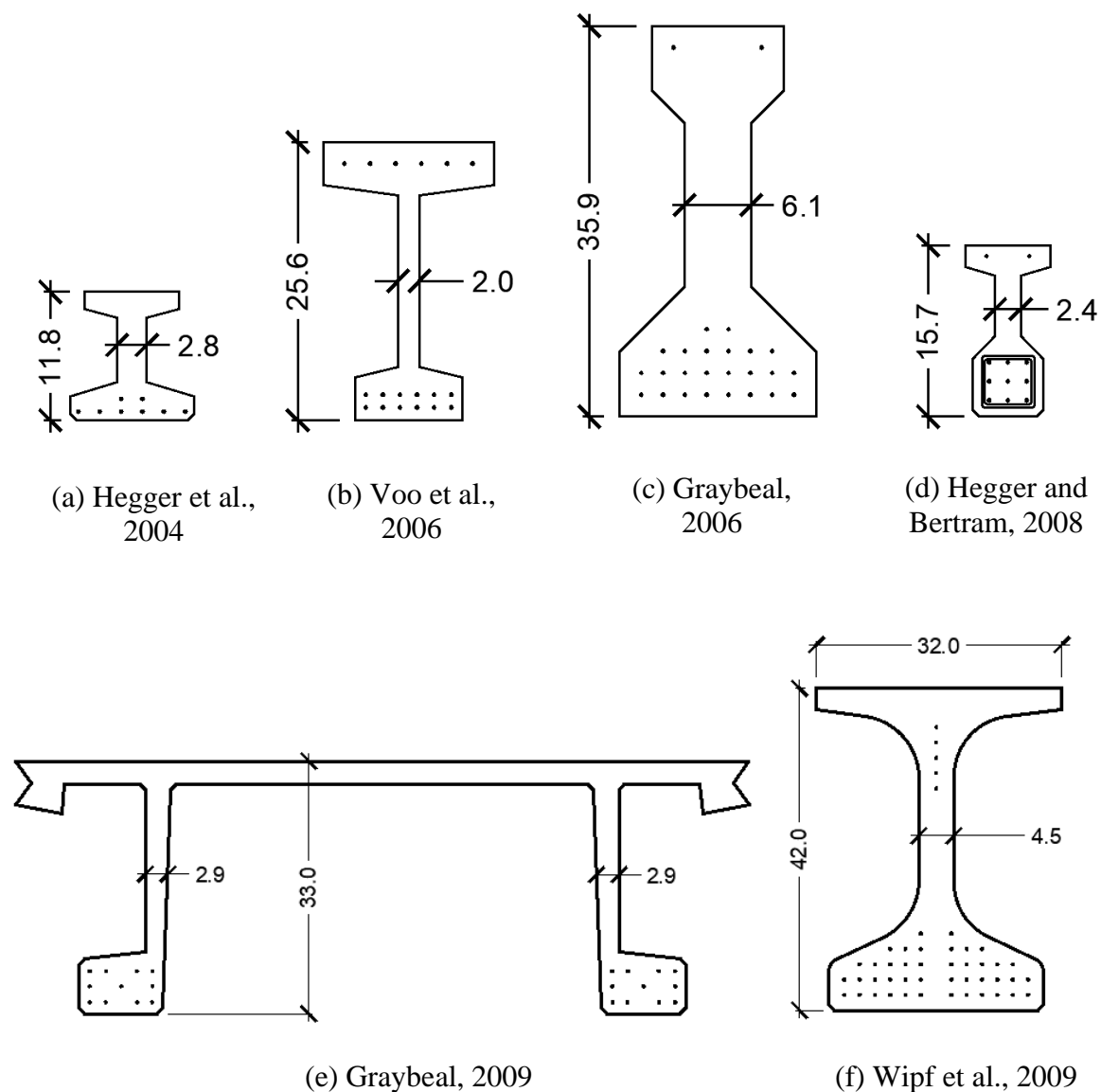
$$\mathcal{E}_s = \frac{\frac{|M_u|}{d_v} + 0.5 N_u + |V_u - V_P| - A_{ps} f_{po} - \gamma f_{t,loc} A_{ct}}{E_s A_s + E_p A_{ps}} \quad (28)$$

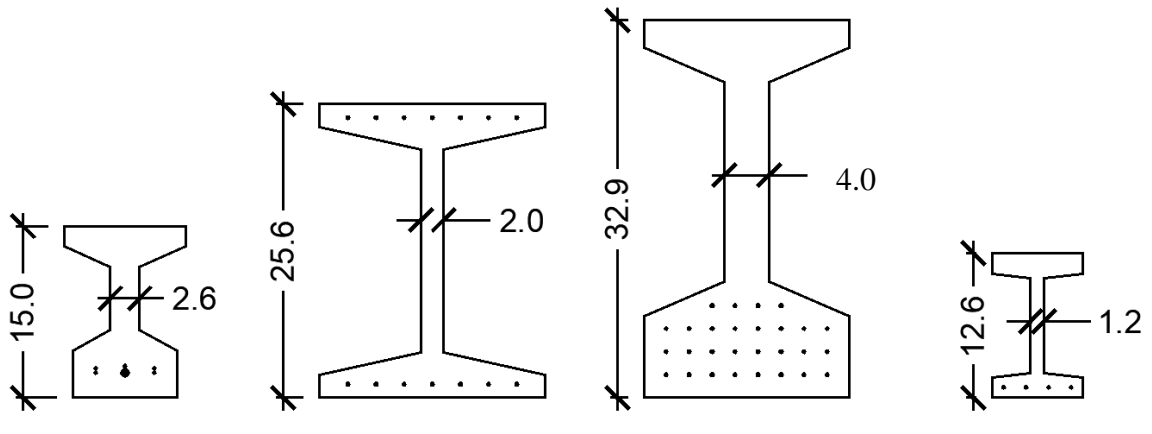
Where, $|M_u|$ is the absolute value of the factored moment at the design section, not to be taken less than $|V_u - V_P| d_v$; N_u is the factored axial force at the design section, taken as positive if tension and negative if compression; V_u is the factored shear force at the design section; A_{ps} and A_s are the area of prestressing steel and non-prestressed steel respectively in the flexural tension side of the member; f_{po} is the parameter taken as modulus of elasticity of prestressing steel multiplied by the locked-in difference in strain between the prestressing steel and surrounding UHPC and could be taken as 70% of the ultimate tensile strength of the strands for appropriate levels of prestressing; A_{ct} is the area of UHPC in the flexural tension side of the member; E_s and E_p are the moduli of elasticity of non-prestressed and prestressing steel respectively; ρ_v is the transverse reinforcement ratio calculated as the area of transverse reinforcement divided by bar spacing and web width; f_y is the stress in transverse reinforcement; \mathcal{E}_2 is the diagonal compressive strain in the section; and \mathcal{E}_v is the vertical strain in transverse reinforcement at the design section. Similar to the PCI-UHPC model, this model is based on the load and resistance factor design and the model also assumes proper reinforcement is provided and developed in the flexural tension side of the critical section.

2.4.2 Test Data of UHPC Beams in Shear

Table 8 and Table 9 present a summary of the shear experiments conducted on UHPC beams without transverse reinforcement and the main variables associated with each

experiment for prestressed and non-prestressed beams respectively. These experiments were collected from fifteen research programs and focus on UHPC beams reinforced longitudinally with conventional reinforcement (f_y ranging between 58 to 87 ksi) or prestressing strands (f_{pu} ranging between 246 to 270 ksi). All UHPC mixes in this study have straight fibers with a tensile strength in the range of 260 to 377 ksi, except Voo et al., 2006 who used a combination of straight and end hooked in some tests. All the specimens considered in this study had a shear span to depth ratio of at least 2.3 and experienced a diagonal tension failure. The rest of this section summarizes each of the shear test programs in the order presented in tables. Figure 32 shows the cross-section, width, and height of the fifteen experimental programs.



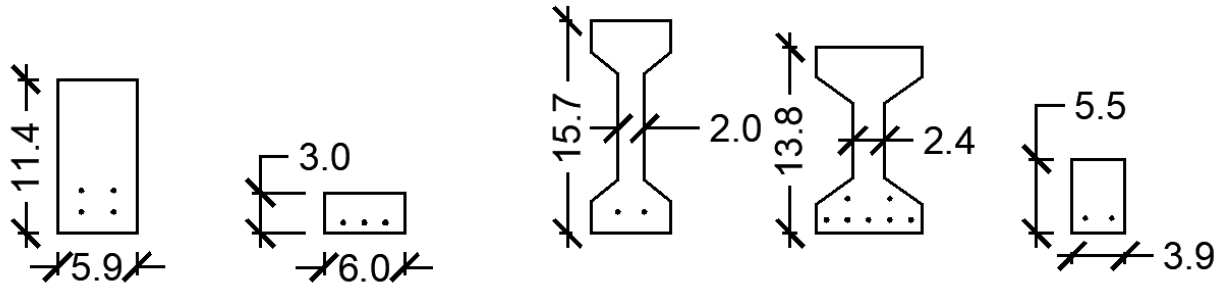


(g) Baby, et al., 2010

(h) Voo et al., 2010

(i) Crane, 2010

(j) Fehling et al., 2012



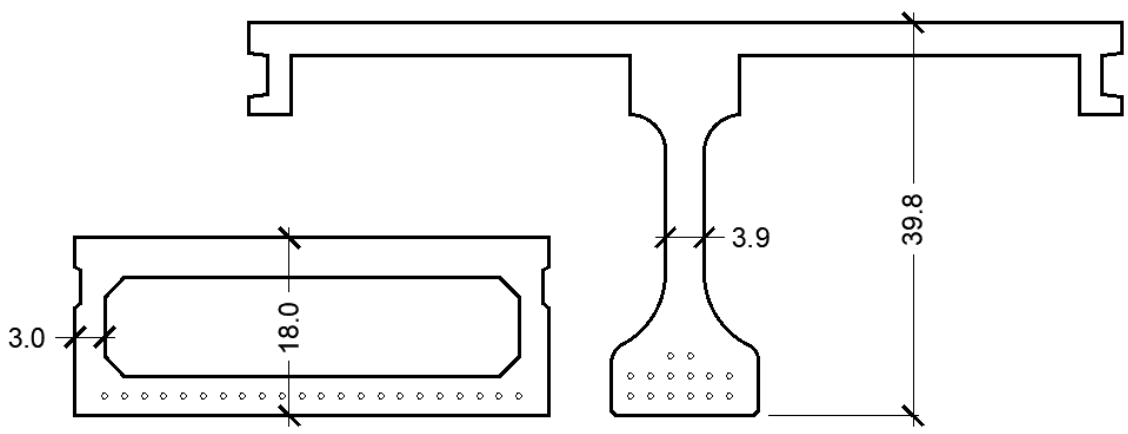
(k) Lim, et al., 2016

(l) Pourbaba, et al., 2018

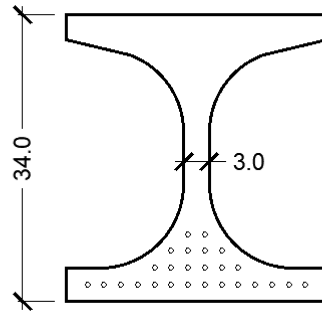
(m) Pansuk, et al., 2017

(n) Meszoly et al., 2018

(o) Ridha, et al., 2018



(p) Tadros et al., 2021



(p) Tadros et al., 2021

Figure 32: Girder cross-sections of the considered sixteen experimental programs, dimensions in inches

Hegger et al., 2004 performed an experiment on an I-beam reinforced with 8 strands on the bottom flange to investigate the bond anchorage behavior of the strands, in addition to the shear strength of the section. The test setup and shear failure mode are shown in Figure 33. Flexural tensile strength of 5.8 ksi was achieved for the 2.5% fiber volume mix having fiber length of 0.5 inch. The UHPC beam showed a brittle shear failure mode similar to other specimens made with high-strength concrete. The degree of utilization of the prestressing force was approximately 80% at the time of failure.



Figure 33: Shear failure mode, courtesy of Hegger et al., 2004

Voo et al., 2006 performed seven shear tests on prestressed I-beams having 12 strands (0.6-inch diameter) on the bottom flange and 6 strands on the top flange. Top strands were tensioned to carry half the prestressing force of the bottom strands. The girder cross-section and shear failure mode are shown in Figure 34. In five beams, the bottom strands were

tensioned to 15% of their yield strength (254 ksi), one beam was not tensioned at all, and one beam had the bottom strands tensioned to 30% of their yield strength. Bearing supports were placed 10 in. from the girder ends. Transfer length is reported to be about 10 in. for the 0.5 in. diameter strands and 14 in. for the 0.6 in. diameter strands, Bertram et al., 2012 and Russell et al., 2013. It was noticed that the failure crack pattern extended horizontally at the transition between the flanges (with prestressing strands) and the web until reaching the supports. The total fiber volume fraction was 2.5%. However, the used steel fibers were a combination of straight (type I) and end-hooked (type II) types. Specimens SB1, SB2, and SB3 contained only type I fibers, while specimens SB4, SB5, SB7 contained 1.25%, 1%, 0.62% type II fibers respectively, and specimen SB6 contained only type II fibers. Measured crack angles ranged between 21 to 37 degrees. Average flexural strength from notched three-point bending tests done on 3.9 x 3.9 in. prisms spanning 15.7 in. and notch depth of 1.0 in. was 3.4 ksi.

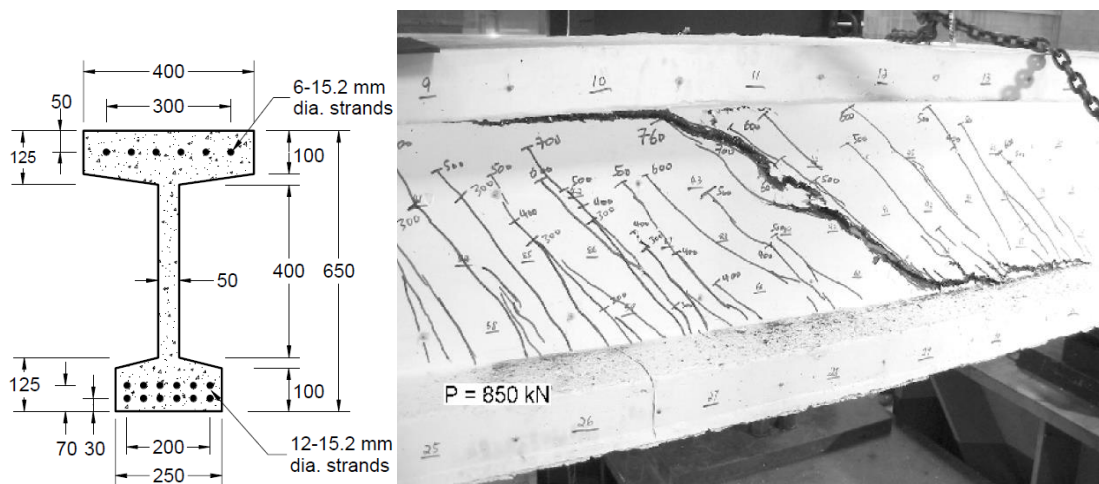


Figure 34: Girder cross-section (left), shear failure mode (right), courtesy of Voo et al., 2006

Graybeal, 2006 performed three shear experiments on prestressed AASHTO Type II girders having 24 strands in the bottom flange (12 strands were debonded). Debonding effects of prestressing strands at the end of the girders were minimized by placing the bearing supports 4 feet from the girder ends (except girder 14S end bearing was placed 5.9 in. from girder end). A simplified prediction model for shear strength was proposed by calculating the diagonal tension carried by UHPC. The girder cross-section and shear

failure mode are shown in Figure 35. The post-cracking diagonal tension strength for girders 24S and 14S was calculated inversely from the measured shear strength and resulted in 2.3, and 1.8 ksi respectively. The same procedure was followed on small-scale tests and the post-cracking diagonal tension strength was estimated to be 1.3 ksi which was considered a lower bound for un-reinforced webs with 2% steel fibers volume fraction.

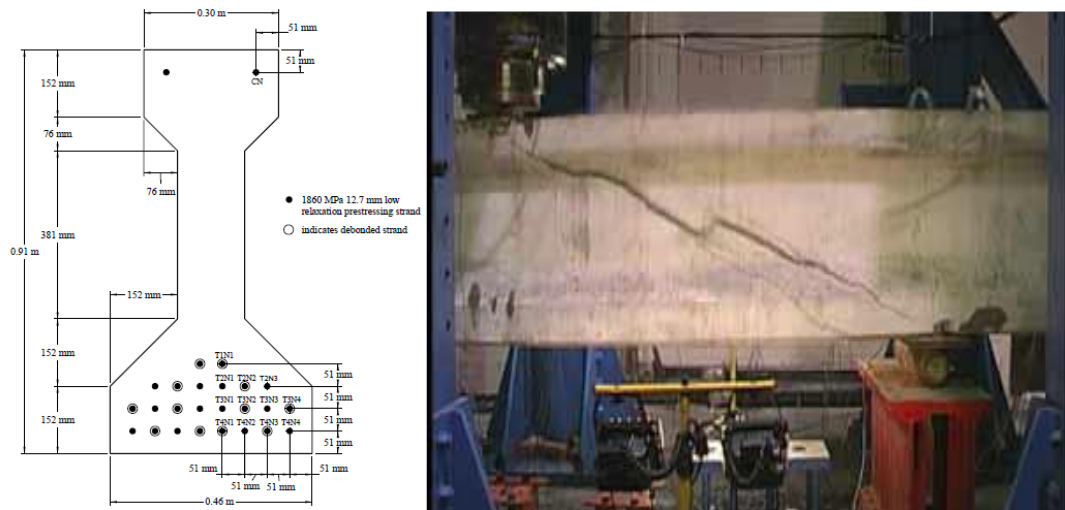


Figure 35: Girder cross-section (left), shear failure mode (right), courtesy of Graybeal, 2006

Hegger and Bertram, 2008 performed shear experiments on prestressed I-beams having 9 bottom strands (with 2 strands de-bonded). The girder cross-section is shown in Figure 36. The testing was done to evaluate the bond anchorage of the strands and the shear strength of the section with and without web openings. Five specimens without web openings were only considered in this study. Crack angle ranged between 20 and 24 degrees for the mixes having 0.9% fiber volume fraction.

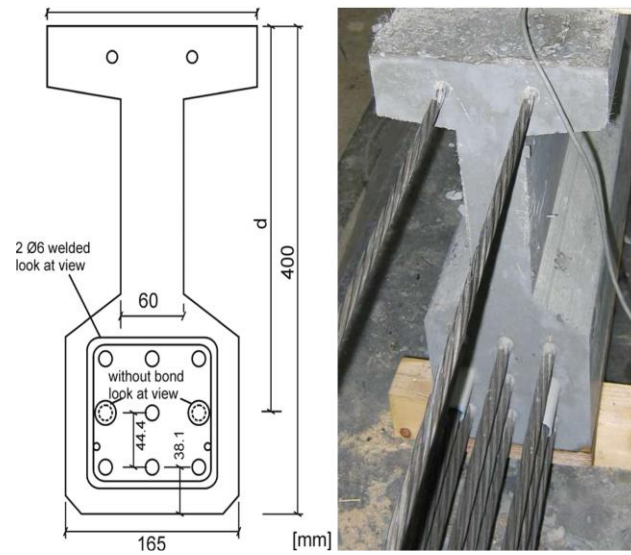


Figure 36: Girder cross-section, courtesy of Hegger and Bertram, 2008

Graybeal, 2009 performed several flexural and shear tests on pi-girders to optimize the design of the section using UHPC. Strands were placed symmetrically in the two bottom flanges, each flange had 11 strands with 3 strands de-bonded for 12 in., and 2 strands de-bonded for 72 in.. Two static shear experiments were performed with different shear spans on girders P2 and P4 that showed diagonal tension failure. For girder P2, supports were placed 24 in. away from the girder end to minimize the effect of debonding strands. While at girder P4 supports were placed only 6 in. from girder end. The prestressing force in the 72 in. de-bonded strands was not considered when predicting the ultimate shear strength as the debonding length is covering a significant portion of the shear span. The test setup and shear failure mode in one test are shown in Figure 37. Split cylinder cracking for the UHPC used in this program was 1.7 ksi, and direct tension cracking strength ranged between 1.4 to 1.6 ksi.



Figure 37: Shear failure mode, courtesy of Graybeal, 2009

Wipf et al., 2009 performed a shear experiment on one large scale prestressed I-beam. The beam had a slightly modified Iowa DOT Bulb Tee C standard cross-section. The beam contained 47 strands in the bottom flange, 8 strands were de-bonded for 42 in., and 16 strands were de-bonded for 78 in., 5 strands were harped towards the top of the web at the girder ends. The prestressing force in the 78 in. de-bonded strands were not considered when predicting the ultimate shear strength in this study as the debonding length is covering a significant portion of the shear span. The measured crack angle at failure was 25.3 degrees. Shear prediction analysis was performed and calibrated according to the test results based on the modified compression field theory and AFGC, 2002. The girder cross-section and shear failure mode are shown in Figure 38. The fiber contribution factor is determined using the maximum tensile strength of UHPC which was recommended to be taken as 1.7 ksi for the used mix having a 2% fiber volume fraction.

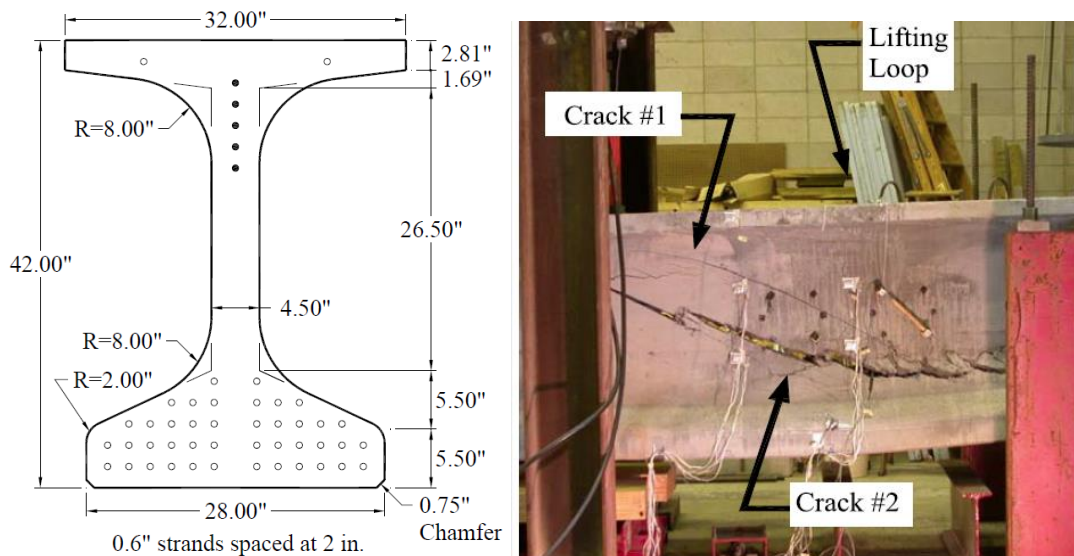


Figure 38: Girder cross-section (left), shear failure mode (right), courtesy of Wipf et al., 2009

Baby, et al., 2010 performed shear experiments on I-beams with the main test variables as the prestressing force (3 tests on prestressed, and 2 tests on non-prestressed beams) and fiber volume fraction (2 or 2.5%). The girder cross-sections for the prestressed and non-prestressed beams are shown in Figure 39. Bearing supports were placed 19.7 in. from the beam end. Test results from this program were later compared to the prediction models of RILEM TC 162-TDF, 2003, *fib* Model Code, 2010, and AFGC, 2002 by Baby, et al., 2013. It was concluded that RILEM TC 162-TDF, 2003 and *fib* Model Code, 2010 give similar predictions that are excessively conservative, while the AFGC, 2002 provided a reasonable and conservative prediction.

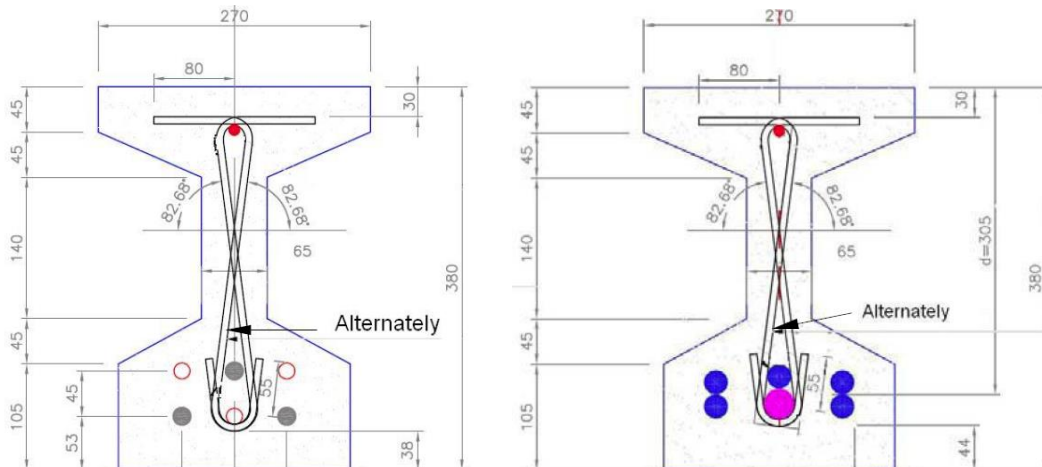


Figure 39: Non-prestressed girder cross-section (left), prestressed girder cross-section (right), courtesy of Baby, et al., 2010

Voo et al., 2010 performed shear experiments on prestressed I-beams having a slender web (2 in. thickness). The beams cross-section was symmetric about the neutral axis and had six strands on the top flange and six strands on the bottom flange having the same prestressing force. Bearing supports were placed 11.8 in. away from the girder end. Failure mode occurred from a tensile fracture across a single dominant crack or from a combination of cracks leading to the formation of a dominant crack. Average flexural strength from unnotched four-point bending tests done on 3.9 x 3.9 in. prisms spanning 11.8 in. was 2.0 ksi for the mixes having 0.6 in. fiber length.

Crane, 2010 performed six shear experiments on 32 in. deep bulb-tee girders with 8 in. thick cast in place high-performance concrete deck having 12.2 ksi compressive strength. Crack angles ranged between 23 to 34 degrees. Due to the large difference in concrete properties between girder and deck, the effective shear depth was based only on the girder and not the composite section. The girder cross-section and shear failure mode in one test are shown in Figure 40. Measured shear capacities were compared against prediction models from two approaches. The first approach was based on calculating the direct tensile strength of the girder web over the failure angle, a direct tension strength of 1.4 ksi was used based on previous research of a similar mix. The second approach was based on the AFGC, 2002 in which a separate fiber contribution term is introduced, the residual rupture/tensile strength was taken as 1.0 ksi based on previous research. It was concluded that the AFGC, 2002 model provided a closer estimate to the measured shear strength than the direct tension approach with an average of less than 15% than the average measured strength.

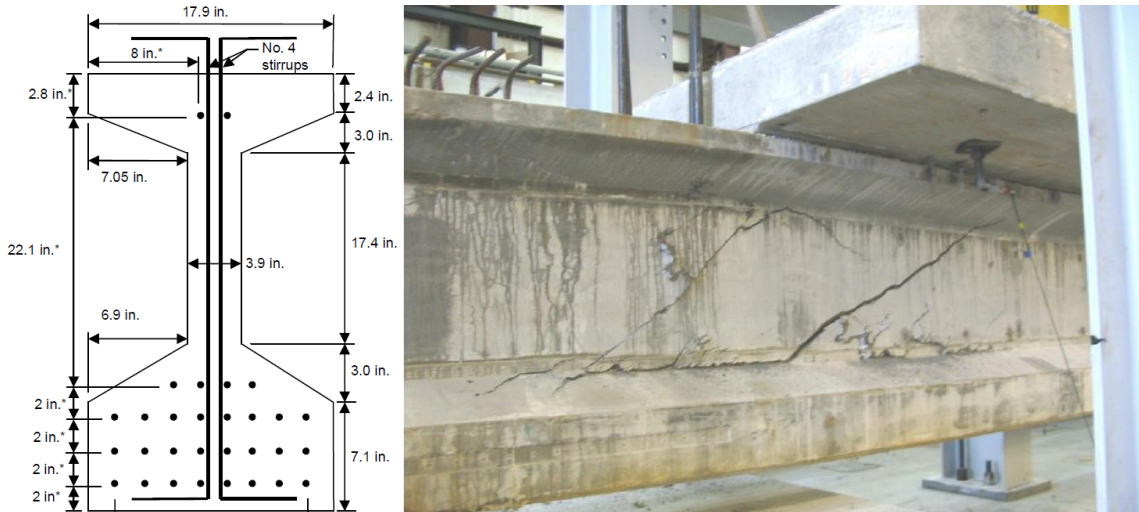


Figure 40: Girder cross-section (left), shear failure mode (right), courtesy of Crane, 2010

Fehling et al., 2012 performed shear experiments on rectangular non-prestressed beams having an I-shaped section on their shear span at which diagonal tension failure occurred, the remainder of the span was a rectangular section. The beam cross-section is shown in Figure 41, and the shear failure mode in one test is shown in Figure 42. Bending tensile strength of 1.6 x 1.6 in. prisms having a length of 6.3 in. was 3.4 ksi for the prisms having 1% fiber volume fraction. Crack angle ranged between 30 and 45 degrees.

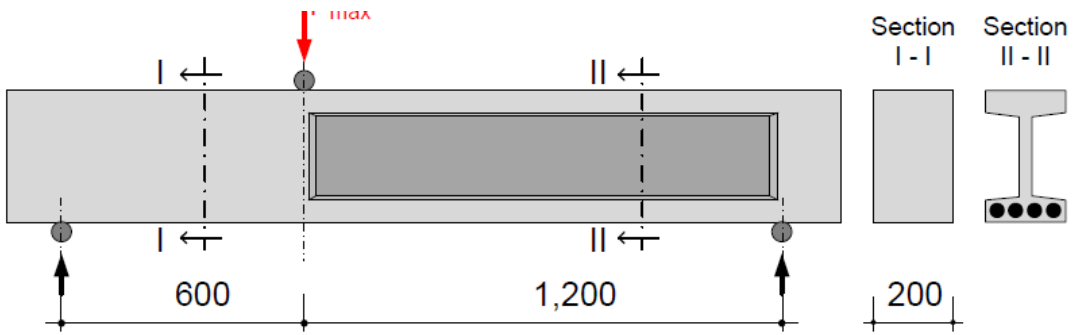


Figure 41: Shear test setup (left), beam cross-sections (right), courtesy of Fehling et al., 2012

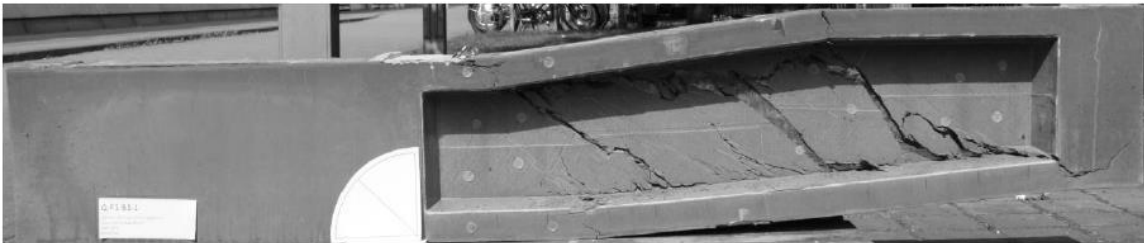


Figure 42: Shear failure mode, courtesy of Fehling et al., 2012

Lim, et al., 2016 performed shear experiments on rectangular beams with the main test variable as the transverse shear reinforcement ratio. Only one specimen (out of four) contained no transverse reinforcement and showed diagonal tension failure which was considered in this study. Shear strength was predicted using several research models, as well as the AFGC, 2013 prediction model. All considered researcher prediction models underestimated the shear strength significantly, while the AFGC, 2013 provided reasonable estimation (1.37 times the measured shear strength). Average direct tensile strength was 1.7 ksi for the used UHPC mix which was used to predict the AFGC, 2013 shear strength.

Pourbaba, et al., 2018 performed several shear experiments on non-prestressed rectangular beams with the main test variables as section dimensions, longitudinal reinforcement ratio, and shear span-to-depth ratio. Measured shear strength was compared against some code prediction models which were found to be excessively conservative.

Pansuk, et al., 2017 performed four shear experiments on I-beams with main test variables as fiber volume fractions and transverse reinforcement ratio. The average splitting tensile strength was 2.4 and 2.2 ksi for 1.6% and 0.8% fiber volume fraction mixes respectively. *fib* Model Code, 2010 and AFGC, 2002 prediction models were compared to measured shear strength. It was concluded that the *fib* Model Code, 2010 model provided a much higher margin of safety compared to AFGC, 2002.

Meszoly et al, 2018 performed shear experiments on I-beams with the main test variables as fiber volume fraction and transverse shear reinforcement. Measured shear strength was compared to the AFGC, 2013 prediction model, ($\sigma_{R,f}$) was determined by performing flexural tests on prisms $5.9 \times 5.9 \times 27.6$ in³. Results were back-calculated with an inverse analysis procedure as recommended and ($\sigma_{R,f}$) was estimated to be 0.73 and 0.91 ksi for the mixes with 1% and 2% fiber volume fraction respectively.

Ridha, et al., 2018 performed shear experiments on rectangular beams with the main test variables as the shear span-to-depth ratio, longitudinal reinforcement ratio, and fiber volume fraction. The test setup and beam cross-section are shown Figure 43. Average

splitting tensile strength was 1.3, 1.6, 2.1, and 2.3 ksi for mixes having 0.5%, 1.0%, 1.5%, and 2.0% fiber volume fraction respectively.

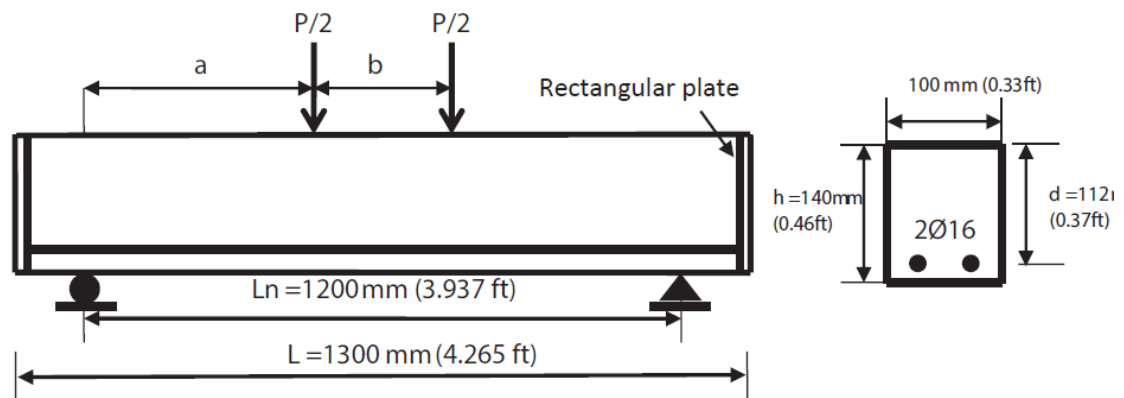


Figure 43: Shear test setup (left), beam cross-section (right), courtesy of Ridha, et al.,

2018

Table 8: Shear experiments review on prestressed UHPC beams

Reference	Specimen ID	Specimen Shape	b_w (in.)	d (in.)	h (in.)	V_f %	a/d	A_{ps}/b_wd	σ_{cp} (ksi)	f'_c (ksi)	l_f (in.)	Φ_f (in.)	$\sigma_{Rd,f}$ (ksi)	V_u (kip)	$(\frac{V_u}{b_wd})$ (ksi)	
Hegger et al., 2004	1	I-beam	2.8	9.8	11.8	2.5	5.4	6.80%	3.9	23.9	0.5	0.006	1.8	61.0	2.3	
Voo et al., 2006	SB2	I-beams	2.0	23.6	25.6	2.5	3.3	2.70%	1.0	23.2	0.5 Type I	0.008 Type I	1.4	111.7	2.4	
	SB3												1.2	96.2	2.0	
	SB4												0.8	75.6	1.6	
	SB5												1.4	98.9	2.1	
	SB6												1.3	74.2	1.6	
	SB7												1.3	89.9	1.9	
Graybeal, 2006	28S	AASHTO Type II	6.1	31.6	35.8	2.0	2.5	1.90%	1.3	28.0	0.5	0.008	1.6	383.9	2.0	
	24S						2.8						1.6	501.9	2.6	
	14S						2.3						1.6	437.7	2.3	
Hegger and Bertram, 2008	T1a	I-beams	2.4	12.5	15.7	0.9	3.8	4.60%	3.6	21.9	0.7	0.006	0.7	52.6	1.8	
	T1b									25.2			0.7	60	2.0	
	T3b					2.5				24.7	0.35		1.6	91.7	3.1	
	T4a					0.9				25.5	0.7		0.7	77.3	2.6	
	T4b									4.4			26.5	0.7	65.4	2.2
Graybeal, 2009	P 2-21S	Pi-girders	6.6	29.4	33.0	2.0	2.9	1.73%	0.9	33.2	0.5	0.008	1.7	430	2.2	
	P4-57SH						2.4						1.5	366.0	1.9	
Wipf et al., 2009	1	I-beams	4.5	36.5	42.0	2.0	2.5	5.6%	3.1	19.8	0.5	0.008	1.7	594	3.6	
Baby et al., 2010	Beam 1-A	I-beams	2.6	12.0	15.0	2.5	2.5	4.10%	2.5	22.6	0.8	0.012	1.7	99.2	3.2	
	Beam 1-A-bis													23.4	99.0	3.2
	Beam 1-B					2.0					24.6			0.5	0.008	115.9
Voo et al., 2010	X-B1	I-beams with Symmetric Prestressing	2.0	24.4	25.6	1.0	3.2	2.60%	2.2	18.1	0.6	0.008	0.6	74.2	1.5	
	X-B2									18.3			0.8	79.8	1.6	
	X-B3									19.6			0.7	81.4	1.7	
	X-B4									2.5			17.7	0.7	102.4	2.1
	X-B5									3.5			20.3	1.0	95.0	1.9
	X-B6									4.5			20.3	1.0	87.8	1.8
	X-B7					1.5				17.7			1.1	117.2	2.4	
Crane, 2010	1-2	Bulb-Tee with cast-in-place HPC decks	3.9	28.3	32.9	2.0	3.4	3.90%	2.4	29.0	0.5	0.008	1.6	431.0	3.9	
	2-1													466.0	4.2	
	3-1													422.0	3.8	

Table 8, continued

Reference	Specimen ID	Specimen Shape	b_w (in.)	d (in.)	h (in.)	V_f %	a/d	A_{ps}/b_wd	σ_{cp} (ksi)	f_c' (ksi)	l_f (in.)	Φ_f (in.)	$\sigma_{Rd,f}$ (ksi)	V_u (kip)	$(\frac{V_u}{b_wd})$ (ksi)			
Tadros et al., 2021	IA1	I-beams	3.0	28.9	34.0	2%	2.9	6.5%	2.6	22.4	0.5	0.008	1.6	359	4.1			
	IA2									17.4			1.0	311	3.6			
	IA3									18.3			1.0	308	3.6			
	IA8									18.2			1.2	359	4.1			
	IA13		2.0					9.8%		2.8			18.3	1.1	236	4.1		
	IA14		4.0					4.9%		2.5			18.3	1.0	410	3.5		
	DIB – Test 1	Decked I-Beam	3.9	36.4	39.8		2.7	2.2%	0.9	20.0			1.5	355	2.5			
	BX-1	Box Section	6.0	16.0	18.0		2.8	3.5%	1.4	19.8			1.2	273	2.8			
	BX-2												1.2	256	2.7			
		Maximum	6.6	36.5	42.0		2.5	5.4	6.80%	3.9			33.2	1.2	0.020	1.8	594	4.2
		Minimum	2.0	9.8	11.8		0.9	2.3	1.73%	0.9			17.7	0.35	0.006	0.6	52.6	1.5

Table 9: Shear experiments review on non-prestressed UHPC beams

Reference	Specimen ID	Specimen Shape	b_w (in.)	d (in.)	h (in.)	V_f %	a/d	$\frac{A_l}{b_w d}$	f_c' (ksi)	l_f (in.)	Φ_f (in.)	$\phi_{Rd,f}$ (ksi)	V_u (kip)	$(\frac{V_u}{b_w d})$ (ksi)	
Voo et al., 2006	SB1	I-beams	2.0	23.6	25.6	2.5	3.3	2.70%	23.3	0.5 Type I 1.2 Type II	0.008 Type I 0.020 Type II	1.6	96.7	2.0	
Baby et al., 2010	Beam 3-A	I-beams	2.6	12	15.0	2.5	2.5	4.80%	22.6	0.8	0.012	1.7	103.7	3.4	
	Beam 3-B					2.0	2.5	4.80%	24.6	0.5	0.008		102.3	3.3	
Fehling et al., 2012	Q-F1-2	Shear span was I-shaped	1.2	11.6	12.6	1.0	4.1	6.60%	29.1	0.5	0.007	1.3	24.3	1.8	
	Q-F1-3								30.0				24.3	1.8	
	Q2-F1-1								26.8				22.5	1.6	
Lim et al., 2016	SB1	Rectangular Beams	5.9	9.5	11.4	1.5	2.8	7.30%	24.2	0.63 and 0.75	0.008	1.4	107.0	1.9	
Pourbaba et al., 2018	B35	Rectangular Beams	6.0	2.2	3.0	1.5	2.7	5.60%	19.9	0.5	0.007	1.4	23.8	1.8	
	B36							4.00%					19.1	1.4	
	B37							2.70%					16.0	1.2	
Pansuk et al., 2017	NS08	I-beams	2.0	13.8	15.8	0.8	2.9	5.50%	21.4	0.5	0.008	1.6	76.4	2.8	
	NS16					1.6			21.3			2.5	119.4	4.4	
Meszoly et al., 2018	B19	I-beams	2.4	11.6	13.8	2.0	3.7	5.06%	18.6	0.6	0.008	1.0	1.6	89.2	3.3
	B20					1.0			18.8				1.0	94.2	3.4
	B24					1.0			20.2				1.0	70.8	2.6
	B25					2.0			21.7				1.6	113.5	4.1
	B29					2.0			21.6				1.0	109.5	4.0
	B30					2.0			20.6				1.6	127	4.6
Ridha et al., 2018	B5	Rectangular Beams	3.9	4.4	5.5	2.0	3.5	2.87%	16.0	0.5	0.008	1.0	18.5	1.1	
	B6						2.5						24.2	1.4	
	B7						3.0						25.3	1.5	
	B10						3.0						28.1	1.6	
	B11						3.5		21.9			1.3			
	B16						3.5		18.1			1.1	21.1	1.2	
	B17						3.5		20.6			1.1	22.7	1.3	
	B18						3.5		21.9			1.1	24.7	1.4	
	Maximum		6.0	23.6	25.6	2.5	4.1	7.30%	30.0	1.2	0.020	2.5	127	4.4	
	Minimum		1.2	2.2	3.0	0.8	2.5	2.70%	16.0	0.35	0.007	1.0	16.0	1.1	

2.4.3 Test Data of CC-UHPC Beams in Shear

2.4.3.1 Aghani et al., 2016

Eight rectangular beams (4.0 x 8.0 in.²) with limited shear reinforcement were tested in a three-point bending test as shown in Figure 44 and summarized in Table 10. Four beams were considered as control beams, while the other four beams were strengthened with prefabricated UHPC sheets having a thickness of 1.2 inches. The UHPC used had a compressive strength of 20.3 ksi, and steel fibers length of 1.2 in. and diameter of 0.03 in. The UHPC sheets were bonded to the concrete beam using epoxy adhesive having a tensile strength of 4.3 ksi. No debonding between the beam and UHPC sheets was reported. UHPC sheets were able to change the failure mechanism of the beams, increase their stiffness, ductility, and failure load significantly.

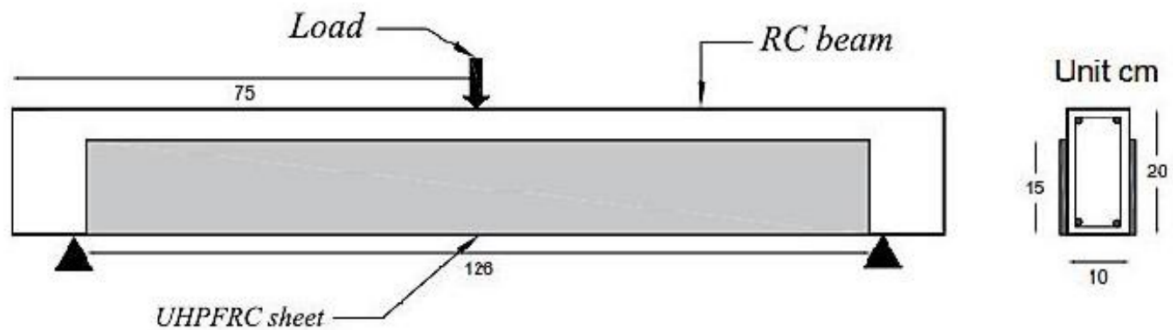


Figure 44: Three-point bending test of a strengthened beam, courtesy of Aghani et al., 2016

Table 10: Summary of tested specimens and failure modes, Aghani et al., 2016

Specimen ID	Specimen Type	A_1 (in ²)	A_v (in ² /ft)	Failure Load (kip)	Failure Mode
S1	Control	0.35	0.067	13.1	Shear
S2				13.4	
S3-re	Strengthened			16.4	Flexure
S4-re				16.3	
B1	Control	0.24		8.1	Flexure-Shear
B4				8.6	
B3-re	Strengthened			10.7	Flexure
B2-re				10.5	

2.4.3.2 Al-Osta et al., 2016

Seven rectangular beams (5.5 x 9.0 in.) shown in Figure 45 were tested in a four-point bending test as summarized in Table 11. The thickness of added UHPC jackets was 1.2 in. constant in all cases. The beams were reinforced longitudinally ($A_1 = 0.24$ in.²) and transversally ($A_v = 0.95$ in.²/ft). Two bonding mechanisms were tested: roughening the base concrete surface by sandblasting then casting UHPC and bonding prefabricated UHPC sheets using epoxy adhesive (tensile strength of 2.9 ksi). The bond strength of the interface was estimated by split tensile testing on composite UHPC-conventional concrete cylinders according to ASTM standards. The sandblasted surface showed a bond strength of 0.54 ksi. The conventional concrete had a compressive strength of 7.8 ksi. While the UHPC used had a compressive strength of 18.6 ksi, split tensile strength of 2.5 ksi, and flexural strength of 2.2 ksi. A mix of straight and end-hooked fibers were used in the UHPC (with a ratio of 1:1), the end-hooked fibers had a length of 1.0 in. and a diameter of 0.008 in., while the straight fibers had a length of 0.5 in. and a diameter of 0.004 in. The addition of UHPC jackets increased the flexural strength significantly, having a 3-sided jacket resulted in almost double the flexural strength.

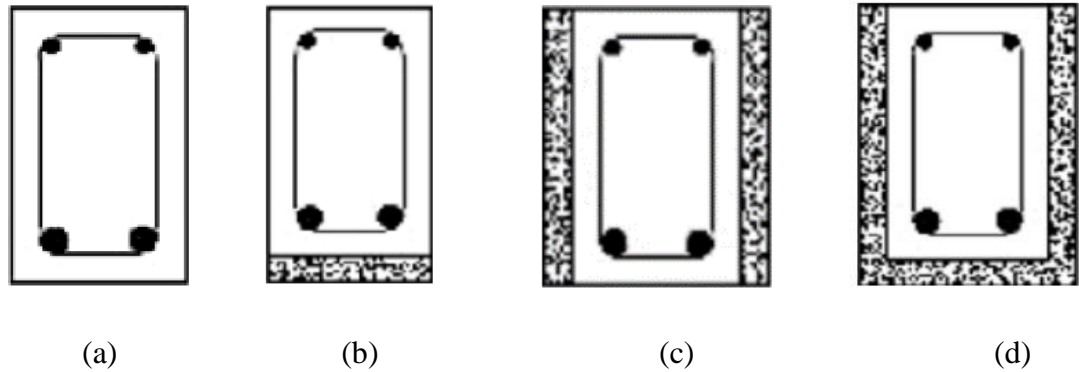


Figure 45: Tested specimens, (a) Control Beam, (b) BOT SJ, (c) 2 SJ, (d) 3SJ, courtesy of Al-Osta et al., 2016

Table 11: Summary of tested specimens and failure modes, Al-Osta et al., 2016

Specimen ID	Specimen Type	Bonding Mechanism	Failure Load (kip)	Failure Mode
Control	Control	N/A	15.7	Flexure
SB – BOTSJ	Bottom jacket	Sandblasting conventional concrete then casting UHPC	18.2	
SB – 2 SJ	Two sides jacket		22.9	
SB – 3 SJ	Three sides jacket		29.7	
EP – BOTSJ	Bottom jacket	Prefabricated sheets bonded by epoxy adhesive	16.9	
EP – 2 SJ	Two sides jacket		21.4	
EP – 3 SJ	Three sides jacket		29.0	

2.4.3.3 Bahraq et al., 2019

Nine rectangular beam specimens (5.5 x 9.0 in.²) were tested in a four-point bending configuration as shown in Figure 46 and summarized in Table 12. The beams were divided into three main groups with variable shear span-to-depth ratio. All beams had bottom longitudinal reinforcement ($A_l = 0.97$ in.²), and top longitudinal reinforcement of 0.35 in.². In each group, a control beam was tested without strengthening as a reference. Then, a 1.2-inch layer of UHPC was cast on the two sides of the beam for one test and the two sides and bottom surface of the beam (U-wrap). The interface between conventional concrete

and UHPC was prepared by sandblasting which remained intact, and no failure was recorded in any of the tests. The used UHPC had a compressive strength of 21.9 ksi, and direct tensile strength of 1.3 ksi (obtained on dogbone shaped specimens tested uniaxially). The controlled beams failed consistently in shear, while the strengthened beams showed considerably higher failure loads in flexure or flexure-shear modes.

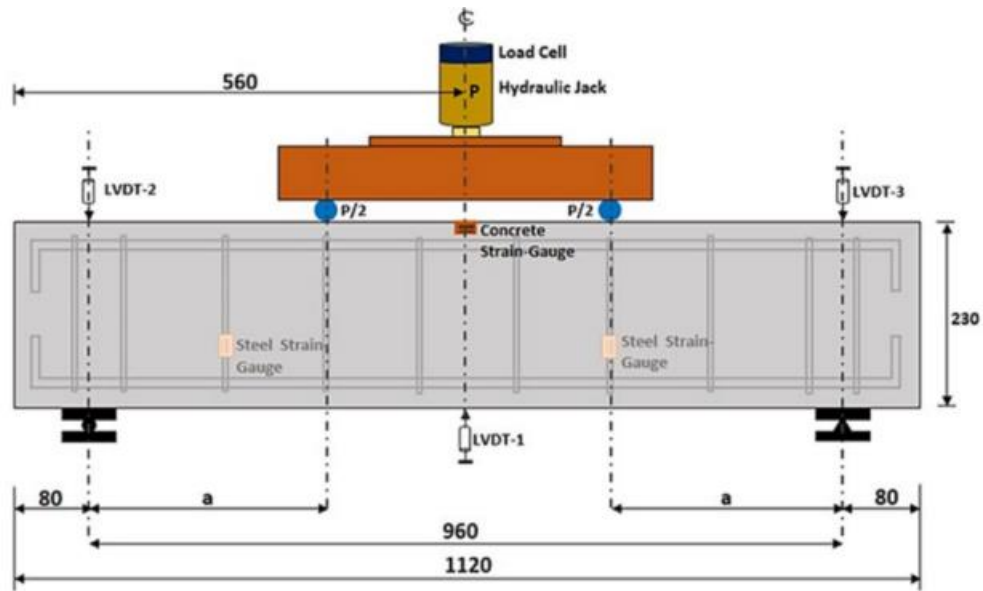


Figure 46: Four-point bending test setup, courtesy of Bahraq et al., 2019

Table 12: Summary of tested specimens and failure load, Bahraq et al., 2019

Specimen	Specimen Type /UHPC Layers Location	Shear span-to- depth	A_v (in. ² /ft)	V_u (kip)	Failure Mode
CT-1.0	Control	1.0	0.20	9.7	Shear
SB-2SJ-1.0	2 Side Layers			14.3	Flexure - Shear
SB-3SJ-1.0	U-Wrap			15.9	Flexure
CT-1.5	Control	1.5		7.2	Shear
SB-2SJ-1.5	2 Side Layers			10.2	Flexure - Shear
SB-3SJ-1.5	U-Wrap			12.2	Flexure
CT-2.0	Control	2.0		7.0	Shear
SB-2SJ-2.0	2 Side Layers			8.7	Flexure - Shear
SB-3SJ-2.0	U-Wrap			8.9	Flexure

2.4.3.4 Sakr et al., 2019

Seven rectangular beams were tested in a four-point bending configuration as shown in Figure 47 and summarized in Table 13. Three control beams were tested: beam (C-S) having limited shear reinforcement to be strengthened in shear, beam (C-F) having higher shear reinforcement representing the target repaired section capacity, and beam (C-S-210) having limited shear reinforcement with larger section dimensions representing the strengthened section dimensions. Prefabricated UHPC layers were bonded on four beams, in which two beams were unreinforced and two contained additional reinforcement, two beams had the UHPC layer bonded on one side and the other two had the UHPC layer bonded on the two sides. Figure 48 shows the strengthening schemes considered in this study. UHPC was bonded to the conventional concrete using an epoxy adhesive having a tensile strength of 3.3 ksi. For the reinforced specimens (ST-1S-R and ST-2S-R) 0.4-inch diameter holes were drilled though an embedment depth of 2.8 inch to connect the

additional transverse reinforcement. The used UHPC in this study had a compressive strength of 19.6 ksi, and a tensile strength of 1.6 ksi. The addition of UHPC sheets increased the failure load significantly reaching a maximum of 145% when comparing the control beam with limited shear reinforcement (C-S) to the strengthened beam with reinforced UHPC (ST-2S).

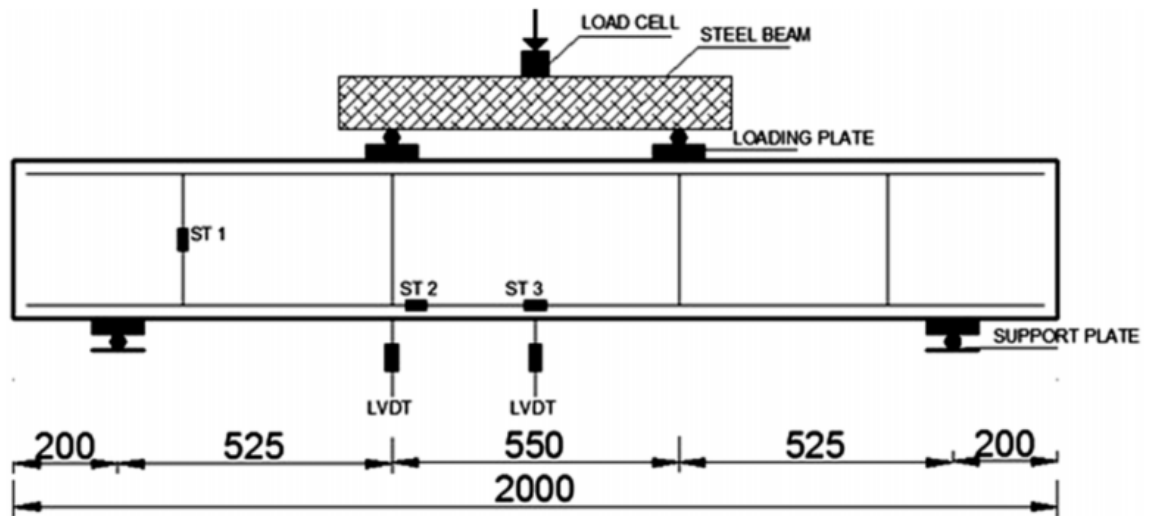


Figure 47: Four-point bending test setup, courtesy of Sakr et al., 2019

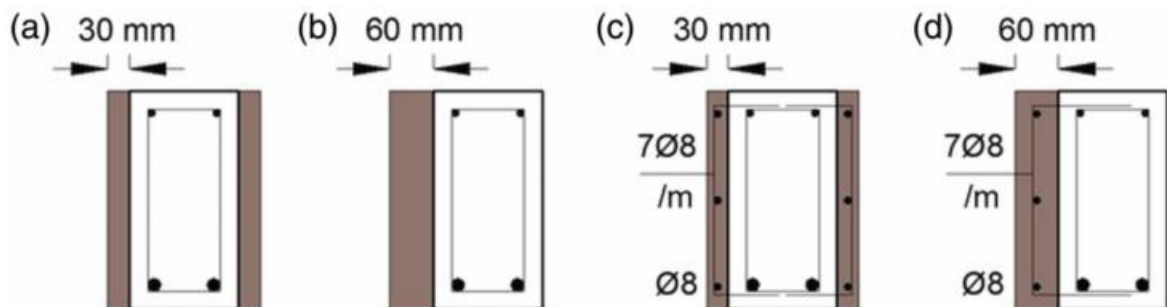


Figure 48: Beam strengthening schemes, courtesy of Sakr et al., 2019

Table 13: Summary of tested specimens and failure load, Sakr et al., 2019

Specimen	Specimen Type	Overall Dimensions (in. x in.)	Longitudinal Reinforcement (in ²)	Transverse Reinforcement (in ² /ft)	Failure Load (kip)	Failure Mode
C-S	Control	5.9 x 11.8	0.79	0.12	13.0	Shear
C-F	Control	5.9 x 11.8		0.48	28.5	Flexure
C-S-210	Control	8.3 x 11.8		0.12	23.7	Shear
ST-2S	2-side Unreinforced UHPC	8.3 x 11.8		0.12	31.6	Flexure
ST-1S	1-side Unreinforced UHPC	8.3 x 11.8		0.12	17.2	Interface
ST-2S-R	2-side Reinforced UHPC	8.3 x 11.8	0.95	0.41	37.2	Flexure - Shear
ST-1S-R	1-side Reinforced UHPC	8.3 x 11.8		0.41	28.3	Flexure - Shear

Table 14 shows a summary on the four testing programs in shear strengthening. Table 15 show an estimation of the UHPC contribution to the shear strength of the strengthened section by comparing the results of the strengthened beams to the reference beams. It can be noticed that the resulting shear strength of UHPC is significantly under the typical values of UHPC beams presented in section 2.4.2. This can be attributed to the flexural failure in all test data causing the UHPC to be significantly under-utilized.

Table 14: Summary of previous testing done on strengthening conventional concrete beams using UHPC jackets in shear

Reference	CC Compressive Strength (ksi)	Specimen ID	Specimen Type/UHPC repair scheme	a/d	b (in.)	d (in.)	h (in.)	UHPC Compressive Strength (ksi)	UHPC location	Bonding Mechanism	A _l (in ²)	A _v (in ² /ft)	V _u (kip)	Failure Mode	($\frac{V_u}{b_w d}$) (ksi)	
Aghani et al., 2016	4.9	S1	Control	3.6	3.9	6.9	7.9	N/A	N/A	N/A	0.35	0.067	6.6	Shear	0.25	
		S2											6.7		0.25	
		S3-re	Prefabricated Sheets 1.2 x 5.9 in ²					6.3	20.3	2 Sides			Epoxy adhesive	8.2	Flexure	0.18
		S4-re						8.2	0.18							
		B1	Control					3.9	N/A	N/A	N/A		4.1	Flexure-Shear	0.16	
		B4						4.3	0.16							
		B3-re	Prefabricated Sheets 1.2 x 5.9 in ²					6.3	20.3	2 Sides	Epoxy adhesive		0.24	5.4	Flexure	0.12
		B2-re												5.3		0.12
Al-Osta et al., 2016	7.8	Control	Control	2.8	5.5	8.1	9.1	18.6	N/A	N/A	0.24	0.95	7.9	Flexure	0.18	
		SB – 2 SJ	Casting UHPC on roughened CC		7.9				9.1	2 Sides			Sandblasting (0.08 in. depth)		11.5	0.18
		SB – 3 SJ			7.9				10.3	U-wrap			14.9		0.23	
		EP – 2 SJ	Prefabricated UHPC strips		7.9				9.1	2 Sides			Epoxy adhesive		10.7	0.17
		EP – 3 SJ			7.9				10.3	U-wrap			14.5		0.23	
Bahraq et al., 2019	8.6	CT-1.0	Control	1.0	5.5	8.0	9.0	21.9	N/A	N/A	0.97	0.20	9.7	Shear	0.22	
		SB-2SJ-1.0	2 Sides		7.9				9.0	2 Sides			Sandblasting	14.3	Flexure - Shear	0.23
		SB-3SJ-1.0	U-Wrap		7.9				10.2	U-Wrap			15.9	Flexure	0.25	
		CT-1.5	Control	1.5	5.5				9.0	N/A			N/A	7.2	Shear	0.16
		SB-2SJ-1.5	2 Sides		7.9				9.0	2 Sides			Sandblasting	10.2	Flexure - Shear	0.16
		SB-3SJ-1.5	U-Wrap		7.9				10.2	U-Wrap			12.2	Flexure	0.19	
		CT-2.0	Control	2.0	5.5				9.0	N/A			N/A	7.0	Shear	0.16
		SB-2SJ-2.0	2 Sides		7.9				9.0	2 Sides			Sandblasting	8.7	Flexure - Shear	0.14
		SB-3SJ-2.0	U-Wrap		7.9				10.2	U-Wrap			8.9	Flexure	0.14	
Sakr et al., 2019	4.3	C-S	Control	3.0	5.9	10.8	11.8	19.6	N/A	N/A	0.79	0.41	0.12	13.0	Shear	0.20
		C-F			5.9								0.48	28.5	Flexure	0.45
		C-S-210			8.3								0.12	23.7	Shear	0.26
		ST-2S	Unreinforced UHPC		8.3				2 Sides	Epoxy adhesive			0.12	31.6	Flexure	0.35
		ST-1S			8.3				1 Side				0.12	17.2	Interface	0.19
		ST-2S-R	Reinforced UHPC		8.3				2 Sides	0.95			37.2	Flexure - Shear	0.41	
		ST-1S-R			8.3				1 Side	28.3			Flexure - Shear	0.32		

Table 15: Calculating UHPC contribution to the shear strength

Reference	Specimen ID	Specimen Type/UHPC repair scheme	b_{UHPC} (in.)	d_{UHPC} (in.)	h_{UHPC} (in.)	$(V_{cc} + V_s)$ (kip)	(V_{UHPC}) (kip)	$(\frac{V_{cc} + V_s}{b_w d})$ (ksi)	$(\frac{V_{UHPC}}{b_w d})$ (ksi)
Aghani et al., 2016	S1	Control	0	0	0	6.7	0	0.25	0
	S2						0.14		
	S3-re	Prefabricated Sheets 1.2 x 5.9 in ²	2.4	4.9	5.9		1.6		0.14
	S4-re					1.6			
	B1	Control	0	0	0	4.2	0	0.16	0
	B4						0.10		
	B3-re	Prefabricated Sheets 1.2 x 5.9 in ²	2.4	4.9	5.9		1.2		0.09
B2-re	1.1								
Al-Osta et al., 2016	Control	Control	0	0	0	7.9	0	0.18	0
	SB – 2 SJ	Casting UHPC on roughened CC	2.4	8.1	9.1		3.6		0.19
	SB – 3 SJ				10.3		7.0		0.36
	EP – 2 SJ	Prefabricated UHPC strips			9.1		2.8		0.14
	EP – 3 SJ				10.3		6.6		0.34
Bahraq et al., 2019	CT-1.0	Control			0	0	0	9.7	0
	SB-2SJ-1.0	2 Sides	2.4	8.0	9.0	4.6	0.24		
	SB-3SJ-1.0	U-Wrap	2.4		10.2	6.2	0.32		
	CT-1.5	Control	0	0	0	7.2	0	0.16	0
	SB-2SJ-1.5	2 Sides	2.4	8.0	9.0		3.0		0.16
	SB-3SJ-1.5	U-Wrap	2.4		10.2		5.0		0.26
	CT-2.0	Control	0	0	0	7.0	0	0.16	0
	SB-2SJ-2.0	2 Sides	2.4	8.0	9.0		1.7		0.09
SB-3SJ-2.0	U-Wrap	2.4	10.2		1.9		0.10		
Sakr et al., 2019	C-S	Control	0	0	0	13.0	0	0.20	0
	C-F					28.5		0.45	
	C-S-210					23.7		0.26	
	ST-2S	Unreinforced UHPC	2.4	10.8	11.8	13.0	18.6	0.20	0.72
	ST-1S		2.4			13.0	4.2	0.20	0.16
	ST-2S-R	Reinforced UHPC	2.4	10.8	11.8	18.5	18.7	0.41	0.72
	ST-1S-R		2.4			18.5	9.9	0.41	0.38

Chapter 3 – UHPC Material Characterization

This chapter discusses the mix design and mechanical properties of UHPC in tension and compression which are used in the prediction models of UHPC and CC-UHPC components in flexure and shear. The commonly used idealized material models are first discussed, then the test methods used to obtain the design values of these methods are then presented. Tension properties of UHPC are significantly important in the design for shear compared to compression properties. Tensile properties are estimated using direct and indirect tests and both are discussed in this chapter with the inverse analysis used to obtain the direct tension properties from indirect tests.

3.1 Mix Design

The UHPC used in this research was produced using a Mortarman vertical shaft non-tilting drum mixer powered by gas. The mix was designed the particle packing method to achieve the highest packing density with locally available materials in the state of Nebraska to reduce material cost, Mendonca et al., 2020. The mix constituents shown in Table 16 were selected as in UNL UHPC 1900 to achieve the highest reported compressive strength. This mix typically achieve a 28-day compressive strength ranging between 17.2 and 18.0 ksi, which satisfies the ASTM C1856 UHPC requirement of 17 ksi. Mechanical testing has been done to characterize the modulus of elasticity and flexural strength as will be discussed later in this chapter.

Table 16: UHPC mix design constituents

Ingredient	Quantity (lb/cy)
Cement (Type I/II)	1,207
Silica Fume	161
Slag (GGBFS)	586
Fine Aggregate (#10 Sand)	1631
Water + Ice	316
Workability Retaining Admixture (WRA)	12
High Range Water Reducer (HRWRA)	45
Steel Fibers (0.5-inch long)	263
Spread (in.)	8

The mix design process was done by reviewing the locally available constituents with respect to their chemical composition, physical properties including particle size distribution, and cost to be considered as viable candidates for UHPC. Figure 49 shows the particle size distribution of the powders (cement, slag, silica fume, and limestone powder), while Figure 50 shows the particle size distribution of sand used in this dissertation.

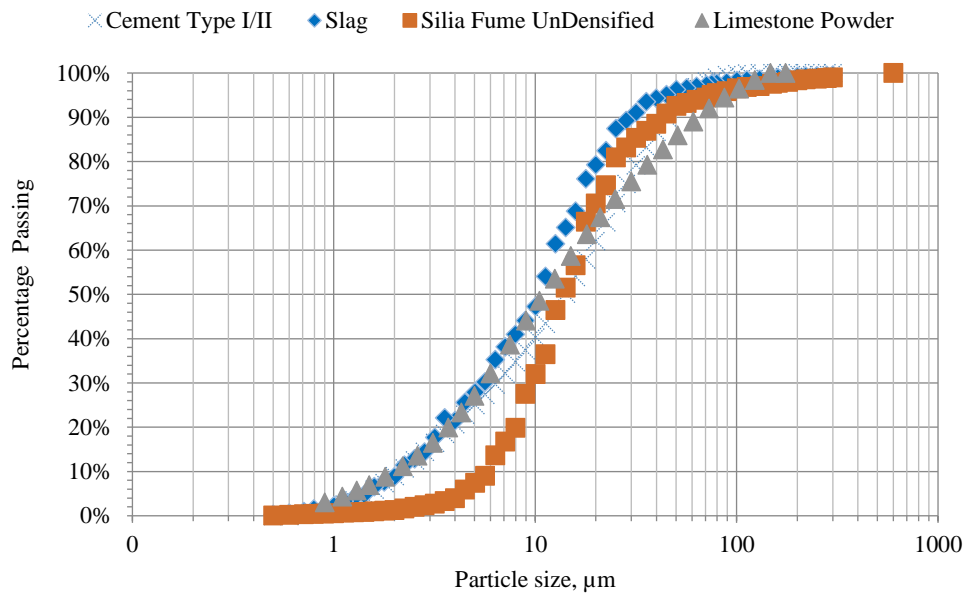


Figure 49: Particle Size Gradations of Powders

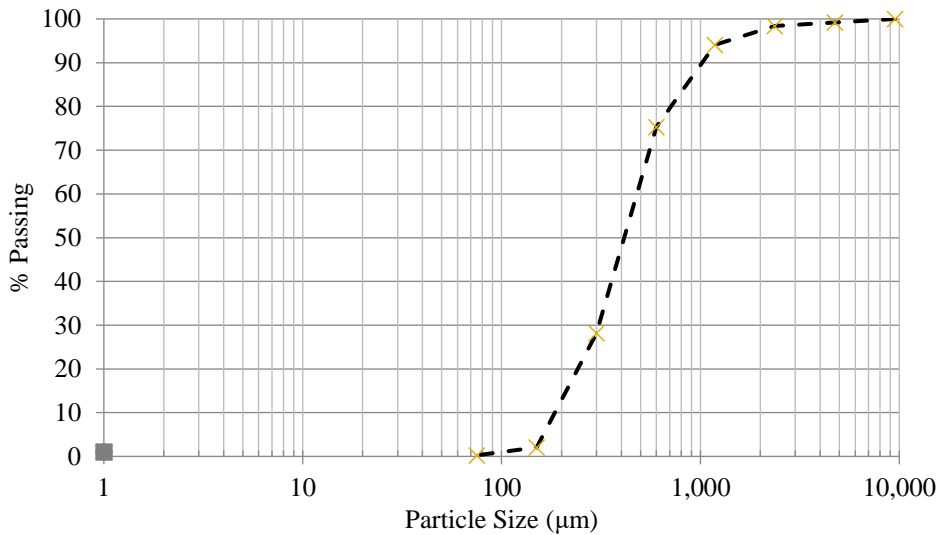


Figure 50: Particle Size Gradation of Sand

UHPC mixture proportions were determined by comparing various combinations of cement, silica fume, slag, quartz flour and sand to a target gradation based on the modified Andreasen and Andersen (A&A) model. The modified A&A model is defined by the equation:

$$P(D) = \frac{D^q - D_{min}^q}{D_{max}^q - D_{min}^q} \quad (29)$$

where $P(D)$ is the percent of particles with a diameter smaller than D ; D_{min} and D_{max} are the minimum and maximum particle diameters, respectively; and q is a shape parameter between 0 and 1. A shape parameter, q , value closer to 1 produces a more coarsely graded mixture, and a q value closer to 0 produces a more finely graded mixture; typical q values selected for UHPC mixtures are in the range of 0.19 to 0.37.

For preliminary mixture identification, D_{min} and D_{max} were selected to be 0.5 and 1,180 microns based on the minimum and maximum particle sizes in the grouping of materials considered, respectively, and q was selected to be 0.22. An optimization algorithm was developed to identify the relative proportions of materials for each combination selected that minimized the difference between the combined gradation and the A&A “ideal” target. Material proportions resulting in optimal gradations were used in developing the trial batches with minor modifications to improve the economy of the mix.

After the mix design was developed, performance evaluation testing was done on each batch to evaluate compressive and flexural tensile strengths, as well as the modulus of elasticity. The performance evaluation testing is discussed in the next sections.

3.2 Compressive Properties

3.2.1 Idealized Material Models

Two idealized compression models are commonly used in the development of UHPC flexural strength prediction models. The first model is a bilinear model shown in Figure 51 and reported by AFGC, 2013 and El-Helou et al., 2019. In this model, the compressive stress increases linearly with strain until reaching the design value of compressive strength (f_{cd}), then, the stress is assumed constant up to the ultimate compressive strain (\mathcal{E}_{cu}). El-

Helou et al., 2019 assumes f_{cd} as 85% of the ultimate compressive strength (f'_c), while the AFGC, 2013 calculates f_{cd} as follows:

$$f_{cd} = \frac{\alpha_{cc} f'_c}{\gamma_c} \quad (30)$$

Where, α_{cc} is a coefficient to consider the adverse long-term effects on the compressive strength and the unfavorable effects resulting from load application (recommended as 0.85), and γ_c is a material partial safety factor for concrete given as 1.5 for the ultimate limit state design of persistent and transient loads, and 1.2 for accidental loads. It should be noted that El-Helou et al., 2019 model is based on the Load and Resistance Factor Design (LRFD), where the material safety factors are included in the strength reduction factor which is multiplied by the component flexural strength.

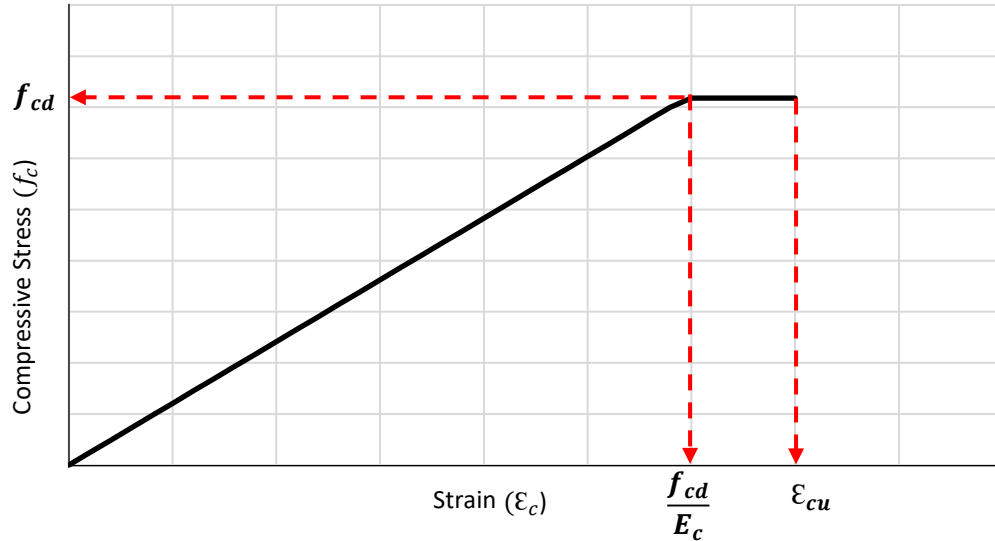


Figure 51: UHPC compression model according to El-Helou et al., 2019 and AFGC, 2013

The ultimate compressive strain (ϵ_{cu}) is assumed by El-Helou et al., 2019 as 0.0035, and calculated by AFGC, 2013 as follows:

$$\epsilon_{cu} = \left[1 + 14 \left(\frac{f_{tu}}{f'_c} \right) \right] \left(\frac{\alpha_{cc} f'_c}{E_c} \right) \quad (31)$$

Where, f_{tu} is the ultimate tensile strength of UHPC, and E_c is the modulus of elasticity of UHPC that is calculated as follows:

$$E_c = k_o \sqrt[3]{f'_c} \quad (32)$$

Where, k_o is the factor that relates the modulus of elasticity to compressive strength and is calibrated by testing. The k_o factor ranges from 2428 to 3035 for three UHPC mixes reported by AFGC, 2013, where E_c is given in [ksi]. El-Helou et al., 2019 estimates E_c as follows:

$$E_c = 1550 \sqrt{f'_c} \text{ [ksi]} \quad (33)$$

The second model is shown in Figure 52 as reported by Haber et al., 2018. The stress-strain behavior is idealized as a non-linear relationship with a reduction parameter (α) that increases exponentially with the increase of strain. The reduction parameter is dependent on f'_c , E_c , and two factors (a) and (b) that are calibrated by test data. The model equations are shown below:

$$f_c = \varepsilon_c E_c (1 - \alpha) \quad (34)$$

$$\alpha = a \varepsilon_n^b \quad (35)$$

$$\varepsilon_n = \frac{\varepsilon_c E_c}{f'_c} \quad (36)$$

$$E_c = 1430 \sqrt{f'_c} \text{ [ksi]} \quad (37)$$

Where, ε_n is the normalized strain, a and b are fit parameters calibrated by test data and will be considered as 0.106 and 2.606 respectively.

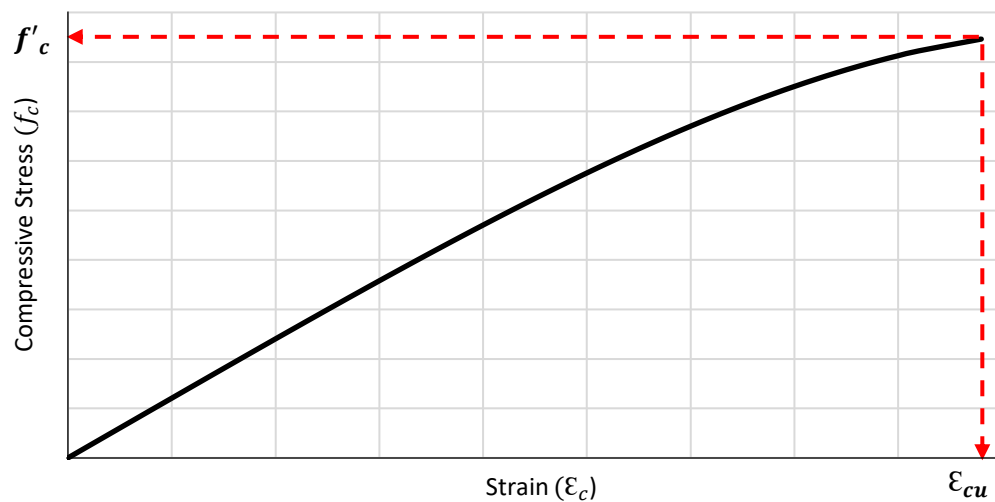


Figure 52: UHPC compression model according to Haber et al., 2018

3.2.2 Compressive Strength Testing

Compressive strength testing was done according to ASTM 1856 on 3x6 in² cylinders. Cylinders were cast in plastic molds at an angle to minimize entrapped air and the molds were tapped on the sides to improve consolidation. The molds were stripped after 24 hours from casting and the cylinders were placed in the curing room at the standard curing temperature. Additional cylinders were subjected to accelerated curing conducted using the procedure and equipment shown in Figure 53. In this procedure, specimens were taken out of the molds and submerged in the water that has a gradually increasing temperature up to 180⁰F. After 48 hours of curing, specimens were cooled gradually down to 80⁰F and placed in the standard curing room until the testing time.

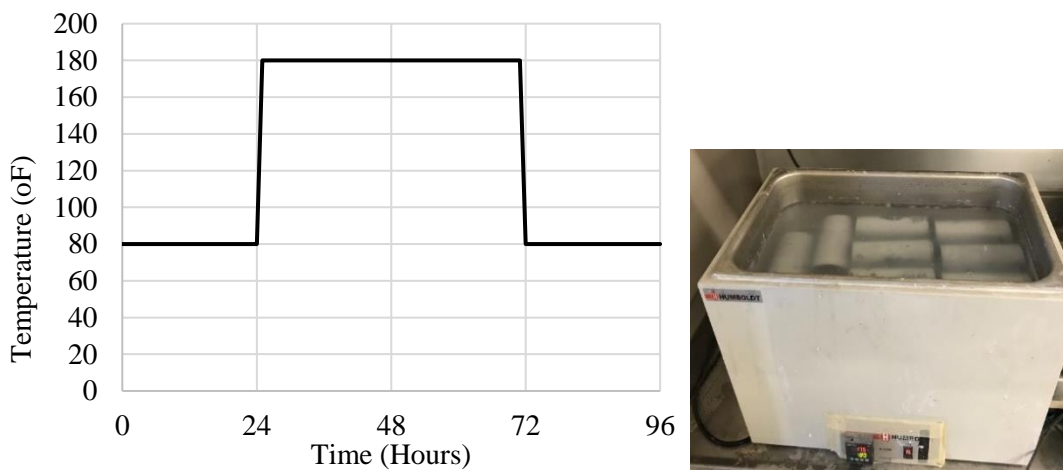


Figure 53: Accelerated curing procedure and equipment

At the time of testing the cylinders ends were ground using an end grinding machine shown in Figure 54. After grinding, the cylinders were allowed to dry for at least 3 hours. A load rate of 150 psi/sec was applied on the test specimens until failure as shown in Figure 54. A minimum of 3 cylinders were tested per each batch done to ensure consistency and quality of the produced UHPC. The used mix achieved a minimum compressive strength of 17.0 ksi which satisfies the ASTM C1856 requirement for UHPC. The resulting spread of that mix was typically ranged between 8 to 9 inches as shown in Figure 55.



Figure 54: End grinding of UHPC cylinders (left), failed cylinder after compressive strength testing (right)



Figure 55: Resulting spread of 8-inches

Table 17 shows the compressive strength test results of one batch done using the UNL UHPC 1900 mix. Extensive testing was done on that batch at the ages of 4, 14, and 28 days using conventional and accelerated curing methods on cylinders and cubes. Figure 56 shows the average compressive strength of moist-cured UHPC cylinders at different ages, where the results achieve the compressive strength requirement for UHPC between 14 and 28 days of age. Figure 57 shows the average 4-day compressive strength of UHPC

cylinders and cubes using different curing methods. These results shows that UHPC can achieve its 28-day compressive strength at 4 days of age when subjected to accelerated curing. In addition, the 2-inch cubes resulted in higher compressive strengths than cylinders especially at early age.

Table 17: Compressive strength UNL UHPC 1900 cylinders and cubes at different age and curing conditions

Specimen No.	Compressive Strength (ksi)					
	4			14	28	
Curing Condition - Specimen Type	Moist Curing - Cylinders	Hot Tub Curing - Cylinders	Hot Tub Curing - Cubes	Moist Curing - Cylinders	Moist-Cured Cylinders	Moist-Cured Cubes
SP-1	13.1	16.7	20.3	14.4	18.3	19.2
SP-2	12.8	18.2	19.6	14.8	19.6	18.9
SP-3	13.1	18.4	20.9	15.7	18.7	19.1
Average	13.0	17.8	20.3	15.0	18.9	19.1

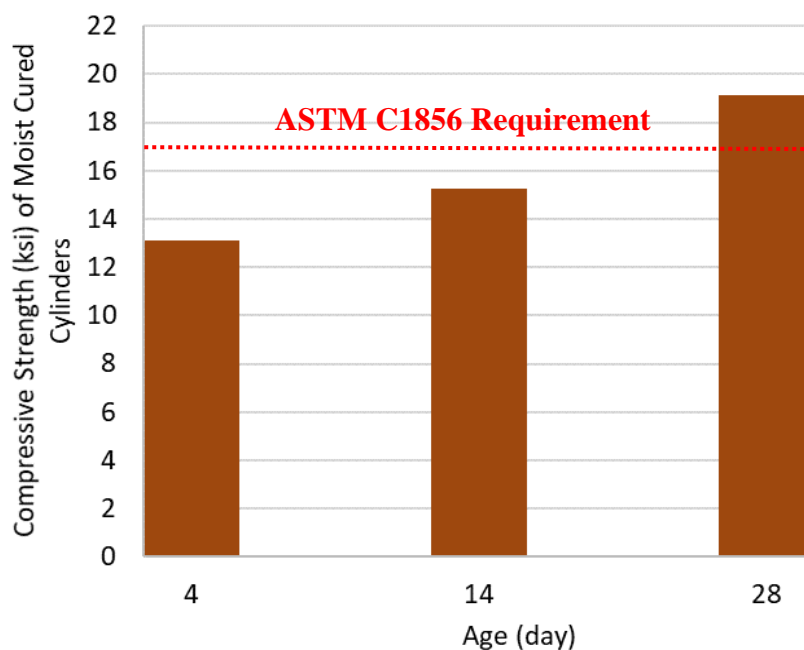


Figure 56: Average compressive strength of moist-cured UHPC cylinders at different ages

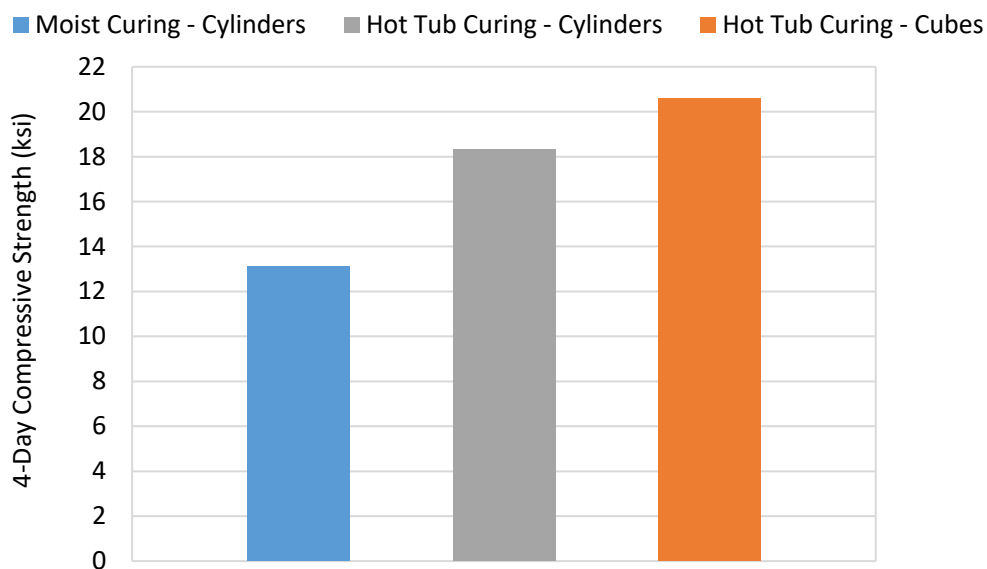


Figure 57: Average 4-day compressive strength of UHPC cylinders and cubes using different curing methods

3.2.3 Modulus of Elasticity Testing

The modulus of elasticity was estimated according to ASTM C469 on 4x8 in² cylinders as shown in Figure 58. Cylinder ends were ground like what was described in the compressive testing procedure. A Compressometer/Extensometer cage was fixed to the cylinder with a gauge length of 5-inches. The cylinder was loaded until reaching approximately 40% of its compression carrying capacity where the modulus of elasticity was calculated. The used mix design achieved a modulus of elasticity of at least 6300 ksi. Table 18 shows the results of the modulus of elasticity done on three prisms fabricated from the same batch discussed in the previous section. The cylinders were moist cured conventionally and the test was done at 28-day of age.



Figure 58: Extensometer cage installed on a UHPC cylinder for the modulus of elasticity testing

Table 18: Modulus of elasticity test results (ksi) of three UHPC cylinders

Cylinder #	Test #1	Test #2	Test #3	Average
1	6297	6229	6263	6263
2	6512	6531	6520	6521
3	6535	6538	6538	6537
Average	6440			

3.3 Tensile Properties

3.3.1 Idealized Material Models

The stress-strain behavior of UHPC in tension is typically linear until cracking with a modulus of elasticity equals to that of UHPC in compression, Graybeal, 2007. The post-cracking behavior is highly dependent on the steel fibers volume fraction, length/diameter ratio, and strength. Strain hardening occurs when the cracking resistance provided by the fibers is higher than that of the concrete matrix, otherwise, strain softening occurs where the post-cracking strength is less than the pre-cracking strength, AFGC, 2013. Three idealized models for UHPC in tension are discussed: simplified, strain-hardening, and

strain-softening models. The first model is shown in Figure 59, which is reported by the AFGC, 2013 as a simplified model for thin elements under pure flexure. This model is also reported by El-Helou et al., 2019 as the simplest idealization where the tensile stress increases linearly with the strain until reaching the design value of tensile strength (f_{td}). Then, the stress remains constant until reaching the ultimate tensile strain (ϵ_{tu}), which is proposed as 0.004 by El-Helou et al., 2019, 0.007 by Graybeal, 2006, and 0.01 by Graybeal, 2008. Direct tensile testing by Haber et al., 2018 showed that UHPC having a fiber volume fraction (V_f) of 2% can sustain most of its tensile strength for a strain up to 0.01. El-Helou et al., 2019 considers f_{td} as 85% of the cracking tensile strength (f_{cr}), while the AFGC, 2013 calculates f_{td} as follows:

$$f_{td} = \frac{f_{tu}}{\gamma_{cf} K} \quad (38)$$

Where, f_{tu} is the ultimate tensile strength of UHPC obtained by flexural or direct tension tests, γ_{cf} is a partial safety factor for UHPC in tension recommended as 1.30 for transient loads and 1.05 for accidental loads, K is a fiber orientation safety factor recommended as 1.25. Sim et al., 2020 proposes the same model to be used for flexure design of beams for the Precast/Prestressed Concrete Institute (PCI) with recommended set values for f_{td} as 0.75 ksi, and for ϵ_{tu} as 0.005.

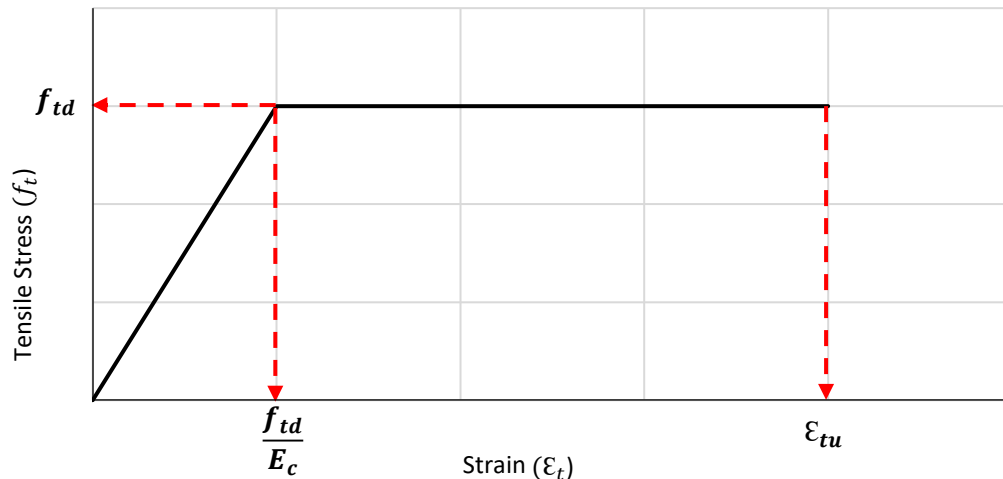


Figure 59: UHPC simplified tension model according to AFGC, 2013 and El-Helou et al., 2019

The second model is shown in Figure 60 as defined by AFGC, 2013 for strain-hardening UHPC and reported by Yoo et al., 2016. In this model, the tensile stresses increase linearly with strain until reaching the cracking tensile strength (f_{cr}) divided by the safety factor γ_{cf} , then increases again until reaching f_{td} at a strain (ϵ_{tu}). The AFGC, 2013 recommends f_{cr} to be taken as 1.3 ksi for the preliminary design of strain-hardening UHPC, while Yoo et al., 2016 and Graybeal, 2008 reports f_{cr} to be 87% of f_{tu} .

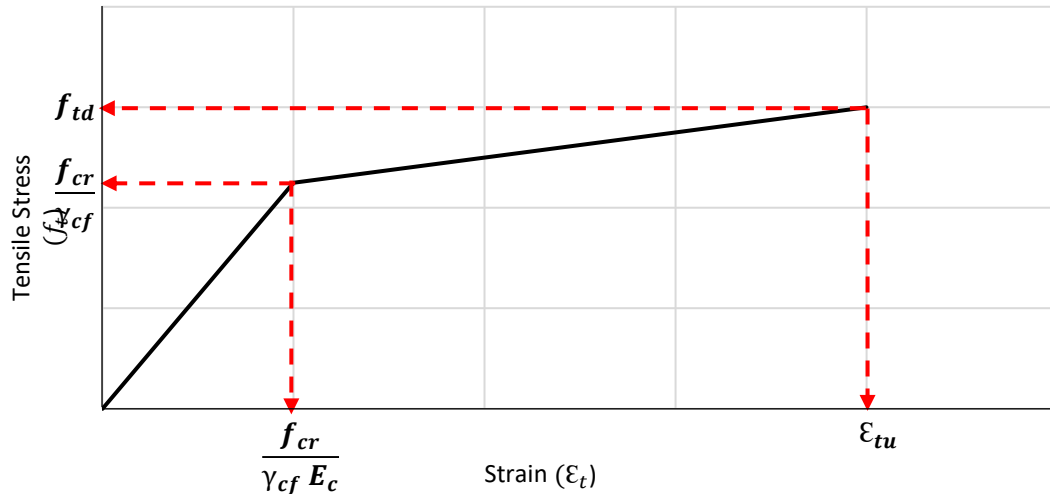


Figure 60: UHPC strain-hardening tension model according to of AFGC, 2013 and Yoo et al., 2016

The third model is shown in Figure 61 as reported by Qi et al., 2018 and Bae et al., 2016. This strain-softening tension model is similar to that of ACI 544.4R-18 for fiber-reinforced concrete. In this model, the tensile stresses increase linearly with the strain until reaching f_{td} , then the tensile stresses drop to the residual tensile strength (f_R) until reaching the ultimate tensile strain (ϵ_{tu}). Qi et al., 2018 considered f_{td} to be equal to the full value of f_{tu} obtained from direct tensile tests without safety factors for flexure strength prediction only. The f_R is achieved through the crack bridging ability of fibers and their interaction with the concrete matrix. Fiber length, diameter, orientation, and bond with the concrete matrix significantly affect f_R and ϵ_{tu} . Qi et al., 2018 estimates f_R based on the experimental work done by Singh, 2015 on the pull-out strength of steel fibers in concrete. A critical fiber length to diameter ratio is defined empirically by Singh, 2015 to determine whether

f_R is governed by the bond between the fibers and matrix or the fibers tensile strength. The residual tensile strength is calculated as follows:

$$f_R = \begin{cases} 0.12 \sqrt{f'_c} \frac{V_f l_f}{d_f} \text{ [ksi]}; & \text{for } \frac{l_f}{d_f} < \left(\frac{l_f}{d_f}\right)_{cri} \\ V_f \sigma_{fu} \text{ [ksi]}; & \text{for } \frac{l_f}{d_f} \geq \left(\frac{l_f}{d_f}\right)_{cri} \end{cases} \quad (39)$$

$$\left(\frac{l_f}{d_f}\right)_{cri} = 1.26 \frac{\sigma_{fu}}{\sqrt{f'_c}} \quad (40)$$

Where, V_f is the fiber volume fraction, l_f is the fibers length, d_f is the fibers diameter, σ_{fu} is the fibers tensile strength [ksi]. The f_R can vary significantly from 50%, according to Prem et al., 2012, Qi et al., 2018, and Yang et al., 2010, to 100% of (f_{tu}), according to Graybeal, 2006, Graybeal, 2008, and Haber et al., 2018.

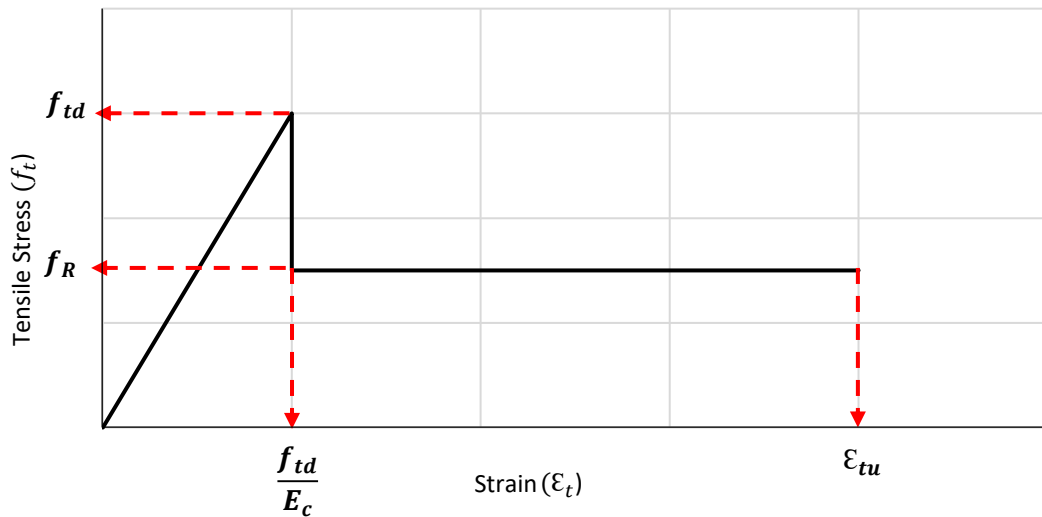


Figure 61: UHPC strain-softening tension model according to Qi et al., 2018 and Bae et al., 2016

3.3.2 Direct Tension Testing

Direct tension testing is typically done by applying uniaxial tension force on (2 x 2 x 17 in³) or (2 x 2 x 12 in³) UHPC prism specimens, Graybeal et al., 2019. The force is typically transferred from the testing machine to the specimens by gripping on the specimen ends through one stationary and one moving head. Tapered grip plates are fixed to the specimen ends using high strength adhesives to allow for the machine to grip on the specimen ends

without inducing eccentric forces and bending moments. The gripping length of the 17-inch-long specimens is larger than that of the 12-inch ones which can reduce the required adhesive strength. Tensile strain measuring devices typically an extensometer is installed over a gauge length to measure the deformation with load increase. The gauge length of the 17-inch-long specimens is 4 inches, while for the 12-inch ones the gauge length is 3 inches.

Figure 62 shows the general behavior of UHPC obtained from tension testing and the characterization of phases according to Graybeal et al., 2013. There are four phases that UHPC under tension goes through before failure. The first phase is the elastic phase where stresses increase linearly with the increase in strain until initial cracking when the tensile strength of the cementitious matrix is reached. The second phase is the formation of multiple cracks in the cementitious matrix across the area under tension in the member or test specimen. In this phase, the number of cracks keeps increasing while each individual crack does not experience widening until the cementitious matrix can no longer sustain any deformation by cracking which is known as crack saturation. After reaching crack saturation of the matrix, the crack straining phase start to happen where the cracks experience widening while they are bridged by the steel fiber reinforcement. The cracks straining phase is governed by the tensile strength of the fibers and their pullout strength as indicated in the previous section. After the multiple cracks exhibits most of their widening or straining capabilities, one of the cracks starts to widen excessively and the localization phase starts to occur. In the localization phase, a specific crack experience continued widening while the rest of the member behaves elastically, and the tensile stresses carried by the specimen keep decreasing until failure at that crack.

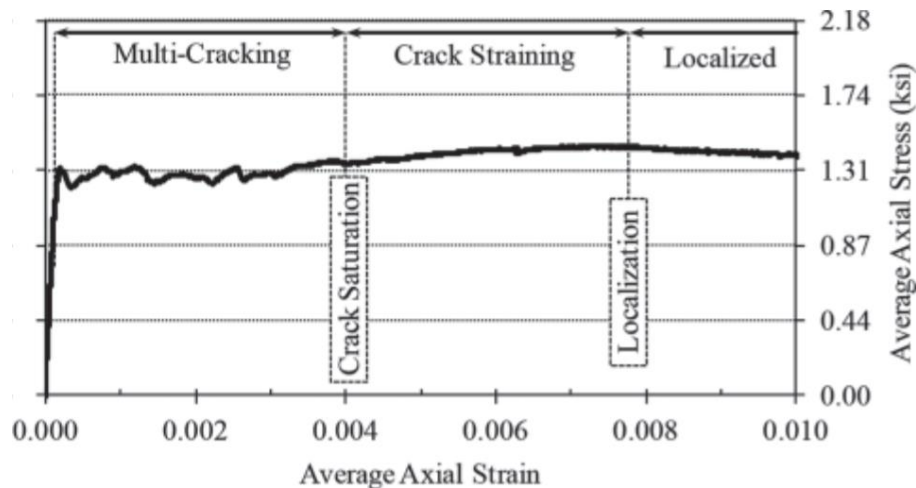


Figure 62: Stress-strain behavior of UHPC in tension, courtesy of Graybeal et al., 2013

3.3.3 Indirect Tension Testing

The flexural tensile properties of UHPC were estimated according to ASTM C1609 as shown in Figure 63. The prism specimens had dimensions of 3.0 x 3.0 x 14 in.³ tested on a four-point bending test setup with a 12-in. span. Specimen dimensions were selected according to ASTM C1856 and the used fiber length (0.5 in.). Load was applied using a displacement rate of 0.003 in./min. until a mid-span deflection of $L/900$ is reached then the rate is increased up to 0.008 in./min until a mid-span deflection of $L/150$ is reached and the test is stopped. The applied load was measured using a 20-kip load cell placed on top of the load spacer plates. While the mid-span deflection was measured using two Linear Variable Differential Transducers (LVDTs) fixed at the base of the supports. Figure 64 shows the stress-deflection plot of 3 prisms tested at 4 days of age, while Figure 65 shows the plot for 3 prisms tested at 14 days, and Figure 66 shows the plot for 2 prisms tested at 28 days with the results of one prism omitted as the failure did not occur under the loading points. Also shown on the plots are the PCI-UHPC requirements for that testing according to Sim et al., 2020 where the requirement for the peak flexural strength is 2.0 ksi, and the requirement for the flexural strength at the first crack is 1.5 ksi. It can be noticed that the results of all plots satisfy these requirements with a considerable safety margin. However,

the flexural strength did not increase significantly from 4 to 14 days of age, while there was a significant increase between the 28- and 14-days flexural strength results. Figure 67 shows the tested prisms after failure for prisms at ages 4, 14, and 28 days. The results of flexural testing were used to obtain the direct tensile properties as will be discussed in the next section.



Figure 63: Flexural testing of UHPC prism

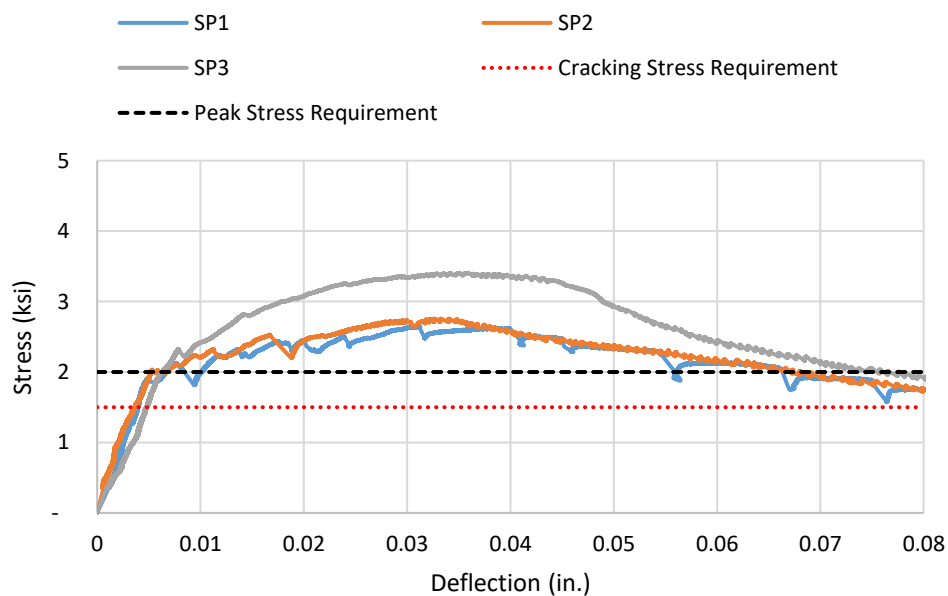


Figure 64: Stress-deflection plot of the UHPC prisms tested at 4 days of age

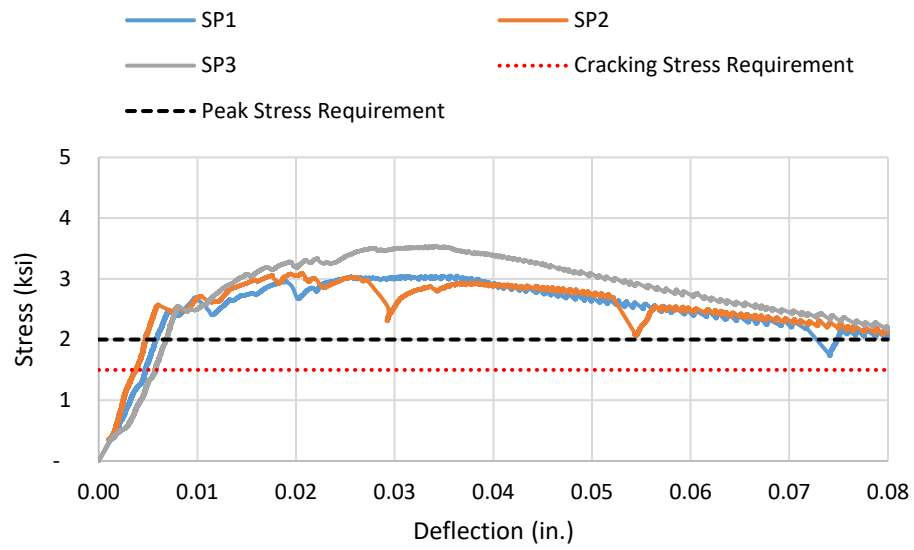


Figure 65: Stress-deflection plot of the UHPC prisms tested at 14 days of age

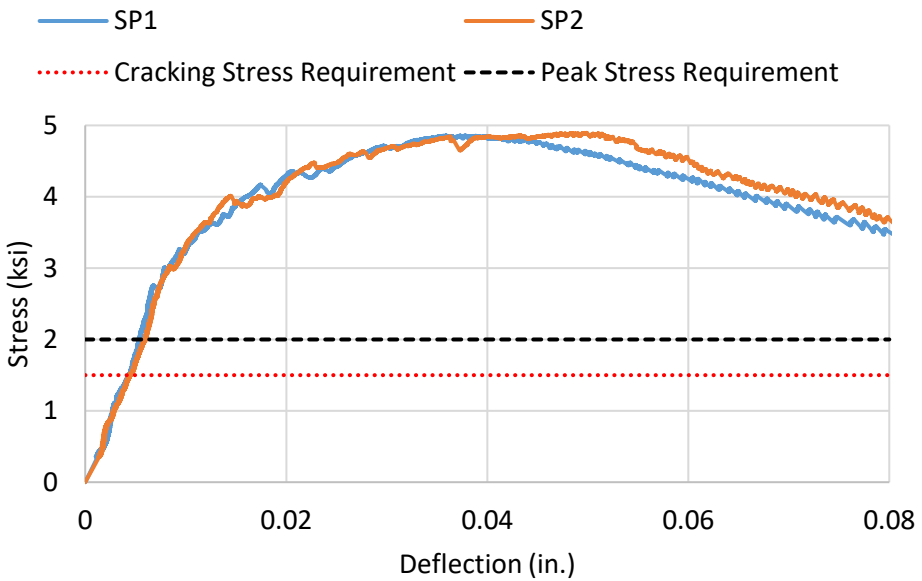


Figure 66: Stress-deflection plot of the UHPC prisms tested at 28 days of age

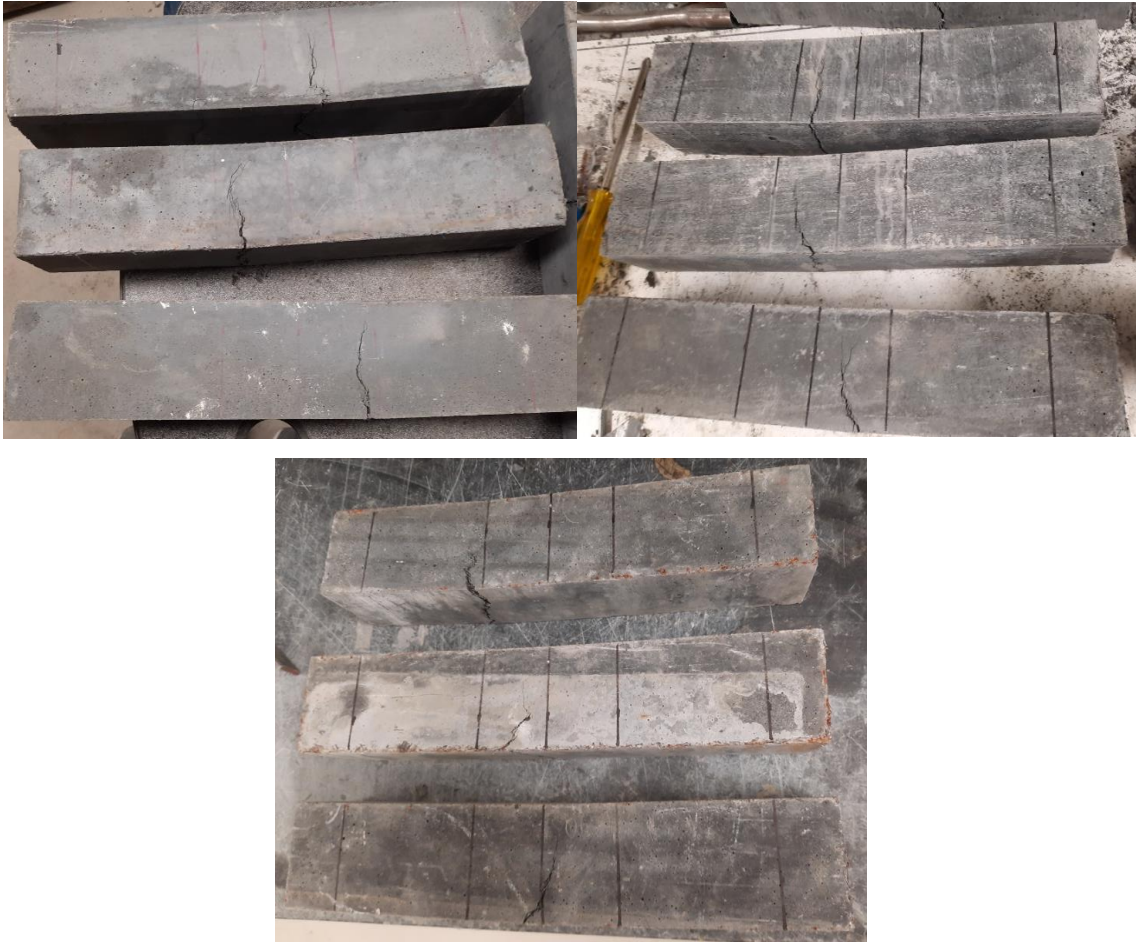


Figure 67: Tested prisms after failure at 4 days (top left), 14 days (top right), and 28 days (bottom)

3.3.4 Inverse Analysis

Flexural testing done on UHPC prisms is considered an indirect test method to obtain the tensile properties of UHPC. The process of obtaining the direct tensile properties using indirect flexural testing is known as inverse analysis, Baby et al., 2013. There are several inverse analysis approaches described as follows:

Method 1: Assuming an idealized tension model like El Helou et al., 2019 (linear-constant), and assuming the crack localization strain (i.e. $\epsilon_{tu} = 0.004$). Use a conversion factor to convert the peak flexural strength obtained from testing to the direct tensile strength (f_{tu}). A conservative conversion factor of 0.383 is recommended by the Swiss standard SIA 2052, 2016. This factor is based on having the neutral axis located at a

distance of 0.82 times the prism height from the outermost tensioned fiber as shown in Figure 68. Another conservative conversion factor of 0.37 is recommended by the German guidelines DAfStb, 2017. The conversion factor can be formulated as shown in the below equation:

$$x = \frac{f_{t,loc}}{f_{t,f}} = 0.37 \quad (41)$$

Where x is the conversion factor multiplied by the flexural strength to obtain the localization strength; $f_{t,loc}$ is the UHPC localization strength; $f_{t,f}$ is the flexural strength obtain from UHPC prism testing.

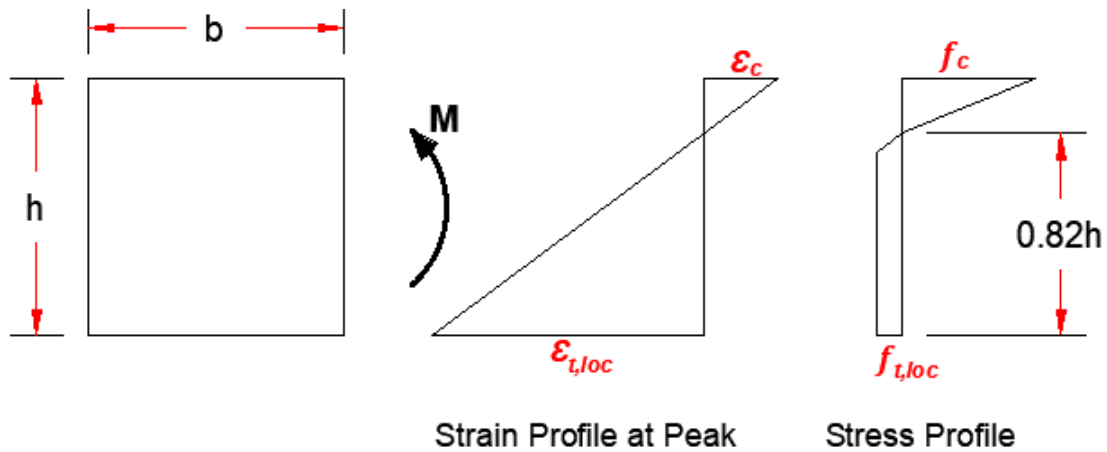


Figure 68: Assumed stress and strain profiles at the measured peak flexural stress, SIA 2052, 2016 (not to scale)

Method 2: Similar approach to Method 1 but with more detailed calculations without having to assume a fixed value for $\epsilon_{t,loc}$. Initial assumptions are made for $f_{t,loc}$, and $\epsilon_{t,loc}$ until the correct value of peak moment is achieved and conversion factors are obtained using closed form equations based on equilibrium of internal forces. A numerical example using this method is presented in the appendix titled “Derivation of Conversion Factors for Inverse Analysis of UHPC Flexure Test Data”. The conversion factors are dependent on the assumed combination of $f_{t,loc}$, and $\epsilon_{t,loc}$ and typically range between 0.37 to 0.43. The conversion factors are calculated as discussed below and in Figure 69 showing the stress and strain profiles at the measured peak flexural stress.

Based on the equilibrium of internal forces between tension and compression zones of the UHPC prism at the peak moment, the following equation can be obtained:

$$b f_{t,loc} k (h - c) = (E_c \mathcal{E}_c) b \frac{c}{2} \quad (42)$$

$$r = \frac{\mathcal{E}_{t,cr}}{\mathcal{E}_{t,loc}} = \frac{f_{t,loc}}{E_c \mathcal{E}_{t,loc}} \quad (43)$$

$$k = 1 - \frac{r}{2} \quad (44)$$

Where, b is the prism width; k is an adjustment factor depending on the ratio between cracking and localization strains (r); h is the prism height; c is the neutral axis depth; E_c is the UHPC modulus of elasticity in tension and/or compression; \mathcal{E}_c is the strain at extreme compression fibers; $\mathcal{E}_{t,cr}$ and $\mathcal{E}_{t,loc}$ are the cracking and localization strains, respectively. Applying the principle of strain compatibility across the prism height provides the below relationship:

$$\frac{\mathcal{E}_c}{c} = \frac{\mathcal{E}_{t,loc}}{(h-c)} \quad (45)$$

The equilibrium of internal forces equation can be rewritten according to the previous relationships as follows:

$$f_{t,loc} k (h - c) = E_c \frac{\mathcal{E}_{t,loc}}{(h-c)} \frac{c^2}{2} \quad (46)$$

$$\frac{(h-c)^2}{c^2} = \frac{E_c \mathcal{E}_{t,loc}}{2 k f_{t,loc}} \quad (47)$$

Taking the square root of the left-hand side of this equation yields a closed-form equation to determine c based on the prism height (h) and UHPC tensile properties ($E_c, f_{t,loc}, \mathcal{E}_{t,loc}$) as follows:

$$\frac{h}{c} = \sqrt{\frac{E_c \mathcal{E}_{t,loc}}{2 k f_{t,loc}}} + 1 \quad (48)$$

$$c = \frac{h}{\sqrt{\frac{E_c \mathcal{E}_{t,loc}}{2 k f_{t,loc}} + 1}} \quad (49)$$

The bending moment capacity of the prism (M_n) and the resulting conversion factor (x) can then be calculated as follows:

$$M_n = [b f_{t,loc} k (h - c)] \left[h - \frac{c}{3} - \frac{k(h-c)}{2} \right] \quad (50)$$

$$x = \frac{f_{t,loc}}{f_{t,f}} = \frac{f_{t,loc}}{\frac{M_n}{S}} \quad (51)$$

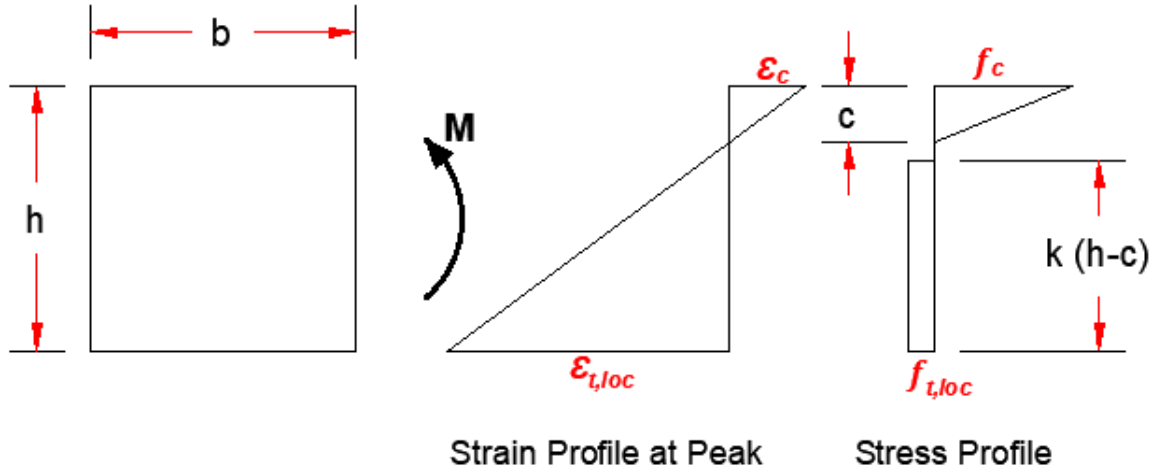


Figure 69: Stress and strain profiles at the measured peak flexural stress, method 2 of inverse analysis

Method 3: Using the measured peak load and its corresponding mid-span deflection to obtain the tensile properties (f_{tu} , and ϵ_{tu}) assuming the “Linear-Constant” idealized model. This method is based on solving three equations based on equilibrium of internal forces, measured peak moment, and measured peak curvature, to obtain three unknowns which are c , f_{tu} , and ϵ_{tu} as shown in Figure 70. A numerical example using this method is presented in the appendix titled “Inverse Analysis of UHPC Flexure Prism (Linear-Constant Model)”. The first equation based on equilibrium of internal forces can be formulated as follows:

$$C = T_1 + T_2 \quad (52)$$

$$\epsilon_c E_c \frac{b c}{2} = b f_{t,loc} \frac{r (h-c)}{2} + b f_{t,loc} (h - c) (1 - r) \quad (53)$$

$$\frac{\epsilon_c}{c} = \frac{\epsilon_{t,loc}}{(h-c)} \quad (54)$$

Where, C is the compression force in UHPC; T_1 is the tension force in the triangular part in UHPC; T_2 is the tension force in the rectangular part in UHPC. The second equation utilizing the measured curvature at peak moment can be written as follows:

$$\Phi_{loc} = \frac{\epsilon_{t,loc}}{h-c} \quad (55)$$

Where, Φ_{loc} is the curvature occurring at the point of peak moment. Φ_{loc} can be directly obtained from the measured deflection, the derivation and calculation procedure is shown in the appendix titled “Conversion of Load-Deflection to Moment-Curvature relationships”. The third equation utilizing the measured peak moment can be written as follows:

$$M_n = b E_c \frac{\epsilon_{t,loc}}{(h-c)} \frac{c^3}{3} + b f_{t,loc} \frac{r^2(h-c)^2}{3} + \frac{b f_{t,loc} (h-c)^2 (1-r^2)}{2} \quad (56)$$

Where, M_n is the measured peak moment calculated from the applied load during testing of the UHPC prism. These three equations contain the three unknowns of c , f_{tu} , and ϵ_{tu} which when solved can obtain the tensile properties of the Linear-Constant model without assumptions as in the previous methods.

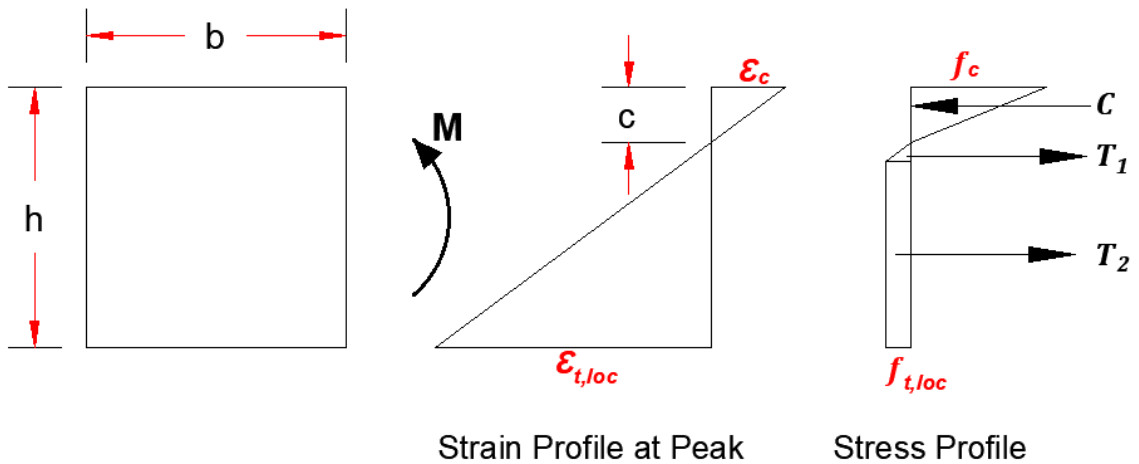


Figure 70: Stress and strain profiles at the measured peak flexural stress, method 3 of inverse analysis

Method 4: Using the measured peak load and its corresponding mid-span deflection and the cracking load to obtain the tensile properties (f_{cr} , f_{tu} , and ϵ_{tu}) assuming the “Strain-

Hardening” idealized model. This method is similar to method 3 in solving the three equations in three unknowns as shown in Figure 71 with the introduction of f_{cr} obtained directly from the measured cracking load. A numerical example using this method is presented in the appendix titled “Inverse Analysis of UHPC Flexure Prism (Strain-Hardening Model)”. The first equation based on equilibrium of internal forces can be formulated as follows:

$$C = T_1 + T_2 + T_3 \quad (57)$$

$$\mathcal{E}_c E_c \frac{bc}{2} = b f_{t,cr} \frac{r(h-c)}{2} + b f_{t,cr} (h-c) (1-r) + \frac{b}{2} (f_{t,loc} - f_{t,cr})(h-c) (1-r) \quad (58)$$

$$\frac{\mathcal{E}_c}{c} = \frac{\mathcal{E}_{t,loc}}{(h-c)} \quad (59)$$

Where, T_1 is the tension force in the top rectangular part in UHPC; T_3 is the tension force in the bottom rectangular part in UHPC. The second and third equations utilizing the measured curvature at peak moment and the peak moment itself can be written as follows:

$$\Phi_{loc} = \frac{\mathcal{E}_{t,loc}}{h-c} \quad (60)$$

$$M_n = b E_c \frac{\mathcal{E}_{t,loc}}{(h-c)} \frac{c^3}{3} + b f_{t,cr} \frac{r^2(h-c)^2}{3} + \frac{b f_{t,cr} (h-c)^2 (1-r^2)}{2} + \frac{b}{2} (f_{t,loc} - f_{t,cr})(h-c)^2 \frac{(1-r)(2-r)}{6} \quad (61)$$

These three equations contain the three unknowns of c , f_{tu} , and \mathcal{E}_{tu} which when solved can obtain the tensile properties of the Strain-Hardening model without assumptions as in the previous methods.

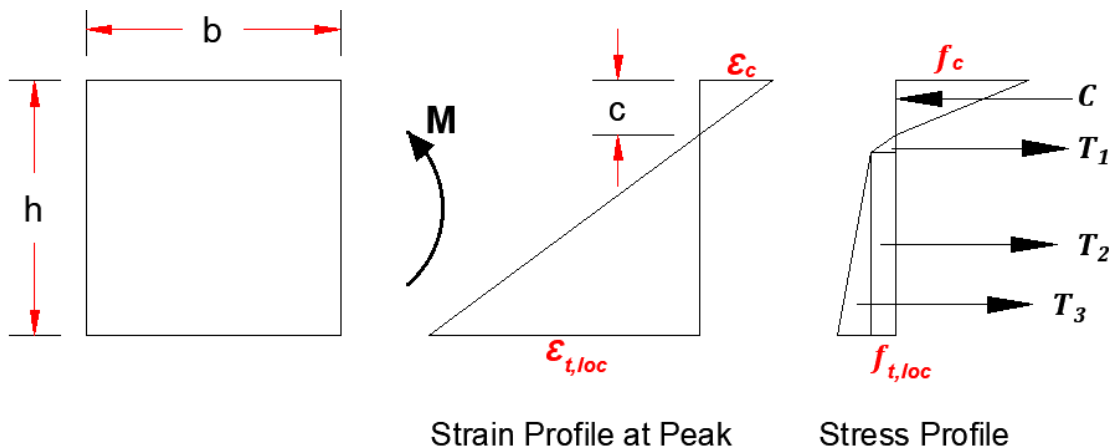


Figure 71: Stress and strain profiles at the measured peak flexural stress, method 4 of inverse analysis

Figure 72 shows the moment-curvature plot of two flexure test results with the prediction provided using the 4 discussed methods with the same results shown in the calculations in the appendix. It can be noticed that method 1 provides the most conservative estimation of the tensile properties. While methods 2 to 4 provides close estimates to each other and to the measured moment-curvature. The post-peak prediction is significantly underestimated in all methods which can be attributed to the fact that the assumed idealized tension models neglect all tensile stress carried by UHPC after ϵ_{tu} is reached.

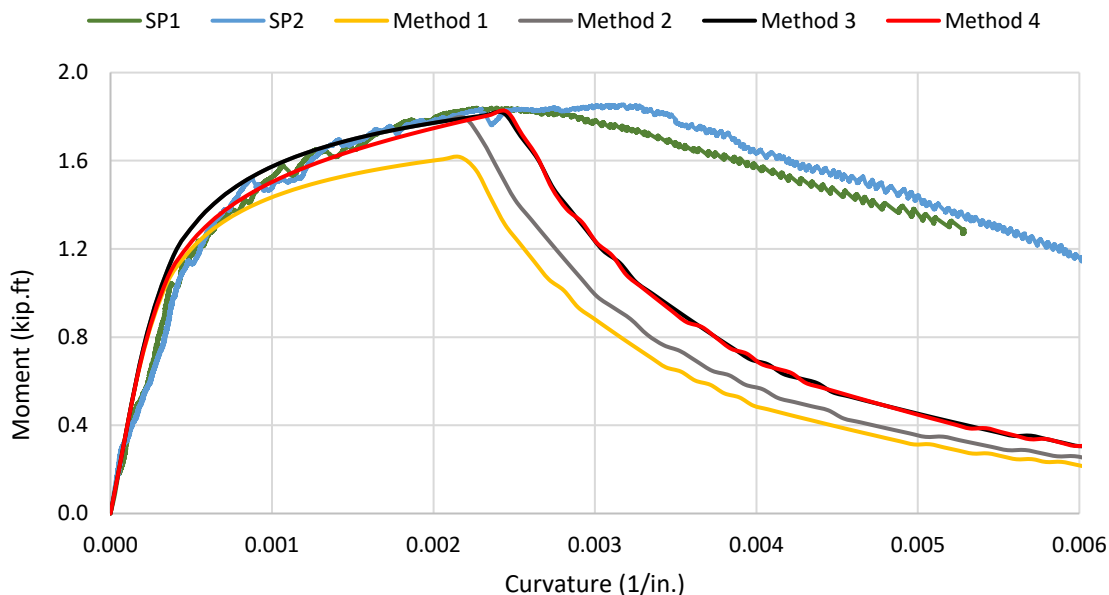


Figure 72: Moment-curvature plot of flexure test results of two specimens and the prediction provided by different inverse analysis methods

Chapter 4 – Flexural and Shear Strength of UHPC Beams

The chapter presents the work done on analyzing flexural and shear test data of UHPC beams collected from the literature. The parameters affecting flexural and shear strength of UHPC beams are also analyzed. Flexure testing of a ribbed UHPC slab is also presented to validate the analysis of flexural strength prediction models of UHPC beams.

4.1 Flexural Strength of UHPC Beams

This section will present a study to evaluate the accuracy of flexure strength prediction models of UHPC beams (discussed in section 2.3.1). UHPC beams flexure test data (discussed in section 2.3.2) are used to compare measured versus predicted flexure strength then the results will be evaluated statistically for their average and standard deviation.

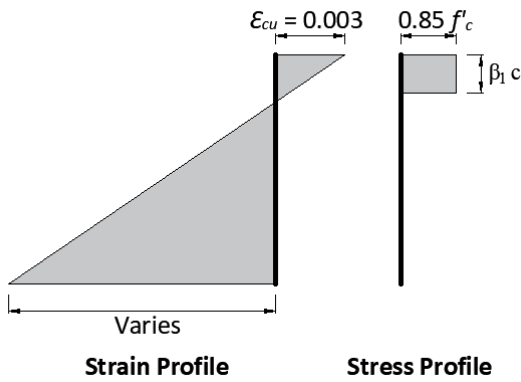
4.1.1 Analysis of UHPC Beams Flexure Test Data

Test data collected in section 2.3.2 were analyzed to evaluate the prediction models of UHPC components. First, several combinations of the commonly used UHPC stress-strain models (discussed in Chapter 3) are used to develop several flexural strength prediction models as shown in Table 19. Figure 73 presents a schematic of the strain and stress profiles of some of these prediction models at curvatures Φ_p and Φ_u . A reference model for CC was evaluated using the equivalent rectangular compression block in compression and neglecting the concrete strength in tension. The parameters of tension model A were taken according El-Helou et al., 2019 ($\mathcal{E}_{cu} = 0.0035$) and ($\mathcal{E}_{tu} = 0.004$). The f_{cr} of tension model B was taken conservatively as 75% of the tensile strength f_{tu} . The f_R of tension model C was taken conservatively as 50% of the tensile strength f_{tu} . Models A1M and A2M were analyzed using the ultimate tensile strain (\mathcal{E}_{tu}) as 0.010 instead of 0.004 to evaluate its effect on the flexural strength.

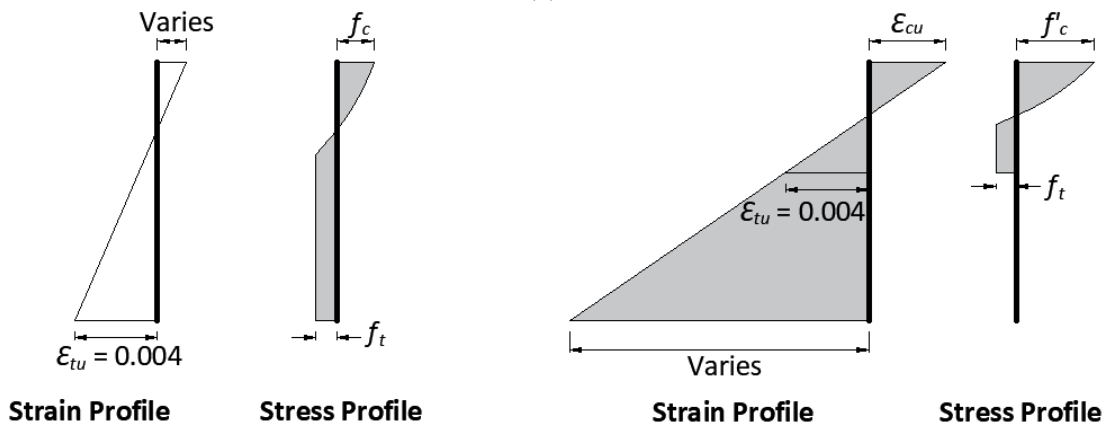
Table 19: Prediction model combinations

	Compression Model 1 (El-Helou et al., 2019)	Compression Model 2 (Haber et al., 2018)
Tension Model A (AFGC, 2013 and El-Helou et al., 2019)	Model A1, A1M*	Model A2, A2M*
Tension Model B (AFGC, 2013 and Yoo et al., 2016)	Model B1	Model B2
Tension Model C (Qi et al., 2018 and Bae et al., 2016)	Model C1	Model C2

* Models A1M and A2M have ϵ_{tu} as 0.010 instead of 0.004



(a) CC Model



(b) Model A2 at curvature Φ_p

(c) Model A2 at curvature Φ_u

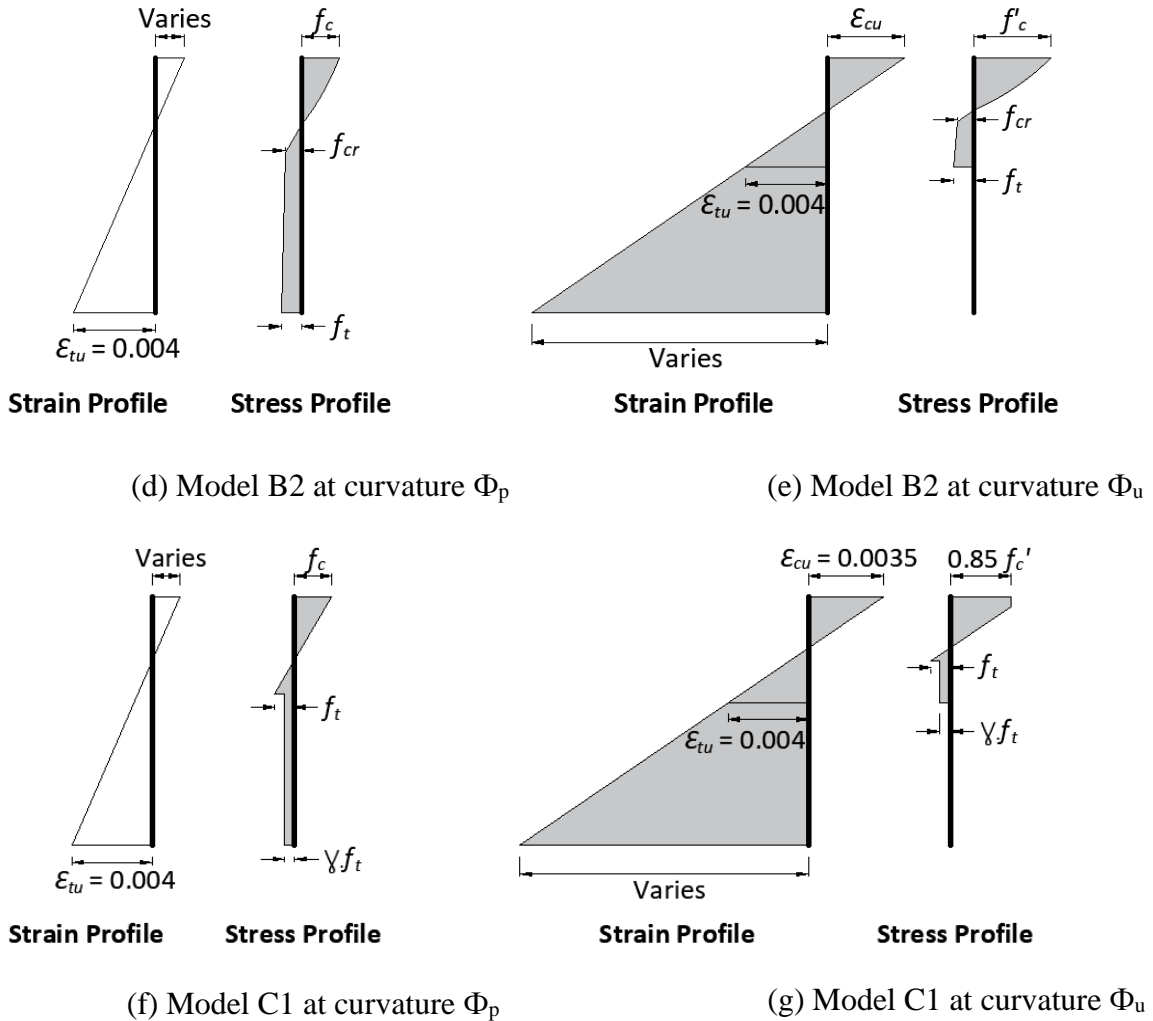


Figure 73: Strain and stress profiles of the prediction models at curvatures Φ_p and Φ_u : a) CC Model; b) Model A2 at curvature Φ_p ; c) Model A2 at curvature Φ_u ; d) Model B2 at curvature Φ_p ; e) Model B2 at curvature Φ_u ; f) Model C1 at curvature Φ_p ; g) Model C1 at curvature Φ_u (not to scale)

Second, the resulting eight material model combinations were used to predict the flexural strength of the collected test data. Figure 74 shows the measured versus predicted flexural resistance factors (R_{measured} vs. $R_{\text{predicted}}$) of the test data using models A1 and the CC models. It shows that the CC model significantly underestimates the flexural resistance factor compared to Model A1. Figure 75 shows R_{measured} versus $R_{\text{predicted}}$ using Model A1 at curvatures Φ_p and Φ_u . Significant difference can be noticed between the two cases where curvature Φ_p provides much closer prediction to the measured flexural resistance factor.

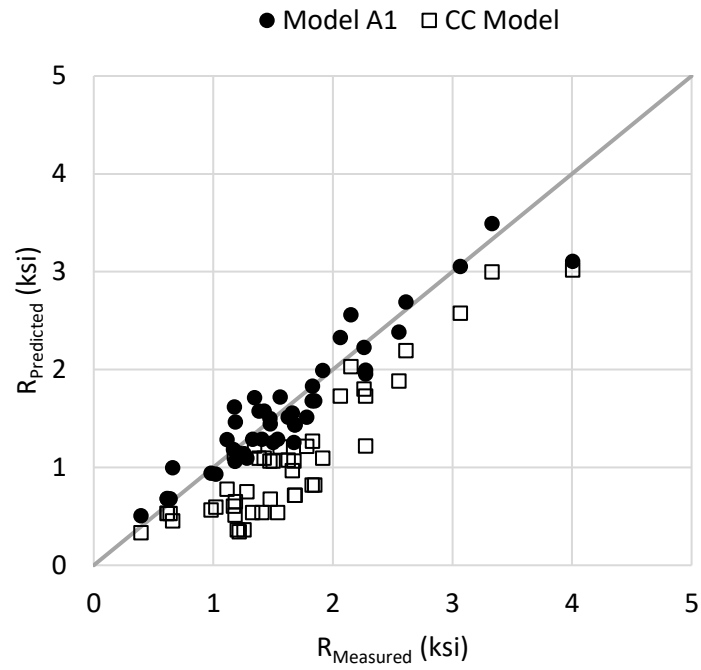


Figure 74: Measured versus predicted flexural resistance using CC and A1 models at curvature Φ_p

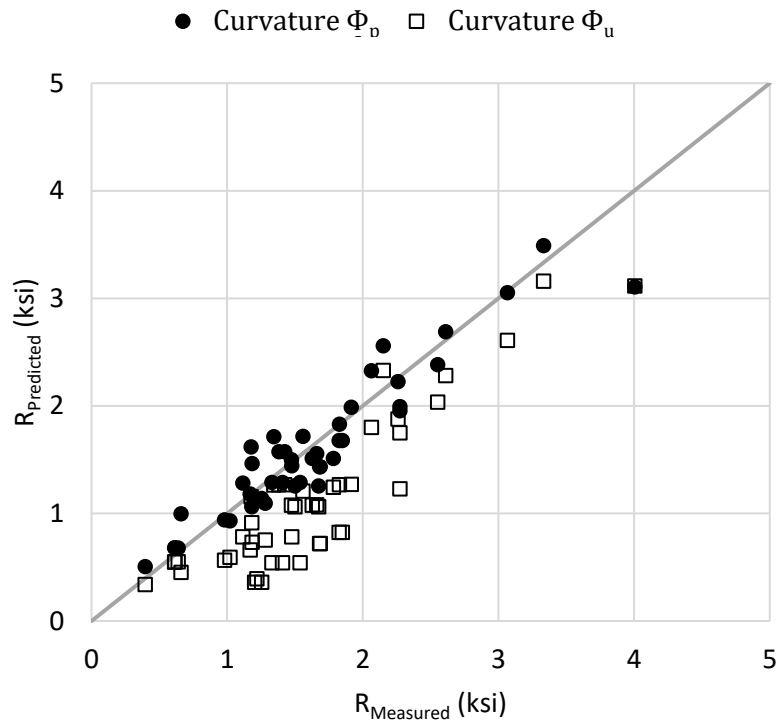


Figure 75: Measured versus predicted flexural resistance using Model A1 at curvatures Φ_p and Φ_u

Figure 76 shows R_{measured} versus $R_{\text{predicted}}$ using Models A1 and A2 at curvature Φ_p . The difference between the two compression models (Models 1 and 2) did not have a significant effect on the prediction for almost all the test data where the points appear to coincide.

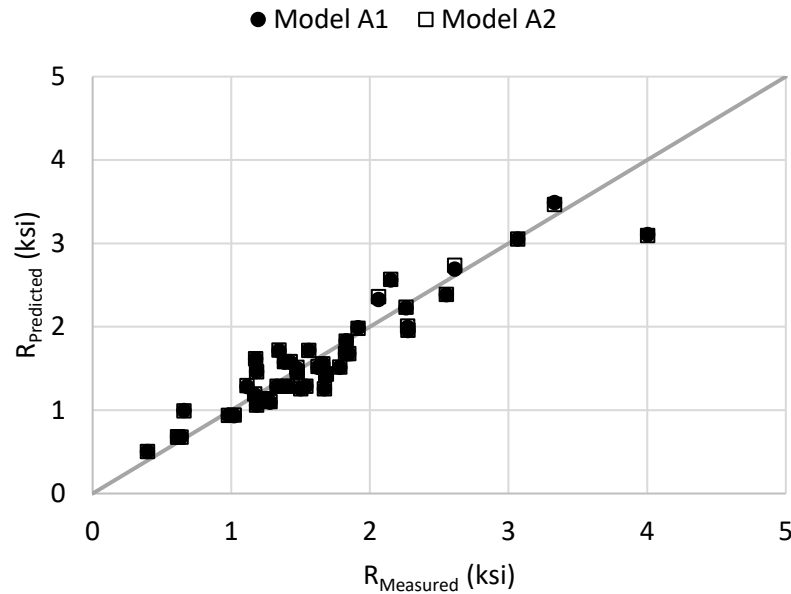


Figure 76: Measured versus predicted flexural resistance using Models A1 and A2 at curvature Φ_p

Figure 77 shows R_{measured} versus $R_{\text{predicted}}$ using Models A1, B1, and C1 at curvature Φ_p . The difference between tension Models A and B did not have a significant effect on the prediction for almost all the test data where the points appear to coincide. This indicates that introducing f_{cr} to the model did not make a significant effect on the prediction. While the difference between tension model C and the other two models (A and B) was more significant, where the tension model C reduces the prediction noticeably. This indicates that introducing f_R to the model underestimated the prediction. This can be attributed to the fact that UHPC in tension is acting across the entire tension height of the cross-section and reducing most of these tensile stresses to its half reduced the overall capacity significantly. However, using the tension Model A as the simplest form of idealization provided the best prediction accuracy for the considered test data.

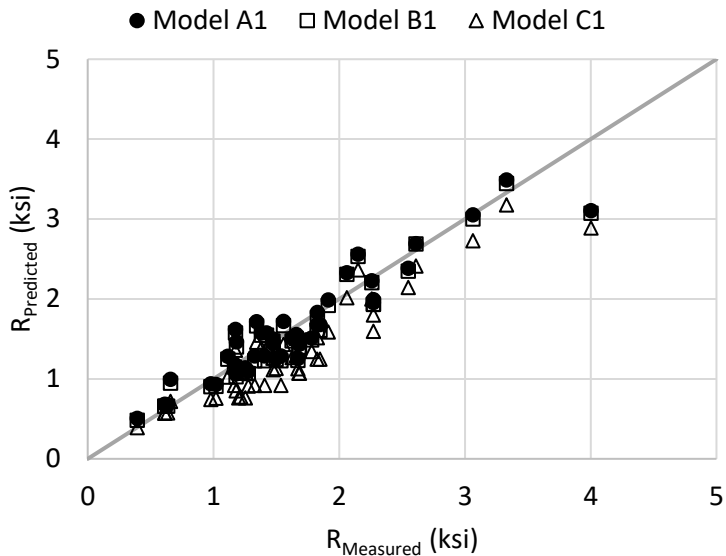


Figure 77: Measured versus predicted flexural resistance using Models A1, B1, and C1 at curvature Φ_p

Figure 78 shows R_{measured} versus $R_{\text{predicted}}$ using Models A1 and A1M at curvature Φ_p . No significant difference can be noticed between the two models. This indicates that using $\epsilon_{tu} = 0.010$ instead of $\epsilon_{tu} = 0.004$ did not have a significant effect on the predicted flexural strength. This can be attributed to the fact that tension reinforcement is yielding in both models, which is the main contributor to the overall flexural strength of the component.

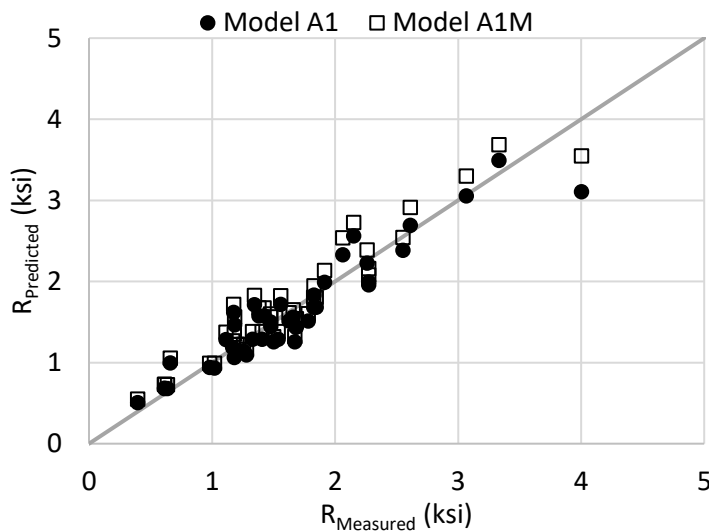


Figure 78: Measured versus predicted flexural resistance using Models A1 and A1M at curvature Φ_p

Table 20 summarizes the average and standard deviation of the measured-to-predicted flexural resistance ratio of the prediction models at curvature Φ_p and Φ_u . The CC model underestimated the prediction by 73%, while models A1 and A2 at curvature Φ_p provided the closest prediction with significantly low scattering. The predicted flexural resistance factor at curvature Φ_p was larger than that at curvature Φ_u by about 60% in tension models A and B, and about 33% in tension model C. The models having ($\mathcal{E}_{tu} = 0.010$) at curvature Φ_p overestimated the flexural strength by about 5%. This indicates that considering ($\mathcal{E}_{tu} = 0.010$) and using the simplest form of idealization in the tensile model (Model A) is not recommended. Having the simplest form of idealization in tension model A and ($\mathcal{E}_{tu} = 0.004$) provided the closest prediction of the measured flexural strength.

Table 20: Summary of the evaluation of the prediction models

Model ID	Measured-to-predicted Resistance Ratio at Curvature Φ_p		Measured-to-predicted Resistance Ratio at Curvature Φ_u	
	Average	Standard Deviation	Average	Standard Deviation
CC Model	N/A	N/A	1.73	0.65
Model A1	1.02	0.15	1.65	0.63
Model A2	1.01	0.15	1.65	0.63
Model A1M	0.94	0.13	1.56	0.67
Model A2M	0.95	0.13	1.59	0.65
Model B1	1.05	0.15	1.65	0.63
Model B2	1.05	0.15	1.65	0.63
Model C1	1.25	0.22	1.66	0.63
Model C2	1.25	0.22	1.66	0.63

4.1.2 Parameters Affecting Flexural Strength Prediction

The study presented in this section aims to investigate if the prediction accuracy is affected by different design parameters in the test data. The prediction provided by Model A2 at curvature Φ_p was selected in this study as it provided the closest prediction to the measured flexural strength. The first step is to identify which parameters have a significant effect on the measured flexural strength of the test data. A multiple regression model was developed

with the measured flexural strength as the response variable, and ρ , f_t , f'_c , and V_f as the explanatory variables. The four considered parameters showed a significant effect on the measured flexural strength where the p-values were 3.3×10^{-20} , 0.007, 0.041, and 0.063 for ρ , f_t , f'_c , and V_f , respectively. The next step is to study the effect of these parameters on the prediction accuracy which can be represented by the measured-to-predicted flexural resistance ratio ($R_{\text{Measured}} / R_{\text{Predicted}}$). Figure 79 plots $R_{\text{Measured}} / R_{\text{Predicted}}$ against the four considered parameter for all test data. It can be noticed that the $R_{\text{Measured}} / R_{\text{Predicted}}$ does not deviate significantly from the 1.0 horizontal line, which indicates that model accuracy is not sensitive to the variation in the study parameters. This shows that the prediction provided by Model A2 at curvature Φ_p provided a reasonable prediction accuracy regardless of the beam characteristics.

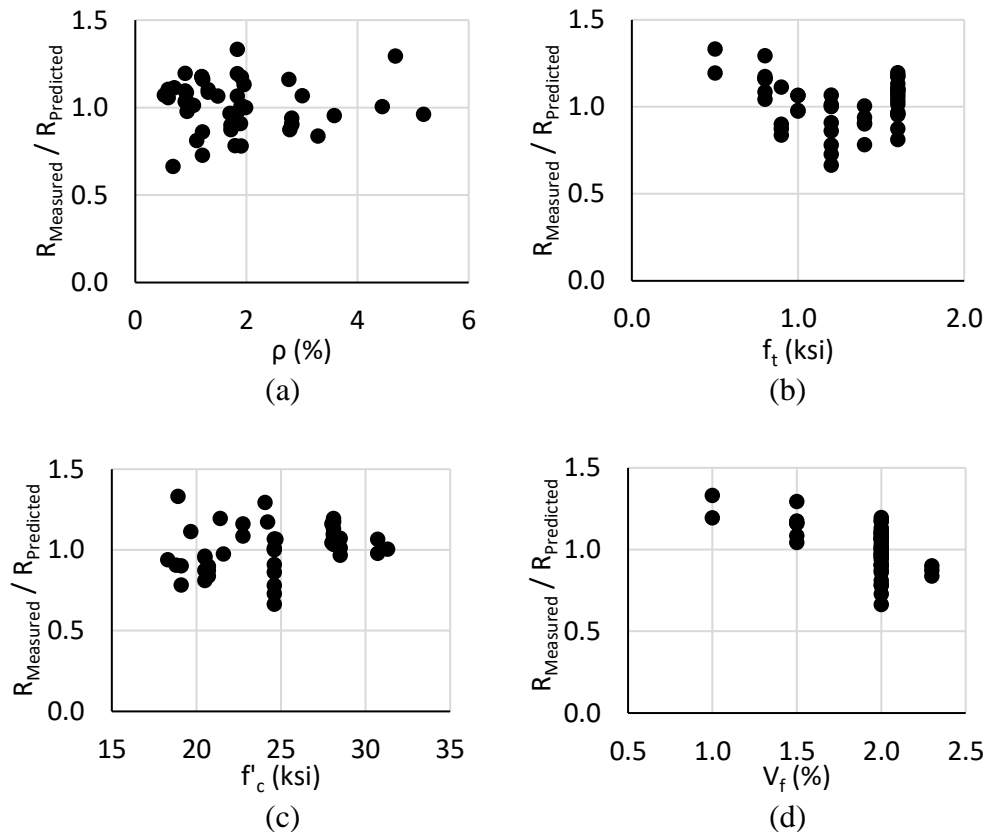


Figure 79: Measured-to-predicted flexural resistance factors versus design parameters:

a) ρ ; b) f_t ; c) f'_c ; and d) V_f

4.1.3 Flexural Testing of a Ribbed UHPC Slab

A flexure test of a UHPC ribbed slab was conducted to validate the prediction models presented earlier. Figure 80 shows the dimensions and detailing of the ribbed slab specimen reinforced with 2M16 (#5) top reinforcement and 2M19 (#6) bottom reinforcement Grade 60 steel. The 28-day compressive strength was 18.4 ksi, and flexural strength was 3.6 ksi which was evaluated according to ASTM C1609 performed on 3 x 3 in² prisms having a 12 in. span. Figure 81 shows the test setup where a mid-span spreader beam was used to apply a concentrated load on the slab up to failure in the tension zone. String potentiometers were used to measure the mid-span deflection and strain gauges were installed to measure the strain in UHPC.

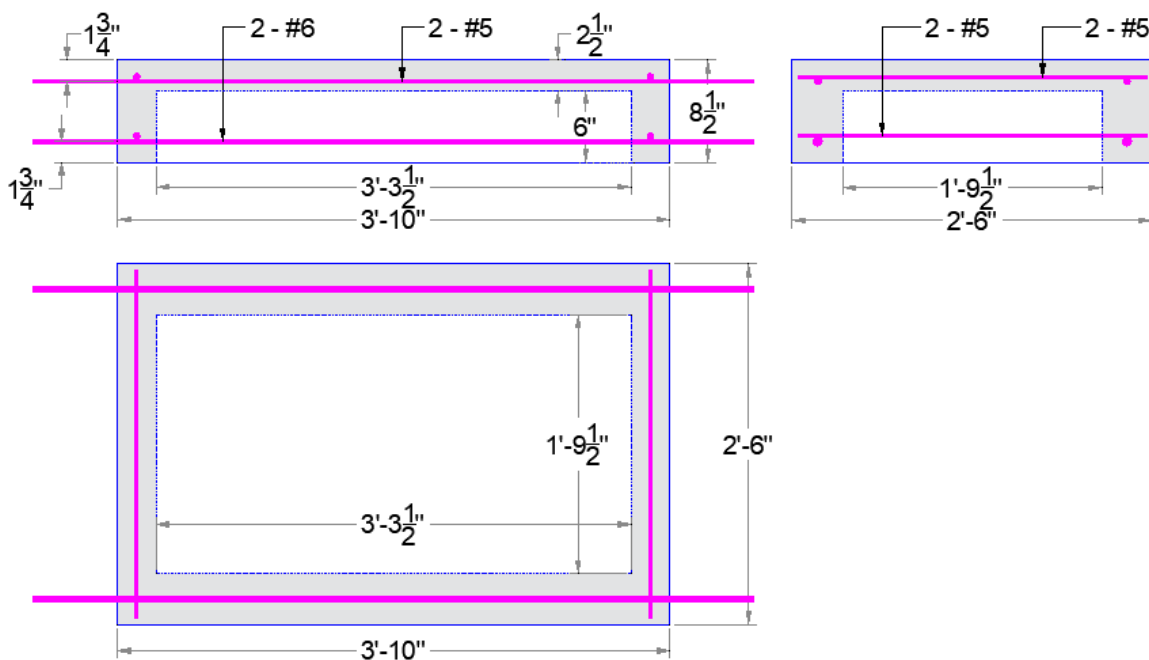


Figure 80: Ribbed slab dimensions and reinforcement



Figure 81: Test setup of the ribbed slab

Figure 82 shows the moment-deflection plot of the ribbed slab where the peak moment reached 63.2 kip.ft at a deflection of 0.46 in.. The predicted M_u was 34.9 kip.ft, while the predicted M_p was 59.3 kip.ft. The load application was stopped after a wide flexural crack was noticed in the tension area, and signs of UHPC crushing in compression started to appear under the spreader beam as shown in Figure 83. The measured-to-predicted flexural strength was 1.07, and 1.81 at curvatures Φ_p , and Φ_u respectively, which indicates reasonable prediction accuracy at curvature Φ_p . It can be noticed that the slab sustained slightly higher flexural strength than M_p for a significant amount of deformation which can be attributed to UHPC capacity to sustain tensile stresses for high deformations.

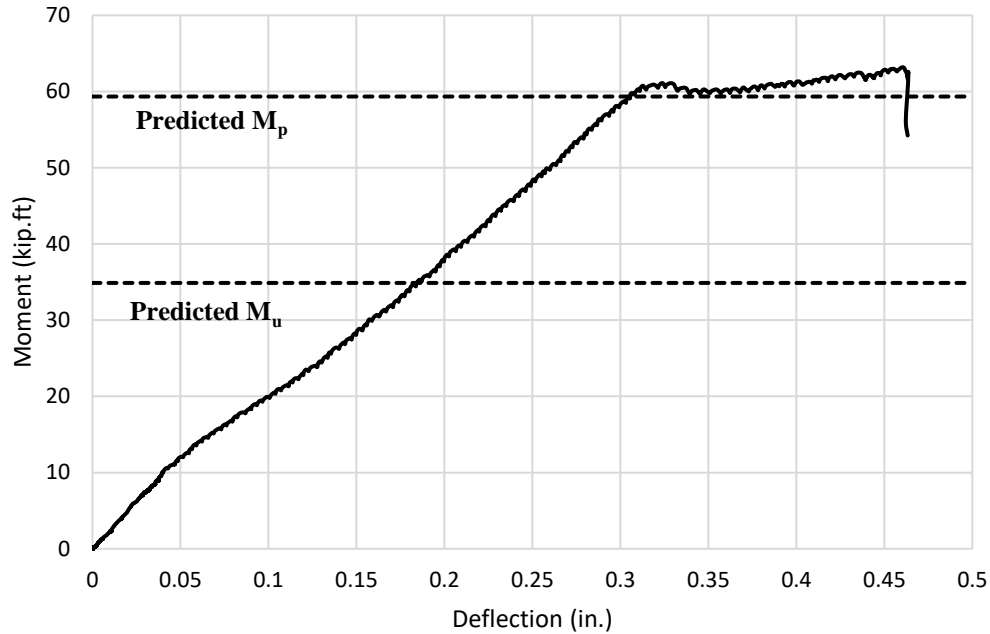


Figure 82: Moment-deflection plot of the flexure test of the ribbed slab



Figure 83: Flexure failure mode in the ribbed slab

4.2 Shear Strength of UHPC Beams

This section will present a study to evaluate the accuracy of shear strength prediction models of UHPC beams (discussed in section 2.4.1). UHPC beams shear test data (discussed in section 2.4.2) are used to compare measured versus predicted shear strength then the results will be evaluated statistically for their average and standard deviation.

4.2.1 Analysis of UHPC Beams Shear Test Data

Prediction models were evaluated by comparing measured versus predicted shear strength for the test data presented earlier. Safety factors were set to 1.0 when calculating the predicted shear strength of UHPC beams. Crack angles that were not reported for some tests were assumed based on shear failure photos. The tensile strength that was not reported for some tests was assumed based on direct tension or flexural test results. A conversion factor was used to convert the tensile strength obtained from flexure testing to that obtained from direct tension test. This conversion factor was found to be 0.377 based on the average of the German guidelines for UHPC, DAfStb-2017, and Swiss standard SIA 2052, 2016. The conversion factor is multiplied by the post-cracking flexural tensile strength to get the axial tensile strength and is based on having the neutral axis located at a distance of about 82% of the prism height from the extreme tension surface. Table 21 presents three-point bending tests conducted in the literature to quantify the residual tensile strength of UHPC. It shows that the size of the prism has a significant effect on the measured tensile strength. Average values from this table were used to estimate the residual tensile strength of UHPC in the terms $f_{R,4}$, f_{ftuk} , $\sigma_{Rd,f}$, f_{rr} , or $f_{t,loc}$ in the five considered prediction models, respectively. For example, for fiber volume fraction of 2%, $f_{R,4}$ would be 4.3 ksi, while for mixes with 2.5% and 1% fiber volume fraction, $f_{R,4}$ would be the 5.8 and 0.4 ksi, respectively. For, mixes with different fiber volume fractions, values are estimated by interpolation.

Table 21: Three-point bending tests on notched prisms to evaluate residual tensile strength

Reference	Fiber Volume Fraction (V_f)	Fiber Length (l_f) (in.)	Fiber Diameter (Φ_f) (in.)	Cylinder Compressive Strength (f'_c) (ksi)	Prism Cross Section (in. ²)	Notch Height (in.)	Span (in.)	Residual Flexural Tensile Strengths ($f_{R,i}$) (ksi)			
								$f_{R,1}$	$f_{R,2}$	$f_{R,3}$	$f_{R,4}$
Prem et al., 2012 (R1 Mix)	2.5%	0.5	0.006	26.1	2.8 x 2.8	0.83	11.8	6.6	7.2	6.2	5.8
Prem et al., 2012 (R2 Mix)	2%	0.5	0.006	24.6	2.8 x 2.8	0.83	11.8	5.4	5.8	5.4	5.0
Yang et al., 2010 (average)	2%	0.5	0.008	27.7	3.9 x 3.9	0.39	11.8	3.9	4.4	4.0	3.6
Graybeal, 2006 (M2P02)	2%	0.5	0.008	18.3	2.0 x 4.0	1.00	16.0	3.2	3.0	--	--
Zagon et al., 2016 (average)	1%	0.4	0.007	20.5	3.9 x 3.9	1.06	15.7	1.7	0.9	0.6	0.4

The upper limit of shear strength of conventionally reinforced concrete beams according to AASHTO LRFD, 2017 and ACI 318, 2014 is plotted as a reference horizontal line with the measured shear strength of UHPC beams. The limits are calculated according to equations 30 and 31 for AASHTO, 2017 and ACI 318, 2014, respectively.

$$\frac{V_c + V_s}{b_w d} \leq 0.25 f'_c \text{ [ksi]} \quad (62)$$

$$\frac{V_c + V_s}{b_w d} \leq 0.41 \sqrt{f'_c} \text{ [ksi]} \quad (63)$$

Where, (V_c) is the concrete contribution to shear strength (lbs); (V_s) is the transverse reinforcement contribution to shear strength (lbs); (f'_c) is the cylinder compressive strength in (ksi); (b_w) is the minimum web width (in.); (d_v) is the effective shear depth between the resultants of the tensile and compressive forces due to flexure (in.).

Girder compressive strength was considered as 10 ksi as an upper limit for the conventional concrete compressive strength as required by AASHTO LRFD, 2017 and ACI 318, 2014. Measured shear strengths of UHPC girders without transverse reinforcement exceeded the

ACI 318, 2014 upper limit for most of the data points, and can meet and exceed the upper limit of AASHTO, 2017 as shown in the below sections.

RILEM TC 162-TDF, 2003

Reasonable assumptions for unreported values of $f_{R,4}$ were made according to Table 21. For example, $f_{R,4}$ was assumed as 4.3 ksi for test data having $V_f = 2.0\%$. Figure 84 plots the measured versus predicted shear strength using RILEM TC 162-TDF model. The average $\frac{(V_u)_{measured}}{(V_u)_{predicted}}$ was 2.7, with a standard deviation of 0.88. It can be noticed that safety margin increases with the increase of the measured shear strength.

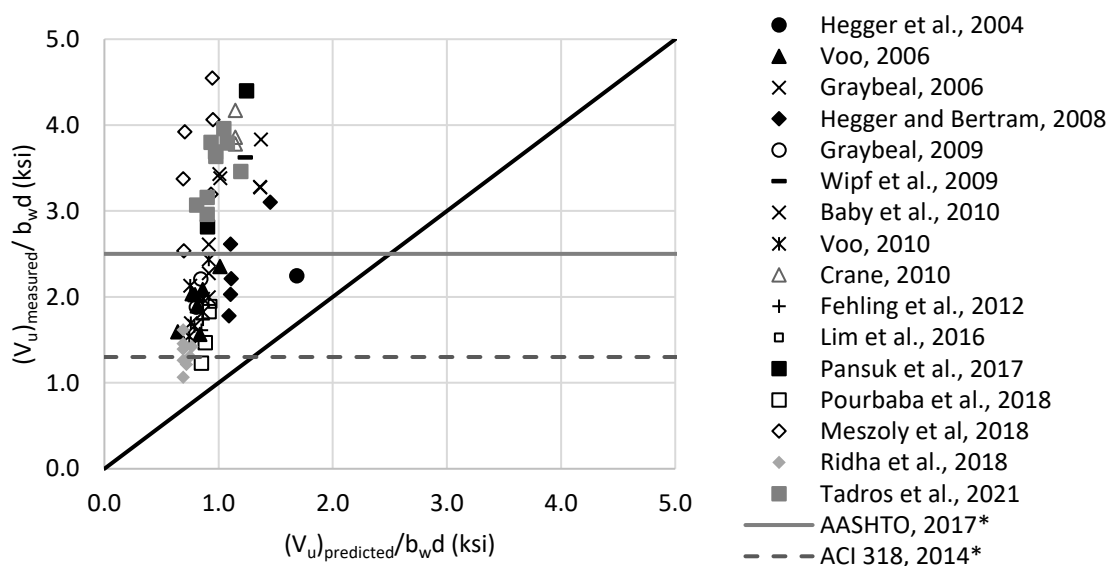


Figure 84: Measured versus predicted shear strength according to RILEM TC 162-TDF, 2003

*Upper limits of the combined contribution of concrete and transverse reinforcement of conventionally reinforced concrete (10 ksi)

fib Model Code, 2010

Reasonable assumptions for unreported values of f_{ftuk} were made according to Table 21. For example, f_{ftuk} was assumed as 1.6 ksi for test data having $V_f = 2.0\%$. This assumption is based on equations (23) and (24) and having the flexural tensile strengths $f_{R,i}$ according to Table 21. Figure 85 shows the measured versus predicted shear capacities plot for the

considered data points. The average $\frac{(V_u)_{measured}}{(V_u)_{predicted}}$ was 2.4, with a standard deviation of 0.74.

It can be noticed that the predicted shear strength is close to what the RILEM TC 162-TDF, 2003 provides.

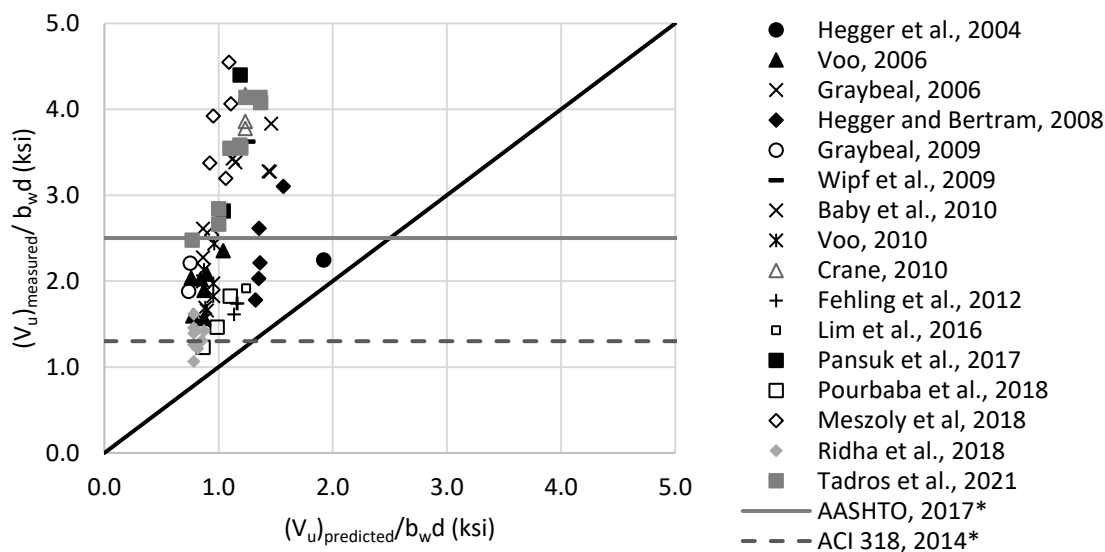


Figure 85: Measured versus predicted shear strength according to the *fib* Model Code, 2010

*Upper limits of the combined contribution of concrete and transverse reinforcement of conventionally reinforced concrete (10 ksi)

French standard, NF P 18-710, 2016

Reasonable assumptions for unreported values of $\sigma_{Rd,f}$ were made according to Table 21. For example, $\sigma_{Rd,f}$ was assumed as 1.6 ksi for test data having $V_f = 2.0\%$. Figure 86 shows the measured versus predicted shear strength plot for the considered data points. The average $\frac{(V_u)_{measured}}{(V_u)_{predicted}}$ was 1.1, with a standard deviation of 0.38. It can be noticed that the data are well distributed around the 45-degree angle line indicating a reasonable consistency in the prediction accuracy.

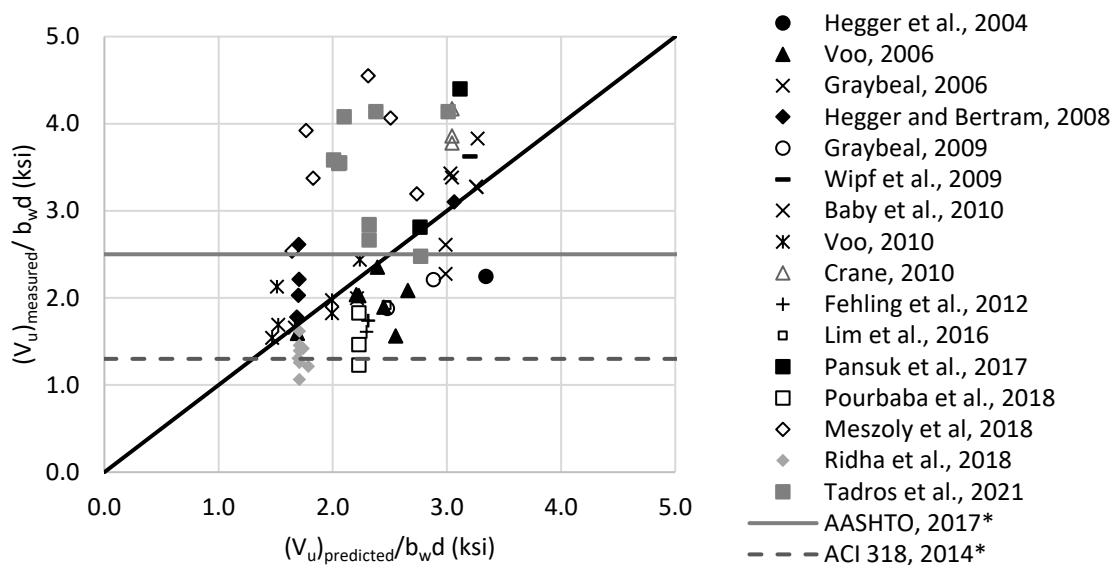


Figure 86: Measured versus predicted shear strength according to French Standard NF P 18-710, 2016

*Upper limits of the combined contribution of concrete and transverse reinforcement of conventionally reinforced concrete (10 ksi)

PCI-UHPC Structures Design Guide, 2021

The assumed value of f_{rr} was limited to 0.75 ksi as recommended by the model. This value is significantly lower than what is typically achieved by commonly used UHPC mixes which caused the predicted shear strengths to be significantly underestimated. Crack angle was calculated according to the suggested procedure of the model and were limited to range between 27.6 and 50.0 degrees as recommended. Figure 87 plots the measured versus predicted shear strength using PCI-UHPC Structures Design Guide model. The average $\frac{(V_u)_{measured}}{(V_u)_{predicted}}$ was 2.5, with a standard deviation of 1.14. It should be noted that the French Standard considers the level of prestressing while the PCI-UHPC model does not consider the level of prestressing term for simplicity. The effect of prestressing is only considered in that model when estimating the crack angle.

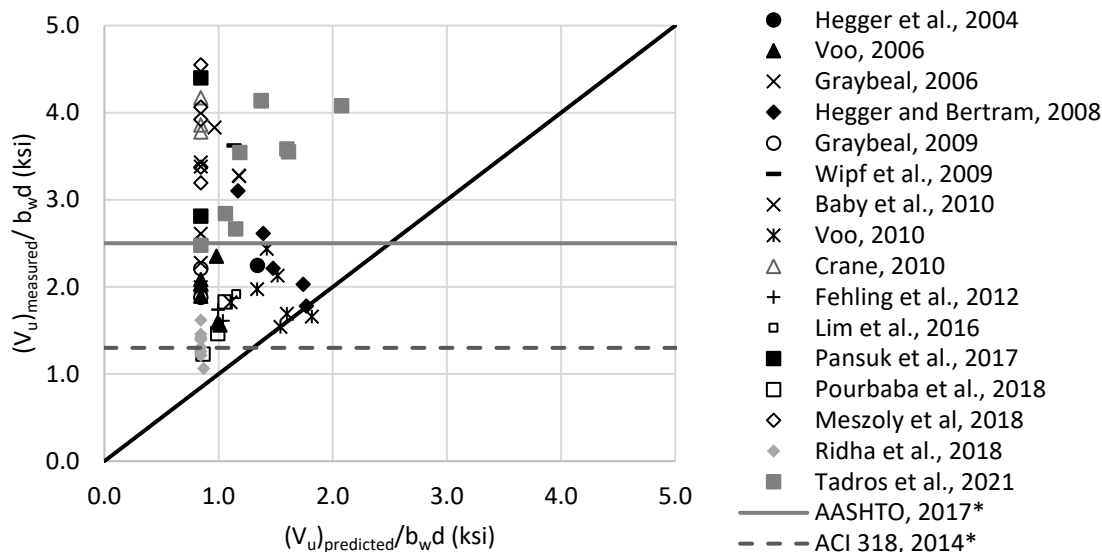


Figure 87: Measured versus predicted shear strength according to PCI-UHPC Structures Design Guide, 2021

*Upper limits of the combined contribution of concrete and transverse reinforcement of conventionally reinforced concrete (10 ksi)

Draft of AASHTO Guide Specification for Structural Design with UHPC, 2021

Reasonable assumptions for unreported values of $f_{t,loc}$ were made according to Table 21. For example, $f_{t,loc}$ was assumed as 11.0 MPa (1.6 ksi) for test data having $V_f = 2.0\%$. The localization strain ($\epsilon_{t,loc}$) was assumed as 0.007 for all test data based on the average of the recommended upper and lower values (0.004 and 0.010) as discussed in section 2.3.1. Figure 88 plots the measured versus predicted shear strength using Draft AASHTO model. The average $\frac{(V_u)_{measured}}{(V_u)_{predicted}}$ was 1.5, with a standard deviation of 0.63. This indicates that the prediction provided by the that model is slightly more conservative than that provided by the French Standard. Similar to the PCI-UHPC Structures Design Guide model, this model does not consider the level of prestressing term and only considers the prestressing effect in the crack angle estimation.

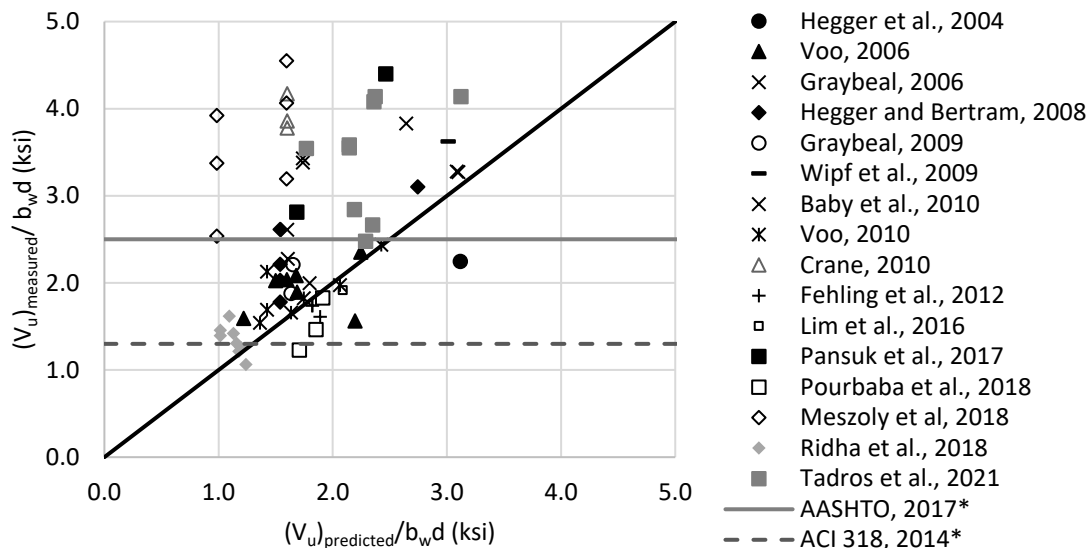


Figure 88: Measured versus predicted shear strength according to Draft of AASHTO Guide Specification for Structural Design with UHPC, 2021

*Upper limits of the combined contribution of concrete and transverse reinforcement of conventionally reinforced concrete (10 ksi)

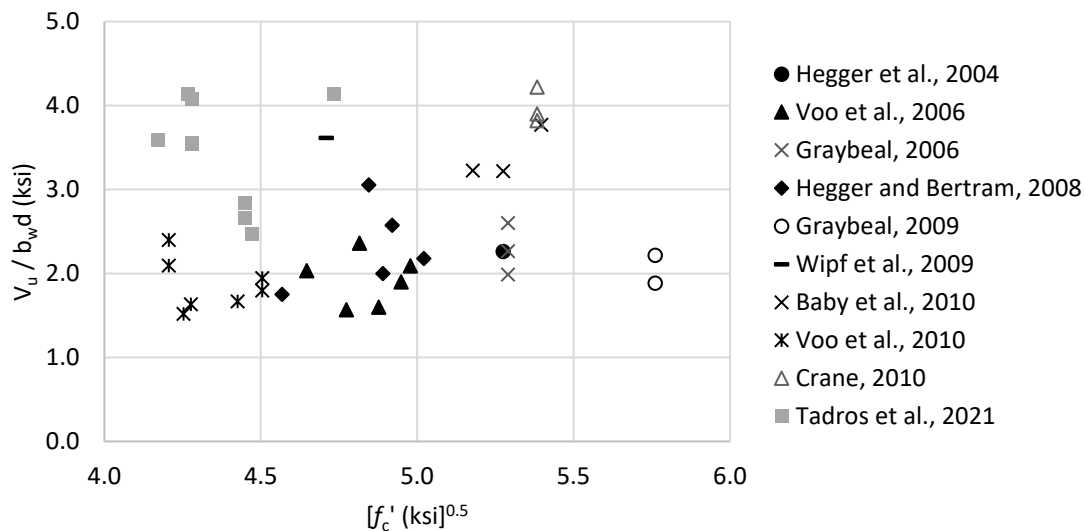
Table 22 summarizes the outcomes of model evaluation. The table shows that the French Standard NF P 18-710, 2016 provided the closest estimation of the shear strength followed by the Draft of AASHTO Guide Specification for Structural Design with UHPC, 2021. The PCI-UHPC Structures Design Guide, 2021 underestimated the predicted shear strength significantly due to the limitation of UHPC tensile strength. The *fib* Model Code, 2010, and RILEM TC 162-TD, 2013 models provided significantly conservative prediction as they were developed for steel fiber-reinforced concrete. The French Standard NF P 18-710, 2016 also provided the least standard deviation, which indicates the highest consistency in the shear strength prediction.

Table 22: Summary of evaluation of prediction models

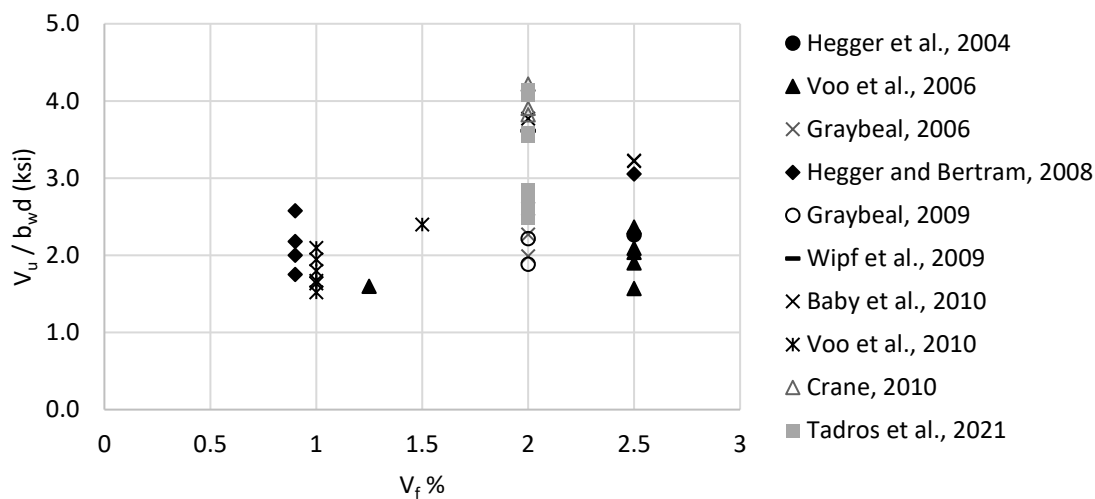
International Practice	Average $\frac{(V_u)_{measured}}{(V_u)_{predicted}}$	Standard Deviation
RILEM TC 162-TDF, 2003	2.7	0.88
<i>fib</i> Model Code, 2010	2.4	0.74
French Standard NF P 18-710, 2016	1.1	0.38
PCI-UHPC Structures Design Guide, 2021	2.5	1.14
Draft of AASHTO Guide Specification for Structural Design with UHPC, 2021	1.5	0.63

4.2.2 Parameters Affecting Shear Strength Prediction

Test data listed in Table 8 were used to evaluate the effect of key parameters, such as compressive strength, fiber content, tensile strength and level of prestressing, on the shear strength of prestressed UHPC beams. Figure 89 a, b, c, and d plot $[f_c']^{0.5}$, V_f , $\mathcal{G}_{Rd,f}$, and \mathcal{G}_{cp} , respectively, versus measured shear strength. These plots indicate there is no strong correlation between any of these parameters and the shear strength of prestressed UHPC beams. Correlation coefficients were calculated using Pearson correlation test and were found to be 0.05, 0.36, 0.44, and 0.33 for $[f_c']^{0.5}$, V_f , $\mathcal{G}_{Rd,f}$, and \mathcal{G}_{cp} , respectively. These coefficients indicate that there is only a moderate correlation between $\mathcal{G}_{Rd,f}$ and the shear strength, which is in agreement with the prediction models presented earlier. In addition, to test for the statistical significance of these key parameters on the shear strength of prestressed beams, a multiple regression analysis was performed for shear strength as the dependent variable and $[f_c']^{0.5}$, V_f , $\mathcal{G}_{Rd,f}$, and \mathcal{G}_{cp} as the independent variables using 5% significance level. Only $\mathcal{G}_{Rd,f}$, and \mathcal{G}_{cp} were found to have significant effects as their P-values were 0.019, and 0.001 respectively, while $[f_c']^{0.5}$, and V_f had P-values of 0.43, and 0.69 respectively, which indicate that their effects are statistically insignificant.



(a) effect of the square root of UHPC compressive strength ($[f'_c]^{0.5}$)



(b) effect of fiber volume fraction (V_f)

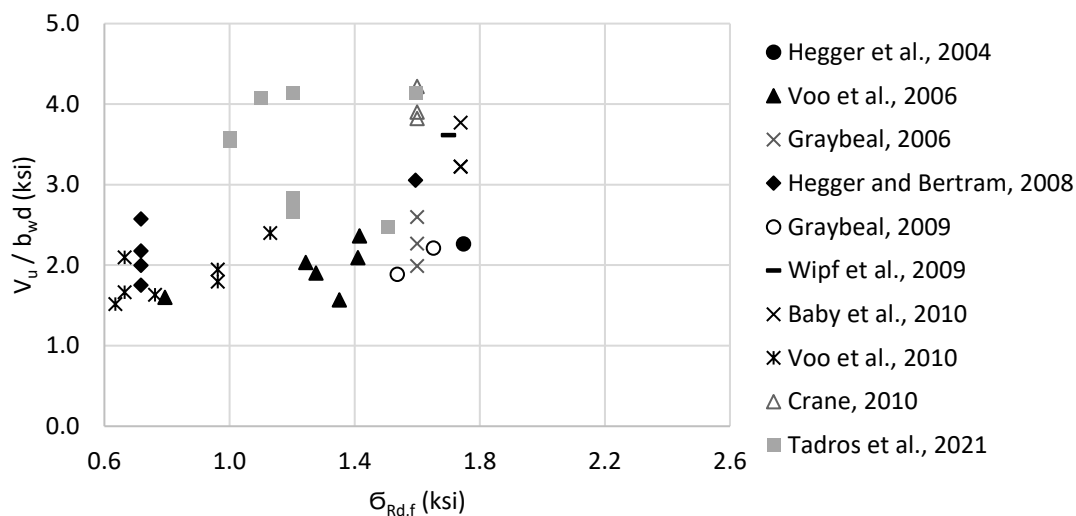
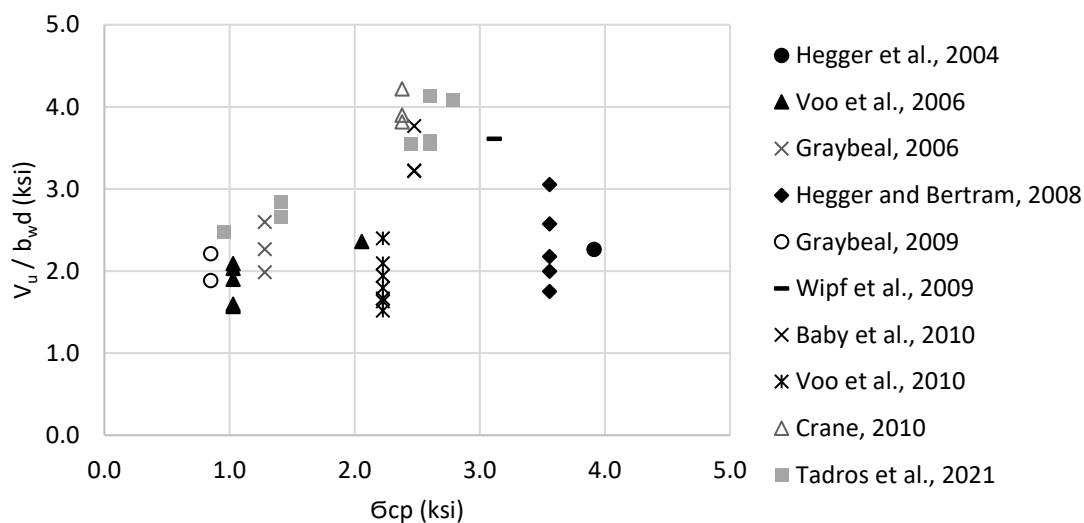
(c) effect of UHPC post-cracking tensile strength ($\sigma_{Rd,f}$)(d) effect of level of prestressing (σ_{cp})

Figure 89: Effect of key parameters on shear strength of prestressed UHPC beams

In order to have a more homogenous group of test data, specimens having fiber volume fraction less than 2% ($V_f < 2.0\%$) were omitted since the commonly used V_f in UHPC mixtures is at least 2%. Also, Hegger et al., 2004 specimen was omitted as the prestressing force was not fully utilized due to strand slippage. The remaining specimens yielded a strong correlation between level of prestressing (σ_{cp}) and the shear strength ($V_u/b_w d$) as

shown in Figure 90. Multiple regression analysis was done on that group and resulted that $\bar{\sigma}_{cp}$ and V_f were statistically significant as the P-value were 1×10^{-7} , and 6×10^{-5} respectively, while $[f_c']^{0.5}$ and $\bar{\sigma}_{Rd,f}$ had P-values of 0.96, and 0.86 respectively. The resulting relation between the shear strength and V_f was very weak which is in agreement with the Pearson correlation test results of the multiple regression analysis.

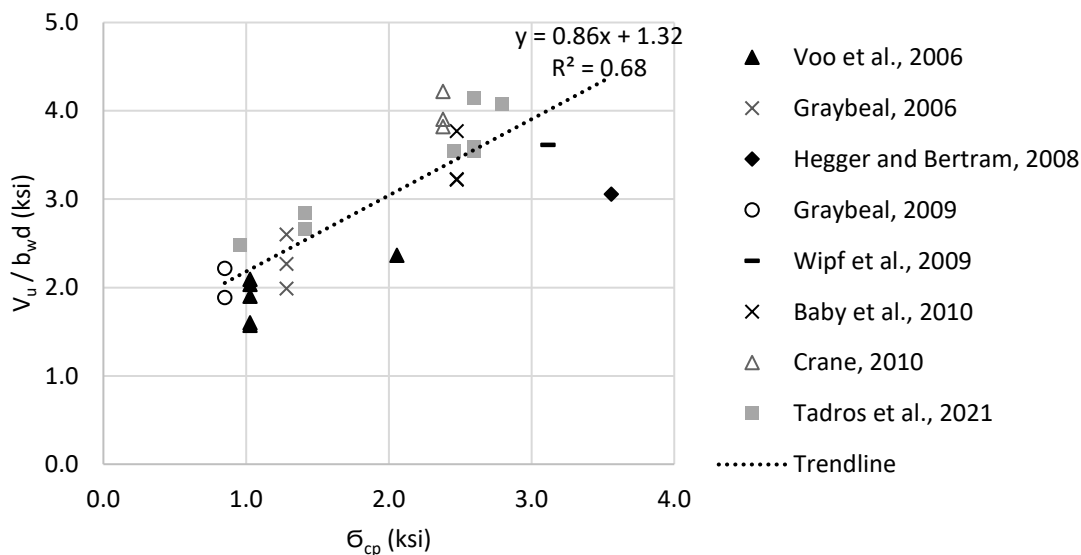
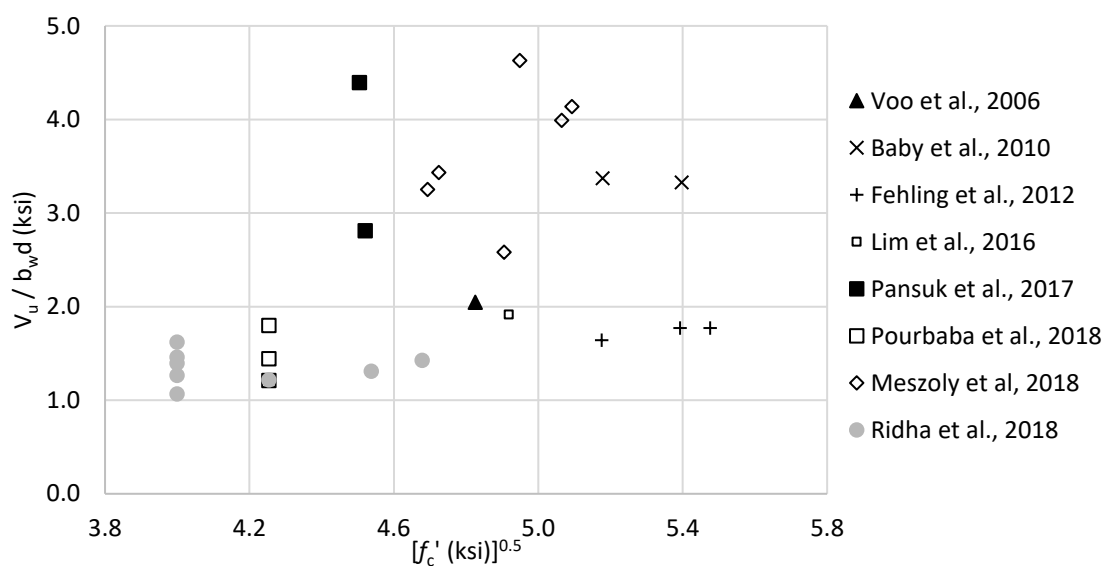


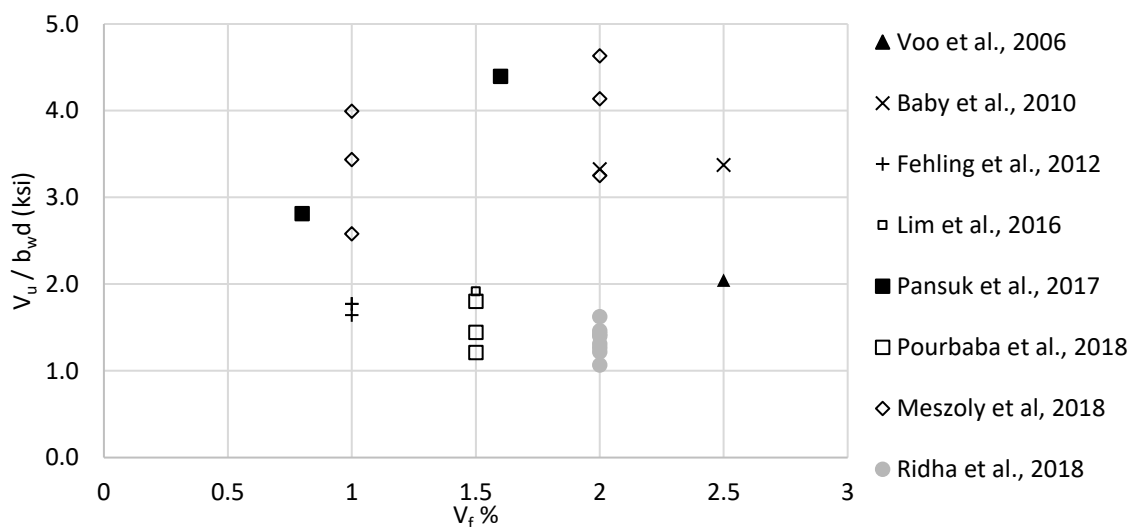
Figure 90: Effect of the level of prestressing ($\bar{\sigma}_{cp}$) on the shear strength for prestressed beam with $V_f \geq 2.0\%$

Test data listed in Table 9 were used to evaluate the effect of key parameters, such as compressive strength, fiber content, tensile strength and reinforcement ratio, on the shear strength of non-prestressed UHPC beams. Figure 91 a, b, c, and d plot $[f_c']^{0.5}$, V_f , $\bar{\sigma}_{Rd,f}$, and A_l/b_wd , respectively, versus measured shear strength. These plots indicate that no strong correlation between any of these parameters and the shear strength of non-prestressed UHPC beams. Correlation coefficients were calculated using Pearson correlation test and were found to be 0.49, -0.05, 0.60, and 0.43 for $[f_c']^{0.5}$, V_f , $\bar{\sigma}_{Rd,f}$, and A_l/b_wd , respectively. These coefficients indicate that there is only a moderate correlation between $\bar{\sigma}_{Rd,f}$ and the shear strength, which is in agreement with the prediction models presented earlier in section 2. In addition, to test for the statistical significance of these key parameters on the shear strength of non-prestressed beams, a multiple regression analysis

was performed for shear strength as the dependent variable and $[f_c']^{0.5}$, V_f , $\mathcal{G}_{Rd,f}$, and $A_l/b_w d$ as the independent variables using 5% significance level. Only $\mathcal{G}_{Rd,f}$ was found to have a significant effect, where the P-value was 0.024, while $[f_c']^{0.5}$, V_f , and $A_l/b_w d$ had P-values of 0.22, 0.92, and 0.90, which indicate that their effects are statistically insignificant.



(a) effect of the square root of UHPC compressive strength ($[f_c']^{0.5}$)



(b) effect of fiber volume fraction (V_f)

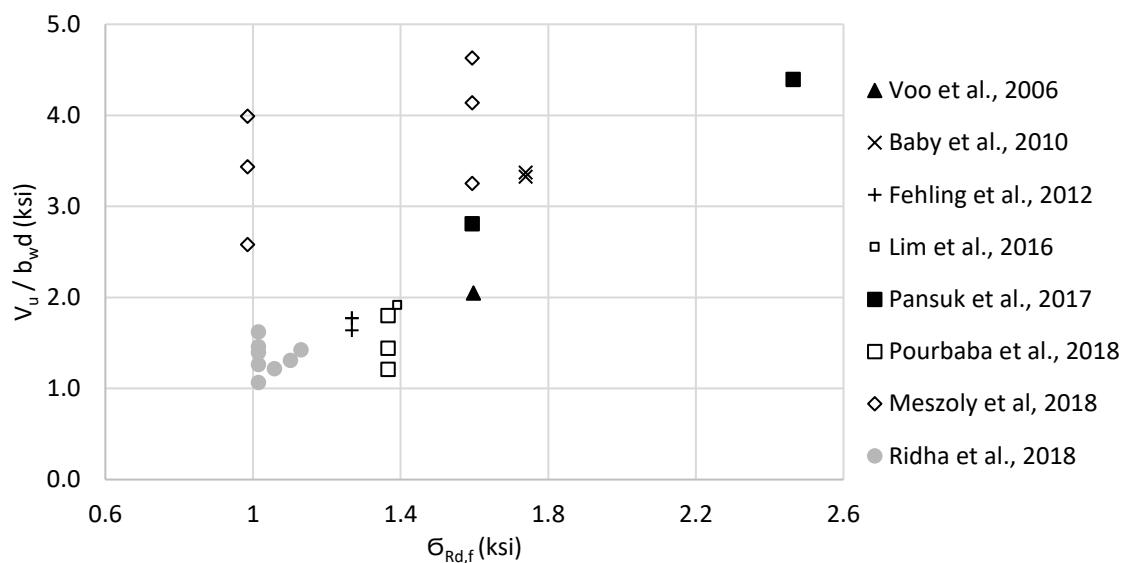
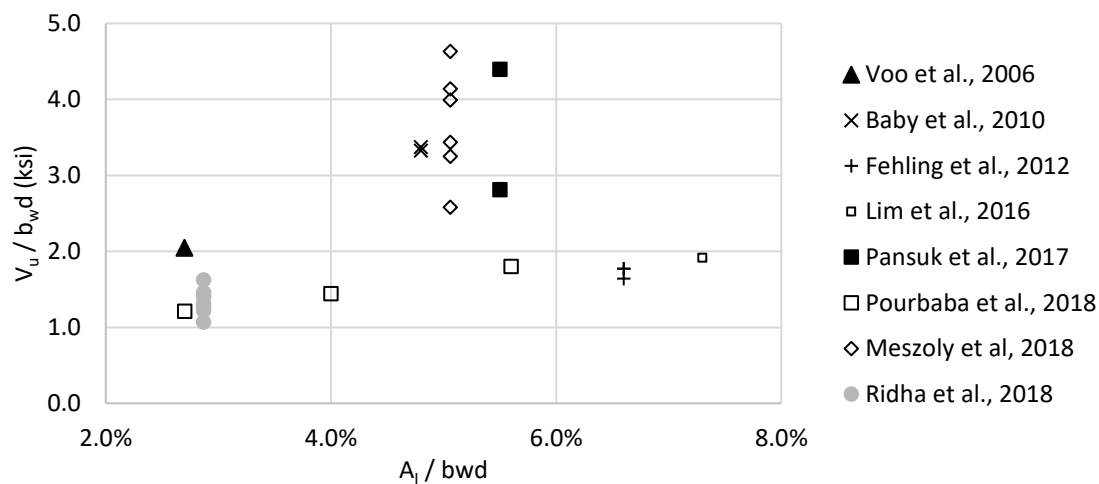
(c) effect of UHPC post-cracking tensile strength ($\sigma_{Rd,f}$)(d) effect of longitudinal reinforcement ratio ($A_l/b_w d$)

Figure 91: Effect of key parameters on shear strength of non-prestressed UHPC beams

In order to have a more homogenous group of test data, specimens having fiber volume fraction less than 2% ($V_f < 2.0\%$) were omitted since the commonly used V_f in UHPC mixtures is at least 2%. The remaining specimens yielded a strong correlation between reinforcement ratio (A_l/b_wd) and the shear strength as shown in Figure 92. Multiple regression analysis was done on that group and resulted that A_l/b_wd was statistically significant as the P-value was 0.024, while $[f_c']^{0.5}$, V_f , and $\sigma_{Rd,f}$ had P-values of 0.82, 0.89, and 0.49 respectively which is in agreement with the Pearson correlation test results.

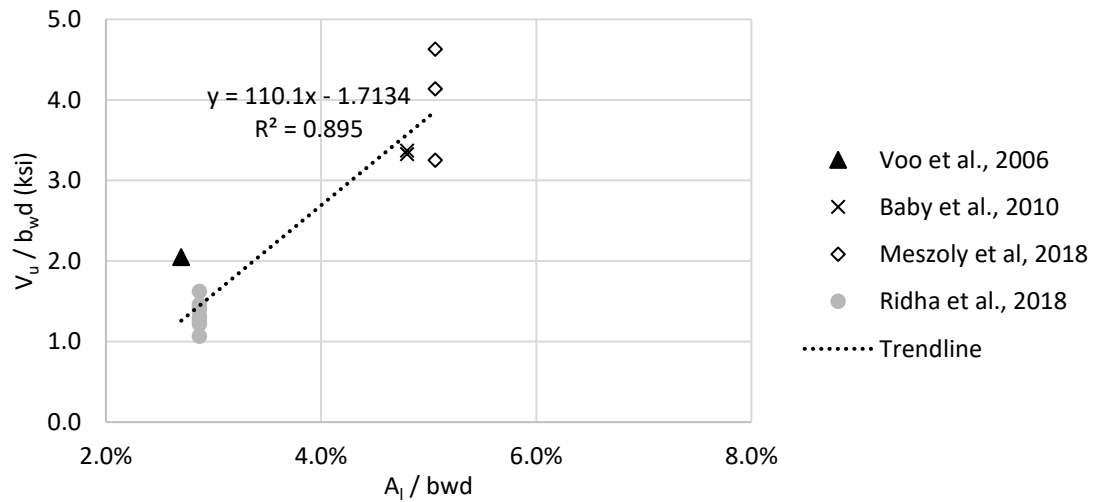


Figure 92: Effect of the longitudinal reinforcement ratio (A_l/b_wd) on the shear strength of non-prestressed UHPC beams with $V_f \geq 2.0\%$

Chapter 5 – Flexural Strengthening using UHPC

This chapter presents the proposed concept of using UHPC in flexural strengthening techniques and utilizing its advantages. The implementation of flexural strengthening techniques in actual projects is presented in the form of construction procedures for a beam example. Then, the design process of a composite (strengthened) CC-UHPC is presented in the form of developing the flexural strength prediction model. Flexure testing of CC-UHPC beams is also presented to validate the prediction of the developed model.

5.1 Construction Procedure and Design

5.1.1 Flexural Strengthening Procedure using UHPC

The general technique of utilizing UHPC in the flexural strengthening of an existing CC beam is presented in Figure 93 where UHPC can be used as an encasement/jacketing layer around the CC beam. The UHPC encasement can be added on the soffit of the existing beam (1 side), or a U-shaped wrap (3 sides) to strengthen in both shear and flexure, or a 4-sided encasement all around the member to strengthen both the tension and compression zones of the member. The additional reinforcement can be non-prestressed or prestressed depending on the strengthening demand. The CC-UHPC interface must be designed to resist the forces carried by the UHPC layers. The interface can be designed with conventional anchors similar to other CC encasement techniques, and it can be designed without anchors depending on the superior interface shear resistance between CC and UHPC. Suggested procedure is proposed similar to other techniques according to the FHWA Bridge Maintenance Reference Manual, 2015.

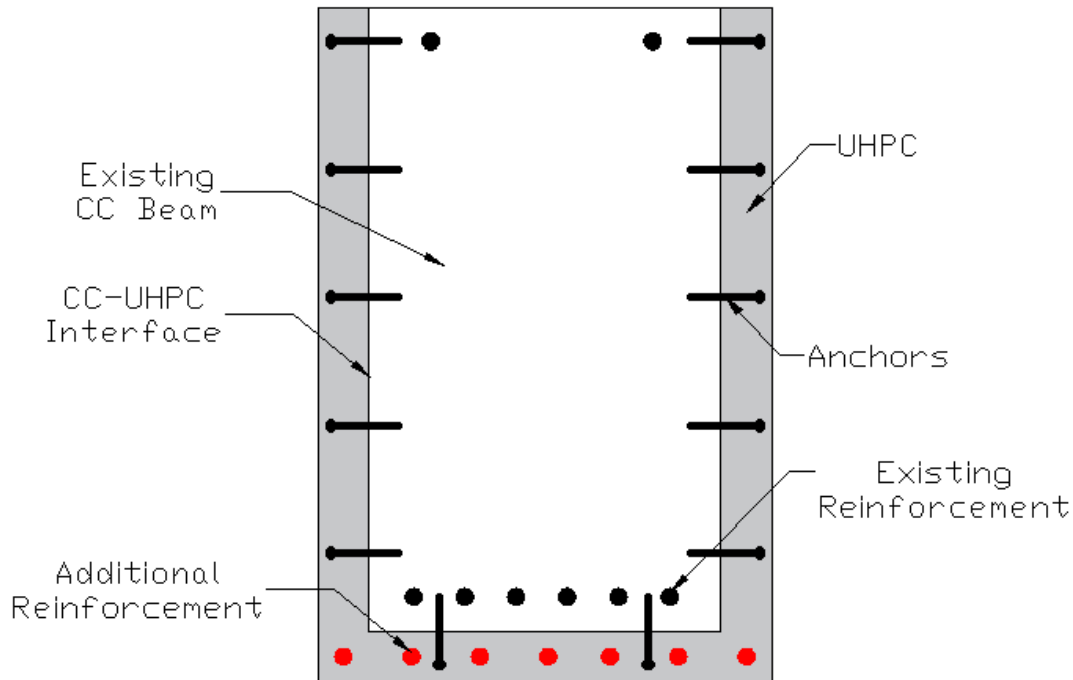


Figure 93: General technique of using UHPC encasement for flexural strengthening of an existing CC beam

When dealing with additional prestressed reinforcement (external post-tensioning), the exposed strands can be removed after UHPC placement. This should help avoid the major disadvantage of the common external post-tensioning technique where the existing component shall be designed to withstand accidental loads. The design example at section 7.1 discusses the procedure of designing flexural strengthening using UHPC with additional prestressed reinforcement. The general construction procedure is presented when the additional reinforcement is non-prestressed and when it is prestressed as follows:

Suggested Construction Procedure for Non-Prestressed Additional Reinforcement:

- 1- Interface Preparation: the existing CC surface should be roughened to increase the interface shear resistance. Then the surface should be cleared of all dust, dirt, oil, grease, or fine particles of concrete that could reduce the interface shear resistance.
- 2- Anchors Installation: Holes should be drilled first and their location and spacing are determined according to the interface design. Then the anchors are fixed

according to manufacturer's recommendations, typically a high-strength epoxy is required.

- 3- Formwork and Rebar Installation: the formwork should be assembled and installed to be rigidly attached to the existing component. The formwork should be watertight since UHPC is highly flowable. The forms should be cleaned and oiled before installation.
- 4- UHPC Placement: Live loads should be reduced or restricted from acting on the existing component before placing UHPC to minimize stresses and deformations before UHPC is placed and gains some of its strength. UHPC can be poured from small opening in the sides or top of the form, opening can be as small as 2-inch diameter circular shafts.
- 5- Formwork stripping: formwork can be stripped after UHPC hardens (typically 6 hours), live loads should fully return to act on the component once UHPC achieves the mechanical properties required by structural design.

Suggested Construction Procedure for Prestressed Additional Reinforcement:

- 1- Anchors Installation: Anchors should be installed along the length of UHPC strengthening according to interface design. Larger anchors should be installed at the ends of strengthening length to allow for external post-tensioning. Holes should be drilled first and their location and spacing are determined according to the interface design. Then the anchors are fixed according to manufacturer's recommendations, typically a high-strength epoxy is required.
- 2- Interface Preparation: the existing CC surface should be roughened to increase the interface shear resistance. Then the surface should be cleared of all dust, dirt, oil, grease, or fine particles of concrete that could reduce the interface shear resistance.
- 3- Casting of End Blocks: End blocks should be casted using CC with a similar procedure to external post-tensioning. The end blocks can be casted using UHPC to reduce their dimensions.
- 4- External Post-Tensioning: strands shall be tensioned through the end block with a similar procedure to the existing post-tensioning technique. The strands can be

tensioned at two live ends, or from one live end and the other one will be considered a dead end.

- 5- Formwork Installation: the formwork should be installed along the tensioned strands and should be watertight to avoid leakage during UHPC placement.
- 6- UHPC Placement: UHPC should be placed along the strands to transfer the forces between the strand and existing CC component.
- 7- Removal of Strand Ends: exposed strand ends can be cut to reduce the vulnerability to vandalism and environmental actions.

5.1.2 Development of Prediction Model of CC-UHPC Beams in Flexure

This section presents the development of the prediction model estimating the flexural strength of CC-UHPC components subjected to pure flexure. The model can predict the strength of non-prestressed and prestressed components and is based on the principles of strain compatibility and internal forces equilibrium.

Model Limitations and Assumptions

The developed prediction model can only be applied to composite CC-UHPC sections that act as fully-composite up to failure. The assumptions used to develop this model are as follows:

1. No interface failure or relative displacement will happen between CC and UHPC up to failure, and the section behaves as fully-composite.
2. The strain compatibility approach is valid across the entire composite section height up to failure.
3. The used UHPC in the repair and strengthening application does not satisfy the mechanical property requirements highlighted in Chapter 3.
4. The strain profile is governed by the material failure modes, the possible failure modes that can happen in the CC-UHPC composite are shown in Figure 94 as follows:
 - a) Tension failure in UHPC (or reaching the crack localization strain)

- b) Tensile fracture of reinforcement in UHPC
- c) Interface failure
- d) Tensile fracture of reinforcement in conventional concrete
- e) Compression failure in CC
- f) Compression failure in UHPC

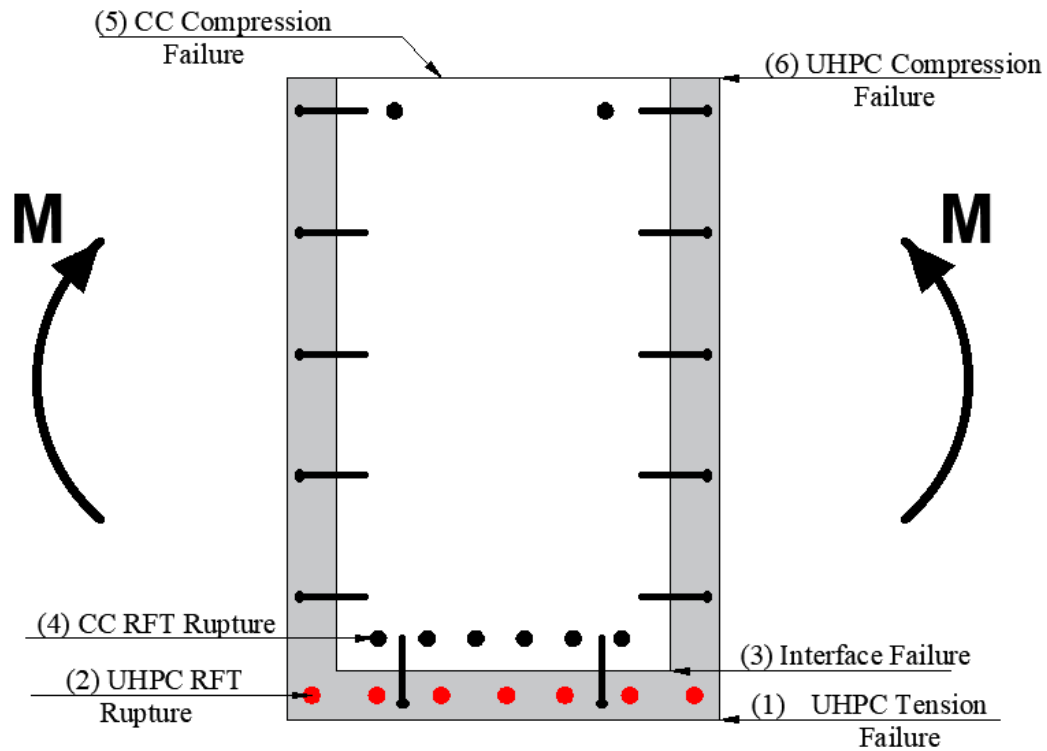


Figure 94: Schematic of possible failure modes in a CC beam strengthened with UHPC

Each failure mode represents a strain profile controlled by the material limit of tensile or compressive strains, as well as the interface strain limit (slippage displacement). Each strain profile will result in a different moment resistance. Several idealizations exist for the tensile stress-strain relationship of UHPC as discussed in the previous section. Tensile testing in the Haber et al., 2018 testing program (FHWA research project) have shown that UHPC prisms were able to sustain their tensile strength for over a strain of (0.01). Conservative idealizations proposed by Graybeal, 2006, and El Helou et al., 2019 consider the ultimate tensile strain of UHPC to be (0.004) then drops to zero with no post-cracking tensile strength. When designing a prestressed girder having a conventional concrete deck, El Helou et al., 2019, found that the strain profile controlled UHPC ultimate tensile strain

provided the largest moment resistance of the section. This causes the ultimate tensile strain limit of UHPC to be crucial in the flexural design calculations of a composite section.

Figure 95 shows a schematic of a composite CC-UHPC beam cross-section and how the proposed model can be used to predict its flexural strength. The beam is composite horizontally and vertically where a 3-sided UHPC wrap is used around the sides of the CC beam. The beam is reinforced with tension and compression reinforcement that can be prestressed or non-prestressed.

Step 1: Obtain the proper stress-strain material models for CC, UHPC, reinforcing and/or prestressing steel. Section 4.1.1 presents a study on the prediction accuracy of UHPC material models in tension and compression.

Step 2: Assume a strain profile based on the predicted failure mode whether in tension, compression, reinforcement, or interface. The strain profile can be assumed using two values, the first value is a strain limit at a certain location (for example, assume the ultimate tensile strain of UHPC at the soffit of the beam), and the second value is the neutral axis depth (c).

Step 3: Divide the composite section into discrete layers, each layer (i) is recommended to have a height smaller than or equal to 0.15 inches.

Step 4: Obtain the strain at the center of each layer (ϵ_i) according to the following equation:

$$\epsilon_i = \begin{cases} \text{if } d_i \leq c, & \epsilon_i = -\epsilon_c \left(\frac{c-d_i}{c}\right) \\ \text{if } d_i > c, & \epsilon_i = \epsilon_c \left(\frac{d_i-c}{c}\right) \end{cases}$$

Where, ϵ_i is the strain at the discrete layer (i); d_i is the depth of the center line of layer (i); (c) is the assumed neutral axis depth; (ϵ_c) is the assumed strain at extreme compression fibers.

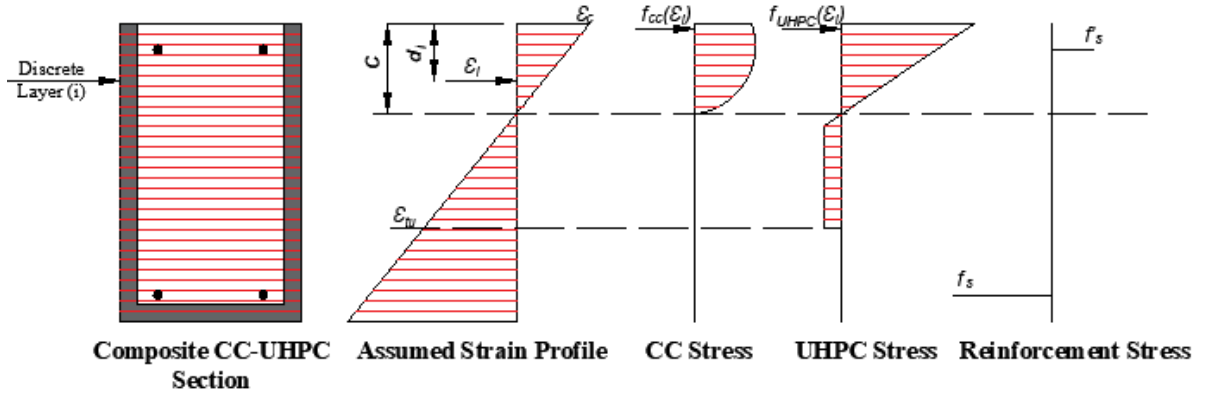


Figure 95: Bases of analysis of the proposed CC-UHPC flexure strength prediction model

Step 5: Calculate the stresses all materials enclosed by layer (i) boundaries based on their material models and ε_i as shown in the below equations as an example:

$$f_{cc} = \begin{cases} \text{if } d_i \leq c, & -f'_c \left[1 - \frac{Z}{1000} \left(\frac{\varepsilon_i - \varepsilon_o}{\varepsilon_o} \right) \right] \\ \text{if } d_i > c, & 0 \end{cases} \quad (64)$$

$$f_{UHPC} = \begin{cases} \text{if } d_i \leq c, & -\varepsilon_i E_{UHPC} (1 - \alpha) \\ \text{if } d_i > c, & \begin{cases} \text{if } \varepsilon_i \leq \varepsilon_{t.loc}, & \max(\varepsilon_i E_{UHPC}, \gamma f_{tu}) \\ \text{if } \varepsilon_i > \varepsilon_{t.loc}, & 0 \end{cases} \end{cases} \quad (65)$$

$$f_s = \begin{cases} \text{if } d_s \leq c, & \min(-\varepsilon_s E_s, -f_y) \\ \text{if } d_s > c, & \max(\varepsilon_s E_s, f_y) \end{cases} \quad (66)$$

$$f_{ps} = \begin{cases} \text{if } d_s \leq c, & \min \left(-\varepsilon_{ps} E_{ps} \left[Q + \frac{1-Q}{\left[1 + \left(\frac{\varepsilon_{ps} E_{ps}}{K f_{pu}} \right)^R \right]^{\frac{1}{R}}} \right], -f_{pu} \right) \\ \text{if } d_s > c, & \max \left(\varepsilon_{ps} E_{ps} \left[Q + \frac{1-Q}{\left[1 + \left(\frac{\varepsilon_{ps} E_{ps}}{K f_{pu}} \right)^R \right]^{\frac{1}{R}}} \right], f_{pu} \right) \end{cases} \quad (67)$$

Where, f_{cc} is the stress in CC calculated according to Hognestad et al., 1955; Z is a constant to control the slope of the curve, commonly used as 150, Wight et al, 2016; ε_o is the strain at peak stress. f_{UHPC} is the stress in UHPC calculated according to Haber et al., 2018 in

compression and El Helou et al., 2019 in tension. The parameters of these models are discussed in detail in section 3.3.1. f_s is the stress in conventional reinforcing steel; f_y is the yield strength of conventional reinforcing steel. f_{ps} is the stress in prestressing strands calculated according to Devalapura et al., 1992. ϵ_s and ϵ_{ps} are the strains at the level of conventional reinforcing steel and prestressing strands, respectively; E_s and E_{ps} are the moduli of elasticity of conventional reinforcing steel and prestressing strands, respectively. f_{pu} is the tensile strength of prestressing strands; Q , K , and R are constants calibrated by test data and can be used according to their recommended values.

In the case of having prestressed reinforcement, the effective prestressing force is used to calculate the initial strain in the prestressed reinforcement and is then added to the value from the strain profile to obtain the total strain.

Step 6: Calculate the internal forces in all materials enclosed by layer (i) boundaries and in the conventional reinforcing steel and prestressing strands. The forces are calculated by multiplying the stresses obtained from the previous step by the material area enclosed by layer (i) boundaries or by the area of reinforcement.

The sign convention in this approach is negative for compressive strain, stress, and force; and for tension values the sign is positive.

Step 7: Calculate the sum of internal forces by adding forces from all layers and all materials.

Step 8: Iterate the value of neutral axis depth (c) and repeat steps 2 through 7 until the sum of internal forces is equal to zero as shown in the below equation. The neutral axis depth obtained is the one that achieves equilibrium when the member is subjected to pure flexure.

$$\sum_{i=0}^{i=n} f_{cc}(\epsilon_i) \cdot A_{cc,i} + f_{UHPC}(\epsilon_i) \cdot A_{UHPC,i} + f_s(\epsilon_s) \cdot A_s + f_{ps}(\epsilon_{ps}) \cdot A_{ps} = 0 \quad (68)$$

Where, n is the total number of discrete layers (i) in the section; $A_{cc,i}$ and $A_{UHPC,i}$ are the areas of CC and UHPC enclosed by layer (i) boundaries, respectively; A_s and A_{ps} are the areas of conventional reinforcing steel and prestressing strands, respectively.

Step 9: Calculate the ultimate flexural strength by taking the moment of all internal forces about any point along the section height. The following equation uses the moment about the extreme compression strain to calculate the ultimate flexural strength:

$$M_n = \sum_{i=0}^{i=n} [f_{cc}(\epsilon_i) \cdot A_{cc,i} + f_{UHPC}(\epsilon_i) \cdot A_{UHPC,i}] d_i + f_s(\epsilon_s) \cdot A_s \cdot d_s + f_{ps}(\epsilon_{ps}) \cdot A_{ps} \cdot d_{ps} \quad (69)$$

Where, M_n is the ultimate flexural strength of the composite section, d_s and d_{ps} are the depths of each layer of conventional reinforcing steel and prestressing strands, respectively.

An Excel spreadsheet was developed to calculate the flexural strength as discussed in steps 1 through 9 for a general section composed of up to 6 layers of material (either UHPC or CC) and up to 6 layers of conventional reinforcing steel, and up to 6 layers of prestressing strands. The sheet can solve for CC and UHPC materials at each layer and they can be composite horizontally or vertically at each layer. The sheet is shown in the appendix section for an example of a UHPC beam.

5.1.3 Interface Design for Flexural Strengthening

After the flexural strength of the composite CC-UHPC is calculated, the interface shall be designed to allow full transfer of the shear forces between the two materials. In order for this model to be valid, the CC-UHPC interface shall be designed to allow full shear transfer of the forces carried by UHPC to the existing CC component. When UHPC is introduced to the top or bottom layers of a CC beam, the interface shall account for the full tension or compression forces carried by UHPC.

The interface can be designed using cohesion and friction factors suggested by Abo El-Khier et al., 2019 or Draft AASHTO UHPC Guidelines, 2021. The Draft AASHTO UHPC Guidelines, 2021 suggests the interface shear resistance to be calculated as follows:

$$V_{ni} = c A_{cv} + \mu (C_1 + C_2 + P_c) \quad (70)$$

Where, V_{ni} is the nominal shear resistance for a given interface; c is the cohesion factor; A_{cv} is the UHPC area contributing to the interface shear resistance; μ is the friction factor, C_1 is the normal clamping force provided by reinforcing steel crossing the interface

(calculated by multiplying the reinforcement area by its yield strength); C_2 is the normal clamping force provided by UHPC recommended to be taken as zero for CC-UHPC interfaces; P_c is the permanent net compressive force acting perpendicular to the interface (zero if tension). Table 23 shows the recommended cohesion and friction factors to be used in the interface design. It can be noticed that the Draft AASHTO UHPC Guidelines, 2021 are far conservative compared to Abo El-Khier and Morcous, 2019 which is based on experimental testing.

Table 23: Cohesion and friction factors recommended for different CC surface conditions

Reference	Draft AASHTO UHPC Guidelines, 2021		Abo El-Khier and Morcous, 2019		
CC Surface Condition	CC Surface not intentionally roughened	Intentionally roughened CC surface (0.25-inch amplitude)	Sandblasted CC surface	Low roughened CC surface	High roughened CC surface
c (ksi)	0.075	0.24	0.59	0.52	0.8
μ	0.6	1	1.42	1.12	1

Another option to design the interface is to neglect the cohesion factor and use the ACI 318 shear friction approach to design the interface. The cohesion factor recommended by Draft AASHTO UHPC Guidelines, 2021 is significantly small for unroughened CC surfaces. The nominal interface shear resistance will be reduced to:

$$V_{ni} = \mu (C_1) = \mu A_{vf} f_y \quad (71)$$

Where, A_{vf} is the reinforcing steel area crossing the interface; and f_y is its yield strength. For short embedment length anchor bars, the pull-out strength of the anchor shall be taken into consideration according to manufacturer's recommendations which can be significantly smaller than the anchor yield strength. In addition, the direct shear strength of the anchors shall be taken into account according to manufacturer's recommendation as typically done in CC jackets. The nominal interface shear resistance becomes to the minimum of these three values as shown below:

$$V_{ni} = \text{minimum}(\mu A_{vf} f_y, V_{PO}, V_{DS}) \quad (72)$$

Where, V_{PO} is the pullout shear resistance of the anchor; V_{DS} is the direct shear resistance of the anchor. The interface design procedure for an example beam is presented in the appendix section using the manufacturer's recommendations for anchor capacity to determine the required number of anchors.

5.2 Flexural Testing of CC-UHPC Beams

This section discusses the testing done on flexure strengthened conventional concrete beams using UHPC having additional reinforcement. The design of specimens and strengthening procedure are discussed first. Then, the test results are presented and used for the validation of the proposed flexural strength prediction model.

5.2.1 Specimen Design

Three 12-foot-long beams were fabricated, one beam was set as the reference without strengthening, and the other two beams were strengthened with a 2-inch UHPC layer at the soffit. Additional reinforcement was added in the UHPC layer to test if UHPC shall transfer the full tension forces in the additional reinforcement. Figure 96 shows the cross-sections of the three beams to be tested in flexure. In order to obtain the highest contribution from UHPC in flexure, the specimens were designed to fail in flexure even after strengthening. The CC section contained three #7 bars (area = 0.60 in²) in the tension side, and one #6 bar (area = 0.44 in²) in the compression side and was reinforced transversally with 2#3 stirrups spaced every six inches. Strengthened beam #1 contained additional two #6 bars, while strengthened beam #2 contained three #6 additional bars. Figure 97 shows a schematic of the flexural test setup of the CC-UHPC beams.

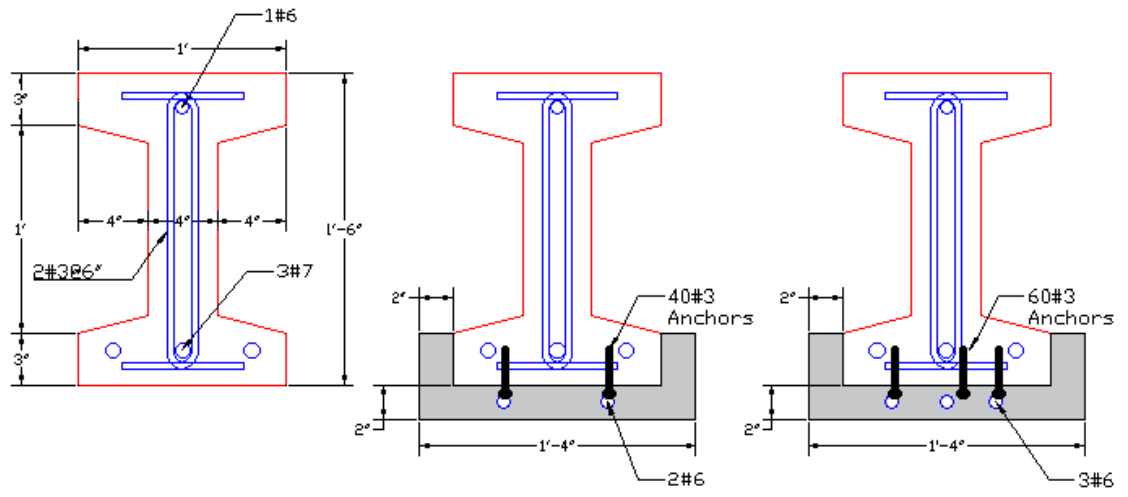


Figure 96: Cross-sections of the strengthened beams in flexure, reference beam (left), strengthened beam #1 (middle), and strengthened beam #2 (right)

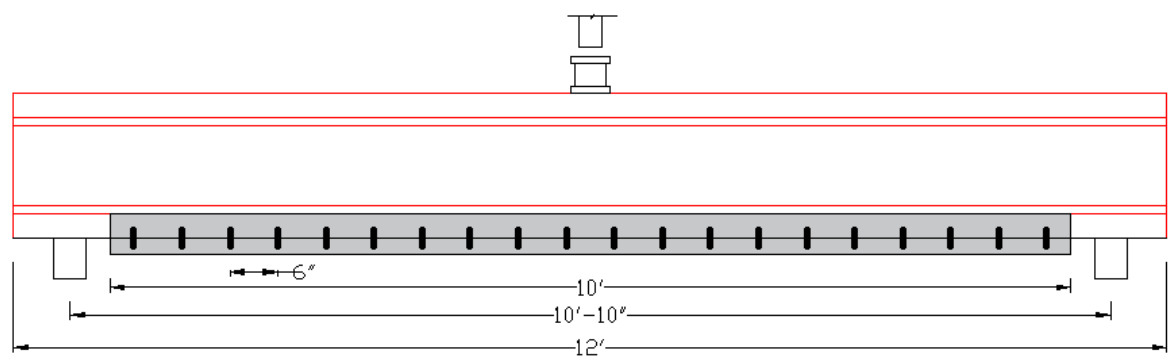


Figure 97: Schematic of the flexural test setup of a CC-UHPC beam

Table 24 shows a summary of the flexural testing with the CC and UHPC compressive strengths during fabrication, as well as, as, the predicted shear and flexure failure loads. The shear capacity was increased as much as possible in order to represent a flexural capacity deficiency. However, for strengthened beam #2 the predicted shear failure load was slightly lower than the predicted flexural failure load. This was acceptable because the shear prediction models are typically more conservative than the flexural prediction models due to the brittle failure mode in shear. And the fact that the predicted shear failure load for strengthened beam #2 was higher than the failure load in strengthened beam #1, so the additional reinforcement effect will be noticeable during testing. The prediction

calculations were done according to AASHTO LRFD, 2017, El-Helou et al., 2019, and Draft AASHTO for UHPC, 2021. The procedure of calculation is presented in the appendix.

Table 24: Summary of test specimens and predicted capacity

Beam ID	CC Compressive Strength (ksi)	UHPC Compressive Strength (ksi)	Longitudinal Reinforcement (CC + UHPC)	Nominal Shear Capacity (V_n) (kip)	Nominal Flexural Capacity (M_n) (kip.ft)	Flexural Failure Load (kip)	Shear Failure Load (kip)
Reference Test	7.2	N/A	3 - #7	41.4	136.8	50.5	82.8
Strengthened Beam #1	7.1	17.0	3 - #7 + 2 - #6	49.1	250.4	92.5	98.2
Strengthened Beam #2	7.1	17.0	3 - #7 + 3 - #6	49.1	285.8	105.5	98.2

Figure 98 shows the predicted moment-curvature relationship of the three beams. The prediction procedure was performed according to sections 2.3.1 and 5.1.2. The effect of fiber contribution of UHPC in tension can be noticed when the predicted M_n at curvature Φ_p is larger than that at curvature Φ_u . While in the reference beam, the well-known moment-curvature behavior of CC beams is observed where the moment capacity tends to keep increasing slightly after the yielding curvature Φ_y .

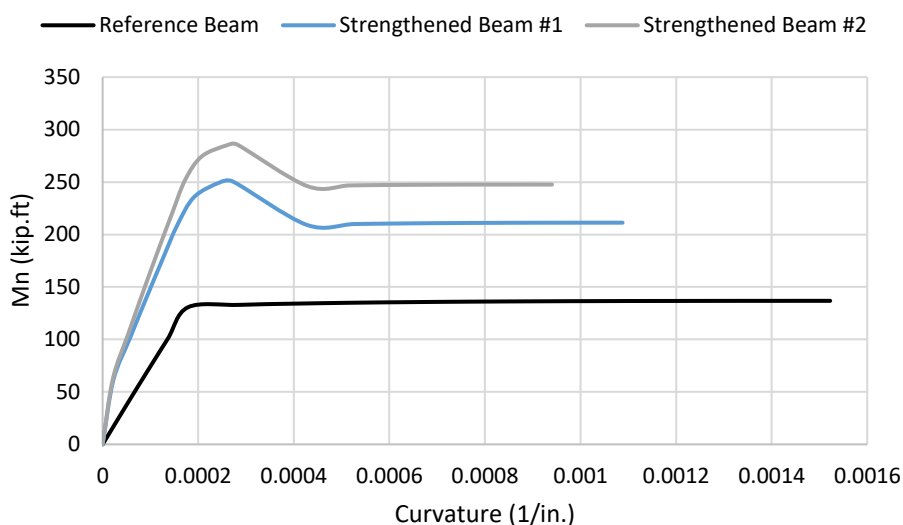


Figure 98: Predicted moment-curvature relationship of the reference and flexural strengthened beams

The CC-UHPC interface was designed to carry the full tension force of UHPC plus additional reinforcement. The interface was roughened by sandblasting to increase the cohesion and friction factors. However, the cohesion between the two materials was not counted when designing the interface similar to the shear friction design in the ACI 318-14. Conventional headed anchors were used to transfer all the shear forces across the interface. Previous research done by Cao et al., 2017 indicated that headed studs with a 1.4-inch length were fully developed in a 2-inch thickness of UHPC. The test setup and anchor dimensions are shown in Figure 99. Test results shows that all studs failed at the interface weld or the stud shank at the bottom towards the interface. The 2-inch UHPC layers were in good condition with no damage which indicated that the full force in the studs was developed in the UHPC layer. The selected screw anchors were embedded in the CC beams using high-strength epoxy and were designed according to the manufacturer’s recommendations taking into account the pull-out and direct shear failure modes.

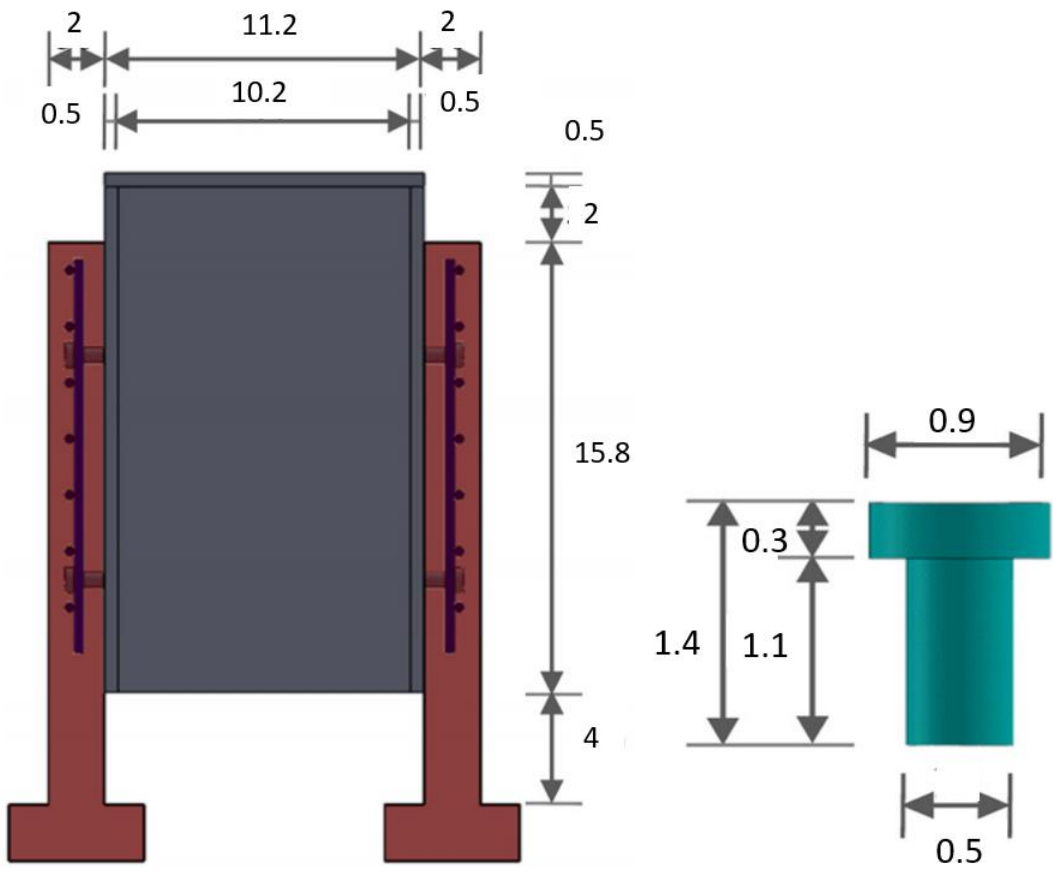


Figure 99: Double shear test setup of headed stud anchors in UHPC (left), anchor dimensions (right), courtesy of Cao et al., 2017

5.2.2 Fabrication

The used CC mix in this research was designed to achieve a compressive strength of at least 4.0 ksi with a slump of 4 to 5 inches. The fabricated specimens achieved compressive strengths ranging between 5.4 to 7.2 ksi according to ASTM C39. Compressive strength testing was done on 4-inch diameter cylinders having a height of 8-inches. Table 25 shows the constituents of the CC mix used to cast the specimens in this research.

Table 25: CC mix design constituents

Ingredient	Quantity (lb/y ³)
Cement (Type I/II)	658
Fine Aggregate (Sand)	880
Coarse Aggregate (#52)	2020
Water	240
Air-Entraining Admixture (MB-AE 90)	0.4
Mid-Range Water Reducer (MasterPolyheed 1020)	39.5

The CC beams were fabricated by casting ready-mixed concrete in wooden formwork as shown Figure 100. Expanded polystyrene foam boards were cut and fixed to the sides of the forms to create the I-shaped cross-section. The top reinforcement bar was fixed in place by the U-shaped transverse reinforcement. The foam pieces on the sides were covered in plastic sheets to allow for easy stripping and multiple reuses as shown in Figure 101.



Figure 100: Formwork and reinforcement of one of the CC beams



Figure 101: Stripping formwork of two CC beams

5.2.3 Strengthening Procedure

Figure 102 shows the first step of the strengthening procedure of the two UHPC strengthened beams in flexure. Sandblasting was used to roughen the CC surface before pouring on UHPC. The used sand size and roughness depth were approximately 1/16-inch. An industrial 10-gallon sandblaster was used with compressed air pressure of 110 psi. Oven-dried fine sand was used as the abrasive material on the CC surface.

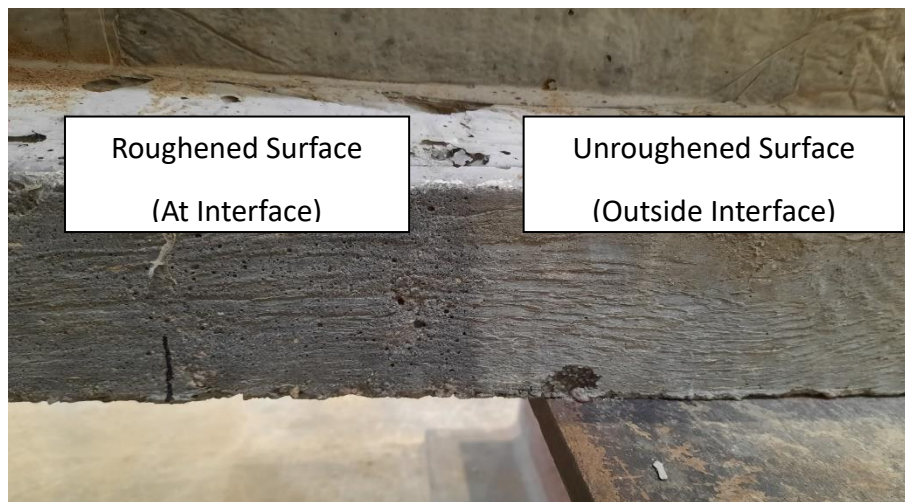


Figure 102: Flexural strengthening procedure, step 1: roughening of the interface

Figure 103 shows the second step of installing the anchors according to the anchor design to develop the full tension forces in the UHPC and additional reinforcement. For strengthened beam #1, forty anchors were distributed into two longitudinal rows along the additional reinforcement and space at six inches. While for strengthened beam #2, sixty anchors were distributed along the additional reinforcement and spaced at six inches with the middle row staggered to avoid hitting the middle rebar in the CC beam.



Figure 103: Flexural strengthening procedure, step 2: installing anchors

Figure 104 shows the third step of installing the additional reinforcement in place. The additional reinforcement was initially fixed in the anchors to make the formwork installation easier. The formwork also contained spacers to maintain the UHPC clear cover which was 5/8-inch.



Figure 104: Flexural strengthening procedure, step 3: installing additional reinforcement

Figure 105 shows the fourth step of assembling the formwork which was done apart from the CC beams for added efficiency in real life bridge girders or beams where the construction time on-site can be minimized. Contractors can fabricate any type of formwork in the shop and erect the formwork directly on-site.



Figure 105: Flexural strengthening procedure, step 4: assembling formwork

Figure 106 shows the fifth step of installing the formwork on the CC beam, six threaded anchors were used to hang the formwork from the top of the beam. The installation procedure was also designed to increase the construction efficiency on site in real project applications, where the anchors can be fixed through holes in bridge decks or slabs in building projects.



Figure 106: Flexural strengthening procedure, step 5: installing formwork

Figure 107 shows the sixth and final step, pouring UHPC through the formwork using buckets. The opening in the formwork were 2-inches wide and no consolidation issues were found during the pouring process of UHPC due to its increased flowability. In the case of bridge girders or building projects with difficult access to the beam soffit, holes can be drilled in the top slab and plastic pipes can be used to pour UHPC from the top surface of the deck or slab.



Figure 107: Flexural strengthening procedure, step 6: pouring UHPC

5.2.4 Test Results

Figure 108 shows the test setup and instrumentation of the reference beam. A 100-kip load cell was used under a hydraulic ram to measure the applied load at mid-span. Two string potentiometers were installed at the beam mid-span to measure displacement. And external

concrete strain gauges were installed at one section along the height of the beam to obtain the strain profile and section curvature at that location. The strain gauge location was selected to be eighteen inches away from the point of load application to be away from the disturbed region.



Figure 108: Reference beam test setup and instrumentation

Figure 109 shows the moment-deflection plot of the reference beam along with the predicted moment capacity. It can be noticed that the beam sustains a significantly higher flexural capacity than the prediction for a considerable amount of deformation. Figure 110 shows the failure mode of the beam where the tension reinforcement bars spall the concrete cover around them and slip.

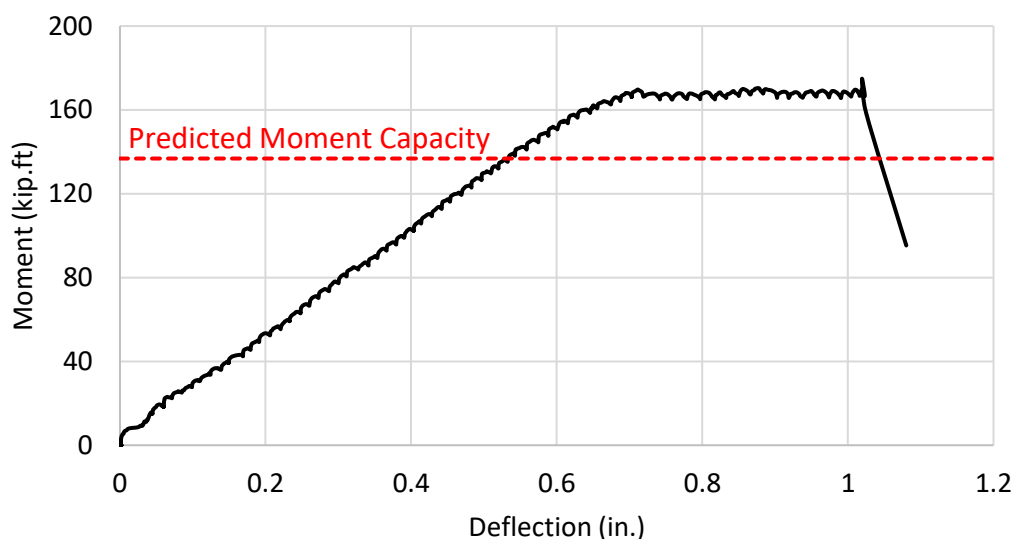


Figure 109: Reference beam moment-deflection plot



Figure 110: Reference beam failure mode

Figure 111 shows the test setup of strengthened beam #1 and the instrumentation used was similar to what was done in the reference beam except for having a larger capacity load cell (400-kip capacity). Also shown in Figure 112 is the instrumentation used to measure any relative displacement between the CC beam and the UHPC end. One Linear Variable Differential Transducer (LVDT) was installed at each end of the UHPC with its base fixed on the CC surface.



Figure 111: Strengthened beam #1 test setup and instrumentation



Figure 112: measuring relative displacement between CC and UHPC in strengthened beam #1

Figure 113 shows the moment-deflection plot of strengthened beam #1 along with the predicted flexural capacity at curvature Φ_p . The beam achieves its predicted flexural capacity which indicates that the 2-inch UHPC layer successfully transferred the forces in the additional reinforcement. Figure 114 and Figure 115 show the failure mode which was similar to that observed in the reference beam. No interface cracks or relative movement were visually noticed between CC and UHPC. Figure 116 shows the measured displacement between the two materials and it can be noticed that the magnitude of displacement is significantly small which indicates no interface failure.

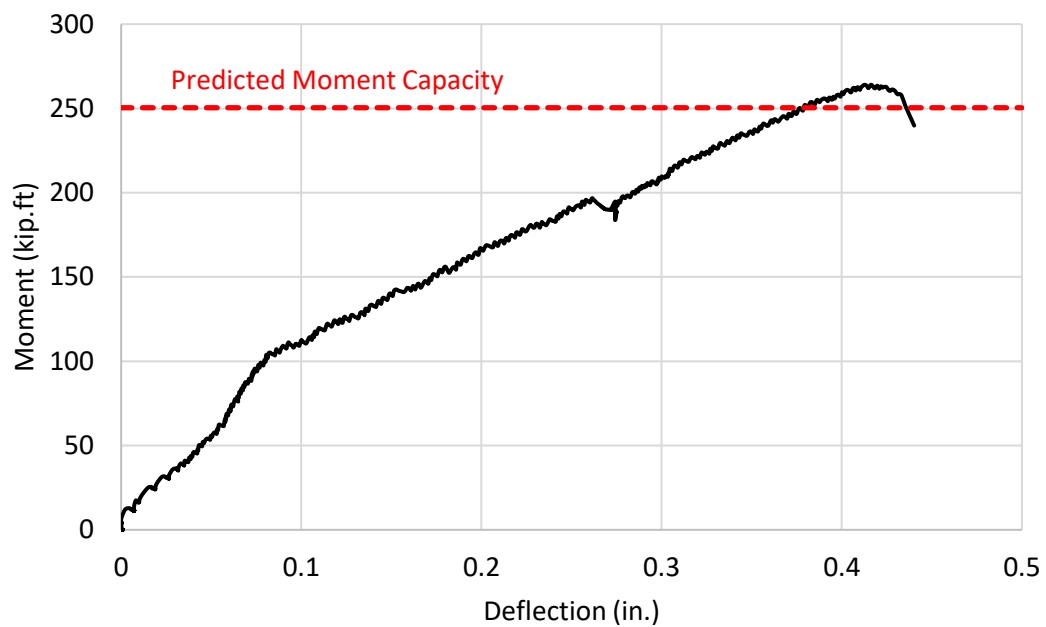


Figure 113: Strengthened beam #1 moment-deflection plot



Figure 114: Strengthened beam #1 failure mode



Figure 115: Strengthened beam #1 failure mode, slippage of CC tension reinforcement

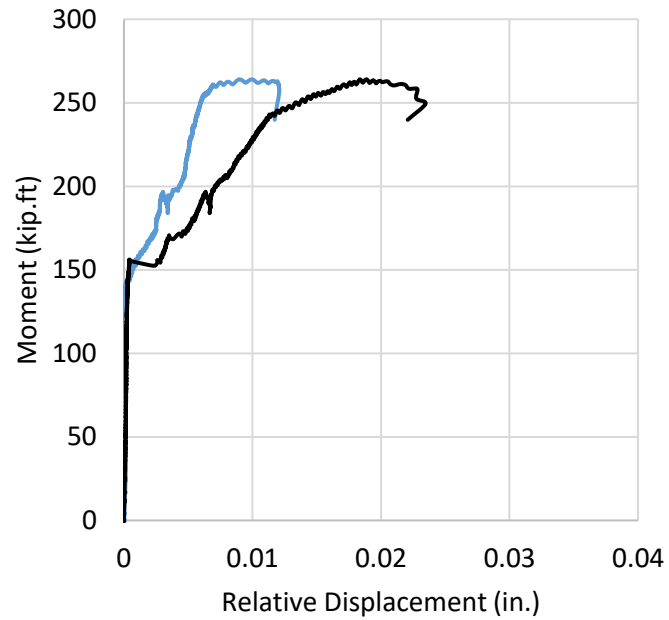


Figure 116: Strengthened beam #1 relative end displacements between CC and UHPC

Figure 117 and Figure 118 show the failure mode of strengthened beam #2. The test setup and instrumentation were similar to what was shown in strengthened beam #1. Also, the failure mode was consistent to what was observed in the reference beam and strengthened beam #1. Figure 119 shows the moment-deflection plot and the predicted flexural capacity at curvature Φ_p . The beam also achieves its predicted flexural capacity which indicates that the 2-inch UHPC layer successfully transferred the forces in the additional reinforcement. Figure 120 shows the measured displacement between the two materials and it can be noticed that the magnitude of displacement is significantly small which indicates no interface failure.



Figure 117: Strengthened beam #2 failure mode



Figure 118: Strengthened beam #2 failure mode, CC tension reinforcement slippage

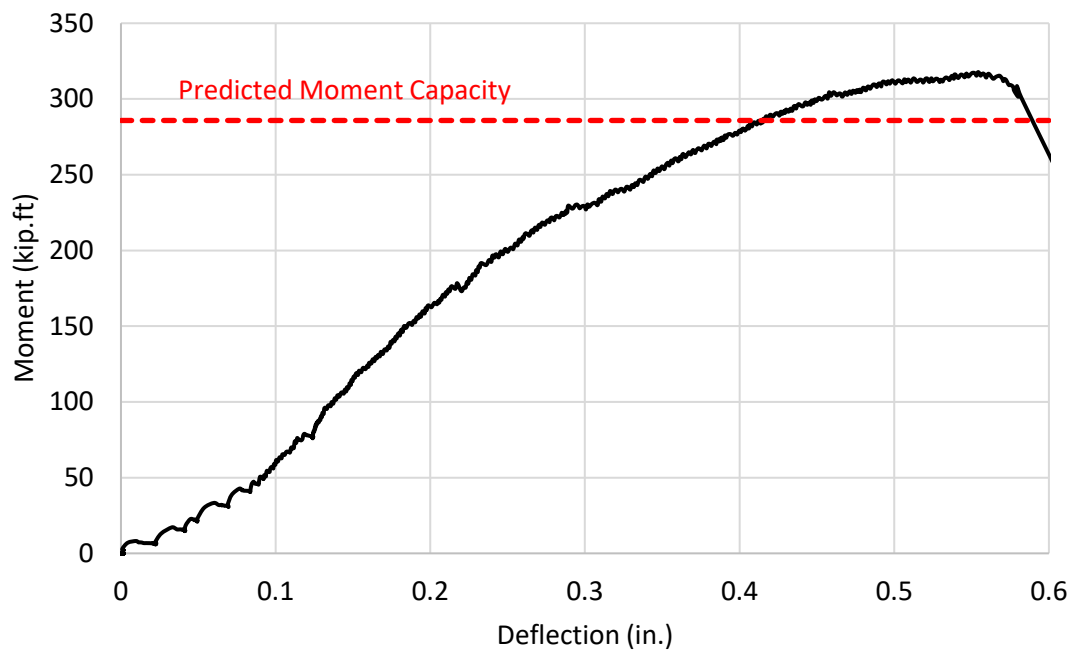


Figure 119: Strengthened beam #2 moment-deflection plot

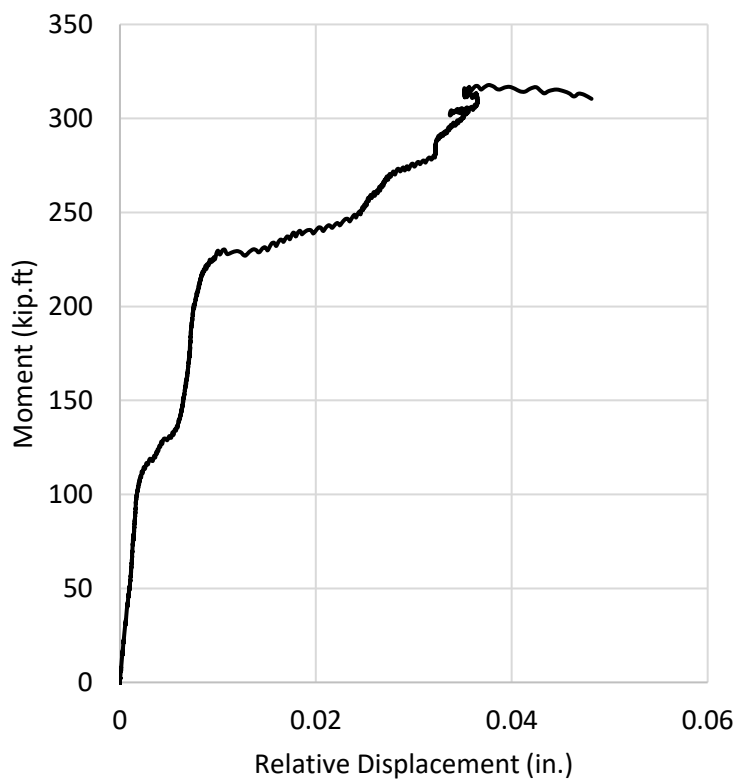


Figure 120: Strengthened beam #2 relative end displacement between CC and UHPC

Figure 121 shows the applied moment versus extreme compressive strain recorded from the top strain gauges for the reference and two strengthened beams. Results show that the compressive strain of the strengthened beams was significantly lower than that recorded for the reference beam at the same level of moment until failure. This indicates that the strengthening procedure and interface design successfully caused the CC-UHPC section to behave fully composite until failure. Other strain gauge measurements were used to calculate the curvature of the section and the results are compared against the predicted moment curvature behavior as will be discussed in the next section.

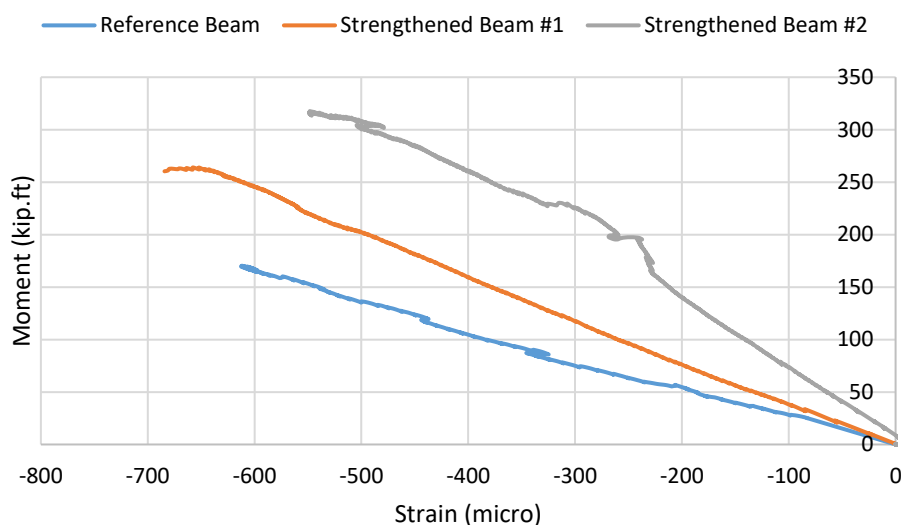


Figure 121: Moment versus measured extreme compressive strain

5.2.5 Validation of The Prediction Model

Figure 122 shows the moment-deflection plot of the three tested beams. It can be noticed that the two strengthened beams stiffness exceeds that of the reference beam significantly which confirms that the 2-inch UHPC is successfully transferring the tension forces and increasing the depth of the beam. The initial stiffness of strengthened beam #1 exceeds that of strengthened beam #2 slightly. However, after a deflection of 0.2-inch the stiffness of strengthened beam #2 exceeds that of strengthened beam #1 because of the extra reinforcement.

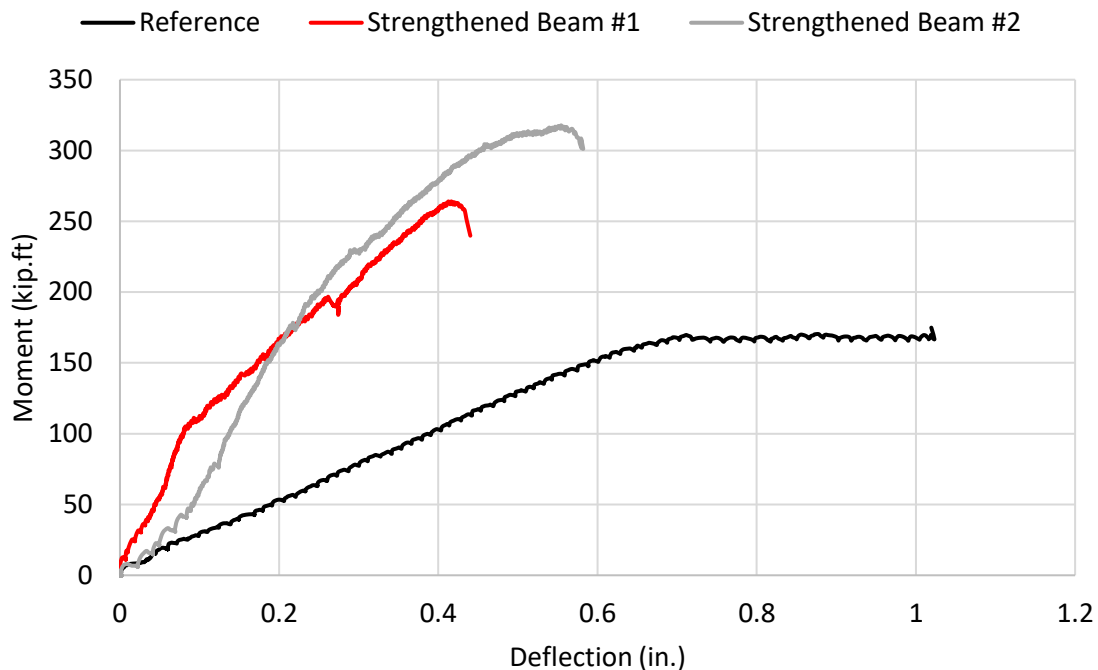


Figure 122: Moment-deflection results of the reference and two strengthened beams

Table 26 summarizes the measured flexural strength of the three tested beams and presents a comparison with the predicted flexural and shear failure values. It can be noticed that the two strengthened beams achieved their respective predicted flexural capacity which validates the prediction model. Figure 123 shows the measured versus predicted moment-curvature relationship of the three tested beams in flexure. The measured curvature values are obtained from the strain gauge readings along the height of the beam. The measured value plots are shown until failure as the strain gauges provides unrealistic reading after significant cracking has occurred on the concrete surface. Reasonable agreement can be noticed between the measured and predicted plots which provides further validation to the proposed model and confirms that the CC-UHPC section was acting as fully composite.

Table 26: Measured versus predicted flexural strength of the tested beams in flexure

	Measured Capacity (kip.ft)	Flexural Prediction		Shear-to-Flexure	
		Predicted Flexural Failure Capacity (kip.ft)	Measured-to-Predicted Flexural Capacity	Predicted Shear Failure Capacity (kip.ft)	Measured-to-Predicted Shear Capacity
Reference Beam	174.9	136.8	1.28	224.3	0.78
Strengthened Beam #1	264.1	250.4	1.05	266.0	0.99
Strengthened Beam #2	317.7	285.8	1.11	266.0	1.19

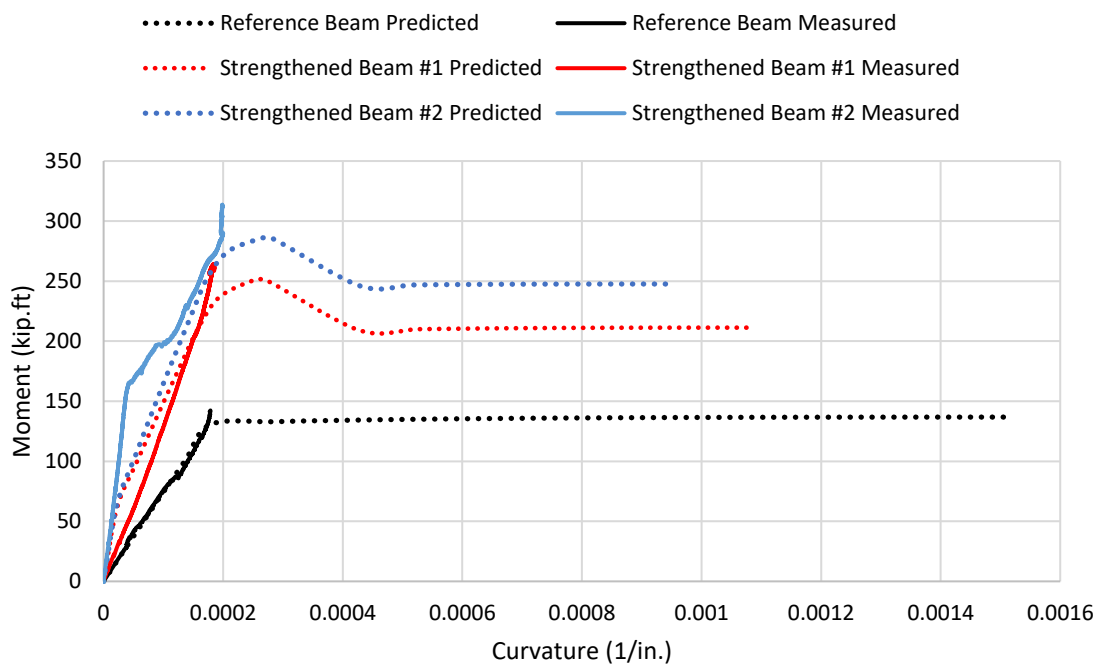


Figure 123: Measured versus predicted moment-curvature relationship of the three tested beams in flexure

Chapter 6 – Shear Strengthening using UHPC

This chapter presents the proposed concept of using UHPC in shear strengthening techniques and utilizing its advantages. The implementation of shear strengthening techniques in actual projects is presented in the form of construction procedures for a beam example. Then, the design process of a composite (strengthened) CC-UHPC is presented in the form of developing the shear strength prediction model. Shear testing of CC-UHPC beams is also presented to validate the prediction of the developed model.

6.1 Construction Procedure and Design

6.1.1 Shear Strengthening Procedure using UHPC

The general technique of utilizing UHPC in the shear strengthening of an existing CC beam is presented in Figure 124 where UHPC can be used as additional side layers at the web area to maximize its contribution to the shear strength. The UHPC layers can be unreinforced, reinforced transversally and/or longitudinally, or prestressed. Having reinforced or prestressed UHPC can increase its contribution significantly in shear and flexure. However, unreinforced UHPC can provide significant shear strength contribution without the need for any reinforcement due to its significantly high tensile strength over the diagonal tension area. The CC-UHPC interface must be designed to resist the shear forces carried by the UHPC layers. The interface can be designed with conventional anchors similar to other CC encasement techniques, and it can be designed without anchors depending on the superior interface shear resistance between CC and UHPC. Suggested procedure is proposed similar to other techniques according to the FHWA Bridge Maintenance Reference Manual, 2015.

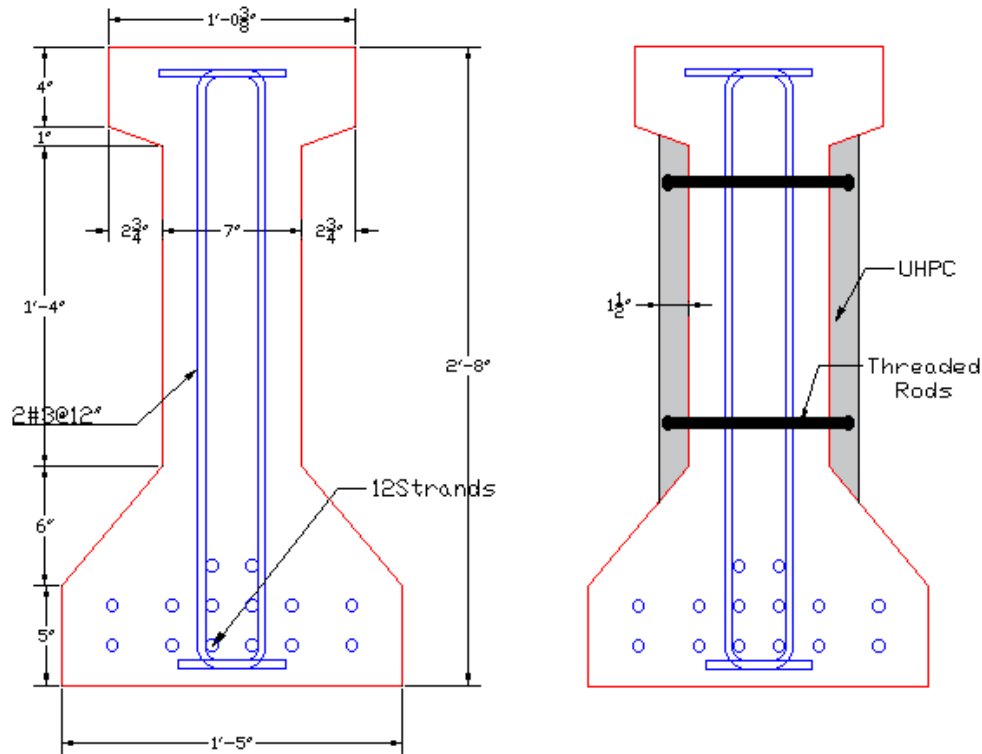


Figure 124: General technique of using 2 UHPC side layers at the web area for shear strengthening of an existing CC bridge girder

The design example at section 7.2 discusses the procedure of designing shear strengthening using UHPC compared to shear strengthening using CFRP wrapping. The general construction procedure is presented here as follows:

Suggested Construction Procedure:

- 1- Interface Preparation: the existing CC surface should be roughened to increase the interface shear resistance. Then the surface should be cleared of all dust, dirt, oil, grease, or fine particles of concrete that could reduce the interface shear resistance.
- 2- Anchors Installation: Holes should be drilled first and their location and spacing are determined according to the interface design. Through web threaded rods can be efficient to eliminate the pull-out failure mode possibility and increase anchor capacity significantly.

- 3- Formwork Installation: side formworks can be rigidly attached to the existing component web area. The formwork should be watertight since UHPC is highly flowable. The forms should be cleaned and oiled before installation.
- 4- UHPC Placement: the easiest and most efficient procedure is to place UHPC through top opening in through the member. For restricted top access, UHPC can be placed from the side of the forms using side opening in the forms, opening can be as small as 2-inch diameter circular shafts. Live loads should be restricted or reduced from acting on the member during placement, otherwise the member can be shored.
- 5- Formwork stripping: formwork can be stripped after UHPC hardens (typically 6 hours), live loads should fully return to act on the component once UHPC achieves the mechanical properties required by structural design.

6.1.2 Development of Prediction Model of CC-UHPC Beams in Flexure

This section presents the development of the prediction model estimating the shear strength of CC-UHPC components. The model can predict the strength of non-prestressed and prestressed components and is based on a similar approach to the repair and strengthening of concrete members in shear using FRP.

When a concrete element is repaired or strengthened, the composite section flexural or shear resistance does not always have to be the algebraic sum of both materials. In other words, the new material resistance is not always fully utilized. When calculating the shear resistance of a concrete beam, the transverse reinforcement becomes fully utilized when it reaches its yielding stress, and its contribution is added algebraically to the resistance. When cracking starts to happen in the base element concrete, stress concentrations start to develop at the new material reducing its contribution to the resistance. In the case of FRP wrapping, the ACI 440.2R-17 limits the utilization of FRP to the effective strain value depending on the repair scheme, anchorage, and FRP mechanical properties. This strain limit was developed based on the effective stress model, Khalifa et al., 1998.

The upper limit of the effective strain in FRP wraps is given by ACI 440.2R-17 as 0.004 as the maximum strain for design of members that are completely wrapped with FRP. This

value is based on testing done by Priestley et al., 1996 and experience. And higher strains in the FRP shear-strengthening applications should not be used. The effective strain model is used to limit the contribution of FRP in the overall shear capacity as the sheets used for shear strengthening tend to rupture at stress levels below their ultimate strength due to stress concentrations, Khalifa et al., 1998.

Previous research suggests that UHPC has a similar strain limit in tension after which the tensile carrying capacity starts to reduce significantly, the strain limit is called the crack localization strain, Draft AASHTO for UHPC, 2021. The localization strain is defined as the strain at which the cracks are localized into a single discrete crack, Haber et al., 2018. The value can be visually chosen on the stress-strain plot of a UHPC prism ($2 \times 2 \times 14 \text{ in}^3$) tends to decrease in a continuous manner. Testing testing done by the FHWA shows that the localization strain can reach 0.007, Graybeal, 2006, and 0.01, Graybeal, 2008. The lower bound is recommended as 0.004, El-Helou et al., 2019 which is equivalent to the upper limit in the FRP strengthening case.

Model Limitations and Assumptions

The developed prediction model can only be applied to composite CC-UHPC sections that act as fully-composite until the localization strain is reached at the highest tensioned location. The assumptions used to develop this model are as follows:

1. No interface failure or relative displacement will happen between CC and UHPC until the larger of the principle tensile strain or longitudinal strain at the level of reinforcement reaches the localization strain limit of UHPC.
2. The longitudinal reinforcement in the tension zone at the critical section is fully developed and anchored.
3. The strain compatibility approach is valid across the entire composite section height up to failure.
4. The used UHPC in the repair and strengthening application does not satisfy the mechanical property requirements highlighted in Chapter 3.

The procedure of predicting the shear strength of a composite CC-UHPC beam shall be done according to the following steps:

Step 1: Calculate the existing CC member capacity ($V_{n,cc}$) and crack angle (θ). V_{cc} shall be calculated according to the original code/standard used to design the existing element. AASHTO LRFD, 2017 was used to predict the vertical shear capacity and crack angle of the conventional concrete beams.

Step 2: Calculate the UHPC contribution term ($V_{n,UHPC}$) and θ in the UHPC according to the Draft AASHTO for UHPC, 2021, which can be calculated as follows:

$$V_{n,UHPC} = V_{UHPC} + V_s \quad (73)$$

Where, $V_{n,UHPC}$ is the UHPC contribution term to the shear strength of the CC-UHPC element; V_{UHPC} is the UHPC contribution term calculated mainly from the fiber's resistance to the diagonal tension cracking, V_s is the transverse reinforcement contribution term of the added reinforcement in UHPC if applicable, V_p is the vertical component of applied prestressing on the UHPC if applicable. V_{UHPC} is calculated as follows:

$$V_{UHPC} = \gamma f_{t,loc} b_{UHPC} d_{v,UHPC} \cot \theta \quad (74)$$

Where, γ is a safety factor for UHPC in tension recommended not to exceed 0.85; $f_{t,loc}$ is the localized tensile strength of UHPC determined by tension testing; b_{UHPC} is the width of added UHPC; $d_{v,UHPC}$ is the effective depth of added UHPC in shear; θ is the angle of inclination of diagonal compressive stresses and calculated by solving the following equations based on the Modified Compression Field Theory (MCFT), Bentz et al., 2006 with some modifications to consider the higher tensile strength of UHPC than CC:

$$\mathcal{E}_1 = \frac{\mathcal{E}_s}{2} (1 + \cot^2 \theta) + \frac{2f_{t,cr}}{E_c} \cot^4 \theta \leq \mathcal{E}_{t,loc} \quad (75)$$

$$\begin{aligned} \mathcal{E}_{t,loc} = & \frac{\mathcal{E}_s}{2} (1 + \cot^2 \theta) + \frac{2f_{t,loc}}{E_c} \cot^4 \theta \\ & + \frac{2\rho_v f_v}{E_c} \sin \alpha \cot^2 \theta [1 + \cot^2 \theta + \cot \alpha (\tan \theta + \cot \theta)] \end{aligned} \quad (76)$$

$$\mathcal{E}_2 = -\frac{2f_{t,loc}}{E_c} \cot^2 \theta - \frac{2\rho_v f_v}{E_c} \sin \alpha [1 + \cot^2 \theta + \cot \alpha (\tan \theta + \cot \theta)] \quad (77)$$

$$\mathcal{E}_v = \mathcal{E}_{t,loc} - 0.5 \mathcal{E}_s + \mathcal{E}_2 \quad (78)$$

$$f_v = E_s \mathcal{E}_v \leq f_y \quad (79)$$

Where, \mathcal{E}_1 is the diagonal tensile strain in UHPC; \mathcal{E}_s : longitudinal strain at the level of reinforcement calculated as follows:

$$\mathcal{E}_s = \frac{\frac{|M_u|}{d_v} + 0.5 N_u + |V_u - V_P| - A_{ps} f_{p0} - \gamma f_{t,loc} A_{ct}}{E_s A_s + E_p A_{ps}} \quad (80)$$

Where, $|M_u|$ is the absolute value of the factored moment at the design section, not to be taken less than $|V_u - V_P|d_v$; N_u is the factored axial force at the design section, taken as positive if tension and negative if compression; V_u is the factored shear force at the design section; A_{ps} and A_s are the area of prestressing steel and non-prestressed steel respectively in the flexural tension side of the member; f_{p0} is the parameter taken as modulus of elasticity of prestressing steel multiplied by the locked-in difference in strain between the prestressing steel and surrounding UHPC and could be taken as 70% of the ultimate tensile strength of the strands for appropriate levels of prestressing; A_{ct} is the area of UHPC in the flexural tension side of the member; E_s and E_p are the moduli of elasticity of non-prestressed and prestressing steel respectively.

And, $f_{t,cr}$ is the cracking tensile strength of UHPC determined by tension testing; E_c is the UHPC modulus of elasticity; $\mathcal{E}_{t,loc}$ is the crack localization strain determined by tension testing; ρ_v is the transverse reinforcement ratio calculated as the area of transverse reinforcement divided by bar spacing and web width; f_v is the stress in transverse reinforcement; \mathcal{E}_2 is the diagonal compressive strain in UHPC; and \mathcal{E}_v is the vertical strain in transverse reinforcement at the design section. Figure 125 shows the principle strains at diagonal tension cracking that are used to develop the MCFT, Bentz et al., 2006. It can be noticed that \mathcal{E}_1 is the largest tensile strain perpendicular to the diagonal tension cracks. The design approach is to limit \mathcal{E}_1 to $\mathcal{E}_{t,loc}$ to control the localization of stresses transmitted from the existing CC member to the UHPC.

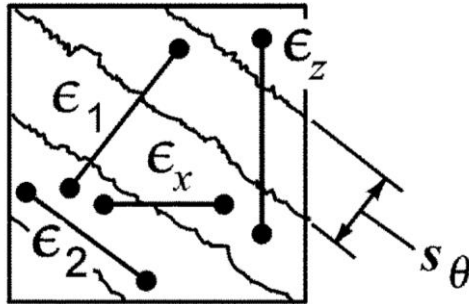


Figure 125: Principal strains at the diagonal tension cracking used to develop the MCFT for CC, courtesy of Bentz et al., 2006

This calculation approach for $V_{n,UHPC}$ ensures that the principle tensile strain (ϵ_1) at the center of the design section and the longitudinal tensile strain at the level of tension reinforcement (ϵ_s) are below $\epsilon_{t,loc}$. $\epsilon_{t,loc}$ is not recommended to exceed 0.004 until further testing is done on CC beams strengthened in shear using UHPC and to have the same effective strain value as in FRP wrapping. The effective strain model is based on the possible slip fields between CC and FRP at the critical shear crack as shown in Figure 126. Having ϵ_1 and ϵ_s below $\epsilon_{t,loc}$ will ensure that the UHPC element facing the shear crack in the existing CC element is still intact and contributing with the full UHPC tensile strength.

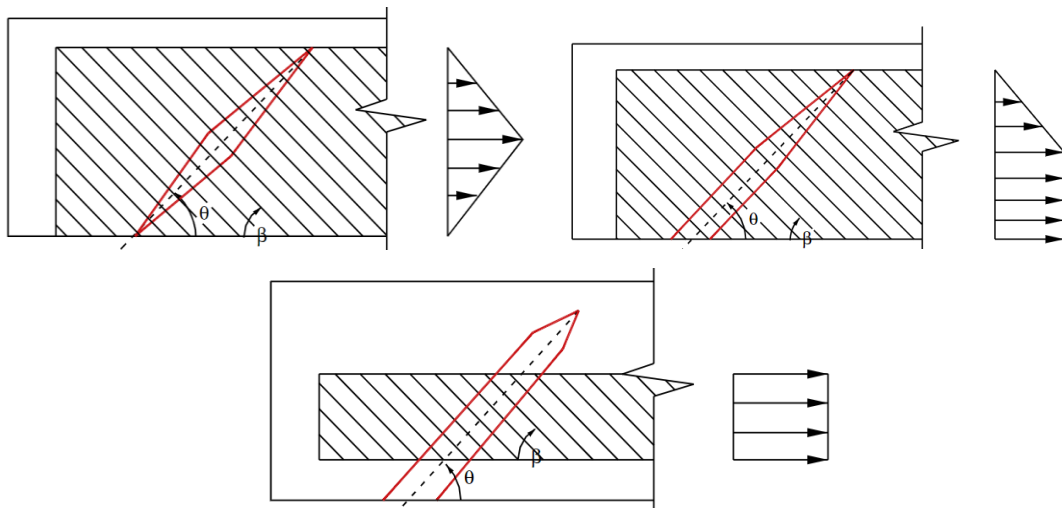


Figure 126: Typical slip fields depending on critical shear crack, courtesy of Lu et al.,

Step 3: Check that f_v obtained in step 2 for UHPC gets the transverse reinforcement in the existing CC element to yield. If not, use f_v as a stress limit for the transverse reinforcement in the existing CC element.

Step 4: Compare θ calculated in the first step for the CC element and the one calculated in the second step for UHPC. The larger of the two angles shall be used as a conservative approach to predict the crack angle when the two calculated angles are different as shown in Figure 127.

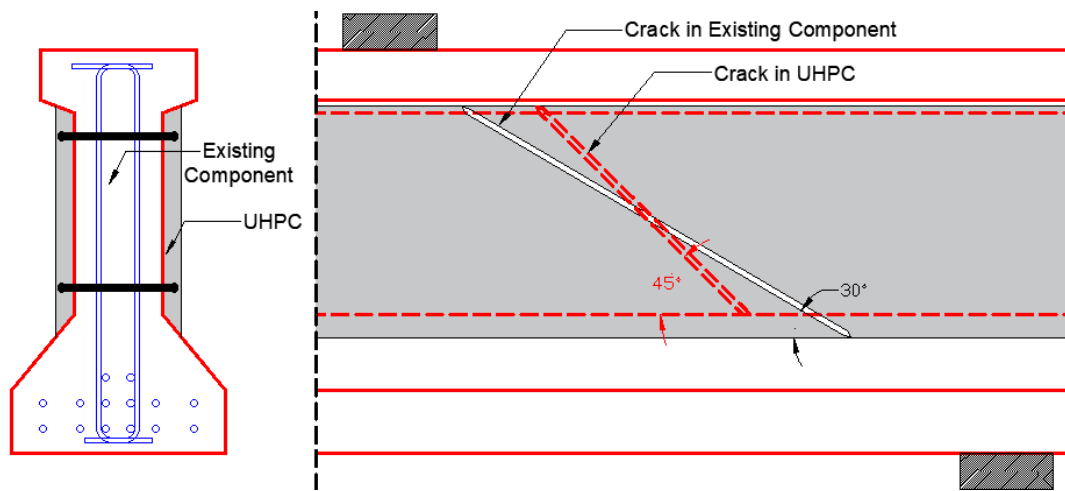


Figure 127: Schematic of different crack angles at the existing girder and UHPC

Step 6: Check the tensile capacity of the longitudinal reinforcement at the critical sections. The tensile reinforcement in both CC and UHPC shall satisfy the following, according to Draft AASHTO UHPC Guidelines, 2021:

$$A_{ps} f_{ps} + A_s f_y + A_{ct} \gamma f_{t,loc} \geq \frac{|M_u|}{d_v \Phi_f} + 0.5 \frac{N_u}{\Phi_c} + \left(\left| \frac{V_u}{\Phi_v} - V_P \right| - 0.5 V_s \right) \cot \theta \quad (81)$$

Where, f_{ps} is the average service stress in prestressing reinforcement at the time of nominal resistance calculation; Φ_f , Φ_v , and Φ_c are the resistance factors according to Draft AASHTO UHPC Guidelines, 2021 for moment, shear, and axial respectively.

Step 7: Calculated the composite CC-UHPC section nominal shear capacity (V_n) as follows:

$$V_n = V_{n,UHPC} + V_{n,CC} \quad (82)$$

It is recommended that the UHPC contribution to the shear strength ($\frac{V_{n,UHPC}}{b_{UHPC} d_{v,UHPC}}$) does not exceed 0.7 ksi until more experimental testing is done on CC-UHPC beams in shear and the test data achieves a higher value than that.

6.1.3 Interface Design for Shear Strengthening

After the shear strength of the composite CC-UHPC is calculated, the interface shall be designed to allow full transfer of the shear forces between the two materials. In order for this model to be valid, the CC-UHPC interface shall be designed to allow full shear transfer of the forces carried by UHPC to the existing CC component. When UHPC is introduced to the sides of a CC beam for shear strengthening, the interface shall be designed for the total vertical shear to be carried by UHPC ($V_{n,UHPC}$). The vertical shear carried by UHPC can be calculated using the ultimate tensile strength of UHPC over the diagonal crack area, similar to the approach used in the shear design UHPC beams (discussed in section 2.4.1). In the case of having the interface not being able to accommodate the full value of the force, $V_{n,UHPC}$ shall be reduced to the CC-UHPC interface shear capacity.

The interface shear resistance can be calculated according to the same procedure discussed in section 5.1.3. Cohesion and friction factors for CC-UHPC interfaces with or without intentional roughening suggested by Abo El-Khier and Morcous, 2019 or Draft AASHTO UHPC Guidelines, 2021 can be used to determine the nominal shear resistance. Another option is to add anchors and design them according to manufacturer's recommendations as in regular CC jackets. When 2-sided UHPC layers are added, the anchors can connect the two sides through the web of the existing element eliminating the pull-out failure mode of the anchor. In that case, the direct shear resistance of the anchor governs the interface design. A design example is discussed in the Appendix section for the interface design of shear strengthening using UHPC.

6.2 Shear Testing of CC-UHPC Beams

This section discusses the testing done on shear strengthened conventional concrete beams using UHPC without additional reinforcement. The design of specimens and strengthening

procedure are discussed first. Then, the test results are presented and used for the validation of the proposed shear strength prediction model.

6.2.1 Specimen Design

Three 12-foot-long beams were fabricated, one beam was set as the reference without strengthening, and the other two beams were strengthened with a 1.5, and 2-inch UHPC layer at the sides of the web for strengthened beam #1 and strengthened beam #2, respectively. Figure 128 shows the cross-sections of the three beams to be tested in shear. In order to obtain the highest contribution from UHPC in shear, the specimens were designed to fail in shear even after strengthening. The CC section contained five #7 bars (area = 0.60 in^2) in the tension side, and one #6 bar (area = 0.44 in^2) in the compression side and was reinforced transversally with a #3 stirrup spaced every six inches. Figure 129 shows a schematic of two shear tests setup of the same CC-UHPC beams, where the supports are moved to allow for the shear span to be at the two opposite ends of the beam.

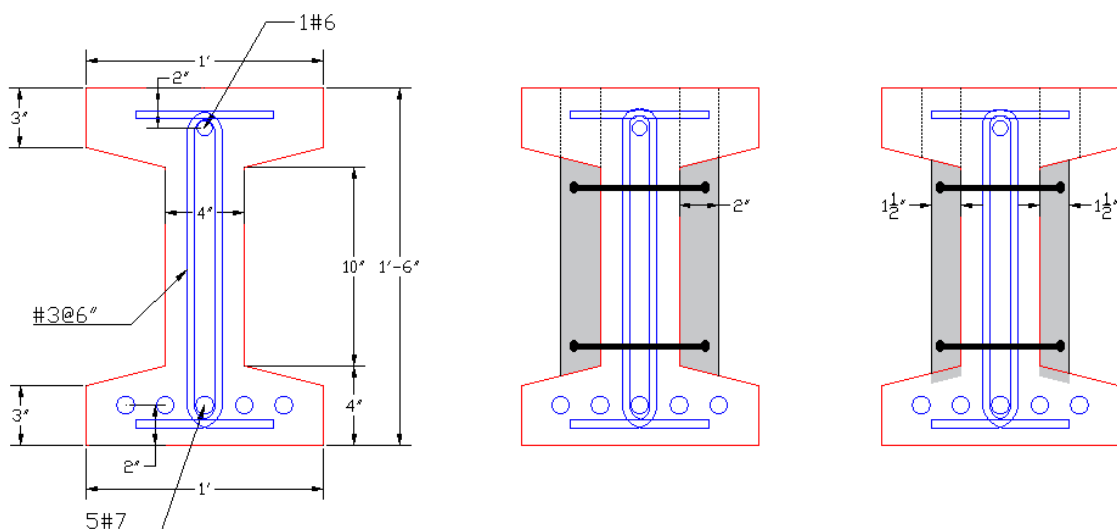


Figure 128: Cross-sections of the strengthened beams in shear, reference beam (left), strengthened beam #1 (middle), and strengthened beam #2 (right)

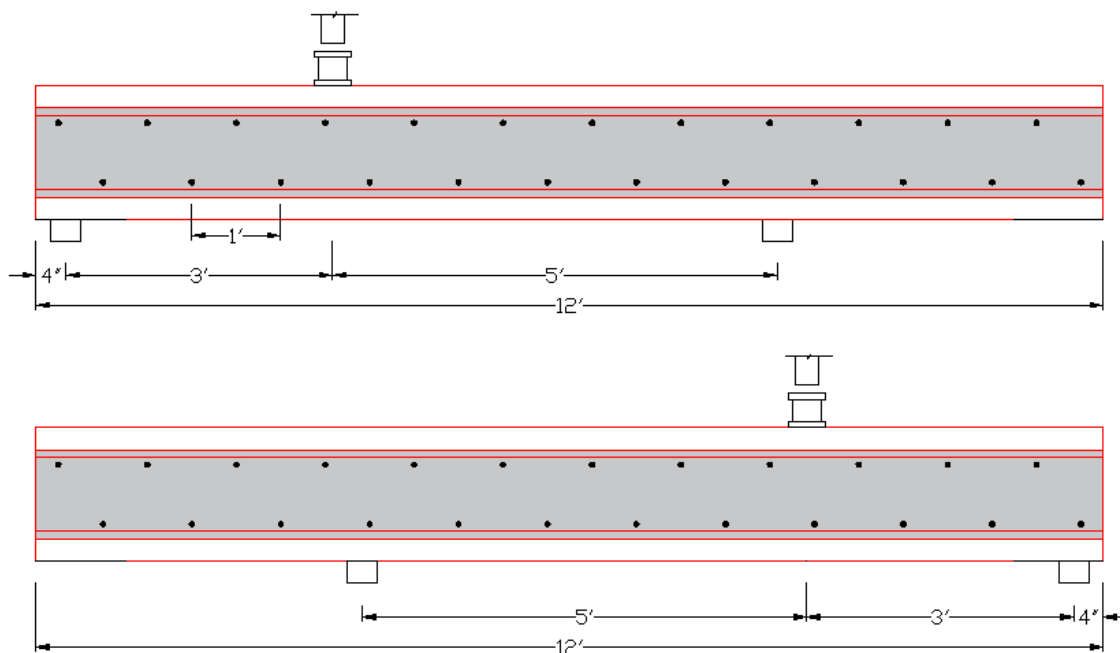


Figure 129: Schematic of two shear tests setup of a CC-UHPC beam, test #1 (top), and test #2 (bottom)

Table 27 shows a summary of the shear testing with the CC and UHPC compressive strengths during fabrication, as well, as, the predicted shear and flexure failure loads. The flexural capacity was increased as much as possible in order to represent a shear capacity deficiency. The prediction calculations were done according to AASHTO LRFD, 2017, El-Helou et al., 2019, and Draft AASHTO for UHPC, 2021. The procedure of calculation is presented in the appendix.

Table 27: Summary of test specimens and predicted capacity

Beam ID	CC Compressive Strength (ksi)	UHPC Compressive Strength (ksi)	Total UHPC Width (in.)	Nominal Shear Capacity (V_n) (kip)	Nominal Flexural Capacity (M_n) (kip.ft)	Flexural Failure Load (kip)	Shear Failure Load (kip)	Flexural Failure Load (kip)
Reference Test	7.2	N/A	N/A	25.6	220.5	117.6	41.0	117.6
Strengthened Beam #1	5.4	17.0	4	60.3	238.7	127.3	96.5	127.3
Strengthened Beam #2	5.4	17.8	3	51.3	233.8	124.6	82.1	124.6

The CC-UHPC interface was designed to carry the full shear forces carried by the two UHPC side layers. The interface was roughened by sandblasting to increase the cohesion and friction factors. However, the cohesion between the two materials was not counted when designing the interface similar to the shear friction design in the ACI 318-14. Threaded anchor rods were used to transfer all the shear forces across the interface through the web. Having a one piece anchor through the CC beam web eliminated the possibility for a pull-out failure mode from the CC beam. The anchors were designed taking into consideration the direct shear failure mode only which helped to significantly increase the anchor capacity. The anchors were considered to be fully developed in the UHPC layers according to the previous research done by Cao et al., 2017 as discussed in section 5.2.1.

6.2.2 Fabrication

The CC and UHPC were both produced with the same mix design discussed in section 5.2.2. The CC beams were fabricated by casting ready-mixed concrete in wooden formwork as shown Figure 100. Expanded polystyrene foam boards were cut and fixed to the sides of the forms to create the I-shaped cross-section. The top reinforcement bar was fixed in place by the U-shaped transverse reinforcement. The foam pieces on the sides were covered in plastic sheets to allow for easy stripping and multiple reuses as shown in Figure 101.



Figure 130: Formwork and reinforcement of two CC beams



Figure 131: Stripping formwork of two CC beams

6.2.3 Strengthening Procedure

Figure 132 shows the first and second steps of the strengthening procedure of the two UHPC strengthened beams in shear. The first step was done through sandblasting where the CC surface was roughened before pouring on UHPC. The used sand size and roughness depth were approximately 1/16-inch. An industrial 10-gallon sandblaster was used with compressed air pressure of 110 psi. Oven-dried fine sand was used as the abrasive material on the CC surface. The second step was to install the anchors according to the anchor design to develop the full shear forces in each of the two UHPC layers. The anchors were spaced every 12-inches and a total of twenty-four anchors were needed as shown in Figure 129. The anchors used were threaded rods having a 3/8-inch diameter and a clear UHPC cover of 1/2-inch. This makes the anchor length to be 7.0, and 6.0 inches for strengthened beam #1 and strengthened beam #2, respectively. A nut was installed at the free ends of the anchor to simulate a similar shape as the headed studs as in Cao et al., 2017. The

anchors were fixed at the CC beam interface using high strength epoxy only to keep the anchor in place while UHPC is poured.



Figure 132: Shear strengthening procedure, steps 1 and 2: roughening of the interface and installing anchors

Figure 133 shows the third step where openings drilled in the top flange of the beams to represent casting from bridge decks. Each side of the beam had two drilled holes towards the beam ends at the shear span testing. Similar pouring procedure was performed in Connecticut, Hain et al., 2021 where UHPC was cast from a 4-inch opening in a bridge deck to repair a corroded steel bridge girder in Connecticut. The openings were initially 2-inches in diameter while strengthened beam #1 was cast. In strengthened beam #2, two adjacent opening were drilled to widen the pouring area slightly as shown in step 6 figure.



Figure 133: Shear strengthening procedure, step 3: drilling top flange openings

Figure 134 shows the fourth step of installing formwork to the sides of the beam. XPS foam boards were cut into the proper dimensions and fixed to plywood to allow for the required UHPC thickness to be created on the sides of the web. This technique can be easily implemented in most bridge girder shapes and beams in buildings.



Figure 134: Shear strengthening procedure, step 4: installing formwork

Figure 135 shows the fifth and sixth steps of the procedure. The fifth step was fixing formwork after installation. Wooden frames spaced at 2-feet were constructed using dimension lumber and were used to prevent the forms from opening when subjected to the fresh UHPC pressure. In the case of having the top surface of the beam or bridge girder inaccessible, steel U-frames could be used as an alternative. Another alternative to these frames is that the vertical elements of the form could be anchored to the CC beam. The sixth step is pouring UHPC from the drilled holes to form the required UHPC thickness.



Figure 135: Shear strengthening procedure, step 5 (left): fixing formwork, step 6 (right): pouring UHPC

Figure 136 shows slight poor consolidation in one side of strengthened beam #1 where UHPC did not fully reach the top flange leaving a small triangular area of unfilled area at one end of the beam, as well as a small triangular area of unfilled UHPC at the middle of the beam. The other side of the beam did not suffer from that issue. In order to avoid this issue in strengthened beam #2, the top flange opening were widened to allow faster pouring. However, the poor consolidation was more significant in strengthened beam #2 as shown in Figure 137. Additional top flange holes were drilled on top of the poorly consolidated areas and UHPC was cast for the second time as shown in Figure 138. No special measures were taken to roughen the interface between the new and old UHPC depending on the high interface shear resistance between two UHPC surfaces.



Figure 136: Poor consolidation in strengthened beam #1



Figure 137: Poor consolidation in strengthened beam #2



Figure 138: Casting UHPC at the poorly consolidated locations in strengthened beam #2

6.2.4 Test Results

Figure 139 shows the test setup and instrumentation of the reference beam. A 100-kip load cell was used under a hydraulic ram to measure the applied load at mid-span. Two string potentiometers were installed at the beam mid-span to measure displacement. And external concrete strain gauges were installed at two sections spaced at 1.0, and 2.0-feet from the support. Four strain gauges were installed at each location to measure the horizontal, vertical, and diagonal strains at that location.



Figure 139: Reference beam test setup and instrumentation

Figure 140 shows the load-deflection plot of the reference beam along with the predicted moment capacity. The predicted capacity was less than half of the measured capacity at failure which can be attributed to the significant conservatism in the shear prediction models. Figure 141 shows the failure mode of the beam where a diagonal tension failure mode occurs at a 45-degree angle.

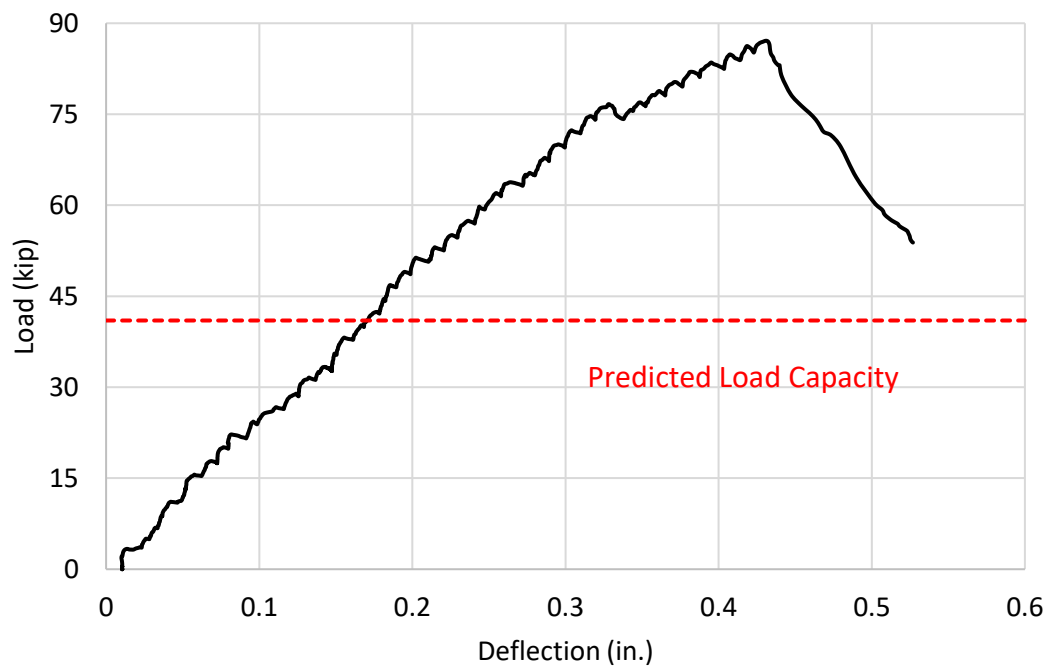


Figure 140: Reference beam load-deflection plot



Figure 141: Reference beam failure mode

Figure 142 shows the test setup of strengthened beam #1 - test #1 and the instrumentation used was similar to what was done in the reference beam except for having a larger capacity load cell (400-kip capacity). Also shown in Figure 143 is the instrumentation used to measure any relative displacement between the CC beam and the UHPC side layer. One Linear Variable Differential Transducer (LVDT) was installed with its base on UHPC at the shear span end and a stiff piece of wood was anchored in the CC end with a spacer wood piece to allow for free movement of UHPC.



Figure 142: Strengthened beam #1 – test #1, test setup and instrumentation



Figure 143: Measuring relative displacement between CC and UHPC in strengthened beam #1 – test #1

Figure 144 shows the load-deflection plot of the two tests done on strengthened beam #1 along with the predicted capacity. The beam achieves and exceeds its predicted shear capacity by 27% for test #1 and 31% for test #2. However, if the results of the reference beam are considered to magnify the prediction, the measured capacity would have been less than the magnified prediction. The original predicted capacity is only shown in the figure. The magnified prediction capacity calculated using the reference beam test results is not shown since the reference beam had higher compressive strength. Figure 145 and Figure 146 show the failure mode and bar slippage in the CC beam at test #1, while Figure 147 shows the failure mode and bar slippage at test #2. The failure mode at the two tests was the same where the longitudinal tension reinforcement in the CC beam spalled their cover and slipped. A diagonal crack is formed as a result of the bar slippage at an angle of approximately 50 degrees with the beam longitudinal axis. No interface cracks or relative

movement were visually noticed between CC and UHPC. Figure 148 shows the measured displacement between the two materials and it can be noticed that the magnitude of displacement is significantly small which indicates no interface failure.

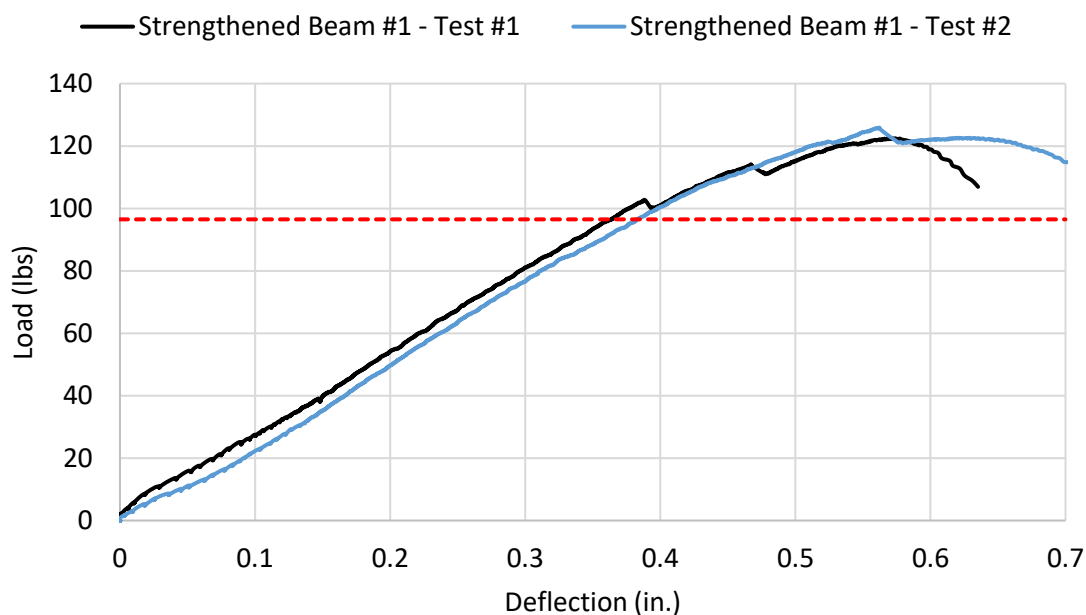


Figure 144: Strengthened beam #1 load-deflection plot for tests #1 and #2

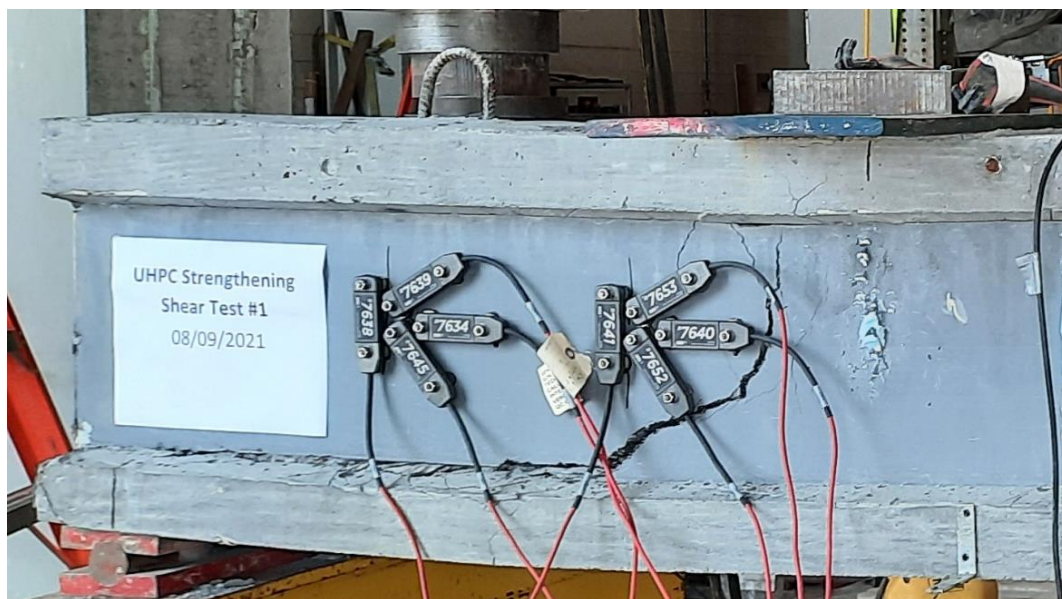


Figure 145: Strengthened beam #1 – test #1 failure mode



Figure 146: Strengthened beam #1 – test #1 bar slippage in the CC beam



Figure 147: Strengthened beam #1 – test #2 failure mode and bar slippage in the CC beam

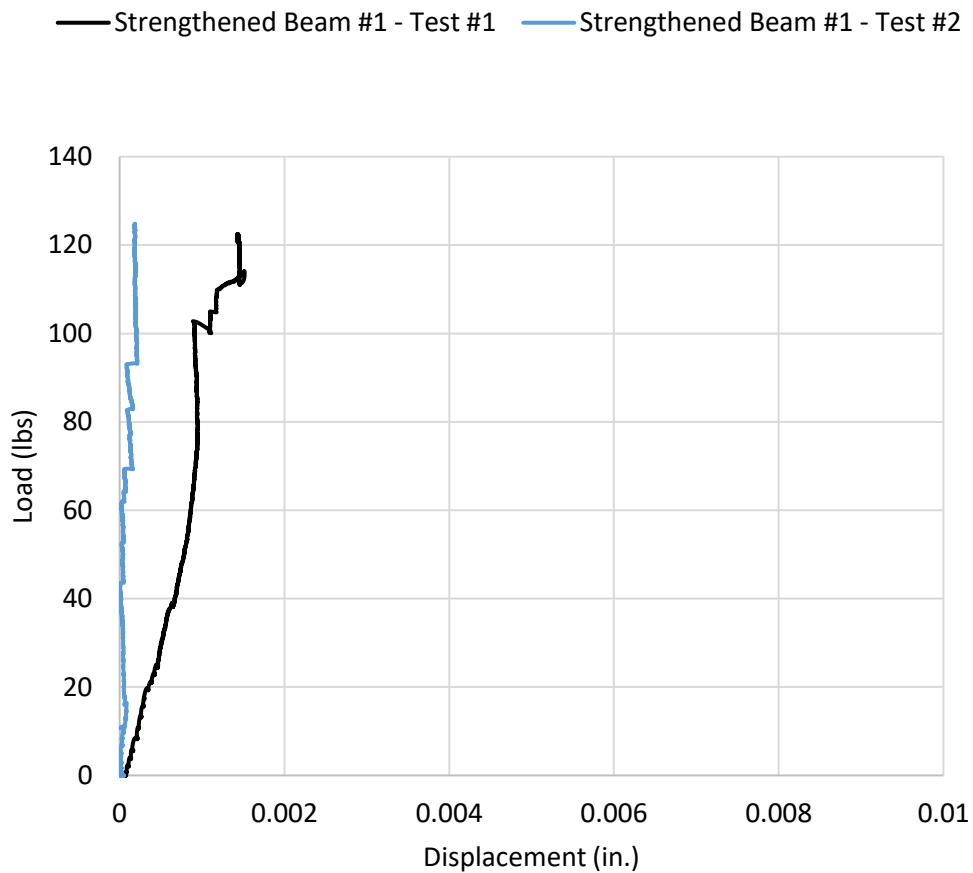


Figure 148: Strengthened beam #1 relative end displacements for tests #1 and #2

Figure 149 and Figure 150 show the test setup and failure mode of strengthened beam #2, tests #1 and #2, respectively. The test setup and instrumentation were similar to what was shown in strengthened beam #1. Also, the failure mode was consistent to what was observed in strengthened beam #1. The longitudinal tension reinforcement in the CC beam slipped and a diagonal crack was formed to the compression zone and having an angle of approximately 70 degrees with the beam longitudinal axis.



Figure 149: Strengthened beam #2 – test #1, test setup and failure mode



Figure 150: Strengthened beam #2 – test #2, test setup and failure mode

Figure 151 shows the load-deflection plot of the two tests done on strengthened beam #2 along with the predicted capacity. The beam achieves and exceeds its predicted shear capacity by 38% for test #1 and 46% for test #2. However, if the results of the reference beam are considered to magnify the prediction, the measured capacity would have been

less than the magnified prediction. The original predicted capacity is only shown in the figure. The magnified prediction capacity calculated using the reference beam test results is not shown since the reference beam had higher compressive strength. No interface cracks or relative movement were visually noticed between CC and UHPC. Figure 152 shows the measured displacement between the two materials and it can be noticed that the magnitude of displacement is significantly small which indicates no interface failure.

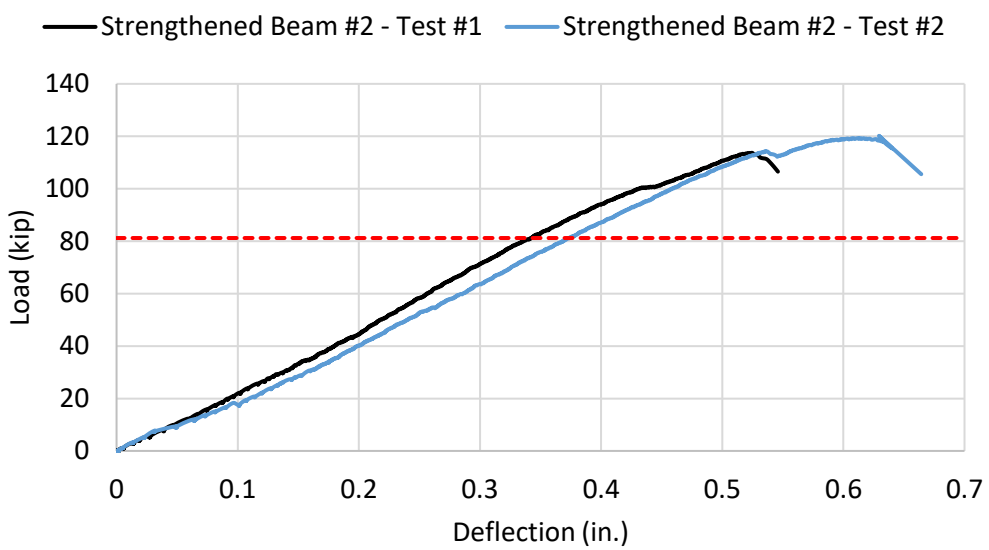


Figure 151: Strengthened beam #2 load-deflection plot for tests #1 and #2

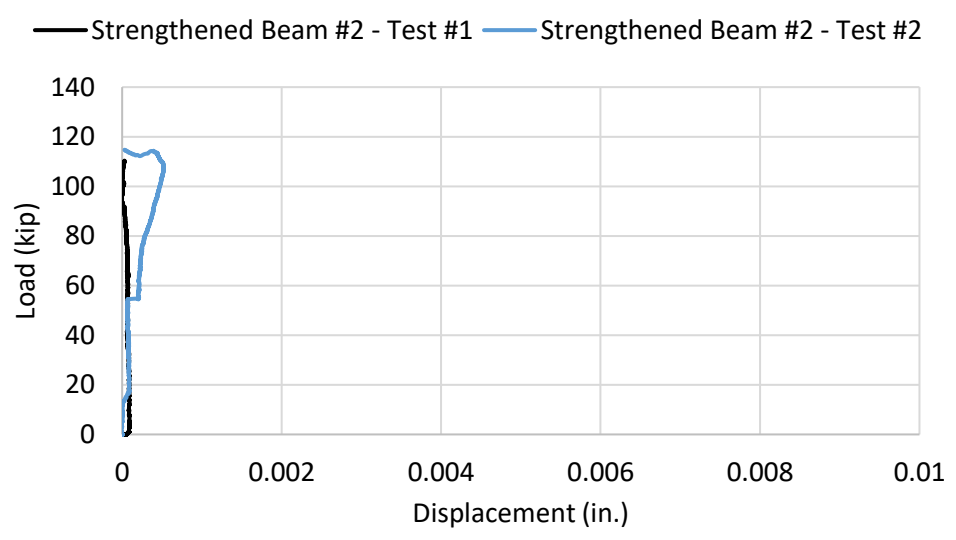


Figure 152: Strengthened beam #2 relative end displacements for tests #1 and #2

Figure 153 shows the measured compressive strains recorded from the diagonal strain gauges in the direction of load path. The measurements are shown for the reference and two strengthened beams, except for Strengthened Beam #1 – Test #1 as the gauges did not measure properly. It can be noticed that the strains in UHPC in the strengthened beams are reduced at the same load compared to the reference beam. This can be attributed to the contribution of UHPC in the shear resistance which reduced the stresses induced in the section from a certain load. Measuring significant compressive strain in UHPC until significantly high loads indicated that CC and UHPC were showing a fully composite behavior which further validates the construction procedure and interface design.

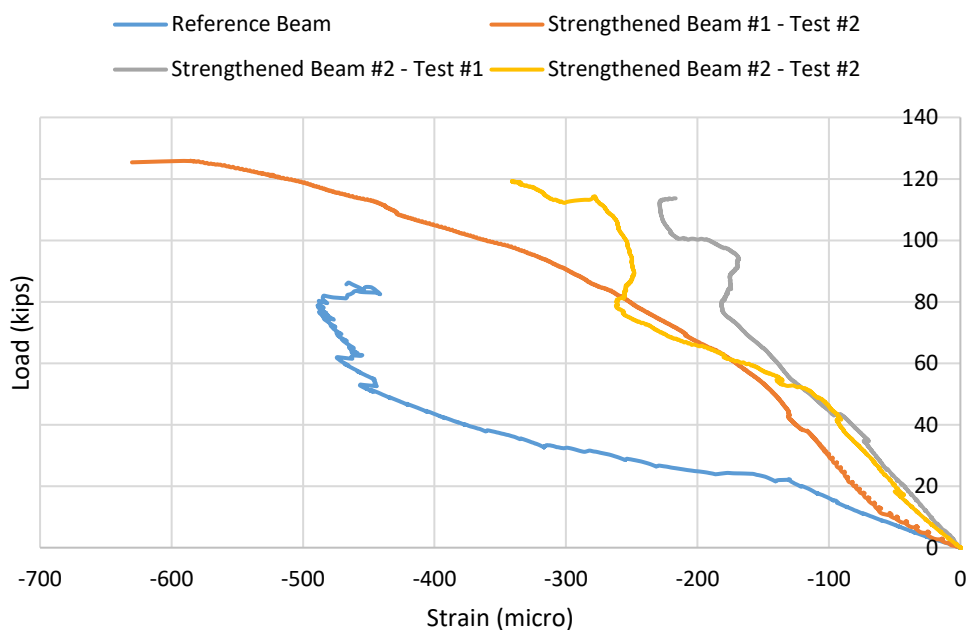


Figure 153: Measured compressive strains

Figure 154 shows the measured tensile strain recorded from the diagonal strain gauges perpendicular to the direction of load path. The measurements are shown for the reference and two strengthened beams, except for Strengthened Beam #1 – Test #1 as the gauges did not measure properly. Concrete strain gauges installed at the surface of concrete in tension do not typically record properly when concrete cracks. However, it can also be noticed that the strain gauges in the strengthened beams recorded significantly smaller strains than the reference beam until reaching a load of 50 kips. After that the strain recording in the

reference beam dropped when cracking occurred. Reading from Strengthened Beam #2 – Test #2 only continued to increase with applied load until reaching 100 kips which indicates that UHPC sustained significant tensile stresses and contributed successfully to the strengthened beam shear strength.

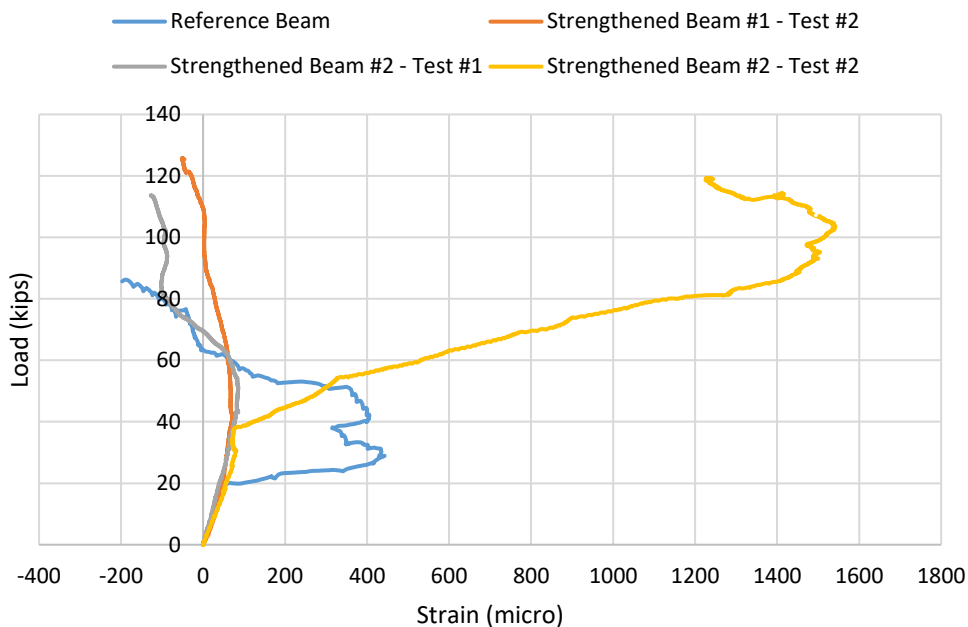


Figure 154: Measured tensile strains

Figure 155 shows the measured horizontal strain recorded from the horizontal strain gauges. The measurements are shown for the reference and two strengthened beams, except for Strengthened Beam #1 – Test #1 as the gauges did not measure properly. Horizontal strain gauges were subjected to tension stress so the relative behavior between the reference and two strengthened beams is similar to that recorded in the diagonal tensile strains. The strain gauges in the strengthened beams recorded smaller strains than the reference beam between an applied load from 20 to 40 kips. After that the strain recording in the reference beam dropped when cracking occurred. Reading from Strengthened Beam #2 – Test #2 only continued to increase with applied load until reaching 100 kips which indicates that UHPC sustained significant tensile stresses and contributed successfully to the strengthened beam shear strength.

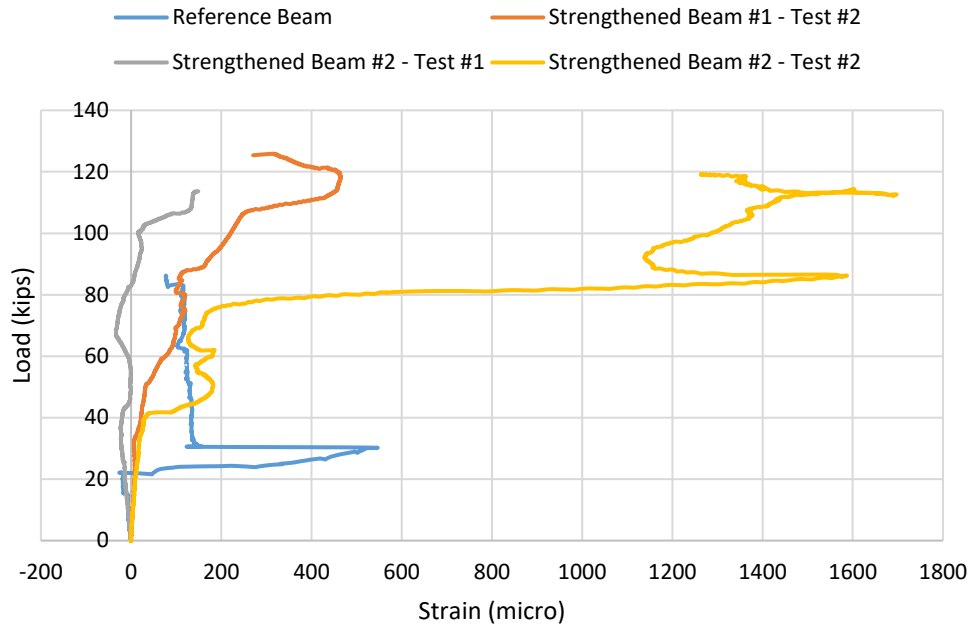


Figure 155: Measured horizontal strains

Figure 156 shows the measured vertical strain recorded from the vertical strain gauges. The measurements are shown for the reference and two strengthened beams, except for Strengthened Beam #1 – Test #1 as the gauges did not measure properly. The gauges were subjected to compression stress so the relative behavior between the reference and two strengthened beams is similar to that recorded in the diagonal compressive strains. The strain gauges in the strengthened beams recorded smaller strains than the reference beam at the same level of applied load. This can be attributed to the contribution of UHPC in the shear resistance which reduced the stresses induced in the section from a certain load. Measuring significant compressive strain in UHPC until significantly high loads indicated that CC and UHPC were showing a fully composite behavior which further validates the construction procedure and interface design.

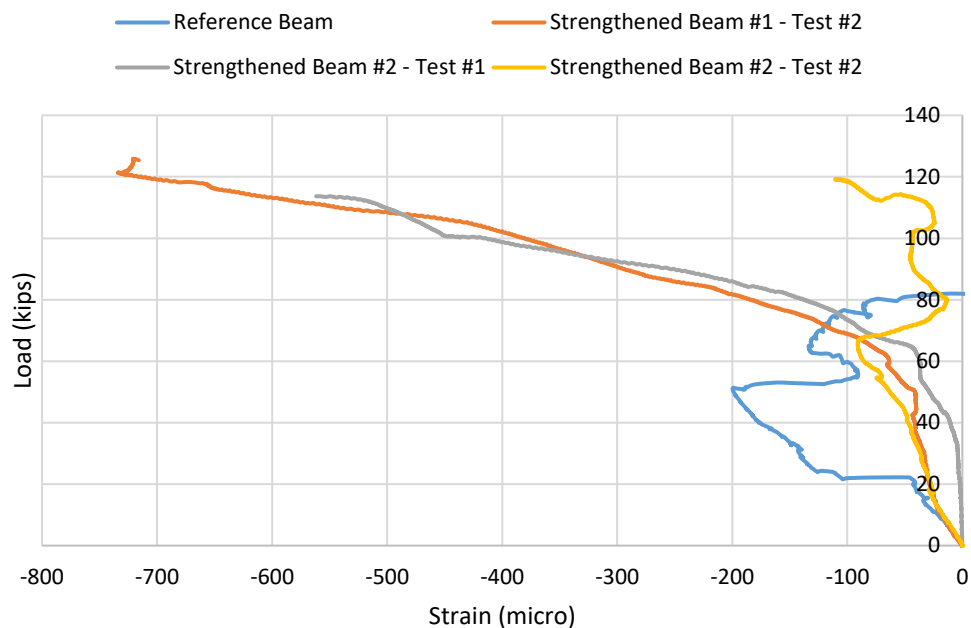


Figure 156: Measured vertical strains

6.2.5 Validation of The Prediction Model of CC-UHPC Beams in Shear

Figure 157 shows the load-deflection plot of the five shear tests done on the reference and two strengthened beams. It can be noticed that the two strengthened beams achieved a significantly higher load capacity and deflection which confirms that the UHPC layers successfully contributed to the shear strength and the ductility of the beams. The stiffness of the strengthened beams was almost the same compared to that of the reference beam. However, it should be noted that the compressive strength of the reference beam is 33% higher than that of the strengthened beams.

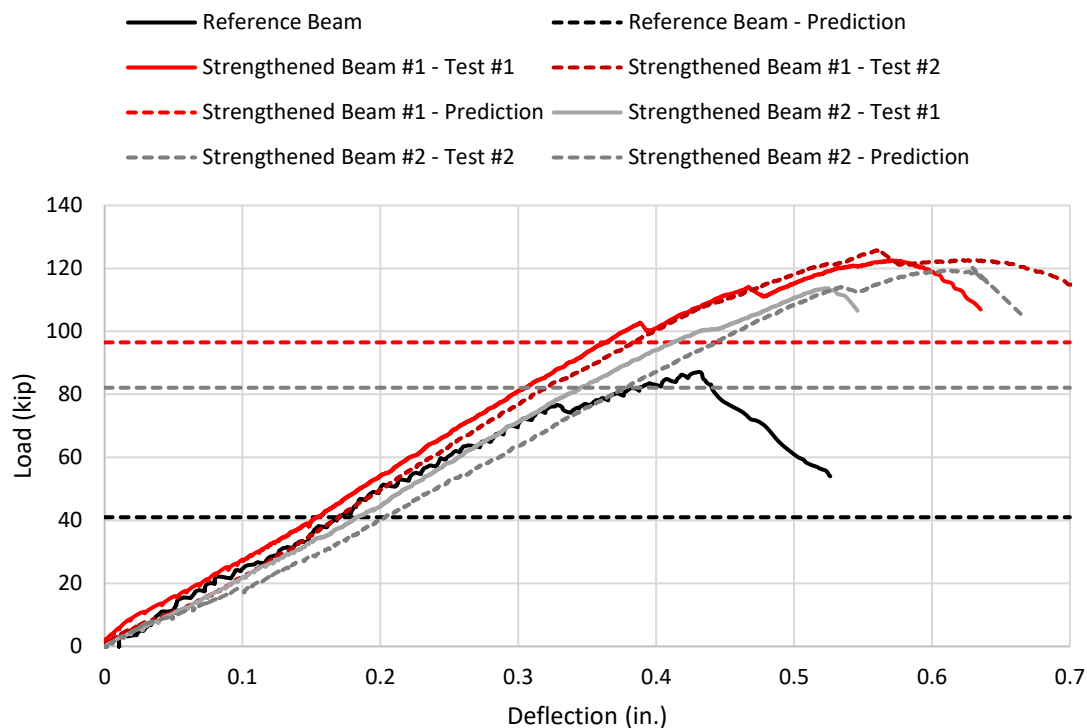


Figure 157: Load-deflection results of the shear testing done on the reference and two strengthened beams

Table 28 summarizes the measured load capacity of the five shear tests done on the reference and two strengthened beams and presents a comparison with the predicted shear and flexure failure values. It can be noticed that the two strengthened beams achieved their respective predicted capacity which validates the prediction model. This also shows how the strengthened beams approached their predicted flexural failure capacity which led to the anchorage failure of the CC beam tension reinforcement.

Table 28: Measured versus predicted load capacities of the tested beams in shear

	Measured Capacity (kip)	Shear Prediction		Flexure-to-Shear	
		Predicted Shear Failure Capacity (kip)	Measured-to-Predicted Shear Capacity	Predicted Flexural Failure Capacity (kip)	Measured-to-Predicted Flexural Capacity
Reference Beam	87.1	41.0	2.12	117.6	1.35
Strengthened Beam #1 – Test #1	122.5	96.5	1.27	127.3	1.04
Strengthened Beam #1 – Test #2	125.9	96.5	1.31	127.3	1.01
Strengthened Beam #2 – Test #1	113.7	82.1	1.38	124.6	1.10
Strengthened Beam #2 – Test #2	120.2	82.1	1.46	124.6	1.04

Figure 158 shows contribution of UHPC to the measured shear strength for the test data collected from the literature and the experimental testing done on strengthened beam #1 (UNL – B1) and strengthened beam #2 (UNL – B2). The contribution was calculated as discussed in Table 15 by subtracting the measured resistance of the reference beam from the strengthened beam to get (V_{UHPC}) and then dividing it by the added width and effective depth of the vertical UHPC layer. It can be noticed that the UHPC contribution in the data points obtained from the testing in this research exceeds the test data from literature significantly, except for one data point from Sakr et al., 2019 where the UHPC had transverse reinforcement. The average UHPC contribution of the UNL test data is 0.7 ksi so it is recommended that the contribution of UHPC is limited to that value until further research is done and larger values are achieved in shear strengthening. The significant contribution of UHPC to the shear strength validates the strengthening procedure despite the fact that a flexure failure mode happened in the test specimens.

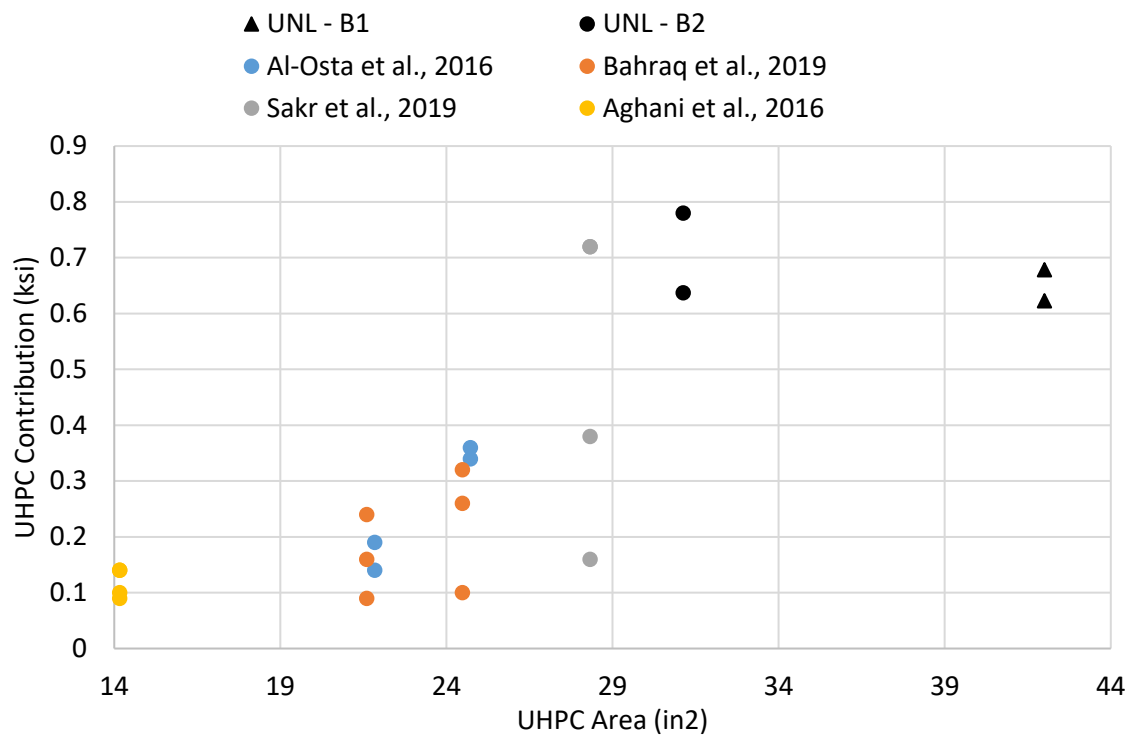


Figure 158: UHPC contribution to the measured shear strength

Chapter 7 – Design Examples

This chapter presents design examples showing the capabilities of UHPC in increasing the flexural and shear strength of existing CC beams. A flexure strengthening design example of a prestressed concrete girder is presented. Then a shear strengthening example of another prestressed girder is discussed. The original and strengthened capacities are compared in both examples.

7.1 Flexure Design Example of a CC-UHPC Beam

The design example is based on an existing prestressed AASHTO Type II girder with 18 bottom strands. Additional strands are added to the tension side and anchored to the existing component with the construction procedure discussed in section 5.1.1. Figure 159 shows the cross sections of the existing and strengthened girders. A 2-inch thick UHPC layer is used to develop the forces in the additional strands to the existing girder. 4 additional strands are used on the side of the bottom flange of the girder to maintain the same road clearances below the girder in that example.

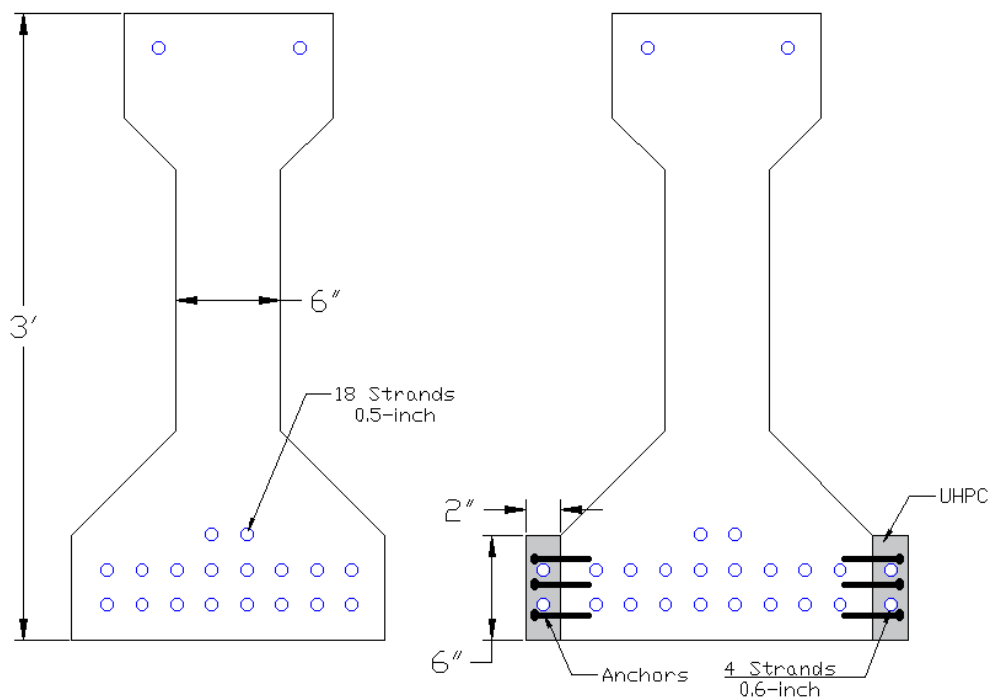


Figure 159: Cross-section of the original (left) and strengthened (right) girders

Figure 160 shows the resulting un-factored moment-curvature plot for the original and strengthened girders, while Figure 161 shows the factored plot for the girders. A 15 percent increase in the flexural strength is achieved just by adding 4 strands on the side of the bottom flange. Additional flexural capacity can be achieved if strands can be added to the soffit of the girder. The advantage offered by UHPC in that case is that it can add a layer of protection to the added strands with minimized thickness. This can help overcome the drawback of external post-tensioning where there is a requirement that the un-strengthened girder can resist unexpected loads if the external post-tensioning is subjected to damage.

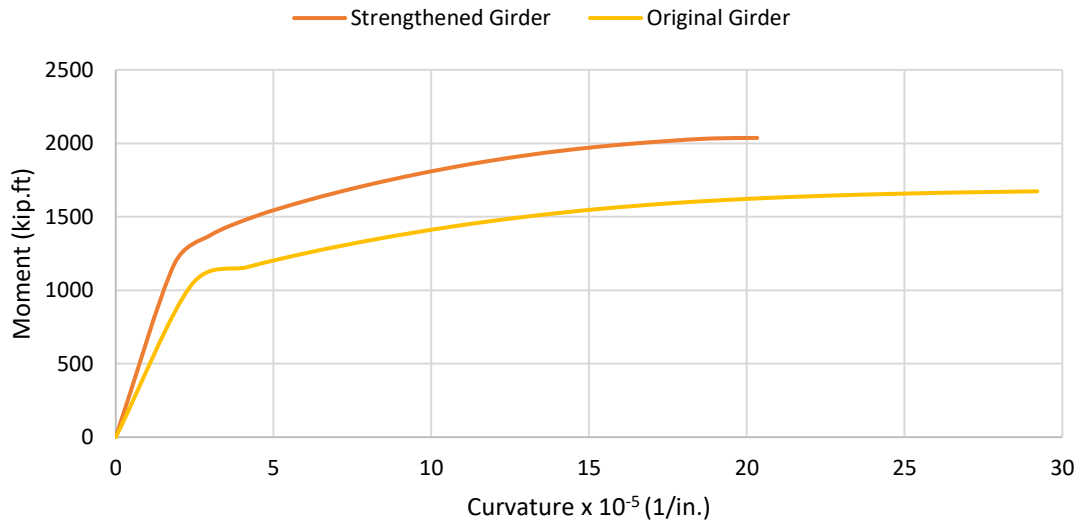


Figure 160: Un-factored flexural strength of the original and strengthened girders

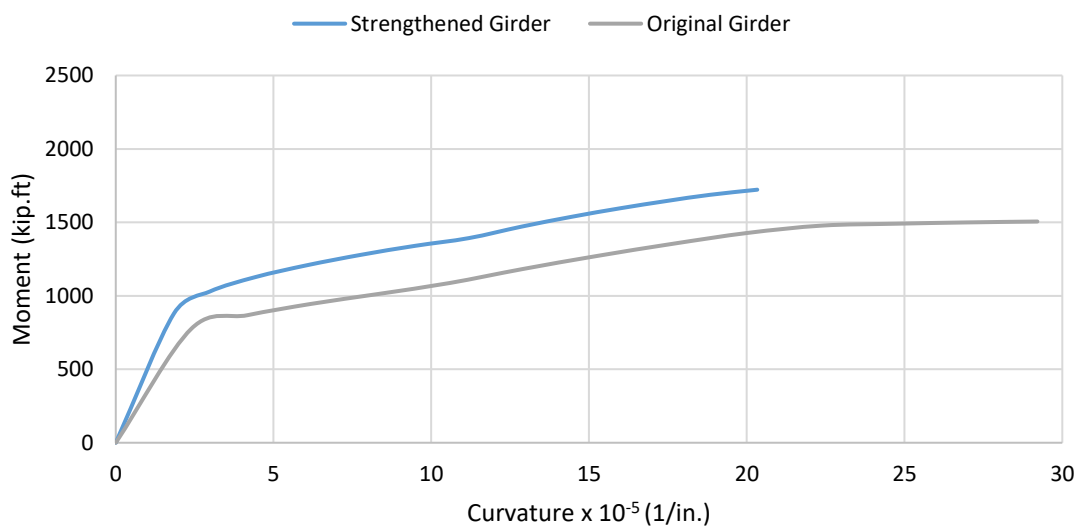


Figure 161: Factored flexural strength of the original and strengthened girders

7.2 Shear Design Example of a CC-UHPC Beam

The design example is based on an example presented by Belarbi et al., 2011 (NCHRP Report 678) on a shear strengthening of a prestressed PC I-beam using a CFRP U-wrap. The calculations are done initially on the existing beam to calculate the un-strengthened capacity. The design shear capacity of the CFRP strengthened beam is then calculated according to the information in the report and was increased by 20%. Then the calculations using two 1.5-inch unreinforced UHPC layers along the web of the beam are presented, and the design shear capacity was increased by 54%. Another alternative using the same two 1.5-inch UHPC layers but with additional reinforcement is presented, and the design shear capacity was increased by 69%. This shows how UHPC can increase the design shear significantly with minimum added dimensions. The 0.7 ksi suggested limit for UHPC contribution in shear was not applied in this design example to show that further testing can increase the contribution significantly if the limit is increased.

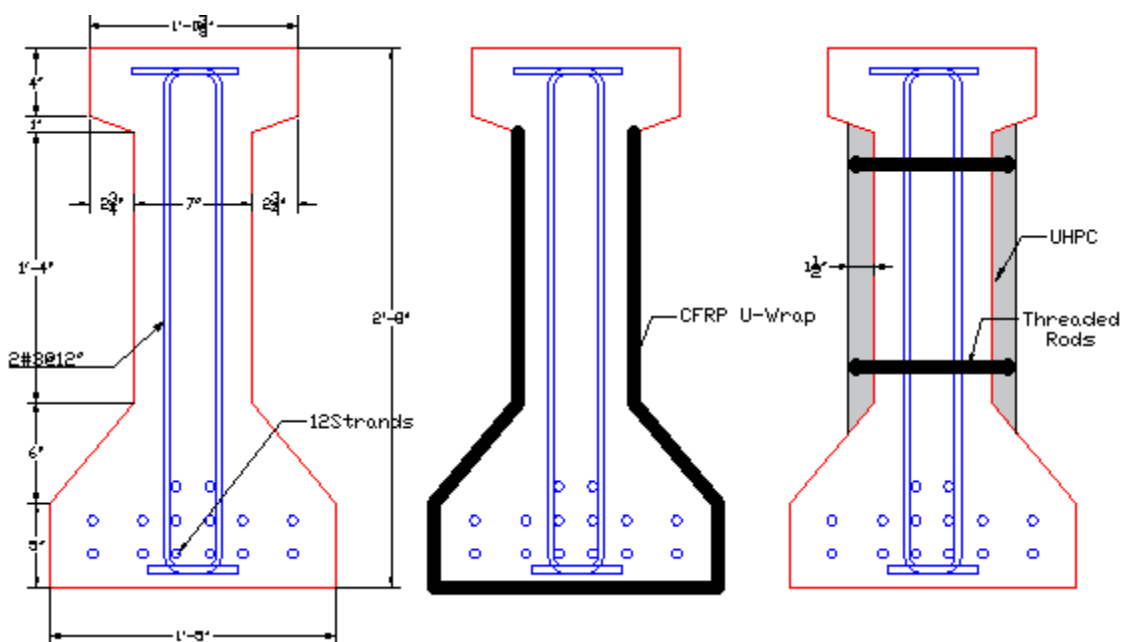


Figure 162: Shear strengthening of the reference girder (left), CFRP strengthened girder (middle), and UHPC strengthened girder (right)

C.G. of Strands from Top of Girder	$d_p := 28.8 \text{ in}$
Shear Depth (AASHTO LRFD, 2017 Section 5.7.2.8)	$d_v := \max(0.9 \cdot d_p, 0.72 h_g) = 25.92 \text{ in}$
Transverse Reinforcement Area	$A_v := 2 \cdot 0.11 \text{ in}^2 = 0.22 \text{ in}^2$
Transverse RFT Yield Strength	$f_{yt} := 60 \text{ ksi}$
Spacing of Transverse RFT (at critical section)	$S := 12 \text{ in}$
Transverse Reinforcement Ratio	$\rho_v := \frac{A_v}{b_w \cdot S} = 0.003$
Yield Strength of Transverse Reinforcement	$f_{y,s} := 60 \text{ ksi}$
Transverse Reinforcement MOE	$E_s := 28500 \text{ ksi}$
Angle of Transverse RFT with Longitudinal Axis	$\alpha := 90 \text{ deg}$

2- Factored Loads (Strength I)

$V_u := 100 \text{ kip}$	
$V_p := 0 \text{ kip}$	Straight Strands
$M_u := 660 \text{ ft} \cdot \text{kip}$	
$N_u := 0 \text{ kip}$	-ve if Compression

3- Existing Girder Capacity

Longitudinal Tensile Strain (AASHTO LRFD, 2017 Section 5.7.3.4)

$$\varepsilon_s := \frac{\max\left(\frac{M_u}{d_v}, |V_u - V_p|\right) + 0.5 N_u + |V_u - V_p| - A_{ps} \cdot f_{po}}{E_p \cdot A_{ps}} = 1.175 \cdot 10^{-5}$$

$$\varepsilon_s := \mathbf{if}(\varepsilon_s < 0, 0, \varepsilon_s) = 1.175 \cdot 10^{-5}$$

Factor of Concrete Ability to Transmit Shear Forces (AASHTO LRFD, 2017 Section 5.7.3.4)	$\beta := \frac{4.8}{1 + 750 \cdot \varepsilon_s} = 4.758$
--	--

Angle of Diagonal Compression Strut (AASHTO LRFD, 2017 Section 5.7.3.4) $\theta := 29 + 3500 \varepsilon_s = 29.041$

Concrete Section Contribution to Shear Resistance (AASHTO LRFD, 2017 Section 5.7.3.4) $V_c := 0.0316 \cdot \beta \cdot \sqrt{f_c'} \cdot \mathbf{ksi} \cdot b_w \cdot d_v = 72.177 \mathbf{kip}$

Transverse RFT Contribution to Shear Resistance (AASHTO LRFD, 2017 Section 5.7.3.4)

$$V_s := \frac{A_v \cdot f_{yt} \cdot d_v \cdot \left(\cot\left(\frac{\pi \theta}{180}\right) + \cot\left(\frac{\pi}{2}\right) \right) \cdot \sin\left(\frac{\pi}{2}\right)}{S} = 51.35 \mathbf{kip}$$

Undamaged Girder Nominal Shear Resistance $V_{n,CC} := V_c + V_s + V_p = 123.5 \mathbf{kip}$

Shear Strength Reduction Factor (AASHTO LRFD, 2017, section 5.5.4.2) $\phi := 0.9$

Existing Girder Nominal Shear Resistance $V_{u,CC} := \phi \cdot V_{n,CC} = 111.2 \mathbf{kip}$

4- Using CFRP U-Wraps at Critical Section (According to AASHTO, 2012, and ACI 440.2R-17)

Thickness of One Layer $t_f := 0.0065 \mathbf{in}$

CFRP Tensile Strength $f_{fu} := 550 \mathbf{ksi}$

Modulus of Elasticity $E_f := 33000 \mathbf{ksi}$

Ultimate Strain $\varepsilon_{fu} := \frac{f_{fu}}{E_f} = 0.017$

Number of CFRP Plies $n_f := 1$

Width of CFRP Sheets $w_f := 8 \mathbf{in}$

Center-to-center Spacing of CFRP Sheets $S_f := 12 \mathbf{in}$

Orientation of CFRP Sheets $\alpha_f := 90 \mathbf{deg}$

Effective Depth of CFRP Sheets $d_f := 26 \mathbf{in}$

Active Bonded Length (ACI 440.2R-17 Section 11.4.1) $L_e := \frac{2500 \mathbf{in}}{\left(n_f \cdot \frac{t_f}{\mathbf{in}} \cdot \frac{E_f}{\mathbf{psi}} \right)^{0.58}} = 2 \mathbf{in}$

Bond Reduction Coefficients (ACI 440.2R-17 Section 11.4.1)	$k_1 := \left(\frac{f'_c}{4000 \cdot \text{psi}} \right)^{\frac{2}{3}} = 1.452$
	$k_2 := \frac{d_f - L_e}{d_f} = 0.922$
Bond Dependent Coefficient (ACI 440.2R-17 Section 11.4.1)	$k_v := \min \left(\frac{k_1 \cdot k_2 \cdot L_e}{468 \cdot \varepsilon_{fu} \cdot \text{in}}, 0.75 \right) = 0.347$
Effective Strain in CFRP Layers (ACI 440.2R-17 Section 11.4.1)	$\varepsilon_{fe.ACI} := \min (k_v \cdot \varepsilon_{fu}, 0.004, 0.75 \cdot \varepsilon_{fu}) = 0.004$
FRP Shear RFT Area (AASHTO, 2012 Section 4.3.2)	$\rho_f := \frac{2 \cdot n_f \cdot t_f}{b_w} = 0.002$
Reduction Factor (AASHTO, 2012 Section 4.3.2)	$R_f := \min \left(\max \left(4 \cdot \left(\rho_f \cdot \frac{E_f}{\text{ksi}} \right)^{-0.67}, 0.088 \right), 1 \right) = 0.254$
Effective Strain in CFRP Layers (AASHTO, 2012 Section 4.3.2)	$\varepsilon_{fe.AASHTO} := R_f \cdot \varepsilon_{fu} = 0.004$
Design Effective Strain in CFRP Layers	$\varepsilon_{fe} := \min (\varepsilon_{fe.ACI}, \varepsilon_{fe.AASHTO}) = 0.004$
Area of CFRP Wraps	$A_{fv} := 2 \cdot n_f \cdot t_f \cdot w_f = 0.104 \text{ in}^2$
Shear Resistance of CFRP Wraps (AASHTO, 2012 Section 4.3.2, and ACI 440.2R-17 Section 11.4.1)	$V_f := \frac{A_{fv} \cdot (E_f \cdot \varepsilon_{fe}) \cdot (\sin(\alpha) + \cos(\alpha)) \cdot d_f}{S_f} = 29.744 \text{ kip}$
Additional Reduction Factor for CFRP U-Wraps (AASHTO, 2012 Section 4.3.1, and ACI 440.2R-17 Table 11.3)	$\psi_f := 0.85$
CFRP Strengthened Girder Shear Resistance	$V_{uf} := \phi \cdot (V_{n.CC} + \psi_f \cdot V_f) = 133.928 \text{ kip}$
Strengthened-to-Original Shear Capacity	$\frac{V_{uf}}{V_{u.CC}} = 1.205$

5- Using UHPC with No Transverse Reinforcement for Strengthening at Girder Web Area (According to Draft AASHTO, 2021)

UHPC Compressive Strength	$f_{c,uhpc}' := 18 \text{ ksi}$
UHPC Modulus of Elasticity	$E_c := 2500 \cdot 1 \cdot \left(\frac{f_c'}{\text{ksi}}\right)^{0.33} \cdot \text{ksi} = 4751.4 \text{ ksi}$
Tensile Strength at Crack Localization	$f_{t,loc} := 1 \text{ ksi}$
Tensile Strength Safety Factor	$\gamma := 0.85$
Tensile Strain at Crack Localization	$\varepsilon_{t,loc} := 0.004$
UHPC Area in Flexural Tension Side	$A_{ct} := 17 \text{ in} \cdot 5 \text{ in} = 85 \text{ in}^2$
Total Width of UHPC	$b_{UHPC} := 3 \text{ in}$
Effective Depth of UHPC	$d_{v,UHPC} := 15 \text{ in}$
Transverse Reinforcement	$\rho_{v,UHPC} := 0$

$$\text{Longitudinal Strain } \varepsilon_s := \max\left(\frac{\left|\frac{M_u}{d_v}\right| + 0.5 N_u + |V_u - V_p| - A_{ps} \cdot f_{po} - \gamma \cdot f_{t,loc} \cdot A_{ct}}{E_p \cdot A_{ps} + E_c \cdot A_{ct}}, 0\right) = 0$$

Guess Values	$\theta := 28 \text{ deg}$ $\varepsilon_v := 0.001$
Constraints	$\varepsilon_{t,loc} = \frac{\varepsilon_s}{2} \cdot \left(1 + (\cot(\theta))^2\right) + \frac{2 \cdot f_{t,loc}}{E_c} \cdot (\cot(\theta))^4 \downarrow$ $+ \frac{2 \cdot \rho_{v,UHPC} \cdot E_s \cdot \varepsilon_v}{E_c} \cdot \sin(\alpha) \cdot (\cot(\theta))^2 \cdot \left(1 + (\cot(\theta))^2 + \cot(\alpha) \cdot (\tan(\theta) + \cot(\theta))\right)$ $\varepsilon_v - \varepsilon_{t,loc} + 0.5 \cdot \varepsilon_s = \frac{-2 \cdot f_{t,loc}}{E_c} \cdot (\cot(\theta))^2 \downarrow$ $- \frac{2 \cdot \rho_{v,UHPC} \cdot E_s \cdot \varepsilon_v}{E_c} \cdot \sin(\alpha) \cdot \left(1 + (\cot(\theta))^2 + \cot(\alpha) \cdot (\tan(\theta) + \cot(\theta))\right)$
Solver	$\text{Solution} := \mathbf{find}(\varepsilon_v, \theta) = \begin{bmatrix} 0.003 \\ 0.518 \end{bmatrix}$

$$\varepsilon_v := \text{Solution}_0 = 0.0027 \quad \theta_{UHPC} := \text{Solution}_1 = 29.664 \text{ deg} \quad f_{v,1} := E_s \cdot \varepsilon_v = 77.019 \text{ ksi}$$

$$f_v := \min(f_{v,1}, f_{y,s}) = 60 \text{ ksi}$$

$$\text{Crack angle for Design} \quad \theta := \max(\theta \cdot \text{deg}, \theta_{UHPC}) = 29.7 \text{ deg}$$

$$\text{UHPC Contribution to Nominal Shear Resistance} \quad V_{UHPC} := \gamma \cdot f_{t,loc} \cdot b_{UHPC} \cdot d_{v,UHPC} \cdot \cot(\theta) = 67.16 \text{ kip}$$

$$\text{Girder Design Shear Resistance} \quad V_{n,UHPC} := V_{UHPC} = 67.2 \text{ kip}$$

$$\text{Resistance Factor in Shear} \quad \phi_v := 0.9$$

$$\text{Resistance Factor in Flexure} \quad \phi_f := 0.9$$

$$\text{Resistance Factor in Compression} \quad \phi_c := 0.75$$

$$\text{Additional Longitudinal Reinforcement in UHPC} \quad A_{s,UHPC} := 0.4 \text{ in}^2$$

Check Longitudinal Reinforcement

$$\text{check} := \text{if} \left(\begin{array}{l} A_{ps} \cdot f_{po} \downarrow \\ + A_{s,UHPC} \cdot E_s \cdot \varepsilon_{t,loc} \downarrow \\ + A_{ct} \cdot \gamma \cdot f_{t,loc} \end{array} > \begin{array}{l} \frac{|M_u| \downarrow}{d_v \cdot \phi_f} \\ + \frac{0.5 \cdot N_u \downarrow}{\phi_c} \\ + \left(\left| \frac{V_u}{\phi_v} - V_p \right| - 0.5 V_s \right) \cdot \cot(\theta) \end{array} , \text{"Ok"}, \text{"Increase"} \right) = \text{"Ok"}$$

$$\text{UHPC Strengthened Girder Shear Resistance (No Transverse Reinforcement)} \quad V_{u,UHPC} := \phi_v \cdot (V_{n,CC} + V_{n,UHPC}) = 171.616 \text{ kip}$$

$$\text{Strengthened-to-Original Shear Capacity} \quad \frac{V_{u,UHPC}}{V_{u,CC}} = 1.544$$

6- Using UHPC with Additional Transverse Reinforcement for Strengthening at Girder Web Area (According to Draft AASHTO, 2021)

Transverse Reinforcement Area $A_{v,UHPC} := 0.22 \text{ in}^2$

Transverse Reinforcement Spacing $S_{UHPC} := 12 \text{ in}$

Transverse Reinforcement $\rho_{v,UHPC} := \frac{A_{v,UHPC}}{b_{UHPC} \cdot S_{UHPC}} = 0.006$

$\theta := 28 \text{ deg}$ $\varepsilon_v := 0.001$

$$\varepsilon_{t,loc} = \frac{\varepsilon_s}{2} \cdot \left(1 + (\cot(\theta))^2\right) + \frac{2 \cdot f_{t,loc}}{E_c} \cdot (\cot(\theta))^4 \downarrow$$

$$+ \frac{2 \cdot \rho_{v,UHPC} \cdot E_s \cdot \varepsilon_v \cdot \sin(\alpha) \cdot (\cot(\theta))^2 \cdot \left(1 + (\cot(\theta))^2 + \cot(\alpha) \cdot (\tan(\theta) + \cot(\theta))\right)}{E_c}$$

$$\varepsilon_v - \varepsilon_{t,loc} + 0.5 \cdot \varepsilon_s = \frac{-2 \cdot f_{t,loc}}{E_c} \cdot (\cot(\theta))^2 \downarrow$$

$$- \frac{2 \cdot \rho_{v,UHPC} \cdot E_s \cdot \varepsilon_v \cdot \sin(\alpha) \cdot \left(1 + (\cot(\theta))^2 + \cot(\alpha) \cdot (\tan(\theta) + \cot(\theta))\right)}{E_c}$$

$Solution := \mathbf{find}(\varepsilon_v, \theta) = \begin{bmatrix} 0.002 \\ 0.568 \end{bmatrix}$

$\varepsilon_v := Solution_0 = 0.0024$ $\theta_{UHPC} := Solution_1 = 32.564 \text{ deg}$ $f_{v,1} := E_s \cdot \varepsilon_v = 67.504 \text{ ksi}$

$f_v := \min(f_{v,1}, f_{y,s}) = 60 \text{ ksi}$

Crack angle for Design $\theta := \max(\theta \cdot \text{deg}, \theta_{UHPC}) = 32.6 \text{ deg}$

UHPC Contribution to Nominal Shear Resistance $V_{UHPC} := \gamma \cdot f_{t,loc} \cdot b_{UHPC} \cdot d_{v,UHPC} \cdot \cot(\theta) = 59.89 \text{ kip}$

UHPC Transverse Steel Contribution

$$V_{s,UHPC} := \frac{A_{v,UHPC} \cdot f_v \cdot d_{v,UHPC} \cdot (\cot(\theta + \cot(\alpha))) \cdot \sin(\alpha)}{S_{UHPC}} = 25.836 \text{ kip}$$

Girder Design Shear Resistance	$V_{n,UHPC} := V_{UHPC} + V_{s,UHPC} = 85.7 \text{ kip}$
Resistance Factor in Shear	$\phi_v := 0.9$
Resistance Factor in Flexure	$\phi_f := 0.9$
Resistance Factor in Compression	$\phi_c := 0.75$
Additional Longitudinal Reinforcement in UHPC	$A_{s,UHPC} := 0 \text{ in}^2$

Check Longitudinal Reinforcement

$$check := \text{if} \left(\begin{array}{l} A_{ps} \cdot f_{po} \downarrow \\ + A_{s,UHPC} \cdot E_s \cdot \varepsilon_{L,loc} \downarrow \\ + A_{ct} \cdot \gamma \cdot f_{L,loc} \end{array} > \begin{array}{l} \frac{|M_u|}{d_v \cdot \phi_f} \downarrow \\ + \frac{0.5 \cdot N_u}{\phi_c} \downarrow \\ + \left(\left| \frac{V_u}{\phi_v} - V_p \right| - 0.5 V_s \right) \cdot \cot(\theta) \end{array}, \text{“Ok”, “Increase”} \right) = \text{“Ok”}$$

UHPC Strengthened Girder Shear Resistance (No Transverse Reinforcement) $V_{u,UHPC} := \phi_v \cdot (V_{n,CC} + V_{n,UHPC}) = 188.331 \text{ kip}$

Strengthened-to-Original Shear Capacity $\frac{V_{u,UHPC}}{V_{u,CC}} = 1.694$

Chapter 8 – Summary, Conclusions, and Recommendations

8.1 Summary

8.1.1 Flexure Strengthening of Conventional Concrete Beams

A flexure strength prediction model was developed for CC-UHPC beams based on the principles of strain compatibility and internal forces equilibrium. The material models of UHPC in tension and compression used in the development of the model were evaluated using the test data of UHPC beams in flexure. The evaluation was done by comparing measured versus predicted flexural resistance. The effect of different idealized models was found to be not significant and the simplest models of UHPC in tension and compression can be used to accurately predict the flexural resistance. The developed model can predict the flexural strength of non-prestressed or prestressed beams where the CC and UHPC are acting fully composite. The interface design was performed to allow the full transfer of forces carried by UHPC in the design for flexure. Concrete anchors were used according to manufacturer's recommendations to develop the force in UHPC, and the design guidelines and construction procedure are documented.

Flexure testing was done on three beams with one beam acting as a reference without strengthening and the other two were strengthened with 2-#6, and 3-#6 additional bars, respectively. A 2-inch layer of UHPC was cast at the soffit of the beams around the additional bars to contribute to the flexural tension zone and transfer the forces in the additional bars to the existing CC beam. The specimens were designed to fail in shear to measure the highest UHPC contribution in flexure. However, a consistent failure mode of slippage of the tension reinforcement in the CC beam occurred after the tension reinforcement exceeded their yield strength. Test results showed that the strengthened beams achieved higher flexural strength and stiffness than the reference beam. Moreover, the measured-to-predicted flexural strength was comparable to a great extent (1.08 for the average of the two strengthened beams) which validates the developed prediction model. No significant displacement was measured between CC and UHPC and no interface cracks were visually noticed indicating that the anchors used, and roughening procedure were successful.

8.1.2 Shear Strengthening of Conventional Concrete Beams

A shear strength prediction model was developed for CC-UHPC beams based on a similar approach to that used in shear strengthening with FRP. The existing shear strength prediction models of UHPC beams were first evaluated by comparing the measured versus predicted shear strength. The French standard, NF P 18-710, 2016 provided that closest prediction to the measured shear strength with the least scatter. The developed model can predict the shear strength of non-prestressed or prestressed beams where the CC and UHPC are acting fully composite. The interface design was performed to allow the full transfer of forces carried by UHPC in the vertical shear design. Through holes were drilled in the beam web area and threaded rods having a nut at their free end were used as the interface anchors. The rods were design according to their tensile and direct shear strength without the consideration of the pullout failure mode as they were connected to the UHPC on both sides. This helped optimize the number of required anchors to develop the vertical shear contribution of UHPC. The anchor design guidelines and construction procedure are documented.

Shear testing was done on three beams with one beam acting as a reference without strengthening and the other two were strengthened with two side UHPC layers at the web area. The first strengthened beam had a total of 4-inch unreinforced UHPC layers added, while the second one had a total UHPC thickness of 3 inches. Test results showed that the strengthened beams achieved higher shear strength than the reference beam. Moreover, the measured-to-predicted shear strength was comparable to a great extent (1.35 for the average of the two strengthened beams) which validates the developed prediction model. No significant displacement was measured between CC and UHPC and no interface cracks were visually noticed indicating that the threaded rods used, and roughening procedure were successful.

8.1.3 Design Examples

Two design examples were presented to show the capabilities of UHPC in shear and flexural strengthening. The flexural strengthening design example was based on.....

The shear strengthening design example was based on strengthening a prestressed bridge beam using CFRP wrapping. Shear strength calculations of the existing, CFRP strengthened, un-reinforced UHPC strengthened, transversally reinforced UHPC beams are presented. Adding a 3-inch un-reinforced UHPC layers at the web area increased the design shear strength by 54% compared to a 20% increase in the case of CFRP wrapping.

8.2 Conclusions

The development and validation of the CC-UHPC beams prediction models yielded the following conclusions:

1. The developed flexure prediction model of strengthened composite CC-UHPC beams provides reasonable accuracy. The average measured-to-predicted flexural strength was 1.08.
2. The developed shear prediction model of strengthened composite CC-UHPC beams provides reasonable accuracy. The average measured-to-predicted shear strength was 1.35.
3. The added 2-inch UHPC layer at the beam soffit allowed increasing the tensile reinforcement and achieving higher flexural strength and stiffness than the reference beam.
4. The added 1.5-inch and 2-inch UHPC layers at the beam webs without transverse reinforcement allowed increasing the shear strength significantly compared to the reference beam.

The strengthening procedure yielded the following conclusions:

1. UHPC strengthening procedures for flexure and shear cases were simple, economical, and efficient. No special forms or casting equipment were required.
2. Interface preparation through light sandblasting and connectors was successful to transfer the interface forces between CC and UHPC. No relative displacement was measured between CC and UHPC, and no visual cracks were observed.
3. No special connectors were required for the interface design. Headed concrete screw anchors were used flexural strengthening, and threaded rods with nuts at free end were used shear strengthening.

The analysis of UHPC beams flexure test data yielded the following conclusions:

1. Conventional concrete material models significantly underestimate the flexural strength of non-prestressed UHPC components as they neglect fiber contribution. The average measured-to-predicted flexural resistance ratio using conventional concrete models was 1.73.
2. UHPC compression models resulted in similar predictions indicating that both models can be used to accurately predict the flexural strength of non-prestressed UHPC beams.
3. Tension models A and B resulted in similar predictions of the flexural strength indicating that cracking tensile strength (f_{cr}) does not have significant effect on flexural strength prediction. However, tension model C resulted in approximately 24% reduction in the predicted flexural strength compared to tension model A. This indicates that introducing the residual tensile strength (f_R) as 50% of the ultimate tensile strength (f_{tu}) underestimates the flexural strength.
4. Assuming UHPC ultimate tensile strain (ϵ_{tu}) as 0.004 or 0.010 did not have significant effect on the predicted flexural strength of non-prestressed beams.
5. The prediction provided by Model A2 at curvature Φ_p was the closest to the measured flexural strength of all test data. Moreover, the prediction accuracy was not affected by the variation of the parameters ρ , f_t , f'_c , and V_f , where the ratio of measured-to-predicted flexural strength did not deviate significantly from 1.0.
6. Experimental testing on the ribbed UHPC slab validated the outcome of the prediction models evaluation. The slab achieved a higher flexural strength than Model A2 prediction at curvature Φ_p , where the measured-to-predicted flexural resistance factors was 1.07.

The analysis of UHPC beams shear test data yielded the following conclusions:

1. Among the parameters affecting the shear strength of prestressed and non-prestressed beams, the tensile strength of UHPC ($\sigma_{Rd,f}$) was found to have a significant positive correlation with the shear strength of UHPC beams.

2. For UHPC beams with fiber volume fraction of at least 2%, the level of prestressing (6_{cp}) and longitudinal reinforcement ratio ($A_l/b_w d$) were found to have significant effect on the shear strength of prestressed and non-prestressed beams respectively.
3. The RILEM TC 162-TDF, 2003, and *fib* Model Code, 2010 prediction models underestimate the shear strength of UHPC beams.
4. The French Standard NF P 18-710, 2016 model provided the closest prediction to the measured shear strength of UHPC beams with the highest consistency of prediction followed by the Draft of AASHTO Guide Specification for Structural Design with UHPC, 2021.

8.3 Recommendations

- 1- Using sandblasting and conventional shear connectors are recommended for CC-UHPC interface preparation for both flexure and shear strengthening. No special connectors or roughening techniques are required.
- 2- Special attention should be given to the longitudinal reinforcement in the tension zone and its anchorage when designing for shear strengthening to prevent premature failure before UHPC contributes fully to the CC-UHPC component capacity.
- 3- The non-proprietary UHPC mix developed by UNL/NDOT (Mendonca et al., 2020) has the required properties as a repair and strengthening material. Special attention should be given to workability retention.
- 4- Further full-scale testing is recommended for the following cases:
 - a. When the existing CC component is prestressed and UHPC is non-prestressed.
 - b. When the existing CC component is prestressed and UHPC is externally post-tensioned. This technique shall utilize the superior mechanical properties of UHPC more than other techniques when UHPC is non-prestressed.
 - c. Columns/piers strengthened with a UHPC encasement.

References

- AASHTO LRFD. (2017). Bridge design specifications. Washington, D.C.: American Association of State Highway and Transportation Officials, eighth edition.
- AASHTO Guide Specification. (Draft, 2021). Structural Design with Ultra-high Performance Concrete. Document developed for consideration by AASHTO CBS T-10 committee (Structural Concrete Design). American Association of State Highway and Transportation Officials.
- Abad, B. F., Lantsoght, E. O., & Yang, Y. (2019). Shear capacity of steel fibre reinforced concrete beams. In Proceedings of the FIB Symposium, Krakow, Poland (pp. 27-29).
- ACI Committee 239. (2014) Ultra-High-Performance Concrete: (ACI 239-18). Farmington Hills, MI :American Concrete Institute.
- ACI Committee 544. (2018) Guide to Design with Fiber-Reinforced Concrete: (ACI 544.4R-18) Farmington Hills, MI :American Concrete Institute.
- AFGC (Association Francaise de Génie Civil). (2002). Ultra high performance fibre-reinforced concretes. Interim Recommendations. AFGC publication, France.
- AFGC (Association Francaise de Génie Civil). (2013). Ultra high performance fibre-reinforced concretes, recommendations. AFGC publication, France.
- Aghani, K., & Afshin, H. (2016). Experimental and Numerical Investigation on Shear Retrofitting of RC Beams by Prefabricated UHPFRC Sheets. Civil Engineering Journal, 2(5), 168-179.
- Alberta Infrastructure and Transportation. (2005). Bridge Engineering Section Technical Standards Branch, Repair Manual for Concrete Bridge Elements.
- Al-Osta, M. A., Isa, M. N., Baluch, M. H., & Rahman, M. K. (2017). Flexural behavior of reinforced concrete beams strengthened with ultra-high performance fiber reinforced concrete. Construction and Building Materials, 134, 279-296.
- Amin, A., Foster, S. J., & Muttoni, A. (2015). Derivation of the σ -w relationship for SFRC from prism bending tests. Structural Concrete, 16(1), 93-105.
- Andrawes, B., Shaw, I., & Zhao, H. (2018). Repair & strengthening of distressed/damaged ends of prestressed beams with FRP composites. Illinois Center for Transportation/Illinois Department of Transportation.

- ASTM, C1609 / C1609M (2019). Standard Test Method for Flexural Performance of Fiber-Reinforced Concrete. American Standards of Testing of Materials (ASTM Standards).
- ASTM C1856 / C1856M (2017). Standard Practice for Fabricating and Testing Specimens of Ultra-High Performance Concrete. American Standards of Testing of Materials (ASTM Standards).
- Baby, F., Marchand, P., Toutlemonde, F., Billo, J., & Simon, A. (2010). Shear resistance of ultra high performance fibre-reinforced concrete I-beams. *FraMCoS7*, 1411-1417.
- Baby, Florent, Pierre Marchand, and François Toutlemonde. (2013). Shear behavior of ultrahigh performance fiber-reinforced concrete beams. I: Experimental investigation. *Journal of Structural Engineering* 140.5: 04013111.
- Baby, Florent, Pierre Marchand, and François Toutlemonde. (2013). Shear behavior of ultrahigh performance fiber-reinforced concrete beams. II: Analysis and design provisions. *Journal of Structural Engineering* 140.5: 04013112.
- Baby, F., Graybeal, B., Marchand, P., & Toutlemonde, F. (2013). UHPFRC tensile behavior characterization: inverse analysis of four-point bending test results. *Materials and structures*, 46(8), 1337-1354.
- Bae, B. I., Choi, H. K., & Choi, C. S. (2016). Flexural strength evaluation of reinforced concrete members with ultra high performance concrete. *Advances in Materials Science and Engineering*.
- Bahraq, A. A., Al-Osta, M. A., Ahmad, S., Al-Zahrani, M. M., Al-Dulaijan, S. O., & Rahman, M. K. (2019). Experimental and numerical investigation of shear behavior of RC beams strengthened by ultra-high performance concrete. *International Journal of Concrete Structures and Materials*, 13(1), 1-19.
- Bertram, G., & Hegger, J. (2012). Bond Behavior of Strands in UHPC—Tests and Design. In *Proceedings of the 3rd international symposium on UHPC, Kassel, Germany* (pp. 525-532).
- Bentz, E. C., Vecchio, F. J., & Collins, M. P. (2006). Simplified modified compression field theory for calculating shear strength of reinforced concrete elements. *ACI Materials Journal*, 103(4), 614.
- Binard, J. P. (2017). UHPC: A game-changing material for PCI bridge producers. *PCI Journal*.
- Carreira, D. J., & Chu, K. H. (1986). Stress-strain relationship for reinforced concrete in tension. In *Journal Proceedings* (Vol. 83, No. 1, pp. 21-28).

- Chen, S., Zhang, R., Jia, L. J., & Wang, J. Y. (2018). Flexural behavior of rebar-reinforced ultra-high-performance concrete beams. *Magazine of Concrete Research*, 70(19), 997-1015.
- Crane, Charles Kennan. 2010. Shear and shear friction of ultra-high performance concrete bridge girders. Dissertation, Georgia Institute of Technology.
- DAfStb-Guideline. German Committee for Structural Concrete, Berlin. 2017. Ultra-High Performance Concrete. (Draft)
- Degen, Brian Everett. (2006). Shear design and behavior of ultra-high performance concrete.
- Devalapura, R. K., & Tadros, M. K. (1992). Stress-strain modeling of 270 ksi low-relaxation prestressing strands. *PCI Journal*, 37(2), 100-106.
- Doiron, G. (2017). UHPC Pier Repair/Retrofit Examples of Completed Projects in North America. In AFGC-ACI-fib-RILEM Int. Symposium on Ultra-High Performance Fibre-Reinforced Concrete.
- Ductal Website, <https://www.ductal.com/en/>, Information obtained in March 2020.
- El-Khier, M. A., Kodsý, A., & Morcous, G. (2018) Precast Concrete Deck-To-Concrete Girder Connection Using UHPC. Proceedings of the 10th International Conference on Short and Medium Span Bridges, Quebec, Canada.
- El-Khier, M. A., & Morcous, G. (2019). Precast Concrete Deck-to-Girder Connection using UHPC.
- El-Khier, M. A., & Morcous, G. (2021). Precast concrete deck-to-girder connection using Ultra-High Performance Concrete (UHPC) shear pockets. *Engineering Structures*, 248, 113082.
- El-Helou, R. G., & Graybeal, B. A. (2019). The ultra girder: A design concept for a 300-foot single span prestressed ultra-high performance concrete bridge girder. In *International Interactive Symposium on Ultra-High Performance Concrete (Vol. 2, No. 1)*. Iowa State University Digital Press.
- ElSafty, A., Graeff, M. K., & Fallaha, S. (2014). Behavior of laterally damaged prestressed concrete bridge girders repaired with CFRP laminates under static and fatigue loading. *International Journal of Concrete Structures and Materials*, 8(1), 43-59.
- European pre-standard: ENV 1992-1-1, (1991): Eurocode 2: Design of Concrete Structures – Part 1: General rules and rules for buildings.

- EN, BS. "14651." Test Method for Metallic Fibre Concrete-Measuring the Flexural Tensile Strength (Limit of Proportionally (LOP), Residual) (2007): 1-20.
- EPFL-Swiss Federal Institute of Technology. (2016). Standard: Ultra-High Performance Fibre Reinforced Cement-based composites (UHPFRC) Construction material, dimensioning and application, SIA 2052.
- Fan, T. (2020). "UHPC for Steel Bridge Repair and Houston Ship Channel Bridge Case Study". 2020 Virtual Transportation Short Course.
- Federal Highway Administration. (2015) Bridge Maintenance Reference Manual, Publication number FHWA-NHI-14-050.
- Federal Highway Administration. (2017) Deficient Bridges by Highway System 2017. <https://www.fhwa.dot.gov/bridge/nbi/no10/defbr17.cfm> (information obtained on August, 2020)
- Fehling, Ekkehard, and Jenny Thiemicke. (2012). Experimental investigations on I-Shaped UHPC-Beams with combined reinforcement under shear load. Ultra High Performance Concrete and Nanotechnology in Construction, 3rd Intl. Symp. on Ultra High Performance Concrete and Nanotechnology for High Performance Construction Materials. Kassel: kassel university press GmbH.
- Fehling, Ekkehard, M., Walraven, J., Leutbecher, T., & Fröhlich, S. (2014). Ultra-high performance concrete UHPC: Fundamentals, design, examples. John Wiley & Sons.
- French standard, NF P 18-710, (2016). National addition to Eurocode 2 — Design of concrete structures: specific rules for Ultra-High Performance Fibre-Reinforced Concrete (UHPFRC).
- Foster, Stephen J., Ankit Agarwal, and Ali Amin. (2018). Design of steel fiber reinforced concrete beams for shear using inverse analysis for determination of residual tensile strength. *Structural Concrete* 19.1: 129-140.
- Graybeal, B. A. (2009). Structural Behavior of a Prototype UHPC Pi-Girder. *TechBrief of FHWA*, 06(November), 1–4. [https://doi.org/HRDI-06/10-09\(100\)E](https://doi.org/HRDI-06/10-09(100)E)
- Graybeal, B.A. (2019). Design and Construction of Field-Cast UHPC Connections, FHWA, U.S. Department of Transportation, Publication No: FHWA-HRT-19-011.
- Graybeal, B. A. (2006). Material property characterization of ultra-high performance concrete. Publication No. FHWA-HRT-06-103. United States. Federal Highway Administration. Office of Infrastructure Research and Development.
- Graybeal, B. A. (2006). Structural Behavior of Ultra-High Performance Concrete Prestressed I-Girders. Publication No. FHWA-HRT-06-115. United States. Federal Highway Administration. Office of Infrastructure Research and Development.

- Graybeal, B. A., Baby, F. (2013). Development of direct tension test method for ultra-high-performance fiber-reinforced concrete. *ACI Materials Journal*, 110(2), 177.
- Habel, K. (2004). Structural behaviour of elements combining ultra-high performance fibre reinforced concretes (UHPRFC) and reinforced concrete (No. THESIS). EPFL.
- Haber, Z. B., De la Varga, I., Graybeal, B. A., Nakashoji, B., & El-Helou, R. (2018). Properties and behavior of UHPC-class materials (No. FHWA-HRT-18-036). United States. Federal Highway Administration. Office of Infrastructure Research and Development.
- Haber, Zachary B., and Benjamin A. Graybeal. (2019). Advancing Bridge Repair and Preservation Using Ultra-High-Performance Concrete. *ASPIRE* magazine.
- Hain, A., and Zaghi, A. (2021). Learnings from the Field Implementation of a Novel UHPC Beam End Repair on a Corroded Steel Girder Bridge in Connecticut. <https://www.youtube.com/watch?v=wIU9CgIIlTmI&t=111s>. Information obtained in 2021.
- Hasgul, U., Turker, K., Birol, T., & Yavas, A. (2018). Flexural behavior of ultra-high-performance fiber reinforced concrete beams with low and high reinforcement ratios. *Structural Concrete*, 19(6), 1577-1590.
- Hegger, Josef, Dirk Tuchlinski, and Boris Kommer. (2004). Bond anchorage behavior and shear capacity of ultra high performance concrete beams. *Proceedings of the International Symposium on Ultra High Performance Concrete*.
- Hegger, J., & Bertram, G. (2008). Shear carrying capacity of Ultra-High Performance Concrete beams. *Proceedings of the International fib Symposium 2008 - Tailor Made Concrete Structures: New Solutions for Our Society*, 96.
- Hognestad, E., Hanson, N. W., & McHenry, D. (1955). Concrete stress distribution in ultimate strength design. In *Journal Proceedings* (Vol. 52, No. 12, pp. 455-480).
- International Federation for Structural Concrete CEB-*fib*. (2012). *CEB-FIP Model Code 2010*”, Final Draft, Vol. 1. Lausanne, Switzerland.
- Kahanji, C., Ali, F., & Nadjai, A. (2017). Structural performance of ultra-high-performance fiber-reinforced concrete beams. *Structural Concrete*, 18(2), 249-258.
- Khalifa, A., Gold, W. J., Nanni, A., & MI, A. A. (1998). Contribution of externally bonded FRP to shear capacity of RC flexural members. *Journal of composites for construction*, 2(4), 195-202.
- Kodsy, A., Morcous, G., and Wood, R. L. (2020). Synthesis of Repair Practices of Damaged Precast/Prestressed Concrete Girders. Nebraska Department of Transportation (NDOT) Project Report.

- Kodsy, A., & Morcou, G. (2021). Flexural strength prediction models of non-prestressed Ultra-High Performance Concrete (UHPC) components. In *Structures* (Vol. 34, pp. 4532-4547). Elsevier.
- Lim, W. Y., & Hong, S. G. (2016). Shear Tests for Ultra-High Performance Fiber Reinforced Concrete (UHPFRC) Beams with Shear Reinforcement. *International Journal of Concrete Structures and Materials*, 10(2), 177–188.
<https://doi.org/10.1007/s40069-016-0145-8>
- Mendonca, F., El-Khier, M. A., Morcou, G., & Hu, J. (2020). Feasibility Study of Development of Ultra-High Performance Concrete (UHPC) for Highway Bridge Applications in Nebraska (No. SPR-P1 (18) M072). University of Nebraska--Lincoln.
- Mészöly, T., & Randl, N. (2018). Shear behavior of fiber-reinforced ultra-high performance concrete beams. *Engineering Structures*, 168(April), 119–127.
<https://doi.org/10.1016/j.engstruct.2018.04.075>
- Mitchell, D., & Collins, M. P. (1974, August). Diagonal compression field theory-a rational model for structural concrete in pure torsion. In *Journal Proceedings* (Vol. 71, No. 8, pp. 396-408).
- Nettleton, D. (2014). *Commercial data mining: processing, analysis and modeling for predictive analytics projects*. Elsevier.
- Noshiravani, T., & Brühwiler, E. (2013). Experimental investigation on reinforced ultra-high-performance fiber-reinforced concrete composite beams subjected to combined bending and shear. *ACI Structural Journal*, 110(ARTICLE), 251-261.
- Pansuk, W., Nguyen, T. N., Sato, Y., Den Uijl, J. A., & Walraven, J. C. (2017). Shear capacity of high performance fiber reinforced concrete I-beams. *Construction and Building Materials*, 157(December), 182–193.
<https://doi.org/10.1016/j.conbuildmat.2017.09.057>
- Prem, P. R., Bharatkumar, B. H., & Iyer, N. R. (2012). Mechanical properties of ultra high performance concrete. *World academy of Science, Engineering and Technology*, 68, 1969-1978.
- Prem, P. R., & Murthy, A. R. (2016). Acoustic emission and flexural behaviour of RC beams strengthened with UHPC overlay. *Construction and Building Materials*, 123, 481-492.
- Priestley, M. N., Seible, F., & Calvi, G. M. (1996). *Seismic design and retrofit of bridges*. John Wiley & Sons.

- Pourbaba, M., Joghataie, A., & Mirmiran, A. (2018). Shear behavior of ultra-high performance concrete. *Construction and Building Materials*, 183, 554-564.
- Pourbaba, M., & Joghataie, A. (2019). Determining shear capacity of ultra-high performance concrete beams by experiments and comparison with codes. *Scientia Iranica*, 26(1), 273-282.
- Qi, J., Wang, J., & Ma, Z. J. (2018). Flexural response of high-strength steel-ultra-high-performance fiber reinforced concrete beams based on a mesoscale constitutive model: Experiment and theory. *Structural Concrete*, 19(3), 719-734.
- Qiu, M., Shao, X., Wille, K., Yan, B., & Wu, J. (2020). Experimental investigation on flexural behavior of reinforced ultra high performance concrete low-profile T-beams. *International Journal of Concrete Structures and Materials*, 14(1), 1-20.
- Qiu, M., Shao, X., Zhu, Y., Zhan, J., Yan, B., & Wang, Y. (2020). Experimental investigation on flexural cracking behavior of ultrahigh performance concrete beams. *Structural Concrete*, 21(5), 2134-2153.
- Ridha, M. M., Al-Shaarbaf, I. A., & Sarsam, K. F. (2018). Experimental study on shear resistance of reactive powder concrete beams without stirrups. *Mechanics of Advanced Materials and Structures*, 1-13.
- Russell, H. G., Graybeal, B. A., & Russell, H. G. (2013). Ultra-high performance concrete: A state-of-the-art report for the bridge community (No. FHWA-HRT-13-060). United States. Federal Highway Administration. Office of Infrastructure Research and Development.
- Safdar, M., Matsumoto, T., & Kakuma, K. (2016). Flexural behavior of reinforced concrete beams repaired with ultra-high performance fiber reinforced concrete (UHPFRC). *Composite Structures*, 157, 448-460.
- Sakr, M. A., Sleemah, A. A., Khalifa, T. M., & Mansour, W. N. (2019). Shear strengthening of reinforced concrete beams using prefabricated ultra-high performance fiber reinforced concrete plates: Experimental and numerical investigation. *Structural Concrete*, 20(3), 1137-1153.
- Shield, C., & Bergson, P. (2018). BR27568—Experimental Shear Capacity Comparison Between Repaired and Unrepaired Girder Ends.
- Sim, C., Tadros, M., Gee, D., & Asaad, M. (2020). Flexural design of precast, prestressed ultra-high-performance concrete members. *PCI Journal*, 65(6).
- Singh, H. (2015). Flexural modeling of steel fiber-reinforced concrete members: analytical investigations. *Practice Periodical on Structural Design and Construction*, 20(4), 04014046.

- Singh, M., Sheikh, A. H., Ali, M. M., Visintin, P., & Griffith, M. C. (2017). Experimental and numerical study of the flexural behaviour of ultra-high performance fibre reinforced concrete beams. *Construction and Building Materials*, 138, 12-25.
- Solhmirzaei, R., & Kodur, V. K. R. (2017). Modeling the response of ultra high performance fiber reinforced concrete beams. *Procedia engineering*, 210, 211-219.
- Tadros M., Lawler J., Abo El-Khier M., Gee D., Kurt A., Lucier G., Wagner E., (2021). Implementation of Ultra-High Performance Concrete in Long-Span Precast Pretensioned Elements for Concrete Buildings and Bridges. Phase II Report. Precast/Prestressed Concrete Institute. <https://doi.org/10.15554/pci.rr.mat-013>
- Vandewalle, L. (2000). Design method for steel fiber reinforced concrete proposed by RILEM TC 162-TDF. In *Fifth International RILEM Symposium on Fibre-Reinforced Concrete (FRC)* (pp. 51-64). RILEM Publications SARL.
- Voo, Y. L., Foster, S. J., & Gilbert, R. I. (2006). Shear strength of fiber reinforced reactive powder concrete prestressed girders without stirrups. *Journal of Advanced Concrete Technology*, 4(1), 123-132.
- Voo, Yen Lei, Wai Keat Poon, and Stephen J. Foster. (2010). Shear strength of steel fiber-reinforced ultrahigh-performance concrete beams without stirrups. *Journal of structural engineering* 136.11: 1393-1400.
- Vandewalle, Lucie. (2000). Recommendations of RILEM TC 162-TDF: Test and design methods for steel fibre reinforced concrete. *Materials and Structures/Materiaux et Constructions* 33.225: 3-5.
- Walpole, R. E., Myers, R. H., Myers, S. L., & Ye, K. (2012). *Probability & statistics for engineers & scientists*. Prentice Hall.
- Wibowo, H., & Sritharan, S. (2018). Use of ultra-high-performance concrete for bridge deck overlays (No. IHRB Project TR-683).
- Wipf, T., Phares, B., Sritharan, S., Degen, B., & Giesmann, M. T. (2009). *Design and Evaluation of a Single-Span Bridge Using Ultra-High Performance Concrete*.
- Wight, J. K., & MacGregor, J. G. (2017). *Reinforced Concrete: Mechanics and Design*, 7th edition. Pearson Education.
- Yang, In Hwan, Changbin Joh, and Byung-Suk Kim. (2010). Structural behavior of ultra high performance concrete beams subjected to bending. *Engineering Structures* 32.11: 3478-3487.

- Yin, H., Teo, W., & Shirai, K. (2017). Experimental investigation on the behavior of reinforced concrete slabs strengthened with ultra-high performance concrete. *Construction and Building Materials*, 155, 463-474.
- Yoo, D. Y., Banthia, N., & Yoon, Y. S. (2016). Predicting service deflection of ultra-high-performance fiber-reinforced concrete beams reinforced with GFRP bars. *Composites Part B: Engineering*, 99, 381-397.
- Yoo, D. Y., Banthia, N., & Yoon, Y. S. (2017). Experimental and numerical study on flexural behavior of ultra-high-performance fiber-reinforced concrete beams with low reinforcement ratios. *Canadian Journal of Civil Engineering*, 44(1), 18-28.
- Yoo, D. Y., & Yoon, Y. S. (2015). Structural performance of ultra-high-performance concrete beams with different steel fibers. *Engineering Structures*, 102, 409-423.
- Zagon, Raul, Stijn Matthys, and Zoltan Kiss. (2016). Shear behaviour of SFR-UHPC I-shaped beams. *Construction*
- Zmetra, Kevin M. (2015). Repair of Corrosion Damaged Steel Bridge Girder Ends by Encasement in Ultra-High Strength Concrete. Dissertation, University of Connecticut.

Appendix

Conversion of Load-Deflection to Moment-Curvature Relationships

Span	$L \rightarrow L$
Distance from Load to Support	$a \rightarrow a$
Inertia	$I \rightarrow I$
Modulus of Elasticity	$E \rightarrow E$
Load	$P \rightarrow P$
Moment	$M := \frac{P \cdot a}{2} \rightarrow \frac{P \cdot a}{2}$
Curvature	$\psi := \frac{M}{E \cdot I} \rightarrow \frac{P \cdot a}{2 \cdot E \cdot I}$
Deflection	$\Delta := \frac{P \cdot a}{48 \cdot E \cdot I} \cdot (3 \cdot L^2 - 4 \cdot a^2) \rightarrow \frac{P \cdot a \cdot (3 \cdot L^2 - 4 \cdot a^2)}{48 \cdot E \cdot I}$
UHPC Prism Test Setup	$L := 12 \text{ in} \quad a := \frac{L}{3} = 4 \text{ in}$
Conversion from Deflection to Curvature	$\frac{\psi}{\Delta} \rightarrow \frac{24}{3 \cdot L^2 - 4 \cdot a^2} = 0.065 \frac{1}{\text{in}^2}$
Conversion from Load to Moment	$\frac{P}{M} \rightarrow \frac{2}{a} = 0.5 \frac{1}{\text{in}}$

Derivation of Conversion Factors for Inverse Analysis of UHPC Flexure Test Data

UHPC Compressive Strength	$f_c' := 18 \text{ ksi}$
Correction Factor for MOE	$K_1 := 1.0$
Modulus of Elasticity	$E_c := 2500 \text{ ksi} \cdot K_1 \cdot \sqrt[3]{\frac{f_c'}{\text{ksi}}} = 6552 \text{ ksi}$
Reduction Factor for Compression	$\alpha := 0.85$
Elastic Compressive Strain	$\varepsilon_{cp} := \frac{\alpha f_c'}{E_c} = 0.0023$
Ultimate Compressive Strain	$\varepsilon_{cu} := 0.0035$
Effective Cracking Strength	$f_{t,cr} := \begin{bmatrix} 0.75 \\ 1.0 \\ 1.5 \\ 2 \end{bmatrix} \text{ ksi}$
Elastic Tensile Strain	$\varepsilon_{t,cr} := \frac{f_{t,cr}}{E_c} = \begin{bmatrix} 0.00011 \\ 0.00015 \\ 0.00023 \\ 0.00031 \end{bmatrix}$
Crack Localization Strain	$\varepsilon_{t,loc} := 0.005$
Ratio of Elastic to Localization Strain	$r := \frac{\varepsilon_{t,cr}}{\varepsilon_{t,loc}} = \begin{bmatrix} 0.023 \\ 0.031 \\ 0.046 \\ 0.061 \end{bmatrix}$
Adjustment Factor	$k := 1 - \frac{r}{2} = \begin{bmatrix} 0.989 \\ 0.985 \\ 0.977 \\ 0.969 \end{bmatrix}$
Section Width	$b := 3 \text{ in}$
Section Depth	$h := 3 \text{ in}$
Tension Force in UHPC	$T = b \cdot f_{t,cr} \cdot k \cdot (h - c)$
Compression Strain in UHPC	$\varepsilon_c = \varepsilon_{t,loc} \cdot \frac{c}{(h - c)}$
Compression Force in UHPC	$C = b \cdot E_c \cdot \varepsilon_c \cdot \frac{c}{2}$
Equilibrium of Forces	$T = C$

$$b \cdot f_{t,cr} \cdot k \cdot (h - c) = b \cdot E_c \cdot \varepsilon_{t,loc} \cdot \frac{c^2}{2(h - c)}$$

$$\frac{(h - c)^2}{c^2} = \frac{E_c \cdot \varepsilon_{t,loc}}{2 k \cdot f_{t,cr}}$$

$$\frac{h}{c} = \sqrt{\frac{E_c \cdot \varepsilon_{t,loc}}{2 k \cdot f_{t,cr}} + 1}$$

Depth of Neutral Axis

$$c := \frac{h}{\sqrt{\frac{E_c \cdot \varepsilon_{t,loc}}{2 k \cdot f_{t,cr}} + 1}} = \begin{bmatrix} 0.526 \\ 0.591 \\ 0.691 \\ 0.768 \end{bmatrix} \text{ in}$$

UHPC Tension Force

$$T := b \cdot f_{t,cr} \cdot k \cdot (h - c) = \begin{bmatrix} 5.5 \\ 7.12 \\ 10.15 \\ 12.98 \end{bmatrix} \text{ kip}$$

Moment Arm

$$y := h - \frac{c}{3} - \frac{k \cdot (h - c)}{2} = \begin{bmatrix} 1.6 \\ 1.62 \\ 1.64 \\ 1.66 \end{bmatrix} \text{ in}$$

Nominal Moment Capacity

$$M_n := T \cdot y = \begin{bmatrix} 0.73 \\ 0.96 \\ 1.39 \\ 1.8 \end{bmatrix} \text{ kip} \cdot \text{ft}$$

Section Modulus

$$S := \frac{b \cdot h^2}{6} = 4.5 \text{ in}^3$$

Corresponding Flexural Strength

$$f_{t,f} := \frac{M_n}{S} = \begin{bmatrix} 1.96 \\ 2.56 \\ 3.7 \\ 4.8 \end{bmatrix} \text{ ksi}$$

Conversion Factors

$$\frac{f_{t,cr}}{f_{t,f}} = \begin{bmatrix} 0.38 \\ 0.39 \\ 0.4 \\ 0.42 \end{bmatrix}$$

Inverse Analysis of UHPC Flexure Prism (Linear-Constant Model)

UHPC Compressive Strength	$f_c' := 18 \text{ ksi}$
Correction Factor for MOE	$K_1 := 1.0$
Modulus of Elasticity	$E_c := 2500 \text{ ksi} \cdot K_1 \cdot \sqrt[3]{\frac{f_c'}{\text{ksi}}} = 6552 \text{ ksi}$
Prism Width	$b := 3 \text{ in}$
Prism Depth	$h := 3 \text{ in}$
Prism Length	$l := 12 \text{ in}$
Measured Peak Load	$P_p := 10.8 \text{ kip}$
Corresponding Deflection at Peak Load	$\delta_p := 0.038 \text{ in}$
Deflection to Curvature Conversion Factor	$k := 0.065$
Peak Moment	$M_n := P_p \cdot \frac{l}{6} = 1.8 \text{ kip} \cdot \text{ft}$
Curvature at Peak Moment	$\phi_{loc} := \frac{\delta_p \cdot k}{\text{in}^2} = 0.0025 \frac{1}{\text{in}}$

$c := 1 \text{ in}$ $\varepsilon_{t,loc} := 0.005$ $r := \frac{\left(\frac{f_{t,loc}}{E_c}\right)}{\varepsilon_{t,loc}}$

$f_{t,loc} := 1 \text{ ksi}$

$$b \cdot E_c \cdot \frac{\varepsilon_{t,loc}}{(h-c)} \cdot \frac{c^2}{2} = b \cdot f_{t,loc} \cdot \frac{r \cdot (h-c)}{2} + b \cdot f_{t,loc} \cdot (h-c) \cdot (1-r)$$

$$\frac{\varepsilon_{t,loc}}{h-c} = \phi_{loc}$$

$$M_n = b \cdot E_c \cdot \frac{\varepsilon_{t,loc}}{(h-c)} \cdot \frac{c^3}{3} + b \cdot f_{t,loc} \cdot \frac{r^2 \cdot (h-c)^2}{3} + \frac{b \cdot f_{t,loc} \cdot (h-c)^2 \cdot (1-r^2)}{2}$$

$Solution := \mathbf{find}(c, \varepsilon_{t,loc}, f_{t,loc}) = \begin{bmatrix} 0.019 \text{ m} \\ 0.006 \\ (1.358 \cdot 10^7) \text{ Pa} \end{bmatrix}$

$c := Solution_0 = 0.7366 \text{ in}$ $\varepsilon_{t,loc} := Solution_1 = 0.0056$ $f_{t,loc} := Solution_2 = 1.97 \text{ ksi}$

Inverse Analysis of UHPC Flexure Prism (Strain-Hardening Model)

UHPC Compressive Strength	$f_c' := 18 \text{ ksi}$
Correction Factor for MOE	$K_1 := 1.0$
Modulus of Elasticity	$E_c := 2500 \text{ ksi} K_1 \cdot \sqrt[3]{\frac{f_c'}{\text{ksi}}} = 6552 \text{ ksi}$
Prism Width	$b := 3 \text{ in}$
Prism Depth	$h := 3 \text{ in}$
Prism Length	$l := 12 \text{ in}$
Section Modulus	$S := \frac{b \cdot h^2}{6} = 4.5 \text{ in}^3$
Measured Cracking Load	$P_{cr} := 4.1 \text{ kip}$
Measured Peak Load	$P_p := 10.8 \text{ kip}$
Corresponding Deflection at Peak Load	$\delta_p := 0.038 \text{ in}$
Deflection to Curvature Conversion Factor	$k := 0.065$
Peak Moment	$M_n := P_p \cdot \frac{l}{6} = 1.8 \text{ kip} \cdot \text{ft}$
Curvature at Peak Moment	$\phi_{loc} := \frac{\delta_p \cdot k}{\text{in}^2} = 0.0025 \frac{1}{\text{in}}$
First Crack Moment	$M_{cr} := P_{cr} \cdot \frac{l}{6} = 0.683 \text{ kip} \cdot \text{ft}$
Effective Cracking Strength	$f_{t,cr} := \frac{M_{cr}}{S} = 1.822 \text{ ksi}$

$$\begin{aligned}
 c &:= 1 \text{ in} & \varepsilon_{t,loc} &:= 0.005 & r &:= \frac{\left(\frac{f_{t,cr}}{E_c}\right)}{\varepsilon_{t,loc}} \\
 f_{t,loc} &:= 1 \text{ ksi}
 \end{aligned}$$

$$b \cdot E_c \cdot \frac{\varepsilon_{t,loc}}{(h-c)} \cdot \frac{c^2}{2} = b \cdot f_{t,cr} \cdot \frac{r \cdot (h-c)}{2} + b \cdot f_{t,cr} \cdot (h-c) \cdot (1-r) + b \cdot (f_{t,loc} - f_{t,cr}) \cdot (h-c) \cdot \frac{(1-r)}{2}$$

$$\frac{\varepsilon_{t,loc}}{h-c} = \phi_{loc}$$

$$\begin{aligned}
 M_n &= b \cdot E_c \cdot \frac{\varepsilon_{t,loc}}{(h-c)} \cdot \frac{c^3}{3} + b \cdot f_{t,cr} \cdot \frac{r^2 \cdot (h-c)^2}{3} + \frac{b \cdot f_{t,cr} \cdot (h-c)^2 \cdot (1-r^2)}{2} \\
 &\quad + b \cdot (f_{t,loc} - f_{t,cr}) \cdot (h-c)^2 \cdot \frac{(1-r)}{2} \cdot \frac{(2-r)}{3}
 \end{aligned}$$

$$\text{Solution} := \mathbf{find} (c, \varepsilon_{t,loc}, f_{t,loc}) = \begin{bmatrix} 0.019 \text{ m} \\ 0.006 \\ (1.437 \cdot 10^7) \text{ Pa} \end{bmatrix}$$

$$c := \text{Solution}_0 = 0.7293 \text{ in} \quad \varepsilon_{t,loc} := \text{Solution}_1 = 0.0056 \quad \varepsilon_{t,loc} := \text{Solution}_2 = 2.085 \text{ ksi}$$

**Shear Strength of a Non-Prestressed Concrete Beam accordi
AASHTO LRFD, 2017, El-Helou et al., 2019 and Draft AASHTO**

1- Material and Section Properties of Un-strengthened Beam

Compressive Strength	$f_c' := 5400 \text{ psi}$
Section Height	$h := 18 \text{ in}$
Section Width	$b_v := 4 \text{ in}$
Reinforcement MOE	$E_s := 29000 \text{ ksi}$
Reinforcement Grade	$f_y := 60 \text{ ksi}$
Number of Bottom Bars	$n := 5$
Area of One Bar	$A_{s1} := 0.6 \text{ in}^2$
Area of Tension Reinforcement	$A_s := n \cdot A_{s1} = 3 \text{ in}^2$
Area of Compression Reinforcement	$A'_s := 0.44 \cdot \text{in}^2$
Depth of Compression Reinforcement	$d' := 2 \text{ in}$
C.G. of Bars from Top of Beam	$d := 16 \text{ in}$
Shear Depth (AASHTO LRFD, 2017 Section 5.7.2.8)	$d_v := \max(0.9 \cdot d, 0.72 h) = 14.4 \text{ in}$
Transverse Reinforcement Area	$A_v := 0.11 \text{ in}^2$
Transverse RFT Yield Strength	$f_{yt} := 60 \text{ ksi}$
Spacing of Transverse RFT (at critical section)	$S := 6 \text{ in}$
Angle of Transverse RFT with Longitudinal Axis	$\alpha := 90 \text{ deg}$

2- Crack Angle Calculation of Un-strengthened Beam

Factor of Concrete Ability to Transmit Shear Forces (AASHTO LRFD, 2017 Section 5.7.3.4)	$\beta := 2$
--	--------------

Angle of Diagonal Compression Strut (AASHTO LRFD, 2017 Section 5.7.3.4) $\theta := 45 \text{ deg}$

Concrete Section Contribution to Shear Resistance (AASHTO LRFD, 2017 Section 5.7.3.4) $V_c := 0.0316 \cdot \beta \cdot \sqrt{f'_c} \cdot \text{ksi} \cdot b_v \cdot d_v = 8.459 \text{ kip}$

Transverse RFT Contribution to Shear Resistance (AASHTO LRFD, 2017 Section 5.7.3.4)

$$V_s := \frac{A_v \cdot f_{yt} \cdot d_v \cdot (\cot(\theta))}{S} = 15.84 \text{ kip}$$

Un-strengthened Beam Nominal Shear Resistance $V_{n,US} := V_c + V_s = 24.3 \text{ kip}$

3- Shear Capacity of The UHPC Part in The Strengthened Beam (According to El-Helou et al., 2019 and Draft AASHTO, 2021)

Modulus of Elasticity of Steel $E_s := 29000 \text{ ksi}$

UHPC Compressive Strength $f_{c,uhpc}' := 18 \text{ ksi}$

Modulus of Elasticity of UHPC $E_c := 2500 \cdot 1 \cdot \left(\frac{f_{c,uhpc}'}{\text{ksi}} \right)^{0.33} \cdot \text{ksi} = 6489 \text{ ksi}$

UHPC Width $b_{UHPC} := 3 \text{ in}$

UHPC Depth $d_{UHPC} := 9 \text{ in}$

UHPC Tensile Strength $f_t := 1 \text{ ksi}$

Safety Factor to account for Fiber Orientation $\gamma_f := 1$

Safety Factor for the Sustained Tensile Cracking Resistance $\gamma_1 := 1$

Tensile Strength at Crack Localization $f_{t,loc} := \gamma_1 \cdot f_t = 1 \text{ ksi}$

Tensile Strain at Crack Localization $\epsilon_{t,loc} := 0.004$

UHPC Transverse Reinforcement Ratio $\rho_v := 0$

Shear Force Component due to Effective Prestressing Force $V_p := 0 \text{ kip}$ Straight Strands

Estimated Factored Shear Force $V_u := 51.3 \text{ kip}$

Estimated Factored Moment

$$M_u := 154 \text{ kip} \cdot \text{ft}$$

$$M_u := \max(M_u, d_v \cdot V_u) = 154 \text{ kip} \cdot \text{ft}$$

Factored Axial Load

$$N_u := 0 \cdot \text{kip} \quad \text{-ve if Compression}$$

Longitudinal Strain

$$\epsilon_s := \max\left(\frac{\left|\frac{M_u}{d_v}\right| + 0.5 N_u + |V_u - V_p|}{E_s \cdot A_s}, 0\right) = 0.002$$

Guess Values	$\theta := 28 \text{ deg}$ $\epsilon_v := 0.001$
Constraints	$\epsilon_{t,loc} = \frac{\epsilon_s}{2} \cdot (1 + (\cot(\theta))^2) + \frac{2 \cdot f_{t,loc}}{E_c} \cdot (\cot(\theta))^4$ $+ \frac{2 \cdot \rho_v \cdot E_s \cdot \epsilon_v}{E_c} \cdot \sin(\alpha) \cdot (\cot(\theta))^2 \cdot (1 + (\cot(\theta))^2 + \cot(\alpha) \cdot (\tan(\theta) + \cot(\theta)))$ $\epsilon_v - \epsilon_{t,loc} + 0.5 \cdot \epsilon_s = \frac{-2 \cdot f_{t,loc}}{E_c} \cdot (\cot(\theta))^2$ $- \frac{2 \cdot \rho_v \cdot E_s \cdot \epsilon_v}{E_c} \cdot \sin(\alpha) \cdot (1 + (\cot(\theta))^2 + \cot(\alpha) \cdot (\tan(\theta) + \cot(\theta)))$
Solver	$\text{Solution} := \mathbf{find}(\epsilon_v, \theta) = \begin{bmatrix} 0.002 \\ 0.634 \end{bmatrix}$

$$\epsilon_v := \text{Solution}_0 = 0.0024 \quad \theta_{UHPC} := \text{Solution}_1 = 36.314 \text{ deg} \quad f_{v,1} := E_s \cdot \epsilon_v = 69.514 \text{ ksi}$$

$$\theta := \max(\theta_{UHPC}, \theta) = 45 \text{ deg}$$

UHPC Nominal Shear Capacity

$$V_{n,UHPC} := \gamma_f \cdot b_{UHPC} \cdot d_{UHPC} \cdot f_{t,loc} \cdot \cot(\theta) = 27 \text{ kip}$$

Strengthened Beam Shear Capacity

$$V_{n,S} := V_{n,UHPC} + V_{n,US} = 51.3 \text{ kip}$$

Corresponding Applied Moment

$$M_a := V_{n,S} \cdot 3 \text{ ft} = 153.898 \text{ kip} \cdot \text{ft}$$

$$\text{Check}_1 := \mathbf{if} \left(\left| \frac{V_u - V_{n,S}}{V_u} \right| \leq 0.2\%, \text{ "Ok"}, \text{ "Reiterate Vu"} \right) = \text{ "Ok"}$$

$$Check_2 := \text{if} \left(\left| \frac{M_u - M_a}{M_u} \right| \leq 0.2\%, \text{"Ok"}, \text{"Reiterate Mu"} \right) = \text{"Ok"}$$

4- Interface Design

Shear Span $l_v := 36 \text{ in}$

Design Interface Shear along Shear Span (per side) $V_i := \frac{V_{n,UHPC}}{2} = 13.5 \text{ kip}$

Yield Strength of Threaded Rod (Anchor) $f_{y,a} := 60 \text{ ksi}$

Cross-section Area of Threaded Rod (Anchor) $A_a := 0.11 \text{ in}^2$

Direct Shear Resistance of Threaded Rod $V_{An} := 0.6 \cdot f_{y,a} \cdot A_a = 3.96 \text{ kip}$

Required Number of Anchors along The Shear Span (at Top and Bottom) $n_{An,L} := \frac{V_i}{2 \cdot V_{An}} = 1.705$

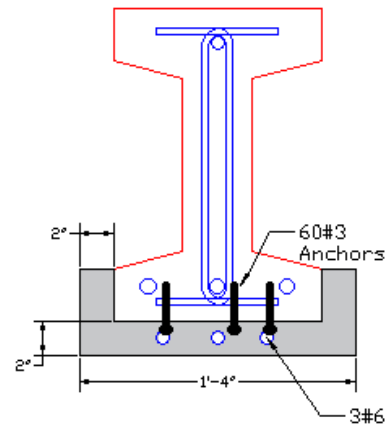
Required Spacing (When through threaded rods are used at top and bottom) $S_a := \frac{l_v}{n_{An,L}} = 21.1 \text{ in}$

Flexural Strength Prediction

Developed Excel Spreadsheet for a General CC-UHPC Section (Composite Horizontally or Vertically)

Input of Dimensions and Material Properties

Layer Arrangement		Material 1 Properties						Material 1 Properties					
Layer # (compression to tension)	Layer Thickness (in.)	Material 1 (f'_c) (ksi)	Layer Width (in.)	UHPC ₁ Tensile Strength (ksi)	UHPC ₁ Ultimate Tensile Strain	Modulus of Elasticity (ksi)	CC ₁ Strain at Peak Stress (ϵ_o)	Material 2 (f'_c) (ksi)	Layer Width (in.)	UHPC ₂ Tensile Strength (ksi)	UHPC ₂ Ultimate Tensile Strain	UHPC ₂ Modulus of Elasticity (Haber et al., 2018) (ksi)	CC ₂ Strain at Peak Stress (ϵ_o)
1	3	6	12			3502.8	0.002					0.0	0.002
2	12	6	4			3502.8	0.002					0.0	0.002
3	3	6	12			3502.8	0.002	17	4	1	0.004	0.0	0.002
4	2	17	16	1	0.004	5896.0						0.0	0.002
5						0.0						0.0	0.002
6						0.0						0.0	0.002



Input and Analysis of Reinforcement and/or Prestressing

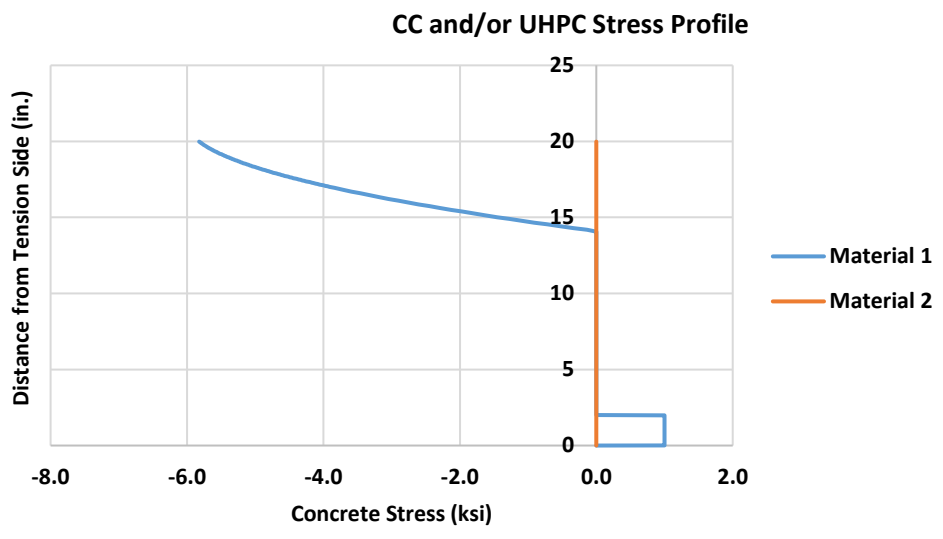
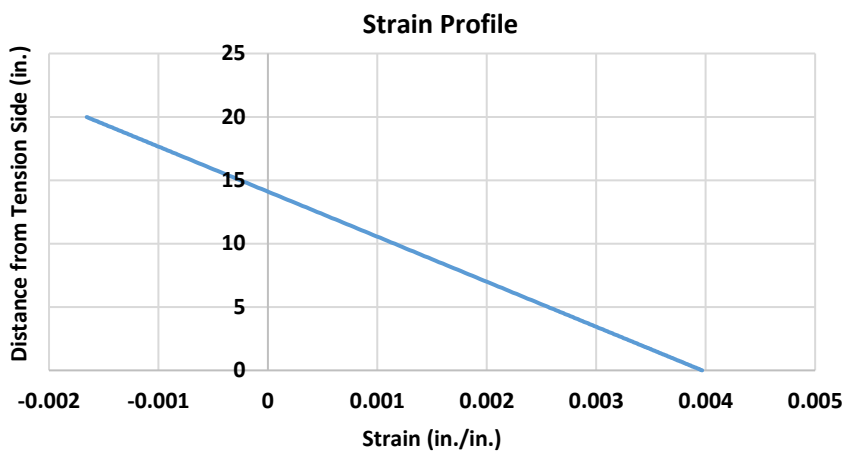
Type	Number of Bars/Strands	Bar/Strand Area (in ²)	Distance from compression side (in.)	Grade (ksi)	Effective Prestress (ksi)	Modulus of Elasticity (E) (ksi)	Total Strain	Bar/Strand Stress (ksi)	Concrete Stress at bar/strand location (ksi)	Internal Forces (kip)	Moment (kip.in)	Change in Strain
Conventional Reinforcement	3	0.6	16	60	0	29000	0.0028	60.0	0.0	108.0	1090.8	0.0028
	1	0.44	2	60	0	29000	-0.0011	-31.8	-4.7	-11.9	46.5	-0.0011
	3	0.44	18.875	60	0	29000	0.0037	60.0	1.0	77.9	1010.5	0.0037
	0	0	0	60	0	29000	-0.0017	-48.1	0.0	0.0	0.0	-0.0017
	0	0	0	60	0	29000	-0.0017	-48.1	0.0	0.0	0.0	-0.0017
Prestressing Reinforcement	0	0	0	270	172	28800	0.0043	124.1	0.0	0.0	0.0	-0.0017
	0	0	0	270	172	28800	0.0043	124.1	0.0	0.0	0.0	-0.0017
	0	0	0	270	172	28800	0.0043	124.1	0.0	0.0	0.0	-0.0017
	0	0	0	270	172	28800	0.0043	124.1	0.0	0.0	0.0	-0.0017
	0	0	0	270	172	28800	0.0043	124.1	0.0	0.0	0.0	-0.0017
	0	0	0	270	172	28800	0.0043	124.1	0.0	0.0	0.0	-0.0017
	0	0	0	270	172	28800	0.0043	124.1	0.0	0.0	0.0	-0.0017
											Max	0.00365

Analysis of Segments in Each Layer of The Section

Strip #	C.G from Top (in.)	Strain	Material 1 Stress (ksi)	Material 2 Stress (ksi)	Distance from Tension Side (in.)	Internal Force (kip)	Moment (kip.in.)
1	0.015	-0.0016558	-5.82	0.00	19.99	-2.1	12.3
2	0.045	-0.0016473	-5.81	0.00	19.96	-2.1	12.3
3	0.075	-0.0016389	-5.80	0.00	19.93	-2.1	12.2
4	0.105	-0.0016305	-5.80	0.00	19.90	-2.1	12.1
5	0.135	-0.001622	-5.79	0.00	19.87	-2.1	12.0
6	0.165	-0.0016136	-5.78	0.00	19.84	-2.1	11.9
7	0.195	-0.0016051	-5.77	0.00	19.81	-2.1	11.8
8	0.225	-0.0015967	-5.76	0.00	19.78	-2.1	11.8
9	0.255	-0.0015882	-5.75	0.00	19.75	-2.1	11.7
.							
..							
...							
595	20	0.0039675	0.00	0.00	0.00	0.0	0.0
596	20	0.0039675	0.00	0.00	0.00	0.0	0.0
597	20	0.0039675	0.00	0.00	0.00	0.0	0.0
598	20	0.0039675	0.00	0.00	0.00	0.0	0.0
599	20	0.0039675	0.00	0.00	0.00	0.0	0.0
600	20	0.0039675	0.00	0.00	0.00	0.0	0.0

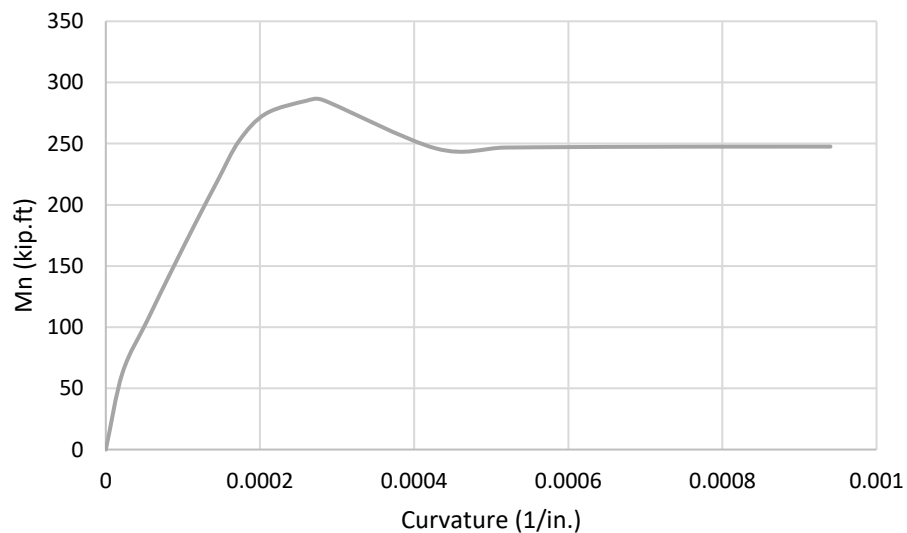
Analysis Results

Sum of Internal Forces	0.00
Ultimate Compressive Strain (ϵ_{cu})	0.0017
Neutral axis depth (c)	5.900
Nominal Moment Capacity (M_n)	285.8
Design Specification	R/C AASHTO
Strength Reduction Factor (ϕ)	0.83
Flexure Resistance (ϕM_n)	237.9



Resulting Moment-Curvature of Flexure Strengthened Beam #2

ϵ_{cx}	c (in.)	M_n (kip.ft)	Curvature (1/in.)
		0	0
0.0002	9.264	62.6	2.16E-05
0.0004	7.4	105.6	5.39E-05
0.0006	7.0	146.5	8.55E-05
0.0008	6.9	184.6	0.000116
0.001	6.9	220.0	0.000145
0.0012	6.9	252.4	0.000173
0.0014	6.7	274.6	0.000208
0.0016	6.1	285.1	0.000260
0.00166	5.9	285.8	0.000281
0.0018	4.2	246.1	0.000428
0.002	3.9	246.8	0.000518
0.0022	3.6	247.2	0.000606
0.0024	3.5	247.5	0.000692
0.0026	3.3	247.6	0.000777
0.0028	3.3	247.6	0.000859
0.003	3.2	247.6	0.00094



Moment-Curvature Plot of Flexure Strengthened Beam #2

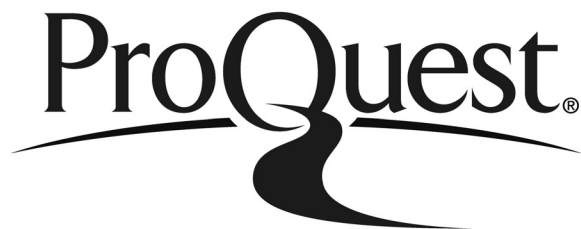
Interface Design for Flexure Strengthened Beam #2

Area of UHPC in Tension	$A_{UHPC} := 2 \cdot 16 \cdot \text{in}^2 = 32 \text{ in}^2$
Tensile Strength of UHPC	$f_{t,UHPC} := 1 \text{ ksi}$
Tensile Force Carried by UHPC	$F_{t,UHPC} := f_{t,UHPC} \cdot A_{UHPC} = 32 \text{ kip}$
Tension Reinforcement Area in UHPC	$A_{s,UHPC} := 3 \cdot 0.44 \cdot \text{in}^2 = 1.32 \text{ in}^2$
Yield Strength of Reinforcement	$f_y := 60 \text{ ksi}$
Tensile Force in Reinforcement	$F_{t,s,UHPC} := f_y \cdot A_{s,UHPC} = 79.2 \text{ kip}$
Largest Force to be Carried by CC-UHPC Interface	$V_i := F_{t,UHPC} + F_{t,s,UHPC} = 111.2 \text{ kip}$
Length of Interface Shear to Transfer the Force	$l_v := \frac{120 \text{ in}}{2} = 60 \text{ in}$
Factored Pullout Resistance of Anchor (according to manufacturer's recommendations)	$V_{PO} := 4.7 \text{ kip}$
Direct Shear Resistance of Anchor (according to manufacturer's recommendations)	$V_{DS} := 4.7 \text{ kip}$
Design Shear Resistance of Anchor	$V_{An} := \min(V_{PO}, V_{DS}) = 4.7 \text{ kip}$
Required Total Number of Anchors along The Shear Span	$n_{An,L} := \frac{V_i}{V_{An}} = 23.66$
Required Spacing for 3 anchors	$S_a := \frac{3 \cdot l_v}{n_{An,L}} = 7.6 \text{ in}$

ProQuest Number: 29067836

INFORMATION TO ALL USERS

The quality and completeness of this reproduction is dependent on the quality and completeness of the copy made available to ProQuest.



Distributed by ProQuest LLC (2022).

Copyright of the Dissertation is held by the Author unless otherwise noted.

This work may be used in accordance with the terms of the Creative Commons license or other rights statement, as indicated in the copyright statement or in the metadata associated with this work. Unless otherwise specified in the copyright statement or the metadata, all rights are reserved by the copyright holder.

This work is protected against unauthorized copying under Title 17, United States Code and other applicable copyright laws.

Microform Edition where available © ProQuest LLC. No reproduction or digitization of the Microform Edition is authorized without permission of ProQuest LLC.

ProQuest LLC
789 East Eisenhower Parkway
P.O. Box 1346
Ann Arbor, MI 48106 - 1346 USA